UNIVERSITY OF CALIFORNIA, SAN DIEGO

NUMERICAL AND EXPERIMENTAL STUDIES OF ETHANOL FLAMES AND AUTOIGNITION THEORY FOR HIGHER ALKANES

A dissertation submitted in partial satisfaction of the

requirements for the degree Doctor of Philosophy

in

Engineering Sciences (Mechanical Engineering)

by

PRIYANK SAXENA

Committee in charge:

Professor Forman A. Williams, Chair
Professor Kalyansundaram Seshadri, Co-Chair
Professor Lynn M. Russell
Professor Sutanu Sarkar
Professor Amitabha Sinha

2007

The dissertation of Priyank Saxena is approved, and it is acceptable in quality and form for publication on microfilm:

_____

_____

_____

_____
Co-Chair

_____
Chair

University of California, San Diego

2007

TABLE OF CONTENTS

LIST OF FIGURES

LIST OF TABLES

ACKNOWLEDGEMENTS

The present work has been accomplished at the Center for Energy Research at the University of California, San Diego, during the period of September 2002 until January 2007. I am deeply indebted to Professor Forman A. Williams for his encouragement, advice, and research support throughout my doctoral studies. I thank him for giving me chances to correct my mistakes during my research work. His energy and dedication to research is a constant source of inspiration to me.

I express my special gratitude to the faculty members of Mechanical and Aerospace Engineering Department, especially Professor Kalyansundaram Seshadri and Professor Sutanu Sarkar for their prompt help regarding both academics and non academics. I also valued tremendously the discussions with Professor Amable Liñan, Professor Antonio Sanchez, and Professor Norbert Peters during their summer-time stays at UCSD.

I am thankful to Venkat Tangirala for his constant encouragement and for always reviving my self confidence in the time of disappointments. I thank Shikha Gupta for helping me in a smooth transition to life in the USA, and her kind assistance in improving my written English. My stay at UCSD was a pleasant experience due to my interactions with all my friends at UCSD; Nick Killingsworth, Gonzalo Del Alamo, Masha Petrova, Maria Da Conceicao, John Buma, Vincent Morin, and Guillaume Mauger to name a few. I also thank my brother and my wife for sharing light moments with me when I was under stress.

Finally, it is impossible to have my research career without my parent's love and constant encouragement for a pursuit for knowledge. It is the guidance of my parents and

teachers that have shaped my ideals and career. I dedicate my dissertation to my parents and teachers.

Chapter 4 of the present dissertation, in part or in full, is a reprint of the material as it appears in the article: P. Saxena and F.A. Williams, "Testing a Small Detailed Chemical-Kinetic Mechanism for the Combustion of Hydrogen and Carbon Monoxide", *Combustion and Flame*, 145, 2006, pp. 316-323. The dissertation author was the primary researcher in that publication.

Chapter 6 of the present dissertation, in part or in full, is a reprint of the material as it appears in the article: P. Saxena and F.A. Williams, "Numerical and Experimental Studies of Ethanol Flames", *Proceedings of the Combustion Institute*, 31, 2007, pp.1149-1156. The dissertation author was the primary researcher in that publication.

Chapter 7 of the present dissertation, in part or in full, is a reprint of the material as it appears in the article: P. Saxena, N. Peters, and F.A. Williams, "An Analytical Approximation for High-Temperature Autoignition Times of Higher Alkanes", *Combustion and Flame*, to appear, 2007. The dissertation author was the primary researcher in that publication.

The research contained in this dissertation was supported by NSF through Grant No. CTS 0129562 and by NASA through Grant No. NCC3-1097.

VITA

January 9th, 1976	Born in Etawah, India
1993-1997	B.E. (Mechanical Engineering), Bhilai Institute of Technology, Bhilai, India
1998-2000	M.Tech. (Aerospace Engineering), Indian Institute of Technology, Kanpur, India
2000-2002	Aerospace Engineer, General Electric Global Research Center, Bangalore, India
2002-2007	Research Assistant, Center for Energy Research, University of California, San Diego, USA
2007	Ph.D., University of California, San Diego

PUBLICATIONS

Journals

1. P. Saxena, N. Peters, and F.A. Williams, "An Analytical Approximation for High-Temperature Autoignition Times of Higher Alkanes", *Combustion and Flame*, to appear 2007.
2. P. Saxena and F.A. Williams, "Numerical and Experimental Studies of Ethanol Flames", *Proceedings of the Combustion Institute*, 31, 2007, pp. 1149-1156.
3. P. Saxena and F.A. Williams, "Testing A Small Detailed Chemical-Kinetic Mechanism for the Combustion of Hydrogen and Carbon Monoxide", *Combustion and Flame*, 145, 2006, pp. 316-323.
4. S. Mittal and P. Saxena, "Hysteresis in flow past a NACA 0012 airfoil", *Computational Methods in Applied Mechanics and Engineering*, 191, 2002, pp. 2179-2189.
5. S. Mittal, P. Saxena, and A. Singh, "Computation of 2D flows past Ram Air Parachutes", *International Journal of Numerical Methods in Fluids*, 35, 2001, pp. 643-667.
6. S. Mittal and P. Saxena, "Prediction of hysteresis associated with the static stall of an airfoil", *AIAA Journal*, 38, No. 5, 2000, pp. 933-935.

Conferences

7. P. Saxena and F.A. Williams, "Experimental and numerical studies of ethanol flames", *ASME TURBO EXPO 2006: Power for Land, Sea and Air*, May 2006, Barcelona, Spain, GT2006-90326.
8. R. Devi, P. Saxena, B. Walter, B. Record, and V. Rajendran, "Pressure Reduction in Intake System of a Turbocharged-Inter cooled DI Diesel Engine using CFD

Methodology", 2004 *SAE Fuels & Lubricants Meeting & Exhibition*, June 2004, Toulouse, France, 2004-01-1874.

Reports

- **M.Tech. Thesis:** "Numerical simulation of turbulent flows using the Baldwin-Lomax model".
- **B.E. Final Year Project**: "Estimation of Primary Energy for Bhilai Steel Plant".

FIELDS OF STUDY

Major Field: Engineering

Studies in Combustion
Professor F. A. Williams

Studies in Physics of Gases and Physical Gas Dynamics
Professor F.A. Williams, Professor S. Krasheninnikov, and Professor R. Cattolica

Studies in Fluid Mechanics and Turbulence
Professor S. Sarkar, Professor P. Linden, and Professor S.L. Smith

Studies in Applied Mathematics
Professor F.A. Williams, Professor S.L. Smith, and Professor W.R. Young

Studies in Numerical Methods and Computational Fluid Dynamics
Professor T. Bewley

ABSTRACT OF THE DISSERTATION

NUMERICAL AND EXPERIMENTAL STUDIES OF ETHANOL FLAMES AND AUTOIGNITION THEORY FOR HIGHER ALKANES

by

Priyank Saxena

Doctor of Philosophy in Engineering Sciences (Mechanical Engineering)

University of California, San Diego, 2007

Professor Forman A. Williams, Chair

Professor Kalyansundaram Seshadri, Co-Chair

In order to enhance the fuel efficiency of an engine and to control pollutant formation, an improved understanding of the combustion chemistry of the fuels at a fundamental level is paramount. This knowledge can be gained by developing detailed reaction mechanisms of the fuels for various combustion processes and by studying combustion analytically employing reduced-chemistry descriptions. There is a need for small detailed reaction mechanisms for alkane and alcohol fuels with reduced uncertainties in their combustion chemistry that are computationally cheaper in multidimensional CFD calculations. Detailed mechanisms are the starting points in identifying reduced-chemistry descriptions of combustion processes to study problems analytically.

This research includes numerical, experimental and analytical studies. The first part of the dissertation consists of numerical and experimental studies of ethanol flames. Although ethanol has gained popularity as a possible low-pollution source of renewable energy, significant uncertainties remain in its combustion chemistry.

To begin to address ethanol combustion, first a relatively small detailed reaction mechanism, commonly known as the San Diego Mech, is developed for the combustion of hydrogen, carbon monoxide, formaldehyde, methane, methanol, ethane, ethylene, and acetylene, in air or oxygen-inert mixtures. This mechanism is tested for autoignition, premixed-flame burning velocities, and structures and extinction of diffusion flames and of partially premixed flames of many of these fuels. The reduction in uncertainties in the combustion chemistry can best be achieved by consistently updating a reaction mechanism with reaction rate data for the elementary steps based on newer studies in literature and by testing it against as many experimental conditions as available. The results of such a testing for abovementioned fuels are reported here along with the modifications of reaction-rate parameters of the most important elementary steps and the addition and deletion of a few key steps relevant to these tests. A mechanism developed in such a hierarchical way starting with simpler fuels such as hydrogen and carbon monoxide to the fuels with one and two carbon atoms has reduced uncertainties in the combustion chemistry of a fuel. This reaction mechanism, consisting of 137 reactions among 30 species, provides a robust building block upon which an ethanol mechanism is developed. The San Diego Mech is extended for ethanol combustion by adding 55 new reactions and 6 new species. Specifically, 33 reactions are added that involve C_2H_5OH or one of the three isomers produced by abstraction of an H atom from it, CH_3CHOH,

CH_2CH_2OH and CH_3CH_2O, and 22 reactions are added that involve acetaldehyde or one of the two isomers produced by abstraction of H from it, CH_2CHO and CH_3CO.

Ethanol combustion is investigated on the basis of a new reaction mechanism, thus developed, consisting of 192 elementary steps among 36 species, augmented by 53 additional steps and 14 additional species to address the formation of the oxides of nitrogen and 43 steps and 7 species to address formation of compounds involving three carbon atoms. The mechanism is tested against shock-tube autoignition-delay data, laminar burning velocities, counterflow diffusion-flame extinction and measurements of structures of counterflow partially premixed and diffusion flames. Measurements on ethanol-air flames at a strain rate of 100 s^{-1}, employing prevaporized ethanol with a mole fraction of 0.3 in a nitrogen carrier stream, were made for the pure diffusion flame and for a partially premixed flame with a fuel-side equivalence ratio of 2.3 and involved thermocouple measurements of temperature profiles and determination of concentration profiles of C_2H_5OH, CO, CO_2, H_2, H_2O, O_2, N_2, CH_4, C_2H_6 and C_2H_2+C_2H_4 by gas chromatographic analysis of samples withdrawn through fine quartz probes. Computational investigations also were made of profiles of oxides of nitrogen and other potential pollutants in similar partially premixed flames of ethanol and other fuels for comparison purposes. The computational results with the present mechanism are in reasonable agreement with experiment and perform as well as or better than predictions of other, generally much larger, mechanisms available in the literature. Further research is, however, warranted for providing additional and more stringent tests of the mechanism and its predictions, especially for condition at higher pressures.

The second part of the dissertation consists of analytical study of autoignition of higher alkane fuels. It is shown that, above about 1000 K, ignition delay times for propane and all higher alkanes, as well as for a number of other fuels, can be calculated well by employing rate parameters of only three types of elementary steps, namely $C_mH_n+HO_2\rightarrow C_mH_{n-1}+H_2O_2$, $H_2O_2+M\rightarrow 2OH+M$ and $2HO_2\rightarrow H_2O_2+O_2$, only the first of which is fuel-specific, the other two clearly being common to all fuels. The prediction of this remarkably simple result relies on a steady-state approximation for HO_2, as well as steady states for more active radicals during induction. The resulting approximation to the chemistry exhibits a slow, finite-rate buildup of H_2O_2 and removal of fuel during the induction period. The criterion employed for termination of the induction period is the complete depletion of the original fuel subject to the approximations introduced. Numerical comparisons of the ignition-time formula with the experiments show that the predictions work well not only for higher alkanes but also for propene and JP-10. The analytical approximation thus produces reasonable results for a wide range of fuels. These results provide a new perspective on high-temperature autoignition chemistry and a general means of easily estimating ignition times of the large number of fuels of practical importance.

CHAPTER 1

INTRODUCTION

1.1 OVERVIEW

Dwindling fossil fuels supplies and rising pollutant levels in the atmosphere are some of the major challenges to fast-paced-power-intensive industrial growth in modern society. The scientific community is trying to tackle these problems by replacing fossil fuels with renewable and cleaner sources of energy. At present, biomass-based fuels seem to be most economically viable option because they can be used in the existing fossil fuel based infrastructure. As a result, a new avenue has been opened for engine designers to develop flex-fuel engines; the engines that can run simultaneously on different fuels.

The present research is a contribution towards these world-wide efforts. Recently, ethanol has piqued the interest of research and industrial communities as a promising biomass fuel. The first part of the present thesis attempts to elucidate ethanol combustion at fundamental level by obtaining improved understanding of ethanol combustion chemistry.

Autoignition delay times of hydrocarbon fuels play a major role in the performance characteristics of new engine concepts such as HCCI (Homogeneous Charged Compression Ignition). There is a need for reduced-chemistry models and simple formula for the autoignition of practical hydrocarbon fuels for flex-fuel complex engine analysis, which are computationally less expensive compared to detailed chemical mechanisms. The second part of this work proposes such a simple chemistry and provides a simple analytical formulation for autoignition of higher alkane fuels.

1.2 ETHANOL AS AN ALTERNATIVE FUEL

Interest in the use of ethanol as a stand-alone fuel and as an oxygenated additive to hydrocarbon fuels is continually increasing. The underlying reasons are the cost of the fuel and environmental effects; as a renewable energy source, ethanol qualifies for consideration in programs designed to conserve precious natural resources [1, 2]. Interest in reducing pollutant emissions in combustion processes also has focused attention on ethanol because many believe that oxygenated fuels or oxygenated fuel additives can decrease emissions of oxides of nitrogen (NO_x) by reducing peak temperatures in flames and also help to oxidize carbon monoxide and lessen soot production by favoring oxidation routes over pyrolysis routes. Although much attention has been given to oxygenated additives other than ethanol in automotive applications, such as ethers that range from methyl tertiary butyl ether (MTBE) to dimethyl ether, these alternatives all are synthetic fuels that, besides exacting in principle an energy-supply penalty in their production, also can be harmful to the environment (witness MTBE in groundwater [3]). To the extent that oxygenated species can reduce air pollution, therefore, increased interest is focused on ethanol for clean burning.

There are, however, considerable uncertainties about the extent to which these possible benefits of ethanol combustion are realizable. There is, for example, concern about possible increased emissions of aldehydes. Since methanol produces very little soot in combustion, prevailing belief is that this may be true for all alcohols, but Spacelab experiments on the combustion of fiber-supported ethanol droplets, performed along with experiments on the combustion of free heptane droplets [4], revealed substantial sooting of ethanol, comparable to that of heptane. With the advent of flexible-fuel cars and high-

octane-rated E85 (85/15 percent ethanol/gasoline) fuel, it thus becomes desirable to assess more critically the suitability of ethanol as an environmentally friendly fuel.

The objective of this study was to understand ethanol combustion at the fundamental level, reduce the uncertainties in the existing combustion-chemistry of ethanol, measure flame structures, and evaluate to what extent the abovementioned advantages are the reasons of excitement and disadvantages are the reasons of concerns. This research has computational and experimental components. The computational part addresses detailed chemical-kinetic descriptions of ethanol combustion chemistry, and experimental part involves experimental testing of predicted flame structures.

1.2.1 CURRENT STATUS OF THE RESEARCH

A number of different authors around the world have contributed to our knowledge of the chemistry of ethanol combustion. This includes work in Ireland [5], Russia [6], France [7], USA [8, 9, 10] and Brazil [11]. As a consequence of these efforts, a number of different detailed chemical-kinetic mechanisms for ethanol combustion now exist that have been tested in a number of ways against different kinds of experimental data. There are experiments with static reactors [12, 13, 14], shock tubes [15, 16, 17], flow reactors [8] and premixed laminar flames [18]. Different experiments pertain to different ranges of conditions. The combustion applications of interest are at temperatures between roughly 800K and 2200K and pressures between 1 bar and 50 bar. The static-reactor experiments tend to be at temperatures and pressures lower than this, while the shock-tube experiments are in the right range and provide useful autoignition data. Flow-reactor temperatures do not extend over the entire range of interest, but flame

experiments, virtually by definition, are central to combustion applications. There are, however, important practical concerns about nonpremixed and partially premixed systems that cannot be addressed by any of these experiments.

Although there have been early experiments on coflow ethanol diffusion flames [19, 20], much better tests of chemical mechanisms can be made in counterflow flames because of the one-dimensional geometry (for all variables except the velocity field) and the availability of readily usable codes to calculate their flame structures with detailed chemistry. The counterflow configuration facilitates thermocouple and gas-sampling measurements by providing horizontal isothermal, isoconcentration surfaces along which the probes can be inserted to minimize sampling errors. These experiments, which are carried out for the first time for ethanol flames, are part of the current research.

1.2.2 A SMALL DETAILED CHEMICAL KINETIC MECHANISM FOR ETHANOL

None of the above mentioned mechanisms were [5-11] found to agree with all the available data and showed uncertainties in predicting the preliminary test results on ethanol flames [21]. This indicates the need for the development of a detailed mechanism for ethanol combustion which is robust.

Because of limitations on computer capabilities, there is a need for detailed chemical-kinetic mechanisms for combustion that are not too large. Our approach differs from that underlying a number of other data bases where larger mechanisms are proposed by including all possible elementary routes for the sake of completeness. The efforts here are directed to keep minimum numbers of species and reactions needed to describe the

high-temperature combustion processes. This in turn reduces the uncertainties in the rate parameters employed. This simplification is achieved by restricting attention to temperatures above about 1000 K, pressure below about 100 bar, equivalence ratios less than about 3 in premixed systems, and potential-flow strain rates greater than about 50 s^{-1}. The simplifications arise from the unimportance of soot formation and cool-flame phenomena (peroxide chemistry) under these conditions.

Hence, as an alternative to mechanisms having thousands of elementary steps, a mechanism for fuels as complex as propane having less than 300 steps [22] was developed, widely known as the San Diego Mech. In the current study, the San Diego Mech, as a starting mechanism, was augmented for ethanol combustion. The ethanol mechanism consists of 192 elementary steps among 36 species, extended by 53 additional steps and 14 additional species to address the formation of oxides of nitrogen and 43 steps and 7 species to address formation of compounds involving three carbon atoms. Out of the 192 reactions 33 reactions are added that involve C_2H_5OH or one of the three isomers produced by abstraction of an H atom from it, CH_3CHOH, CH_2CH_2OH and CH_3CH_2O, and 22 reactions are added that involve acetaldehyde, which is an important intermediate in ethanol combustion, and CH_2CHO and CH_3CO. For the pressure dependent reactions, the third-body efficiencies of various species are assigned constant values, which are the mean over 1000 K to 2000 K for temperature-dependent third-body efficiencies. This helps in keeping the structure of the mechanism simple. Also, generic third-body efficiencies [23] with respect to nitrogen are assigned for all the pressure-dependent reactions. In many detailed mechanisms, it is observed that some reactions are assigned third-body efficiencies related to nitrogen while others have efficiencies

assigned equal to that of nitrogen. This can be a cause of concern especially in simulating experiments consisting of water vapor in the fuel mixture or the possible errors in the rates of recombination reactions which occurs when a lot of carbon dioxide, carbon monoxide and water vapor exist in the oxidation layer in the system.

Important aspects that need to be addressed in an ethanol mechanism are fuel pyrolysis three-body reactions which are also pressure dependent, and the three routes of H abstraction. Previous studies [8, 9, 10] have addressed the branching ratios of H-abstraction steps extensively, and the flame-structure data in this research provides validation to these branching ratios of the H-abstraction reactions. Also an estimation of the rates for two significant pyrolysis steps with pressure fall-off are reported.

The numerical predictions from the mechanism were tested against shock-tube autoignition data, laminar burning velocities, diffusion-flame extinction and measurements of structures of counterflow partially premixed and nonpremixed flames, the last of these were performed and reported here for the first time. In the process of development, the mechanism was also tested for the intermediate fuels such as hydrogen, carbon monoxide, formaldehyde, methane, methanol, ethane, ethylene, acetylene, and acetaldehyde against various experimental data of interests available in the literature.

Computational studies included numerical integration of the conservation equations with detailed chemistry, radiation and transport effects, the last of which is not active in shock-tube autoignition delay time calculations. The computer programs CHEMKIN [24] and FlameMaster [25] were employed for this purpose. San Diego Mech is freely available on the web [26] for academic, research and noncommercial applied purposes in both CHEMKIN and FlameMaster formats.

1.2.3 EXPERIMENTAL CONDITIONS

The experimental conditions adopted in the present work correspond to diffusion flames and partially premixed flames at a plug-flow strain rate of 100 s^{-1}, in a counterflow setup. The diffusion flame that was probed in detail consists of prevaporized fuel, with mole fraction of 0.3, diluted with nitrogen in the fuel stream, and air as the oxidizer stream. The partially premixed flame that was measured includes prevaporized fuel in air partially premixed to an equivalence ratio of 2.3 in the fuel stream, and air as the oxidizer stream. This last configuration yields a two-stage flame: There is a pale green fuel-rich premixed flame in the fuel stream and a brighter blue diffusion flame in the vicinity of the stagnation plane. Temperature profiles were measured by a thermocouple, and concentration profiles of stable species such as C_2H_5OH, CO, CO_2, H_2, H_2O, O_2, N_2, CH_4, C_2H_6 and C_2H_2+C_2H_4 were measured by gas chromatography of samples withdrawn by a fine probe.

There are two reasons for including partially premixed flames in the measurements along with the diffusion flames. One is the prevalence of partially premixed flames in the applications, and the other is for improved experimental accuracy. At a sufficiently large extent of premixing, the partially premixed flames exhibit two reaction zones, a rich premixed reaction zone and a diffusion-flame reaction zone. This serves to spread the flame structure over a few millimeters and lessens the necessity of obtaining fine submillimeter spatial resolution. Proper alignment enables half-millimeter spatial resolutions to be obtained with proper design and operation of the sampling probes, but it is very difficult to go beyond quarter-millimeter resolution. In many

respects, the structures of the partially premixed flames have more character and are more revealing.

1.3 THEORY FOR AUTOIGNITION OF HIGHER ALKANE FUELS

In both propulsion and explosion-safety applications, as well as in fundamental investigations such as computational approaches to descriptions of combustion processes, there is a need for simple analytical expressions for autoignition induction times. Expressions of that type can be obtained empirically from experiment, as they often have been [27-31], but this requires experiments to be performed for each fuel over the full range of conditions of interest. At the opposite extreme, programs are now readily available [24, 25] that enable autoignition times in homogeneous, adiabatic systems to be computed readily with full detailed chemical-kinetic mechanisms, and empirical fits to the computational results can be made. This, however, does not aid in understanding or in extension to conditions that have not been computed.

Autoignition times of most fuels, especially higher hydrocarbons, seem to be remarkably similar in both value and temperature dependence in the temperature range between about 1000 K and 2500 K. This suggests that the length of the induction period may be controlled by chemistry that the fuels have in common, not strongly dependent on the specific fuel and not reliant on the full complex details of the true chemical mechanism. A simple set of key elements of that common chemistry, however, has not yet been identified. Once that set is determined, if it is simple enough then it can readily be used to derive a general analytical autoignition-time formula from basic first principles. Identifying a reduced chemistry for autoignition by systematic reduction and

deriving such a formula was the objective of the present study. A formula which depends on one fuel-dependent step and two fuel-independent steps is developed and reported here. The most important assumption that goes in this study is that the rapid-radical build-up doesn't happen until all the fuel, which absorbs all the reactive radicals, is completely consumed, hence, the ignition occurs [32].

1.4 THESIS ORGANIZATION

Chapter 2 to 6 covers the ethanol combustion study while chapter 7 presents autoignition theory. A survey of the literature for ethanol combustion chemistry, issues related to current mechanisms, and a method for detailed mechanism development is described in Chapter 2. Chapter 3 presents details of experimental setup, experimental conditions, and the procedure for measuring counterflow diffusion flame structures for ethanol. Chapter 4 and Chapter 5 present a detailed study for testing of submechanisms for intermediate fuels in the ethanol mechanism such as hydrogen, carbon monoxide, formaldehyde, methane, methanol, ethane, ethylene, acetylene, and acetaldehyde. Testing of the mechanism for the combustion of hydrogen and carbon monoxide is presented in Chapter 4 while fuels with C_1 and C_2 hydrocarbons and acetaldehyde in Chapter 5. In Chapter 6, ethanol mechanism development, experimental measurements of the flame structures and tests of ethanol mechanism against these flame data, and the data from the literature for autoignition delay times, laminar burning velocities and flame extinction are reported.

Chapter 7 is devoted completely to identifying a simplified chemistry for high-temperature autoignition of higher alkanes, and development of an analytical formula for

the same. The numerical results are compared with the experimental data, and the validity of the theory is discussed.

Finally in Chapter 8, major conclusions from the current studies and the future extensions to this research are discussed.

1.5 REFERENCES

1. U.S. Department of Energy, "Biofuels: Ethanol for sustainable transportation", DOE/GO-10099-736, April, 1999.

2. California Energy Commission, "Evaluation of biomass-to-ethanol potential in California: A report to the Governor and the Agency Secretary", California Environmental Protection Agency, 1999.

3. California Environmental Protection Agency, "MTBE (methyl tertiary butyl ether)", Briefing Paper, April 24, 1997.

4. Nayagam, V., Haggard, Jr., J.B., Colantonio, R.O., Marchese, A.J., Dryer, F.L., Zhang, B.L. and Williams, F.A., "Microgravity n-heptane droplet combustion in oxygen-helium mixtures at atmospheric pressure", AIAA Journal, 36, 1998, pp. 1369-1378.

5. Dunphy, M.P., Patterson, P.M. and Simmie, J.M., "High-temperature oxidation of ethanol. Part 2.-Kinetic Modeling", Journal of the Chemical Society, Faraday Transactions, 87, 1991, pp. 2549-2559.

6. Borisov, A.A., Zamanskii, V.M., Konnov, A.A., Lisyanskii, V.V., Rusakov, S.A. and Skachkov, G.I., "A mechanism of high-temperature ethanol ignition", Soviet Journal of Chemical Physics, 9, 1992, pp. 2527-2537.

7. Dagaut, P., Boettner, J.C. and Cathonnet, M., 1992, "Kinetic modeling of ethanol pyrolysis and combustion", Journal de Chimie Physique, 89, 1992, pp. 867-884.

8. Norton, T.S. and Dryer, F.L., "An experimental and modeling study of ethanol oxidation kinetics in an atmospheric pressure flow reactor", International Journal of Chemical Kinetics, 24, 1992, pp. 319-344.

9. Marinov, N.M., “A detailed chemical kinetic model for high temperature ethanol oxidation”, International Journal of Chemical Kinetics, 31, 1999, pp. 183-220.

10. Li, J., “Experimental and numerical studies of ethanol chemical kinetics,” PhD Thesis, Princeton University, 2004.

11. Benvenutti, L.H., Marques, C.S.T. and Bertran, C.A., “Chemiluminescent emission data for kinetic modeling of ethanol combustion”, Combustion Science and Technology, 177, 2005, pp. 1-26.

12. Cullis, C.F. and Newitt, E.J., “The gaseous oxidation of aliphatic alcohols. 1. Ethyl Alcohol – The products formed in the early stages”, Proceedings of the Royal Society of London A, 237, 1956, pp. 530-542.

13. Brown, J. and Tipper, C.F.H., “Cool flame combustion of ethanol”, Proceedings of the Royal Society of London A, 312, 1969, pp. 399-415.

14. Borisov, A.A. Zamanskii, V.M., Konnov, A.A., Lisyanskii, V.V. , Rusakov, S.A. and Skachkov, G.I., “High-temperature pyrolysis of ethanol”, Soviet Journal of Chemical Physics, 8, 1991, pp. 121-141.

15. Natarajan, K. and Bhaskaran, K.A., “An experimental and analytical investigation of high temperature ignition of ethanol”, Thirteenth International Symposium on Shock Waves, 1982, pp. 834-842.

16. Dunphy, M.P. and Simmie, J.M., “High temperature oxidation of ethanol. Part 1.- Igniton delays in shock waves”, Journal of the Chemical Society, Faraday Transactions, 87, 1991, pp. 1691-1696.

17. Curran, H.J., Dunphy, M.P., Simmie, J.M., Westbrook, C.K. and Pitz, W.J., “Shock tube ignition of ethanol, isobutene and MTBE: Experiments and modeling”, Proceedings of the Combustion Institute, 24, 1992, pp. 769-776.

18. Egolfopoulos, F.N., Du, D.X. and Law, C.K., 1992, “a study of ethanol oxidation kinetics in laminar premixed flames, flow reactors and shock tubes”, Proceedings of the Combustion Institute, 24, 1992, pp. 833-841.

19. Smith, S.R. and Gordon, A.S., “Studies of diffusion flames. II. Diffusion flames of some simple alcohols”, Journal of Chemical Physics, 60, 1956, pp. 1059-1062.

20. Lieb, D.F. and Roblee, Jr., L.H.S., “A radioisotopic tracer study of carbon formation in ethanol-air diffusion flames”, Combustion and Flame, 14, 1970, pp. 285-296.

21. Redell, F.H., “Experimental investigation of the structure of a partially premixed planar ethanol flame”, M.S. Thesis, University of California, San Diego, 2000.

22. Petrova, M.V. and Williams, F.A., “A small detailed chemical-kinetic mechanism for hydrocarbon combustion”, Combustion and Flame, 144, 2006, pp. 526-544.

23. GRI MECH: http://www.me.berkeley.edu/gri_mech/

24. Kee, R.J., Rupley, F.M., Miller, J.A., Coltrin M.E., Grcar, J.F., Meeks, E., Moffat, H.K., Lutz, A.E., Dixon-Lewis, G., Smooke, M.D., Warnatz, J., Evans, G.H., Larson, R.S., Mitchell, R.E., Petzold, L.R., Reynolds, W.C., Caracotsios, M., Stewart, W.E., Glarborg, P., Wang, C., Adigun, O., Houf, W.G., Chou, C.P. and Miller, S.F., Chemkin Collection, Release 3.7.1, Reaction Design Inc., San Diego, CA, 2003.

25. Pitsch, H., “Entwicklung eines Programmpakets zur Berechnung eindimensionaler Flammen am Beispiel einer Gegenstromdiffusionflamme”, M.S. Thesis, RWTH Aachen, Germany, 1993.

26. CER website: http://maemail.ucsd.edu/combustion/cermech/

27. Williams, A. and Cooke, D.F., “Shock tube studies of methane and ethane oxidation”, Combustion and Flame, 24, 1975, pp. 245-256.

28. Spadaccini and Colket III, M.B., “Ignition delay characteristics of methane fuels”, Progress in Energy and Combustion Science, 20, 1994, pp. 431-460.

29. Petersen, E.L., Davidson, D.F. and Hanson, R.K., “Kinetic modeling of shock-induced ignition in low-dilution CH4/O2 mixtures at high pressures and intermediate temperatures”, Combustion and Flame, 117, 1999, pp. 272-290.

30. Colket III, M.B. and Spadaccini, L.J., “Scramjet fuels autoignition study”, Journal of Propulsion and Power, 17, 2001, pp. 315-323.

31. Horning, D.C., Davidson, D.F. and Hanson, R.K., “Study of the high-temperature autoignition of n-Alkane/O_2/Ar mixtures”, Journal of Propulsion and Power, 18, 2002, pp. 363-371.

32. Peters, N., Paczko, G., Seiser, R. and Seshadri, K., “Temperature cross-over and non-thermal runaway at two-stage ignition of n-heptane”, Combustion and Flame, 128, 2002, pp. 38-59.

CHAPTER 2

METHOD FOR DETAILED MECHANISM DEVELOPMENT

2.1 OVERVIEW

The first part of this research consists of numerical and experimental studies of ethanol flames. In the numerical studies a detailed reaction mechanism for ethanol is developed. A detailed reaction mechanism, also called chemical-kinetic mechanism, for a fuel is a system of elementary reactions among different species (molecules and radicals) that are observed to occur during the combustion of that fuel. The critical part in the development of a mechanism is to determine different routes of formation and consumption of each species, and the rate at which the reactants are converted into products. A brief overview of the methods used in the development of a reaction mechanism is presented here. The implementation of the procedures is discussed in details in Chapters 4, 5, and 6 where the development of the San Diego Mech is conducted.

The first step of a detailed reaction mechanism development is to identify routes of fuel consumption, and the formation and consumption of various intermediate stable species and radicals. The second step is to identify the experiments that will cover all the aspects of the combustion processes that are desired in the mechanism, and testing of the mechanism against these experiments. The third step involves sensitivity analysis, reaction-flux analysis, and rate of heat release per reaction to identify key steps and non-significant steps for a particular process. In the fourth step, rate parameters of the key

reactions are chosen after studying the uncertainties in their values from different literature sources and their effect in predictions of different experiments. Finally in the fifth step, the non-significant elementary steps can be eliminated by testing their effects in extreme conditions of pressure, temperature, and equivalence ratio ranges that the mechanism is designed for.

In developing a mechanism for complex fuels, it is important that sub-mechanisms for the simpler fuels are developed and tested as described above. The development of a mechanism in such a hierarchical way simplifies the task of mechanism validation, since only those reactions and rates which have been added to account for the next level of complexity require special attention [1]. However, in order to be sure of the robustness of a mechanism, any modification to the mechanism requires testing the effect of that modification on all the fuels, which in turn requires validating the predictions against the experimental data for each of the fuels. Nevertheless, because of the numerous uncertainties that exist in quantitative data for reaction-rate constants, thermodynamic data, transport data, etc. and in the qualitative descriptions of the chemistry, a chemical-kinetic mechanism can never be proven to be correct; it can only be disproved [2].

These mechanisms, once validated over a wide range of experimental conditions, are available for use in modeling combustion processes in practical devices over similar ranges and can also be used in identifying reduced-chemistry models – for example, to study flame structures analytically.

2.2 EXISTING MECHANISMS

Natarajan and Bhaskaran [3] reported a detailed mechanism for their experiments on ethanol autoignition in a shock-tube. However, they included only one path (isomer formed by H atom abstraction) of fuel consumption but recommended investigation of the effect of the other two isomers formed by H atom abstraction. Later mechanisms were proposed by Dunphy et al. [4], and Curran et al. [5] for shock tube autoignition delay times, Egolfopoulos et al. [6] and Gülder [7] for laminar burning velocities and Cullis [8], Brown [9] and Borisov [10] for static reactors experiments. It is only in the flow reactor study of Norton et al. [11] that a comprehensive mechanism was reported. An extensive exploration of the branching ratios of the formation of the three different isomers formed by H atom abstraction of the ethanol molecule was discussed [11]. Marinov [12] extended the ethanol study by proposing a mechanism for laminar flame speeds, ethanol oxidation profiles from jet stirred and turbulent flow reactors, and autoignition data. The branching ratios for the three different isomers were re-evaluated and rate parameters for fuel pyrolysis steps were estimated. Li [13] proposed a new mechanism by updating the mechanisms proposed in [11] and [12] based on newer rate data in the literature and tests against flame structure in variable pressure flow reactor. Recently, a mechanism [14], mostly based on Dagaut et al. [15] mechanism, was tested for data on chemiluminescence.

None of the above mentioned mechanisms were found to agree with all the available data and showed uncertainties in predicting the preliminary test results on ethanol flames [16]. This indicates the need for the development of a detailed mechanism for ethanol combustion which is robust.

2.3 THE SAN DIEGO MECH

The San Diego Mech grew out of rate-constant evaluations for hydrogen-air diffusion flames [17], augmented by carbon monoxide [18, 19], then methane [20], methanol [21, 22], ethane [23], ethylene [24], acetylene [25, 26], and further extended to propane, propene, propyne and allene [27]. Ethanol seems to be a natural extension to this mechanism, and that is what has been achieved in this study.

Over the years newer experimental data for different fuels have appeared in the literature, and there have been updates in the rate constants of elementary steps based on experimental and theoretical, such as Rice-Ramsperger-Kassel-Marcus (RRKM), studies. As a result of these new rate studies, variations of up to one-order of magnitude in the rate constant values for a few important steps have been observed. Also, potential-surface analysis has shown that a few steps cannot occur. Hence, availability of newer data, revision of rate constants of elementary reactions based on recent studies, and reevaluation of certain paths motivate us to revise the San Diego Mech for the above-mentioned fuels. This way a comprehensive mechanism can be developed in a hierarchical manner as was suggested by Westbrook et al. [1]. By doing this, confidence in the rates of major routes of fuel breakdown as well as formation and consumption of important intermediates, especially pollutants, is achieved.

Recently, tests have been made for hydrogen autoignition [28]. However, when the hydrogen submechanism was tested for freely propagating flames, it overpredicted the burning velocities for mixtures at atmospheric pressure and room temperature. Hence, before developing the ethanol mechanism, a thorough testing and revisions were made in

this study for hydrogen, carbon monoxide, and then all the abovementioned fuels, which are intermediate fuels in the combustion of ethanol.

As a result, a starting mechanism was developed consisting of 137 steps among 30 species augmented by 43 steps among 7 species related to three carbon atoms. After a thorough literature review for different routes of ethanol oxidation and pyrolysis, branching ratios of H-atom abstraction reactions from the ethanol molecule, and the ethanol decomposition reactions, the Li [13] mechanism (based on previous studies of Norton and Dryer [11] and Marinov [12], and modified based on flow reactor experiments) is taken as a basic submechanism for ethanol. The mechanism is chosen since it is the most recent and comprehensive data available. The peroxides species and related reactions, which are important only for low-temperature kinetics, are eliminated. Fall-off for ethanol decomposition steps are proposed after correlating rate constants from different literature sources and experimental results. A new chemical-kinetic mechanism for ethanol is developed, consisting of 192 elementary steps among 36 species, augmented by 53 additional steps and 14 additional species to address the formation of oxides of nitrogen and 43 steps and 7 species to address formation of compounds involving three carbon atoms. The San Diego Mechanism for ethanol developed in this study is tabulated in Appendix 1.

2.4 NUMERICAL METHODS

The best way to reduce the uncertainties in a mechanism is by validating its predictions against as many experimental data as are available. Hence, during the process of development for the San Diego Mech, numerical predictions were compared against

the data of selected experimental conditions. Numerical simulations of the experimental systems were performed using the CHEMKIN [29] and FlameMaster [30] codes. The CHEMKIN subroutines such as AURORA, PREMIX, and OPPDIFF were employed for homogeneous autoignition, freely propagating flames, and diffusion flame structures and extinctions, respectively.

These codes solve the following conservation equations [2] for multicomponent, reacting, ideal-gas mixtures with appropriate assumptions based on the experimental setup.

Mass conservation:

$$\partial\rho/\partial t + \nabla\cdot(\rho v) = 0 \quad , \tag{1}$$

where ρ is density, t is time and v is velocity of the fluid.

Momentum conservation:

$$\partial v/\partial t + v\cdot\nabla v = -(\nabla\cdot \mathrm{P})/\rho + \sum_{i=1}^{N} Y_i f_i \, , \tag{2}$$

where P is the pressure tensor and $\sum_{i=1}^{N} Y_i f_i$ is the sum of all body forces over the mass fraction for each species i.

Energy conservation:

$$\rho\frac{\partial}{\partial t}\left(h+\frac{1}{2}v^2\right)+\rho v\cdot\nabla\left(h+\frac{1}{2}v^2\right)=\frac{\partial p}{\partial t}+\nabla\cdot\left[\left(pU-\mathrm{P}\right)\cdot v\right]+\rho\sum_{i=1}^{N}Y_i f_i\cdot\left(v+V_i\right)-\nabla\cdot q \tag{3}$$

where h is enthalpy and V_i is the diffusion velocity.

Species conservation:

$$\partial Y_i/\partial t+v\cdot\nabla Y_i=w_i/\rho-\left[\nabla\cdot\left(\rho Y_i V_i\right)\right]/\rho\,, \tag{4}$$

where w_i is the rate of production of species i by a chemical reaction.

In equation 2 and 3, the pressure tensor is given by

$$\mathrm{P}=\left[p+\left(\frac{2}{3}\mu-\kappa\right)\left(\nabla\cdot v\right)\right]U-\mu\left[\left(\nabla v\right)+\left(\nabla v\right)^T\right]$$

The ideal gas law, $p=\rho R^0 T\sum_{i=1}^{N}\left(Y_i/W_i\right)$, applies here.

In equation 3, the heat flux vector is given by

$$q = -\lambda \nabla T + \rho \sum_{i=1}^{N} h_i Y_i V_i + R^0 T \sum_{i=1}^{N} \sum_{j=1}^{N} \left(\frac{X_j D_{Ti}}{W_i D_{ij}} \right) \left(V_i - V_j \right) + q_R$$

where λ is thermal conductivity and D_{Ti} is the thermal diffusion coefficient of species i, and q_R is the radiation heat flux. The second to last term is the called Dufor effect.

The relation of diffusion velocity with the thermodynamic parameters and concentrations is given by

$$\nabla X_i = \sum_{j=1}^{N} \left(\frac{X_i X_j}{D_{ij}} \right) \left(V_j - V_i \right) + \left(Y_i - X_i \right) \left(\frac{\nabla p}{p} \right) + \frac{\rho}{p} \sum_{j=1}^{N} Y_i Y_j \left(f_i - f_j \right)$$

$$+ \sum_{j=1}^{N} \left[\left(\frac{X_i X_j}{\rho D_{ij}} \right) \left(\frac{D_{Tj}}{Y_j} - \frac{D_{Ti}}{Y_i} \right) \right] \frac{\nabla T}{T}, \quad \text{i} = 1,..., \text{N}.$$

where D_{ij} is binary diffusion coefficient of species i and j. The last term in the above equation is called Soret effect.

The enthalpy in equation 3 is given by

$$h = \sum_{i=1}^{N} h_i Y_i$$

where $h_i = h_i^o + \int_{T^0}^{T} c_{p,i} dT, \quad \mathrm{i} = 1,..., \mathrm{N}$, which is a sum of chemical and thermal enthalpy.

The source terms in equation 4, which depend on the reaction-rate parameters of each elementary step, in species and energy equations are provided by,

$$w_i = W_i \sum_{r=1}^{M} \left(\nu_{ir}'' - \nu_{ir}'\right) B_r T^{\alpha r} e^{-\left(E_r / R^0 T\right)} \sum_{j=1}^{N} \left(\frac{X_j p}{R^0 T}\right)^{\nu_{j,r}'},$$

where for a particular reaction r, prefactor B_r, temperature exponent α_r, and activation reaction E_r are obtained experimentally or theoretically. The pressure dependence of Arrhenius reaction rate constants, $k = B_r T^{\alpha r} e^{-\left(E_r / R^0 T\right)}$ are given by the formulation in [31].

In the case of autoignition of a homogeneous mixture in a shock tube, where reaction timescales are relatively small compared to the diffusion timescales, the transport effects become insignificant. Hence a zero-dimensional time-dependent initial-value problem was solved using AURORA. The system was considered adiabatic by assuming no heat transfer through the walls. This assumption is valid since for the conditions in a shock-tube the chemical timescales are much smaller than the timescales involved in heat transfer. In addition, all the calculations were performed assuming isochoric system.

In the case of a steady freely-propagating flame, the system of equations is a one dimensional boundary-value problem with burning velocity as an eigenvalue of the

system. The transport effects such as multicomponent diffusion and thermal diffusion (Soret effect), and radiation effects (CO_2 and H_2O bands) are included in calculating the flame propagation. These calculations were performed using PREMIX code.

In simulating counterflow setup for diffusion flame structures and extinctions, flame was regarded to be steady, laminar, and axisymmetric, where momentum equations in radial and axial directions were solved with appropriate boundary conditions such as jet inlet velocities and the mixtures' inlet temperatures and compositions at the ducts' exit. OPPDIFF was employed in performing these calculations. Transport effects such as multicomponent and mixture-averaged diffusion, thermal diffusion (Soret effect), and radiation effects were included.

In case of diffusion-flame extinction, a converged solution was obtained at lower strain-rate value. Then the strain-rate was increased gradually by increasing the nozzle-exit velocities and maintaining momentum balance at the mid plane. The extinction strain rate was the strain rate at which the flame extinction happens. The care must be taken by tracking the strain-rate increments only along the stable branch of the extinction S-curve.

In all the above calculations, body-force terms, Dufor effect, and dependence of diffusion velocity on pressure and body forces are assumed to be negligible.

In the above calculations, various input databases are required, namely mechanism file, thermodynamic database, and transport database. In a mechanism file, the elementary reactions and the reaction-rate constants for forward reactions, k_f, are documented in a desired format depending on the requirements of the code used. The k_f values are obtained either experimentally or theoretically from the literature. In order to obtain k_b, thermodynamic data for each species is required to calculate equilibrium

constants. A thermodynamic database provides the entropy, heat of formation, and specific heat values for each species. This data is mainly based on Burcat's thermodynamic database [32], which is the most up-to-date in light of recent publications. A discussion on the thermodynamic data selection was presented in [27]. Another required database is the transport database, which provides information about the coefficients of diffusivity, viscosity, and conductivity for all the species. This data is mainly taken from the CHEMKIN transport database [29]. The mechanism files, thermodynamic data and transport data are available on the CER website [33].

During the simulations, grid independence of the solution was ensured and the mesh adaptation parameters were utilized to resolve the gradients in the variables as accurately as possible. In flame calculations, the grid size of approximately 1000 grid points were found to be sufficient for the calculations of hydrogen and carbon monoxide systems and approximately 600 grid points for hydrocarbons.

Besides numerical predictions of the desired experimental conditions, tools such as sensitivity analysis and reaction-flux analysis were utilized in assessing the uncertainties in rate parameters of elementary steps. In sensitivity analysis, effect of variation in rate parameters of each elementary step on the desired measured quantity such as ignition delay times, burning velocities or flame temperatures are determined, and are tabulated hierarchically. Reaction pathway analysis provides useful information regarding the formation and consumptions of different species and their percentage due to different routes.

2.5 SOURCES OF REACTION-RATE PARAMETERS

The most important source of uncertainty in mechanism development is due to uncertainty in rate parameters for elementary steps. Other sources of uncertainty are due to uncertainties in thermodynamic and transport data. However, thermodynamic and transport data are better known and the improvements are seen to be marginal, if any. For example as an improvements in thermodynamic data for OH radical in recent publication [34] the value for heat of formation was found to be 5% lower than the earlier value.

In the literature, there are three approaches to estimate the rate constant of elementary steps i.e. experimental, theoretical, and numerical optimization. Most of the experimental sources are based on shock-tube studies where the transport effects are negligible. Hence, the rate of consumption of species can be measured with confidence. However, the uncertainties in other elementary steps contribute towards the errors in determination of the rate parameters for the elementary step under study. Another important source for rate parameters is theoretical studies based on quantum mechanical (RRKM) calculations. Here the potential-surface calculations provide information about what products are possible and what are impossible for a particular elementary step, along with the probable rate for each route [35, 36]. The reaction mechanisms based on numerical optimization are available, for example GRI Mech [37], and are widely used among the scientific community. However, the accuracy of the recommendation of the rate constant of an elementary step in a optimized mechanism greatly depends on the uncertainties in the rate constants of other key elementary steps.

The compilations of these elementary steps and their rate parameters are provided in [38-41]. In these databases, for particular elementary reactions, authors tabulated and

plotted the reaction rates from different sources such as experimental and theoretical studies.

2.6 CONCLUDING REMARKS

A framework for the development of the San Diego Mech for ethanol has been laid out in this chapter. A discussion has been provided on the models, the accompanying assumptions, and the computer programs used in the calculations. In the next chapter the experiments are selected for which the reaction mechanism is developed so as to cover all the aspects of high-temperature combustion. Then in Chapters 4, 5, and 6 development of the San Diego mechanism in a hierarchical way as described in this chapter is done. All the fuels that occur as intermediate species in ethanol flames are tested extensively against the experimental conditions that encompass aspects of high-temperature combustion. The updates to the San Diego mechanism as a result of these tests are reported and discussed in details in these chapters.

2.7 REFERENCES

1. Westbrook, C.K. and Dryer, F.L., "Chemical kinetics and modeling of combustion processes", Proceedings of the Combustion Institute, 18, 1981, pp. 749-767.

2. Williams, F.A., Combustion Theory, ed. 2nd, Addison-Wesley, 1985, 559.

3. Natarajan, K. and Bhaskaran, K.A., "An experimental and analytical investigation of high temperature ignition of ethanol", Thirteenth International Symposium on Shock Waves, 1982, pp. 834-842.

4. Dunphy, M.P. and Simmie, J.M., “High temperature oxidation of ethanol. Part 1.- Igniton delays in shock waves”, Journal of the Chemical Society, Faraday Transactions, 87 (11), 1991, pp. 1691-1696.

5. Curran, H.J., Dunphy, M.P., Simmie, J.M., Westbrook, C.K. and Pitz, W.J., “Shock tube ignition of ethanol, isobutene and MTBE: Experiments and modeling”, Proceedings of the Combustion Institute, 24, 1992, pp. 769-776.

6. Egolfopoulos, F.N., Du, D.X. and Law, C.K., “A study of ethanol oxidation kinetics in laminar premixed flames, flow reactors and shock tubes”, Proceedings of the Combustion Institute, 24, 1992, pp. 833-841.

7. Gülder, O.L., “Laminar burning velocities of methanol, ethanol, and isooctane-air mixtures”, Proceedings of the Combustion Institute, 19, 1982, pp. 275-281.

8. Cullis, C.F. and Newitt, E.J., “The gaseous oxidation of aliphatic alcohols. 1. Ethyl Alcohol – The products formed in the early stages”, Proceedings of the Royal Society of London A, 237, 1956, pp. 530-542.

9. Brown, J. and Tipper, C.F.H., “Cool flame combustion of ethanol”, Proceedings of the Royal Society of London A, 312, 1969, pp. 399-415.

10. Borisov, A.A. Zamanskii, V.M., Konnov, A.A., Lisyanskii, V.V. , Rusakov, S.A. and Skachkov, G.I. , “High-temperature pyrolysis of ethanol”, Soviet Journal of Chemical Physics, 8, 1991, pp. 121-141.

11. Norton, T.S. and Dryer, F.L. “An experimental and modeling study of ethanol oxidation kinetics in an atmospheric pressure flow reactor”, International Journal of Chemical Kinetics, 24, 1992, pp. 319-344.

12. Marinov, N.M., “A detailed chemical kinetic model for high temperature ethanol oxidation”, international journal of chemical kinetics, 31, 1999, pp. 183-220.

13. Li, J., “Experimental and numerical studies of ethanol chemical kinetics”, PhD Thesis, Princeton University, 2004.

14. Benvenutti, L.H., Marques, C.S.T. and Bertran, C.A., “Chemiluminescent emission data for kinetic modeling of ethanol combustion”, Combustion Science and Technology, 177, 2005, pp. 1-26.

15. Dagaut, P., Boettner, J.C. and Cathonnet, M., 1992, “Kinetic modeling of ethanol pyrolysis and combustion”, Journal de Chimie Physique, 89, 1992, pp. 867-884.

16. Redell, F.H., "Experimental investigation of the structure of a partially premixed planar ethanol flame", M.S. Thesis, University of California, San Diego, 2000.

17. Balakrishnan, G. and Williams, F.A., "Turbulent combustion regimes for hypersonic propulsion employing hydrogen-air diffusion flames", Journal of Propulsion and Power, 10, 1995, pp. 434-437.

18. Rightley, M.L. and Williams, F.A., "Structures of CO diffusion flames near extinction", Combustion Science and Technology, 125, 1997, pp. 181-200.

19. Rightley, M.L. and Williams, F.A., "Analytical approximation for structures of wet CO flames with one-step reduced chemistry", Combustion and Flame, 101, 1995, pp. 287-301.

20. Li, S.C. and Williams, F.A., "NO_x formation in two-stage methane-air flames", Combustion and Flame, 118, 1999, pp. 399-414.

21. Li, S.C. and Williams, F.A., "Experimental and numerical studies of two-stage methanol flames", Proceedings of the Combustion Institute, 26, 1996, pp. 1017-1024.

22. Li, S.C. and Williams, F.A., "Formation of NO_x, CH_4, and C_2 species in laminar methanol flames", Proceedings of the Combustion Institute, 27, 1998, pp. 485-493.

23. Waly, M.M.Y., Li, S.C. and Williams, F.A., "Experimental and numerical studies of two-stage ethane-air flames", Journal of Engineering for Gas Turbines and Power, 122, 2000, pp. 651-658.

24. Varatharajan, B. and Williams, F.A., "Ethylene ignition and detonation chemistry, Part 1: Detailed modeling and experimental comparison", Journal of Propulsion and Power, 18, 2002, pp. 344-351.

25. Waly, M.M., Li, S.C. and Williams, F.A., "Structures of non-sooting counterflow diluted acetylene-air flames", Proceedings of the Combustion Institute, 28, 2000, pp. 2005-2012.

26. Varatharajan, B. and Williams, F.A., "Chemical-kinetic descriptions of high-temperature ignition and detonation of acetylene-oxygen-diluent systems", Combustion and Flame, 125, 2001, pp. 624-645.

27. Petrova, M.V. and Williams, F.A., "A small detailed chemical-kinetic mechanism for hydrocarbon combustion", Combustion and Flame, 144, 2006, pp. 526-544.

28. Del Alamo, G., Williams, F.A. and Sanchez A. L, "Hydrogen-oxygen induction times above crossover temperatures", Combustion Science and Technology, 176, 2004, 1599-1626.

29. Kee, R.J., Rupley, F.M., Miller, J.A., Coltrin M.E., Grcar, J.F., Meeks, E., Moffat, H.K., Lutz, A.E., Dixon-Lewis, G., Smooke, M.D., Warnatz, J., Evans, G.H., Larson, R.S., Mitchell, R.E., Petzold, L.R., Reynolds, W.C., Caracotsios, M., Stewart, W.E., Glarborg, P., Wang, C., Adigun, O., Houf, W.G., Chou, C.P. and Miller, S.F., Chemkin Collection, Release 3.7.1, Reaction Design Inc., San Diego, CA, 2003.

30. Pitsch, H., "Entwicklung eines Programmpakets zur Berechnung eindimensionaler Flammen am Beispiel einer Gegenstromdiffusionflamme", M.S. Thesis, RWTH Aachen, Germany, 1993.

31. Gilbert, R.G., Luther, K. and Troe, J., "Theory of thermal unimolecular reactions in the fall-off range. II. Weak collision rate constants", Ber. Bunsenges. Phys. Chem., 87, 1983, pp. 169-177.

32. Burcat, A., http://garfield .chem.elte.hu/Burcat/burcat.html (2005)

33. CER website: http://maemail.ucsd.edu/combustion/cermech/

34. Ruscic, B., Feller, D., Dixon, D.A., Peterson, K.A., Harding, L.B., Asher, R.L., and Wagner, A.F., "Evidence for a lower enthalpy of formation of hydroxyl radical and a lower gas-phase bond dissociation energy of water", The Journal of Physical Chemistry A, 105, 2001, pp. 1-4.

35. Michael, J.V., Sutherland, J.W., Harding, L.B. and Wagner, A.F., "Initiation in H_2/O_2: Rate constants for $H_2+O_2 \rightarrow H+HO_2$ at high temperature", Proceedings of the Combustion Institute, 28, 2000, pp. 1471-1478.

36. Park, J., Xu, Z.F. and Lin, M.C., "Thermal decomposition of ethanol. II. A computational study of the kinetics and mechanism for the $H+C_2H_5OH$ reaction", Journal of Chemical Physics, 118, 2003, pp. 9990-9996.

37. GRI Mech website: http://www.me.berkeley.edu/gri-mech/

38. Warnatz, J., "Rate coefficients in the C/H/O system". In W.C. Gardiner (ed.), Combustion Chemistry, Springer-Verlag, Berlin, pp. 197-360, 1984.

39. Baulch, D.L., Cobos, C.J., Cox, R.A., Esser, C., Frank, P., Just, Th., Kerr, J.A., Pilling, M.J., Troe, J., Walker, R.W. and Warnatz, J., Journal of Physical and Chemical Reference Data, 23, 1994, pp. 847-1033.

40. Tsang, W. and Hampson, R.F., "Chemical kinetic database for combustion chemistry. 1. Methane and related compounds", Journal of Physical Chemistry Reference Data, 15, 1986, pp. 1087-1276.

41. NIST website: http://kinetics.nist.gov/kinetics/index.jsp

CHAPTER 3

EXPERIMENTAL METHODS

3.1 OVERVIEW

In Chapter 2 the methods for development of a chemical-kinetic model were discussed. After the elementary steps in a chemical-kinetic model are identified and assembled along with their rate constants, the best way to test a mechanism's range of validity is by testing it against as many experimental data as possible. An important requirement of an experimental method is that convective and diffusive effects and their interaction with chemistry are well defined. It should also provide easy access for data acquisition. There are various combustion experiments available in the literature catering to different combustion processes under different conditions. Some of the simple experimental configurations are static reactor, flow reactor, well stirred reactor, rapid compression machine, autoignition in shock-tube, laminar premixed and diffusion flames. The temperatures involved in static and flow reactors are lower than the temperatures encountered in combustion processes of practical engines, while temperatures involved in ignition delay from shock tube and flame experiments lie in the region of interest.

3.2 SELECTED EXPERIMENTAL CONDITIONS

The San Diego Mech is developed to interpret experiments which represent high-temperature combustion. Hence, four different experimental conditions were chosen, namely autoignition in a shock-tube, laminar burning velocities, diffusion-flame extinction and their chemical structures.

3.2.1 Autoignition in Shock Tube

Shock-tubes are widely used to study autoignition characteristics of combustible mixtures at temperature above those achievable in conventional static or flow reactor experiments. The fuel/O_2/inert mixture compressed to a desired temperature and pressure is ignited behind the incident or reflected shock wave. The onset of the ignition is inferred from a pressure trace or the emission spectra from an intermediate species (example OH, CH). Care must be taken in interpreting the autoignition delay time data based on different ignition criteria.

Although the advantage of these experiments is that fluid mechanics interactions with the chemistry are negligible, when the ignition times are larger than 500 μs, there is a departure from the ideal behaviors. For example, formation of boundary layers and their interactions with the reflected shock may be a cause of concern. Also, in order to rule out the heterogeneous wall effects, a shock-tube with an appropriate diameter for a particular pressure must be used. Other sources of complication in the measurement of induction time in shock-tube experiments are the presence of two distinct ignition modes and non-equilibrium processes such as vibrational relaxation of the post shock mixtures. The guidelines for evaluating shock-tube data are documented in a review [1].

3.2.2 Laminar Burning Velocities

The burning velocity data for a freely propagating flame lie directly in the range of temperatures that occur in a flame inside a combustion chamber, and provide information regarding the extent of interaction of chemistry with the diffusion effects. Many different techniques to measure burning velocities are listed in the literature, such

as soap bubble, constant volume bomb, burner stabilized, counterflow twin-flame technique. The accuracy of the data depends on the corrections applied to the measured values such as strain-rate corrections and markstein number. In counterflow setup, the burning velocity reported at strain rate → 0, as in [2], is most trustworthy. However, the formation of cellular structures at leaner-flame conditions provides erroneous flamespeed measurements in the counterflow setup.

3.2.3 Counterflow Diffusion-Flame Extinction

The counterflow setup is described in greater details in the following sections. The extinction strain-rate data for a diffusion flame provides a measure of the interaction of the chemical timescales to the flow timescales for a particular mixture. The biggest advantage of extinction data obtained from such a configuration is that these measurements are nonintrusive.

All the above measured quantities are global quantities. A detailed reaction mechanism can be tested more rigorously against the flame-structure data. There is, however, no data available in the literature for the structures of ethanol flames in counterflow setup.

3.2.4 Counterflow Diffusion-Flame Structures

The flame structure provides chemical structure of the flame at different locations of the reaction zone. Hence, it provides a stringent test to the mechanism, especially in the formation and consumption of the trace (such as pollutant) species. The accuracy of the experimental data depends on the validity of the plug-flow condition at duct exits,

moderate value of strain-rate to facilitate flat, stationary luminous zone, correct measurement of concentration of the vaporized liquid fuel, and sampling of the data from the reaction zone. The plug-flow condition is where flow at the ducts exit has only non-zero axial velocity component. The flame is stretched by applying higher flow strain rates which in turn facilitates a flat, stationary luminous zone by eliminating buoyancy induced instabilities. In a counterflow setup the variation in temperature and species concentrations are in axial direction only, except the velocity field. The readily available 1-D codes, such as CHEMKIN can be used to validate the mechanism.

3.3 PREVIOUS EXPERIMENTAL DATA

In the process of development of the San Diego Mech for ethanol, the mechanism was validated against the experimental data from the literature mentioned in following paragraphs. The intermediate fuels in the San Diego Mech such as hydrogen, carbon monoxide, formaldehyde, methane, methanol, ethane, ethylene, acetylene, and acetaldehyde were also tested for the selected experimental conditions mentioned above. These conditions are reported along with the discussion on these tests in Chapters 4 and 5.

Autoignition delay times from shock tube

Natarajan and Bhaskaran [3] reported ignition delay time for $C_2H_5OH/O_2/Ar$ gas mixtures for equivalence ratios of 0.5, 1.0 and 2.0 at 1.0 and 2.0 atm over the temperature range of 1300-1700 K. The ignition was studied behind the reflected shock wave with first visible light emission and pressure inflection as ignition criteria.

Dunphy et al. [4] investigated ignition delay for $C_2H_5OH/O_2/Ar$ mixtures behind reflected shock wave between 2-4.6 atm over the temperature range of 1120-1600 K. The mixture equivalence ratio of 0.25, 0.5, 1.0 and 2.0 were used. Ignition time was determined by rapid pressure rise and the maximum of the product of the CO and O concentrations.

Curran et al. [5] studied ignition delay in a shock tube for an equivalence ratio of 1.0 at pressures 2, 3 and 4.5 bar over a temperature range of 1100-1500 K. Ignition delay was defined based on the onset of a rapid pressure rise, and maximum emissions from OH and CO_2 chemiluminescence.

Laminar burning velocities

Egolfopoulos et al. [6] studied laminar burning velocities using the counterflow twin-flame technique for ethanol/air mixtures. The burning velocities were reported for mixture equivalence ratio in the range of 0.5-1.9 at 1 atm and initial temperatures of 298, 363, 428, and 453 K.

Prior to this Gülder [7] investigated laminar burning velocities using a constant volume spherical bomb for ethanol/air mixture in equivalence ratio range 0.7-1.4 at 1 atm and initial temperature 298 K. Also dependence of laminar burning velocities on temperature and pressure was studied over a temperature range of 300-500 K and a pressure range of 1-8.0 atm for mixture-equivalence ratios between 0.7-1.4.

Diffusion-flame extinction

Seiser and Seshadri [8] experimentally determined extinction strain rates in a counterflow setup at normal pressure for fuel streams of prevaporized ethanol in nitrogen with fuel mass fractions varying between 0.18 and 0.39, flowing against air at room temperature.

3.4 FLAME CONFIGURATIONS

There are, however, important practical concerns about partially premixed and nonpremixed systems that cannot be addressed by any of the experiments listed above. Although there have been early experiments on coflow ethanol diffusion flames [9], much better tests of chemical mechanisms can be made in counterflow flames because of the one-dimensional geometry (for all variables except the velocity field) and the availability of codes to calculate their flame structures with detailed chemistry. Such experiments have been performed for methanol [10, 11] but not for ethanol flames. Hence, in the present study, flame structure measurements are performed in a counterflow setup for two flame configurations: partially premixed flame and nonpremixed flame for ethanol.

The experimental conditions adopted in the present work correspond to diffusion flames and partially premixed flames at a plug-flow strain rate of 100 s^{-1}, in a counterflow setup. The diffusion flame that was probed in detail consists of prevaporized fuel, with mole fraction of 0.3, diluted with nitrogen in the fuel stream, and air as the oxidizer stream. The partially premixed flame that was measured includes prevaporized fuel in air partially premixed to an equivalence ratio of 2.3 in the fuel stream, and air as the oxidizer stream. This last configuration yields a two-stage flame: There is a pale

green fuel-rich premixed flame in the fuel stream and a brighter blue diffusion flame in the vicinity of the stagnation plane. Figure 3.1 shows the photographs of the flames observed in these two different configurations, and dimensions of the counterflow setup.

3.5 CONTERFLOW EXPERIMENTAL SETUP

Diffusion flame structures for flames in two different configurations were measured using counterflow setup. The factors critical to the accuracy of the measurements when using liquid fuel are the vaporization of liquid fuel to a desired mole fraction, prevention of condensation of the fuel in the lines, establishment of accurate flow rates of the fuel and oxidizer streams.

The experimental setup consists of a vaporizer, counterflow burner, and instrumentation such as flowmeters, thermocouple, sampling probe and gas chromatograph. The detailed description of the vaporizer and the burner can be found in [12]

3.5.1 Vaporizer

Figure 3.2 shows a cross section of the vaporizer. It consists of an aluminum cylinder of 116 mm inner diameter and a height of 600 mm. It was filled with liquid ethanol to about half the volume. This level was maintained during the course of data sampling by monitoring the level and manually refilling of vaporizer. At the bottom of the vaporizer, an insert holds a porous brass sinter metal plate which was used for the nitrogen inlet. The nitrogen flow was evenly distributed into fine bubbles that percolate through the heated liquid bath. This ensures a homogeneous mixture of the evaporated

ethanol fuel and the nitrogen gas. Appropriate heating is provided by heating tapes (Themolyne BIH102-100) wrapped around the vaporizer at elevated temperature. The heated lower section was used to vaporize the liquid fuel mixture while the heated upper section was to prevent condensation of evaporated fuel mixture during transfer to the burner. The heating tapes were powered by a variable transformer (STACO3PN1010B). The temperature of the tapes was controlled by the applied voltage; with a maximum voltage of 140 V a power of 250 W for each tape can be achieved. Fiberglass was used to provide insulation on the surfaces exposed to the surrounding air to prevent the heat loss. The temperature inside the vaporizer was measured using a K-type thermocouple which was located within 25 mm below the level of ethanol. The liquid ethanol and ethanol vapor are assumed to be in equilibrium. This ensures that the measured temperature is the temperature of the ethanol/nitrogen flow exiting the ethanol bath. The mole fraction of ethanol in the fuel stream is given by, $X_{ethanol} = P_{ethanol}/P_{total}$, where, P_{total} =1.013 bar, and $P_{ethanol}$ is vapor pressure of ethanol.

The relation of the desired partial pressure and the temperature to which the mixture should be elevated was determined by Classius-Clayperon equation or by Antoine equation. Appendix 2 presents the involved calculations. The vaporizer temperatures were determined based on the fuel mole fraction desired in the nonpremixed flame and partially premixed flame configurations.

The performance of the vaporizer was tested [12] by vaporizing water and examining the effluent with the hygrometer; saturation above 99% was observed for flow conditions comparable to those in the experiments. Also, a test was made before conducting the experiments in the current study by collecting the sample of the

fuel/nitrogen mixture exiting from the vaporizer and analyzing it using gas chromatograph. Accurate mole fractions for fuel and nitrogen corresponding to the desired temperature were ascertained.

The fuel/nitrogen mixture from the vaporizer was transported to the exit of the bottom burner. All the flow lines were heated and insulated between vaporizer and burner to prevent any fuel condensation. The temperature was maintained at about 15 K higher than the evaporation temperature. The fuel-stream temperature at the duct exit was measured using a thermocouple to validate the boundary condition at the exit of fuel stream.

There was a bypass flow mainly used for nitrogen which may be used for controlling the dilution in the fuel stream. The bypass nitrogen stream was heated to the temperature maintained in the vaporizer by heat transfer. In the case of the partially premixed configuration, oxygen was made to flow through the bypass, which constituted desired fuel/air mixture at the exit of the vaporizer. This precautionary step was taken to avoid any fire hazard.

3.5.2 Counterflow Burner

The burner consists of two parts; the bottom burner on the fuel side and the top burner on the oxidizer side. Figure 3.3 shows a cross-section view of the burner. The top burner is made of brass and the bottom burner is made of aluminum.

The bottom burner consists of an inner duct with an inner diameter of 23.1 mm for fuel stream, an annular duct of cross sectional area 664.6 mm^2 for the nitrogen curtain, and an outermost concentric duct for the suction (using a vacuum pump) of

exhaust gases from the flame to the ventilation system. The fuel and curtain ducts are kept at temperatures 15 K higher than the evaporation temperature of the fuel. An additional thin shield is mounted around the curtain duct which prevents cold water or gases in the exhaust section from directly contacting the hot curtain duct. During the experiment, the bottom burner was cooled by a water-cooled circuit. The spray nozzles (Type BETE PJ15) were used to spray water in order to cool the hot products and to prevent autoignition of accumulated ignitable gases in the exhaust duct. Furthermore, the section where hot gases from the flame enter into the exhaust was narrowed down to provide preliminary cooling and quenching of the flame before the section of water mist was reached. The small flange above the spray nozzles was intended to prevent any water particles from traveling towards the flame zone.

Similar to the bottom burner, the top burner consists of an inner duct of inner diameter 23.1 mm for oxidizer stream, and an annular duct of cross section area of 638.7 mm^2 for the nitrogen curtain. Since the oxidizer stream is at room temperature, there is no cooling system required in the top burner.

An important boundary condition in this configuration, for both the top and bottom burner, is a plug-flow boundary condition. This condition was ensured by using three layers of wire meshes (200 x 200 mesh/in). The screens were mounted using four stainless steel rings of 1 mm thickness; between each screen layer a ring was placed. The velocity and temperature of the nitrogen-curtain streams were adjusted to ensure no momentum and heat transfer between them and the reactants streams. Seiser [12] verified plug-flow boundary conditions at the exit of the inner ducts by quantifying the

velocity field on the oxidizer side of the flame using a Particle Imaging Velocimetry (PIV) system.

The top burner was mounted and aligned with the bottom burner with the adjustable screws. The desired distance between the duct exits for a particular strain rate was maintained by adjusting the screws manually.

A separator, which is connected to the ventilation system, was used at the exit of the exhaust pipe connected to the bottom burner to separate the gaseous components from the liquid and solid components by gravity.

3.5.3 Measurements and Instrumentation

3.5.3.1 Flow Measurement

The flows of fuel and oxidizer streams were controlled by mass flowmeters in such a way that the oxidizer-side strain rate of 100 s^{-1} was maintained as calculated by the formula [13]

$$a_2 = 2\frac{|V_2|}{L}\left(1+\frac{|V_1|\sqrt{\rho_1}}{|V_2|\sqrt{\rho_2}}\right)$$

Here, V denotes the velocity and ρ the density. Subscripts 1 and 2 refer to the fuel stream and oxidizer stream, respectively. The separation distance between the two ducts was L=12 *mm*. In order to maintain the stagnation plane at the mid-plane, the momentum balance, $\rho_1 V_1^2 = \rho_2 V_2^2$, was invoked. Using the above relations and the information

about the values of strain rate, vaporizer temperature, fuel and oxidizer streams temperature, and fuel and oxygen concentration, velocities for the fuel and oxidizer streams were determined.

During the experiments rotameter, massflow meter, and flow controllers were used depending on their availability for the experimental setup. In the nonpremixed case, nitrogen curtain flows in the top and bottom burners were metered by separate rotameters, which provided volume flow rates. These rotameters are rated at an accuracy of $\pm 3\%$. The fuel-side nitrogen flow and the oxidizer-side air flow were maintained by Matheson Tri-gas Inc. massflow meters. These massflow meters are rated at an accuracy of $\pm 1\%$.

In the setup for partially premixed flame, nitrogen curtain flows were maintained by the rotameters, oxidizer-side air flow by Matheson Tri-gas Inc. massflow meter, and oxygen and nitrogen flows in the fuel stream by two separate computer controlled Hastings Inc. electronic massflow controllers. These flow controllers are rated at an accuracy of $\pm 1\%$.

Before the experiments were conducted, all the flow meters were calibrated using a Precision Scientific Inc. wet-test meter. This was done to establish the linear behaviour of the flow meters, and to obtain quantitative values of the scale readings versus volume flow rates. For the calibration, the wet-test meter was connected in the actual experimental setup under actual conditions such as temperature, strain rate, and the gas type. Before taking the readings, equilibrium was established in the wet-test meter between the gas flow and the water vapor by running the flow for 5 to 10 minutes. The wet-test meter had a volume reading, a pressure guage, and a temperature reading. The

pressure corrections were applied to the measured values by subtracting the effect of vapor pressure of the water vapor on the gas flow at atmospheric pressure. The corrected pressure was used in determining the volume flow rate at standard temperature and pressure using ideal-gas laws. A linear correlation for each flow meter was determined for scale reading versus volume flow rate at STP. The correlations were further tested by Hastings Inc. flow controllers to ensure the accuracy for each of the rotameters and massflow meters. These tests were made for the desired flow rates for each flow meter as was used in the experimental setup.

3.5.3.2 Temperature Measurement

Temperature profiles were measured by an uncoated Pt-Pt13%Rh (Type R) thermocouple, except in the high-temperature region of the partially premixed flame. The maximum temperature experienced in the partially premixed flame was much higher than that in the diffusion flame and surpassed the melting point of Pt, necessitating use of an uncoated Pt-6%Rh vs. Pt-30%Rh (Type B) thermocouple for near-flame-temperature measurements in the partially premixed flame. The Type R thermocouple with wire diameter 0.088 mm and bead diameter 0.21 mm, and the Type B thermocouple with wire diameter 0.2 mm and bead diameter 0.33 mm were used. Both the thermocouples were shielded in two separate holes in a capillary ceramic tube to hold them in place, to avoid electrical short-circuiting by contact of the wires, and to protect them from bending and other mechanical stress. The ends of the wires were cased in a connector which leads to a digital temperature display unit. The care had been taken in reducing the conduction heat

transfer effects by keeping the wires parallel to the flow field. The measured temperatures were corrected for radiative losses [14] assuming a spherical bead,

$$T_{corrected} = T_g + \varepsilon\sigma T_g^4 \left(\frac{d_{bead}}{\lambda Nu} \right),$$

where, emissivity $\varepsilon = 0.2$, the Boltzmann constant $\sigma = 5.7 \times 10^{-8}$ W/m^{2}K^4, Nusselt number $Nu = 2.0$, and λ denotes the temperature-dependent thermal conductivity of the wire,

$$\lambda = 4.6942.10^{-3} + 8.1225.10^{-5}\, T_g - 1.4547.10^{-8}\, T_g^2$$

T_g stands for gas temperature. The catalytic effects were neglected, leading to temperatures estimated to be about 120 K too high at the highest temperatures, based on experimental observations and the ideas in the literature [14].

3.5.3.3 Sampling with a Quartz Microprobe

The gas samples from the reaction zone were collected using a quartz microprobe. The tip of the microprobe has an inner diameter and an outer diameter of 88 μm and 168 μm, respectively. The diverging nozzle was shaped in accordance with [15], where the shape ensures sonic speed at the throat. This provides rapid decompression of the sample, and hence prevents any further reactions inside the probe. As shown in Fig. 3.4, a tapered copper shield was used around the tip of the probe to reduce heat transfer from the flame to the front part of the probe. In addition, a heated coil maintained at about 380 K was

wrapped around the probe to keep the water and fuel vapors from condensing. By proper balance of the temperature with the pressure of the sampling lines and the sample loop, condensation of sampled vapors was prevented.

Positioning of the thermocouple and sampling probe

The sampling probe and the thermocouple were mounted on a 3D translator. For a particular flame measurement, a digital photograph (using Canon EOS D30) was taken and image processing with a coordinate evaluation feature in Corel Photo-Paint 8 was done to determine the location of the tip of the sampling probe and the bead of the thermocouple in the flow field. A pixel size corresponds to a distance in the flow field of approximately 17 μm. The coordinates of the left and the right rims of the projections in the inner ducts of the top and bottom burners are known. The location of the thermocouple bead and the tip of the microprobe were determined with reference to these coordinates using linear interpolation in a plane. The bead of the thermocouple and the tip of the probe were placed 5 mm off the axis of symmetry. At this position a small radial component of the flow velocity exists towards the probe, which decreases the influence of the probe on the flow field. It was observed that the variation in the species concentrations and temperatures along the horizontal surfaces are negligible. They were the functions of the vertical coordinates only.

3.5.3.4 Concentration Measurements – The Gas Chromatograph

Once the sample was drawn from the flame, the various components were analyzed using a gas chromatograph. A gas chromatograph consists of columns where

species were separated and detectors where their concentrations are quantified. An inert gas called carrier gas is used to transport the sample to the columns. Helium was used as a carrier gas in the experimental setup. The working principle of a gas chromatograph is that the sample enters a column and gets adsorbed by it. Various species pass through the columns with different speeds depending on the species' vapor pressure and affinity for the stationary column bed. Further downstream, the concentrations of these eluting species are determined in detectors.

Columns

In the present experiments a model SRI 8160C gas chromatograph was used. It consists of two types of columns: a 4.5 ft mole sieve 5 Å (80/100 mesh), which is a capillary column, and a 12 ft long Porapak Q column, which is porous polymer based. The mole sieve was used to separate hydrogen, oxygen+argon, nitrogen, methane, and carbon monoxide, while Porapak Q was used to separate carbon dioxide, ethane, ethylene+acetylene, water vapor, propene, propyne, and ethanol.

The performance of a column depends on the species retention time and clear separation of the species with narrow peak width. Short retention times decreased the analysis duration. In order to optimize performance characteristics of the columns, valve switching and temperature programming of the ovens, where these columns are located separately, was employed.

Valve switching is critical in preventing CO_2 from reaching the mole sieve, which causes poisoning of the mole sieve. Figure 3.5 shows the flow of sample through different columns to the detectors, and the switching involved.

The temperature programming helps in obtaining the ideal temperature range for the separation of each component. Each component is sensitive to a temperature range in which it migrates and separates within the column. Prior to reaching this ideal temperature range, each substance is “frozen” or condensed at the head of the column waiting to be separated at a higher temperature. In general a temperature programming is performed so that initially the temperature is low for the most volatile and therefore less dissolved components. Then in order to reduce analysis time the temperature is raised for the later eluting species. This way the temperature programming was used to improve, simplify, or accelerate the separation, identification, and determination of sample components. It allows the proper selection of a temperature which results in well-resolved, nicely shaped peaks, and a total analysis time shorter than isothermal operation. Higher temperature of the mole sieve oven affects each species differently. For example, the retention time of CH_4 was much less sensitive to temperature than CO.

The temperature programming of the mole sieve oven is shown in Fig. 3.6. The initial temperature was room temperature. Five minutes into the experiment, the temperature was raised at a rate of approximately 20 K/min until the second switch of the valve at 12.5 minutes. The mole sieve was then cooled down again to room temperature. The temperature programming of the mole sieve column oven was controlled manually by switching on and off a power supply (variable AC-transformer) at the required time.

The temperature programming of the Porapak Q column oven is shown in Fig. 3.7. The initial temperature was 37 °C. After the second switch of the valve, the temperature was raised at a rate of 5 K/min until the temperature reached 205 °C. The temperature was then held constant until the analysis was terminated. The temperature

programming of the column oven was controlled by a software provided with the gas chromatograph.

Detectors

The gas chromatograph consists of two detectors: The Thermal Conductivity detector (TCD) and Flame Ionization Detector (FID). The TCD was used to detect hydrogen, oxygen, nitrogen, water vapor and other non-hydrocarbons, and the FID was used to detect hydrocarbons. The working principle of both the TCD and FID are described below.

TCD: A TCD consists of an electrically heated wire or thermistor. It measures the thermal conductance of an unknown gas by monitoring the resistance of the heated wire in the gas flow. The unknown gas conducts heat to the body of the TCD and therefore cools the wire. By comparing the resistance to an identical wire in a reference channel, the unknown gas can be identified. The reference gas in the reference channel, which was helium in the present study, has a well known thermal conductance. To measure the resistance a Wheat-stone bridge circuit is employed. The detection limit of TCD is approximately 100 ppm.

FID: An FID is used to determine the presence of total hydrocarbons concentrations in a gaseous sample. The sample containing hydrocarbons is introduced into a hydrogen-air flame and ions are generated either by thermal ionization or oxidation. A high polarizing voltage is applied between the two electrodes immediately

adjacent to the flame and produces an electrostatic field. Negative ions migrate to the collector electrode and positive ions migrate to the high voltage electrode. This generates ionization current between the two electrodes that is directly proportional to the hydrocarbon concentration in the sample burnt by the flame. The FID can detect hydrocarbons containing molecules as low as 100 ppb. Since water is produced in the combustion process, the detector must be heated to at least 125 °C to prevent condensation of water and high boiling samples.

Calibration of detectors: The area under the curve in a chromatogram from a detector output for a particular species is mV-min, where signals are in mV and the x-axis is time in minutes. In order to obtain the absolute concentration of a species, a calibration factor, given as a concentration/mV-min is determined. The calibration factor for a particular species is determined by comparing the known concentration of that species with the corresponding detector output. A certified mixture of nine gases was used to obtain calibration factor for hydrogen, carbon monoxide, carbon dioxide, methane, ethylene, ethane, propene, propane; air was used for oxygen and nitrogen. The composition of the nine-gas sample was: hydrogen (2.11), carbon monoxide (4.99), carbon dioxide (10.00), methane (2.00), ethylene (3.00), ethane (1.01), propene (1.00), propane (3.00), balance nitrogen, where the numbers in parentheses corresponds to percentage by volume. The calibration factors for water and ethanol were obtained by vaporizing them in separate containers and by determining the area under the curve from the detector output, where their molefractions were 100% in each case. The samples for calibration gases were introduced at pressures similar to the pressures at which the flame

samples were collected. Also, the linearity of the detectors output was determined by measuring the output at 150 mbar and 250 mbar. These measures ensured the confidence in required interpolation or extrapolation in calibration factors.

3.6. CONNECTIONS AND PROCEDURE

Figure 3.8 shows a schematic of the experiemental setup including the counterflow burner, the vaporizer, the gas sampling system, and the gas chromatograph. The probe was connected to the gas chromatograph by stainless steel lines which were heated to prevent condensation.

Once the desired fuel concentration in the fuel-stream and strain rate are established, the flame was ignited using a torch. The gas samples were drawn from the flame at various axial locations. First, the sampling lines and the sample loop were evacuated using a vacuum pump. The sample was then taken from the flame through the probe into the lines and the sample loop of volume 1 cc. The samples were injected into the gas chromatograph at a pressure around 280 mbar in order to prevent condensation of water vapor and fuel. The temperature of the sample loop of the gas chromatograph was measured using a thermocouple; the pressure using a strain gauge pressure transducer. Thus, the absolute number of moles in the sample loop could be calculated assuming an ideal gas mixture, and the absolute mole fraction of a species of a specific sample could be determined, independent of the concentrations of other species in the sample. These samples were transported to columns by a carrier gas, where different species were separated and released to the detectors where they were quantified.

During the experiments, continuous flow of helium gas is very important for the correct operation of gas chromatograph. In order to prevent contamination of the system 99.999% pure helium was used. It prevents the overheating of the system which can lead to column and detector damage. The flow rate of helium was measured in the beginning using a cathetometer, and was maintained constant throughout the experiment by maintaining the constant flow pressures in the lines. The flow rate effects the transportation of sample gas to the columns and hence their retention time. It also affects the detection output from the TCD as peak area is inversely proportional to the carrier gas flow rate. Also, desired flow rates for hydrogen and air for FID were maintained in order to maintain a constant flame in the detector.

Ideally, one expects a peak in a chromatogram to be symmetric and Gaussian, and to have a well defined start, end, and height. As peak shape becomes further removed from this expectation, interpretation of its features, including area, height, and retention time, becomes increasingly more difficult. A peak with a tailing edge as it appears for water occurs when the species' ability to dissolve with the column bed decreases with higher concentrations. A symmetric peak is observed when the ability of a component to dissolve with the column is independent of the concentration. Leading edges occur when the ability to dissolve with the column increases with higher concentrations.

Argon elutes together with oxygen from the columns of the gas chromatograph. By assuming the Lewis number of argon and the Lewis number of the main species to be equal, the amount of argon at any point in the flow field was determined from the mixture fraction (calculated using the carbon mass fraction from the measured species) and the amount of argon in the oxidizer stream (Y_{AR}=0.01313). Ethylene and acetylene appear in

the gas chromatogram as a single peak and were reported as their sum using the calibration factor for ethylene since earlier work [16] indicates that its concentration is the larger of the two.

The experimental data from the literature and the one measured in counterflow flames for ethanol are presented in Chapter 6, along with the comparison with the numerical calculations using the San Diego Mech developed for ethanol.

3.7 MEASUREMENT OF FORMALDEHYDE, ACETALDEHYDE, AND KETENE

The presence of acetaldehyde, formaldehyde, and ketene in the atmosphere has serious health hazards. All of these are considered to be possible human carcinogen. They are also observed to cause irritation to the eyes, nose, throat, and lungs. These three species are a few of the major intermediate species that are observed to constitute big portion of the pollutants in ethanol flames. It is of a great interest to the scientific community to measure the concentration of acetaldehyde, formaldehyde, and ketene in the ethanol flames studied in Chapter 6. This could not be achieved during this study due to three reasons – the requirement of a different column to separate these species, difficulties in calibration at the low concentrations encountered in ethanol flames, and difficulties in sampling. A Hayes Separation Column D by Hayes Separation Inc. made of divinylbenzene can be used for separation of acetaldehyde. Hayes Separation Column T by Hayes Separation Inc. made of ethyleneglycoldimethacrylate can be used for separation of formaldehyde and ketene. Formaldehyde and ketene are very reactive and

get consumed in the sampling probe, while acetaldehyde is observed to be formed in sampling probe. These issues have been discussed in details in [17].

3.8 CONCLUDING REMARKS

A brief review of the experiments that are selected for the development of the San Diego Mech is presented. A list of the experimental conditions for the ethanol combustion from the literature for which the ethanol mechanism is developed in Chapter 6 is given here. In addition, a detailed description is provided for the counterflow technique along with the experimental setup and the involved instrumentation. The results of these experiments are presented in Chapter 6 along with the comparisons with the predictions from the mechanism developed in this study.

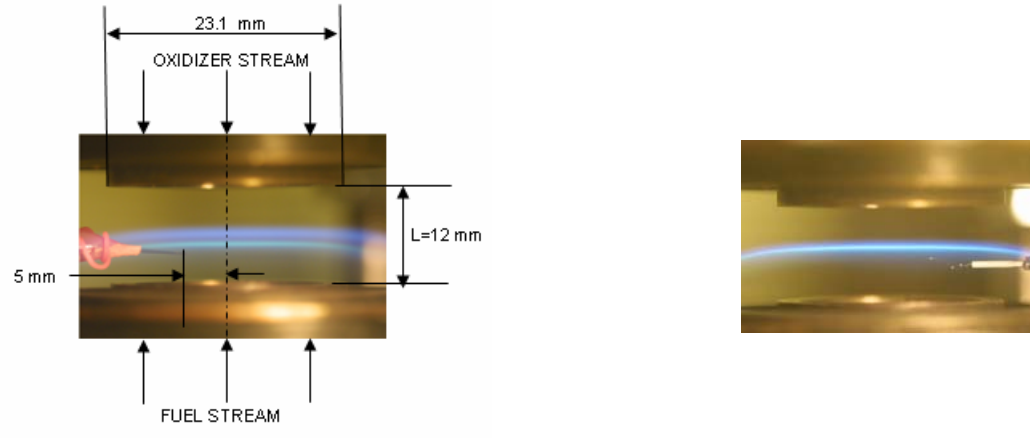

(a) (b)

Figure 3.1 Photographs and dimensions of the counterflow setup used in the experiments for (a) partially premixed flame and (b) nonpremixed flame

(a)

(b)

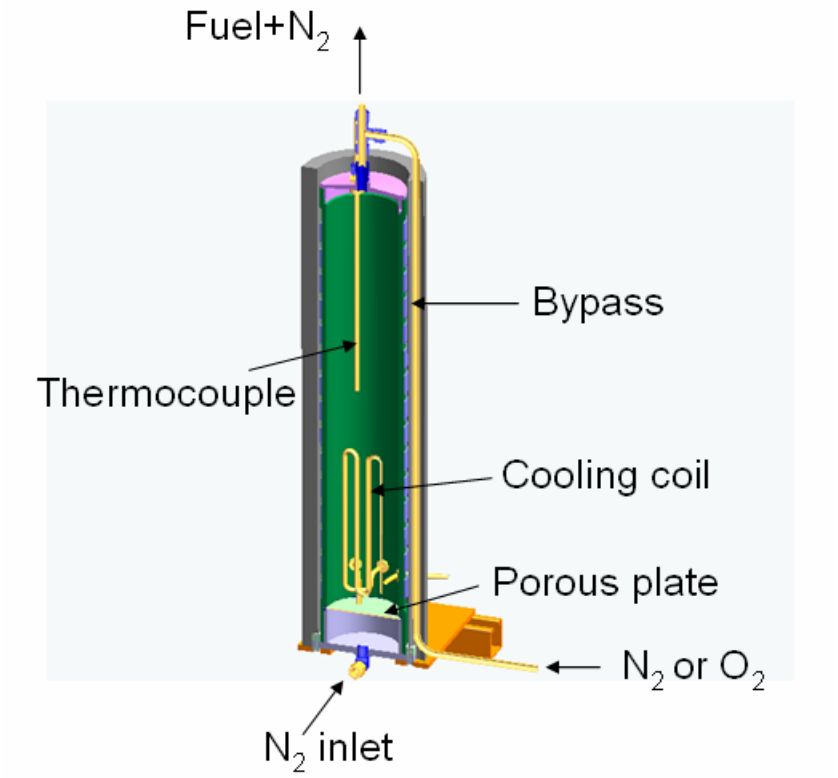

Figure 3.2 (a) Photograph of the vaporizer (b) A section of a solid model of the vaporizer

(a)

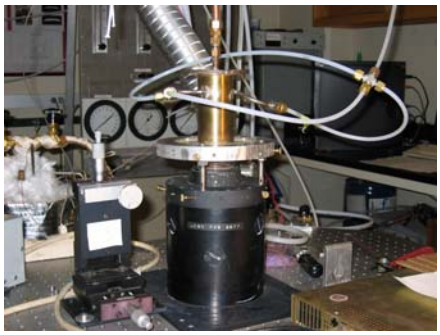

(b)

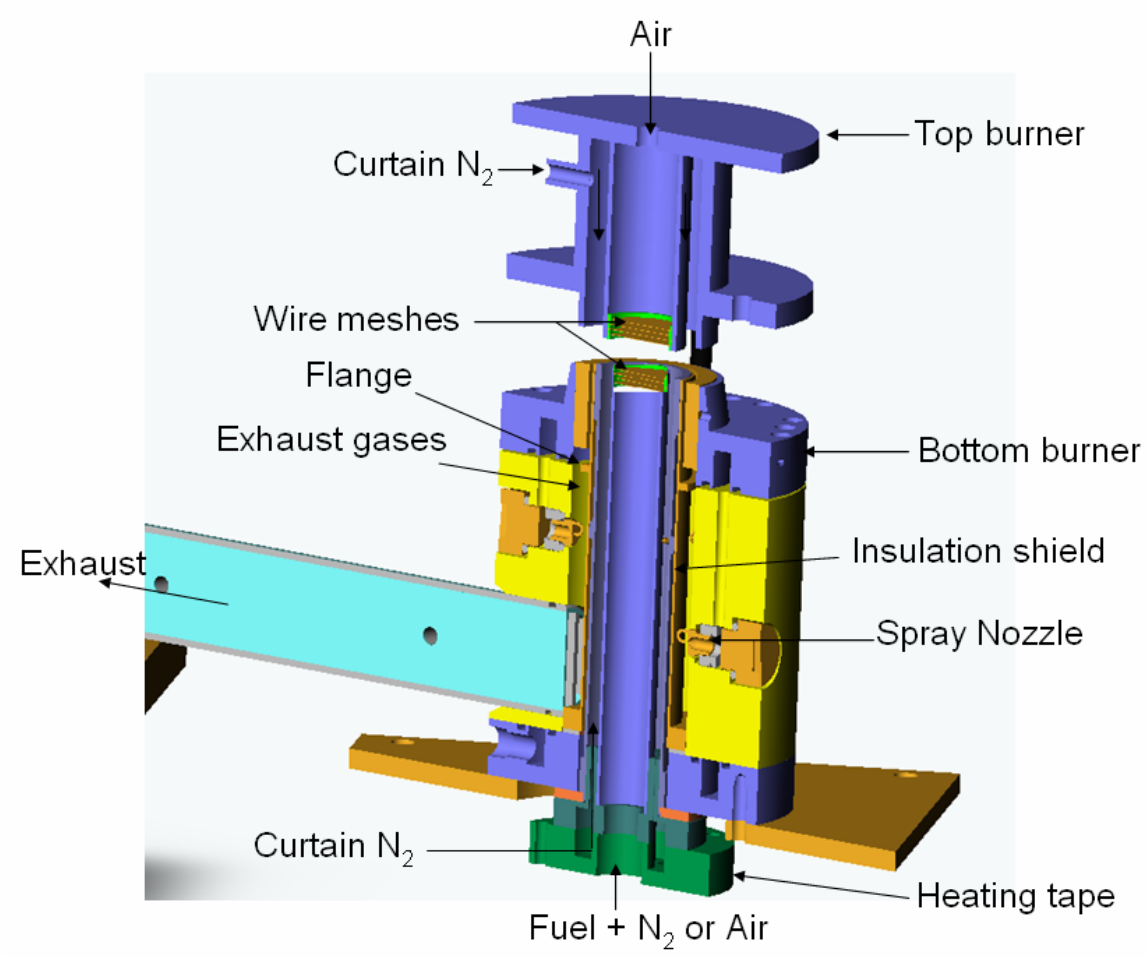

Figure 3.3 (a) Photograph of the counterflow burner assembly (b) A section of a solid model of the counterflow burner

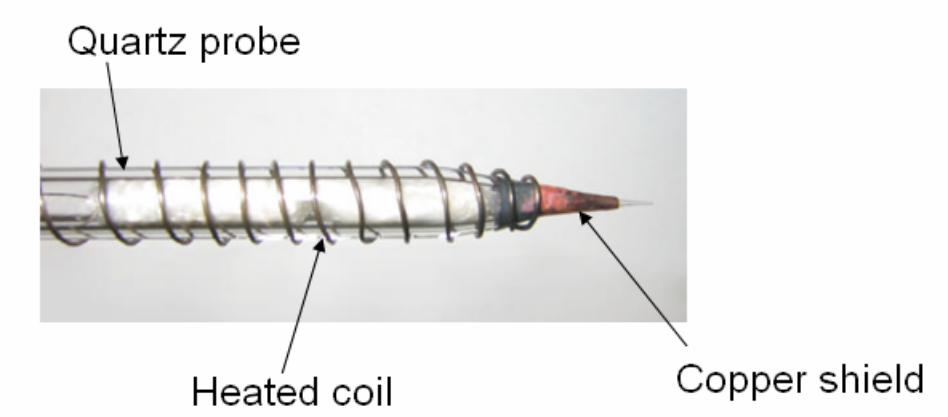

Figure 3.4 Quartz microprobe assembly

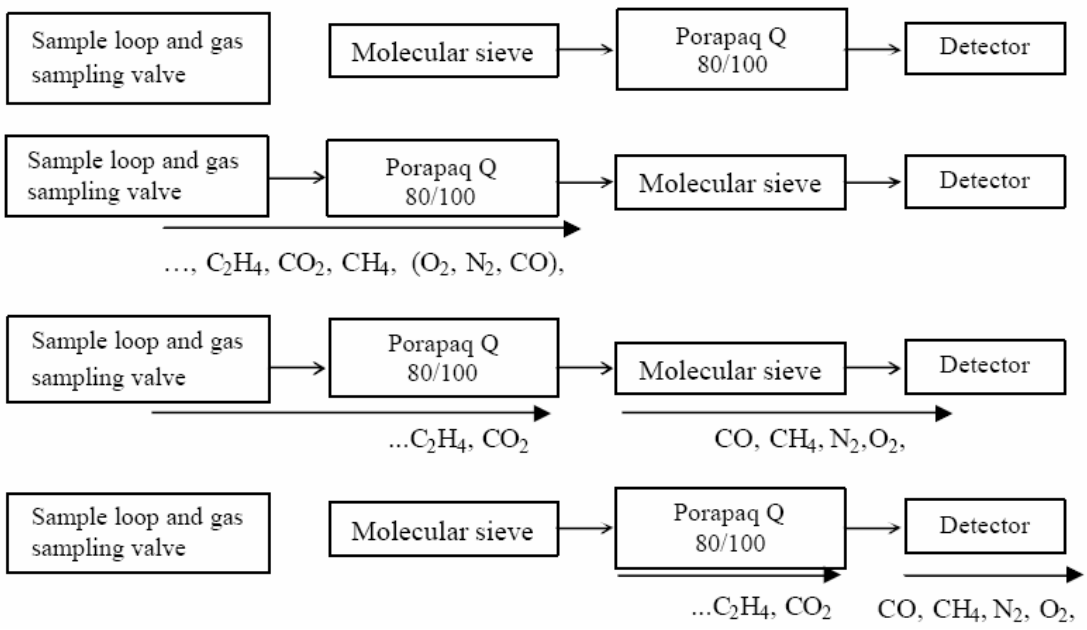

Figure 3.5 Flow of the sampled stable species through the mole sieve and Porapak Q columns to the detectors, and the valve switching involved

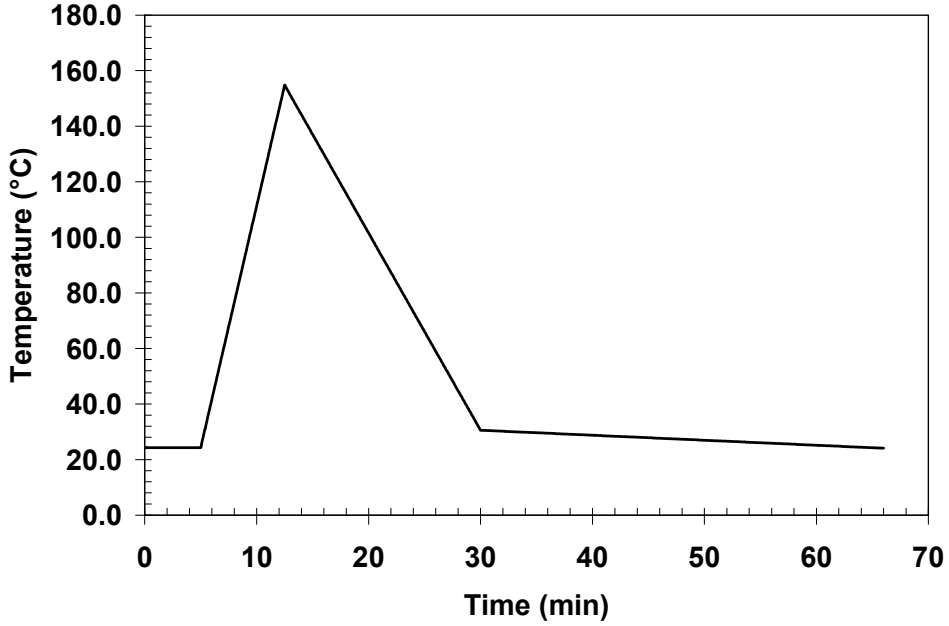

Figure 3.6 Temperature programming of the mole sieve column

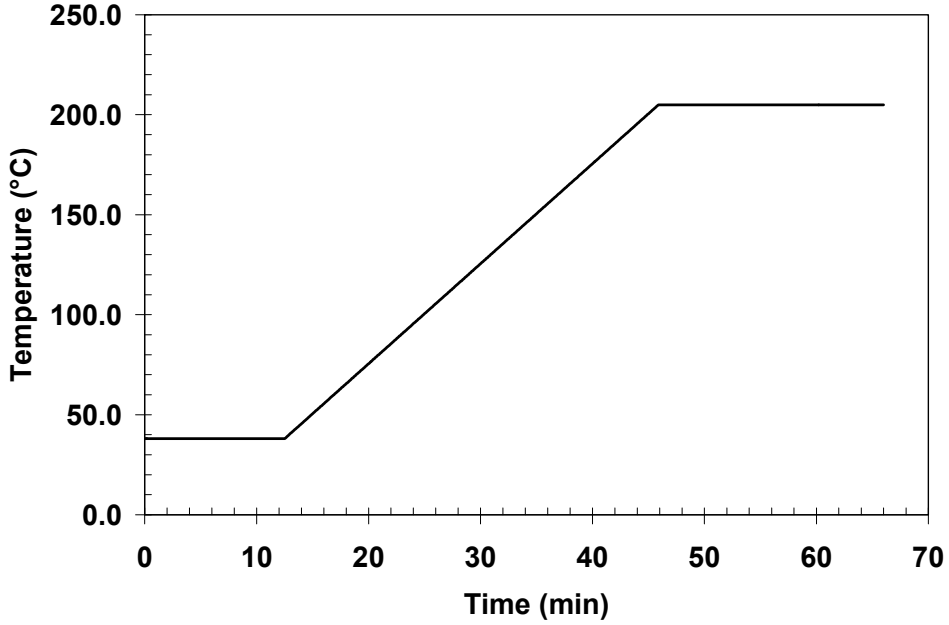

Figure 3.7 Temperature programming of the Propak Q column

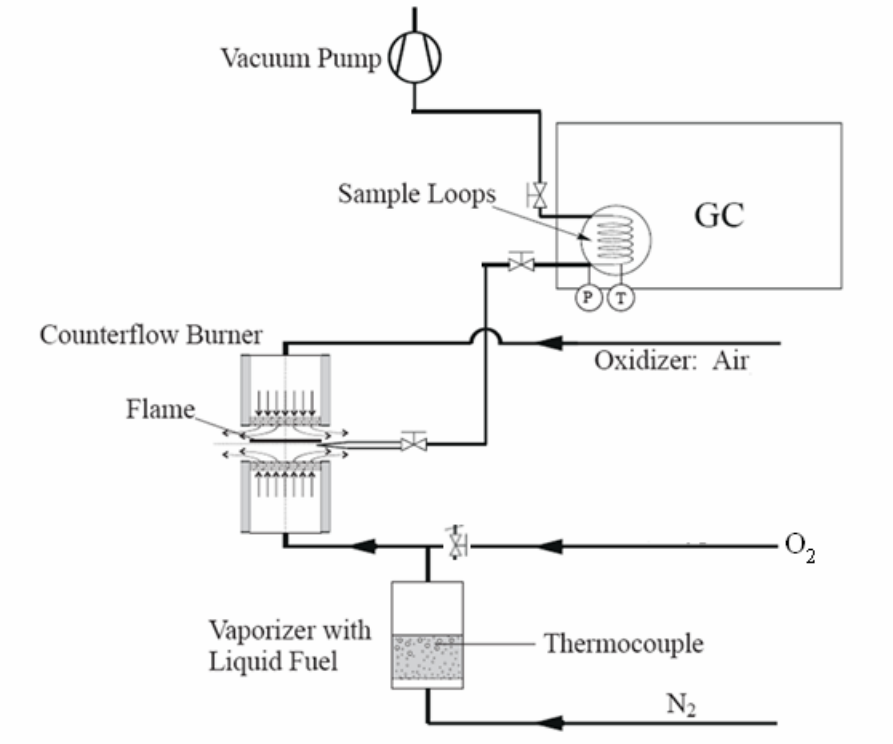

Figure 3.8 Schematic of the experimental setup including the counterflow burner, the vaporizer, the gas sampling system, and the gas chromatograph

3.7 REFERENCES

1. Davidson, D.F. and Hanson, R.K., "Interpreting shock tube ignition data", International Journal of Chemical Kinetics, 36, 2004, pp. 510-523.

2. Vagelopoulos, C.M. and Egolfopoulos, F.N., "Direct experimental determination of laminar flame speeds", Proceedings of the Combustion Institute, 27, 1998, pp. 513-519.

3. Natarajan, K. and Bhaskaran, K.A., "An experimental and analytical investigation of high temperature ignition of ethanol", Thirteenth International Symposium on Shock Waves, 1982, pp. 834-842.

4. Dunphy, M.P. and Simmie, J.M., "High temperature oxidation of ethanol. Part 1.- Igniton delays in shock waves", Journal of the Chemical Society, Faraday Transactions, 87 (11), 1991, pp. 1691-1696.

5. Curran, H.J., Dunphy, M.P., Simmie, J.M., Westbrook, C.K. and Pitz, W.J., "Shock tube ignition of ethanol, isobutene and MTBE: Experiments and modeling", Proceedings of the Combustion Institute, 24, 1992, pp. 769-776.

6. Egolfopoulos, F.N., Du, D.X. and Law, C.K., "A study of ethanol oxidation kinetics in laminar premixed flames, flow reactors and shock tubes", Proceedings of the Combustion Institute, 24, 1992, pp. 833-841.

7. Gülder, O.L., "Laminar burning velocities of methanol, ethanol, and isooctane-air mixtures", Proceedings of the Combustion Institute, 19, 1982, pp. 275-281.

8. Seiser, R. and Seshadri, K., "Counterflow extinction of premixed and nonpremixed methanol and ethanol flames", Western States Section, The Combustion Institute, 2002 Spring Meeting, University of California at San Diego, La Jolla, CA 92093-0411, March 25-26, 2002, Paper # 02S-27.

9. Smith, S.R. and Gordon, A.S., "Studies of diffusion flames. II. Diffusion flames of some simple alcohols", Journal of Chemical Physics, 60, 1956, pp. 1059-1062.

10. Li, S.C. and Williams, F.A., "Experimental and numerical studies of two-stage methanol flames", Proceedings of the Combustion Institute, 26, 1996, pp. 1017-1024.

11. Li, S.C. and Williams, F.A., "Formation of NO_x, CH_4, and C_2 species in laminar methanol flames", Proceedings of the Combustion Institute, 27, 1998, pp. 485-493.

12. Seiser, R., "Nonpremixed combustion of liquid hydrocarbon fuels", Ph.D. thesis, Technical University of Graz, 2000.

13. Seshadri, K. and Williams, F.A., "Laminar flow between parallel plates with injection of a reactant at high reynolds number", International Journal of Heat and Mass Transfer, 21, 1978, pp. 251-253.

14. Shaddix C.R., "Practical aspects of correcting thermocouple measurements for radiation loss", Western State Section/The Combustion Institute, University of Washington, Seattle WA, Oct. 26-27, 1998, WSS/CI 98F-24.

15. Fristrom, R.M., and Westenberg, A.A., Flame Structures, McGraw-Hill, New York, 1965.

16. Seiser, R., Truett, L., Trees, D., and Seshadri, K., "Structure and extinction of non-premixed n-heptane flames", Proceedings of the Combustion Institute, 27, 1998, pp. 649-657.

17. Redell, F.H., "Experimental investigation of the structure of a partially premixed planar ethanol flame", M.S. Thesis, University of California, San Diego, 2000.

CHAPTER 4

TESTING MECHANISM FOR THE COMBUSTION OF HYDROGEN AND CARBON MONOXIDE

4.1 OVERVIEW

Because of limitations on computer capabilities, there is a need for detailed chemical-kinetic mechanisms for combustion that are not too large. As an alternative to mechanisms having thousands of elementary steps, a mechanism having less than 300 steps is being developed [1]. This simplification is achieved by restricting attention to temperatures above about 1000 K, pressures below about 100 bar, equivalence ratios less than about 3 in premixed systems, and strain rates greater than about 50 s^{-1} in nonpremixed or partially premixed systems. The simplifications then arise mainly from the unimportance of soot formation and cool-flame phenomena under these conditions.

Fuels that have been studied previously with the San Diego Mech include methane [2], ethane [3], ethylene [4], acetylene [5, 6], propane [1], propene, [1], propyne [1], allene [1] and methanol [7, 8]. Tests also have been made recently for hydrogen autoignition [9], and some time ago premixed and diffusion flames of carbon monoxide were addressed [10, 11]. There have, however, been no recent tests for premixed hydrogen flames and no tests at all for autoignition of mixtures containing carbon monoxide. Since the hydrogen and carbon monoxide submechanisms are essential to the mechanisms for all of the other fuels, and since there is also substantial interest in these two fuels themselves, testing of the mechanism for them is completed here.

The comparisons to be reported lead to small revisions of rate parameters for a few elementary steps. The resulting steps and rate parameters for this submechanism are given in Table 4.1, in which all steps are considered to be reversible, with backward rates obtained from listed forward rates by use of equilibrium constants. The revisions improve agreements in the present comparisons. The revised values are in agreement with those in some of the more recent literature, and the changes are well within fundamental uncertainties in rates of elementary steps. These uncertainties were considered for all of the steps, and possibilities of revising rate parameters for many additional steps were investigated but finally rejected as insufficiently useful or not justified well enough from fundamental considerations. In addition, one reaction is deleted that has been demonstrated recently to be unlikely to occur, and one has been added that previously had been thought to be unimportant but was found to exert a small but noticeable effect.

In the following sections comparisons are made first for premixed hydrogen systems, next for hydrogen diffusion-flame extinction, then for burning velocities of premixed flames of carbon monoxide with different amounts of hydrogen, and finally for autoignition of mixtures of carbon monoxide and hydrogen. The rate-parameter revisions are discussed in connection with the test for which they are most relevant. The computations for the comparisons were performed with CHEMKIN [19] programs, although the FlameMaster program [20] was also employed to make sure that predictions from the two different programs were the same.

4.2 HYDROGEN BURNING VELOCITIES AND AUTOIGNITION

There is a wealth of data available for laminar flame speeds for hydrogen-air systems for a wide range of equivalence ratios at normal atmospheric pressure and initially room temperature. In the earliest predecessor of the present mechanism for hydrogen [21], comparisons were made with data taken prior to 1990. These results exhibited a great deal of scatter, but more recent data are much more accurate. The measurements that we judge to be most reliable were selected for comparisons in the present work. These include hydrogen-air data at 1 atm and an initial temperature of 298 K for equivalence-ratio ranges of 0.23 to 4.5 [22], 0.25 to 1.5 [23], 0.4 to 4.0 [24] and 0.6 to 4.5 [25]. These results are in remarkably good agreement with each other. In addition, for these same conditions good data are available [25] for hydrogen-oxygen mixtures diluted by argon and by helium at 1 atm, and also [24] at pressures up to 20 atm for this last diluent.

Figures 4.1 and 4.2 compare the present burning-velocity predictions with this data. The computational results were obtained with CHEMKIN 3.7 PREMIX including multicomponent diffusion and Soret effects but excluding radiant energy loss, which would decrease predicted burning velocities only slightly under these conditions. Throughout the present work, calculations also were made including radiant loss from H_2O and CO_2 bands in an optically thin approximation, and results differed approximately by the thickness of the lines.

A dilution factor may be defined as

$$f = [O_2]/([O_2] + [I]),$$

where the brackets denote concentrations and I stands for the inert; f = 0.214 in figure 4.1, and f = 0.08 in figure 4.2. The agreements between predictions and experiments are

quite good in these figures, comparable with the agreements obtained previously [26] by a more complex mechanism. Although measured burning velocities in air for very lean mixtures consistently exceed predictions, the exceptionally strong tendency towards forming cellular flames under these conditions make experiments very difficult and would tend to produce measured burning velocities that are higher than those of a planar, unstretched flame, to which the computations apply.

The small mechanism originally had 22 elementary steps for hydrogen combustion, but recent calculations of potential-energy surfaces [27] show clearly that one of the two chain-initiation steps that had been included, namely $H_2+O_2 \rightarrow 2OH$, is highly unlikely, leaving only the reverse of step 12, $H_2+O_2 \rightarrow HO_2+H$, for initiation. The unlikely step therefore now is deleted. Although this step influenced autoignition times at higher temperatures, coupled with the other rate-parameter modifications indicated below, its deletion does not degrade reported [9] ignition-time comparisons. (The results for hydrogen autoignition with the current hydrogen mechanism are shown in Appendix 3). The comparisons in figures 4.1 and 4.2 therefore pertain to a 21-step hydrogen combustion mechanism, the first 21 entries in Table 4.1.

When the mechanism was first tested against this data, it gave burning velocities noticeably higher than shown in figure 4.1 for air over most of the equivalence-ratio range and much lower than shown in figure 4.2. The rate parameters therefore were reviewed again for all steps, and certain revisions were made on the basis of more recent literature and to obtain the agreements seen in figures 4.1 and 4.2.

The rate of the recombination step 6, $H+OH+M \rightarrow H_2O+M$, was increased by about 80% to reduce high-temperature hydrogen-air burning velocities, on the basis of

newer literature [28, 29, 30], which supports this revision, the listed rate being an average of the rates in the newer literature. The rate of the step 11, $HO_2+H\rightarrow 2OH$, had been decreased to reduce predicted propane-air burning velocities [1], improving agreements, and that similarly helps for hydrogen-air flames. Associated with this decrease, considerations of rate and branching-ratio results [31, 32] prompted recommending a corresponding reduction in the rate of step 12, $HO_2+H\rightarrow H_2+O_2$ [15]. The specific reaction-rate constant

$$k = AT^n e^{-E/RT}$$

with the recommended [15] parameter values listed as entry 12 in Table 4.1 is therefore now adopted for this step, improving agreements slightly for both burning velocities and autoignition times. Revision of the rate of step 17, $2HO_2\rightarrow H_2O_2+O_2$, was considered but rejected as not well justified at the high temperatures of interest.

All of the other changes that were made pertain to the three-body recombinations. Newer [13] rate parameters were adopted for $O+H+M\rightarrow OH+M$, (entry 8 of Table 4.1) with the recommended chaperon efficiencies. The rate parameters for $O+O+M\rightarrow O_2+M$ (entry 7) also were taken from this reference, although chaperon efficiencies of 0.2 were introduced for argon and helium to avoid employing separate reactions for these third bodies, the selected value representing an average over the temperature range of interest here (1000 K to 2500 K). All rate parameters are written consistently with a chaperon efficiency of unity for nitrogen. For step 5, $H+H+M\rightarrow H_2+M$, the recommendation of Baulch et al. [16] was adopted; these authors give values only for argon as the chaperon, whose efficiency with respect to nitrogen was assumed to be 0.5, slightly improving fuel-rich burning-velocity agreements in figure 4.1 and resulting in rates that lie between those

of Li [26] and of the optimized mechanism of Davis et al. [30], whose common relative efficiencies [26, 30] were adopted. For reaction 9, O+OH+M→HO_2+M, chaperon efficiencies are now introduced which are the same as those of O+H+M→OH+M, while the rate is slightly reduced (by 20%) from our previous value [33]. The Troe [34] rate parameters and falloff recommendations for step 10, H+O_2+M→HO_2+M, for nitrogen as the bath gas (e.g., F_c=0.5) were adopted, improving both burning-velocity agreement for high-pressure experiments with helium dilution and ignition-time agreement. To avoid having to introduce either a different rate expression or temperature-dependent chaperon efficiencies for argon as the bath gas for this reaction, just as was done for the other recombination processes discussed above, constant chaperon efficiencies were selected, a high value for water being used for agreement with measured autoignition times and diffusion-flame extinction by water addition, and a value for argon being selected consistent with autoignition times. Finally, for step 16, OH+OH+M→H_2O_2+M, the listed rate parameters [9] are obtained from those for nitrogen of Baulch et al. [35] (who write the reaction in the opposite direction) by use of equilibrium constants, but the argon efficiency was decreased from 0.7 to 0.4, a better average, between 1000 K and 2500 K, of the temperature-dependent recommendation of Baulch et al. [35].

4.3 HYDROGEN DIFFUSION-FLAME EXTINCTION

The mechanism with these updated rate parameters also was tested against counterflow diffusion-flame extinction experiments. Comparisons are shown in figures 4.3 and 4.4. The extinction strain-rate data in figure 4.3 [36] are seen to lie below the solid curve, calculated using CHEMKIN 3.7 OPDIFF with complete transport. Since

there is an indication of inaccurate transport data for hydrogen (as well as helium) in the code [37], for comparison purposes the calculation also was performed with the Soret effects excluded, to obtain an idea of how important light-species transport may be. The results, show by the dashed curve, agree better with the data, about as good as the agreement obtained [36] with an early version of the present mechanism. In view of the non-negligible influences of transport uncertainties for these experiments, until improved transport properties for hydrogen and helium can be incorporated into the computations, the agreement with the updated mechanism is considered acceptable.

Figure 4.4 tests the influence of water addition on the extinction strain rate, employing data [38] against which other mechanisms have been tested earlier. The agreement seen in this figure is somewhat better than found earlier [38], largely as a consequence of the increased chaperon efficiency for water in the step 10, $H+O_2+M \rightarrow HO_2+M$, which decreases the extinction strain rate with increasing water concentrations more rapidly than predicted earlier. Although even better agreement can be obtained with falloff [39] for H_2O different than that for N_2, it was preferred to accept the agreement shown for the sake of not having to treat the reaction with H_2O as a separate reaction.

4.4 BURNING VELOCITIES OF CARBON MONOXIDE

Since flames of carbon monoxide are dominated by hydrogen chemistry in practice, it is necessary only to add the three species CO, CO_2 and HCO, along with nine additional reversible elementary steps, to the hydrogen-oxygen mechanism, to obtain a workable thirty-step mechanism among eleven species for the combustion of carbon

monoxide, as seen in Table 4.1. Figure 4.5 tests predictions of this mechanism against recent burning-velocity data as a function of equivalence ratio for two different mixtures of hydrogen and carbon monoxide in air [40]. Figure 4.6 similarly tests the dependence on the fraction of carbon monoxide in the fuel for stoichiometric mixtures [40]. The excellent agreement in these two figures indicates that slightly revised rate parameters for the step 22, $CO+OH \rightarrow CO_2+H$, [26] and revised rate parameters for step 23, $CO+HO_2 \rightarrow CO_2+OH$, [41], motivated mainly by experiments at temperatures lower than those of interest here, are unnecessary for the present purposes, it being sufficient to retain the earlier [10] rates unchanged.

An earlier version of the mechanism was tested previously [11] for flames of carbon monoxide with trace amounts of hydrogen and water. Figure 4.7 repeats that test with the updated mechanism and exhibits agreements no worse than before.

4.5 AUTOIGNITION OF CARBON MONOXIDE

The mechanism has not been tested previously for autoignition of mixtures of carbon monoxide and hydrogen, even though there are shock-tube data [43, 44] on which such tests can be made. These tests were performed here using the homogeneous, adiabatic, isochoric option of CHEMKIN 3.7 AURORA. Figure 4.8 shows comparisons with one set of data [43] based on three different definitions of ignition times, all derived from profiles of the measured concentration of carbon dioxide. Figure 4.9 shows comparisons with another set of data [44] at lower pressure, based on a different ignition-time criterion. In all comparisons, the computational and experimental ignition-time criteria are the same. The agreements are comparable with or better than those obtained

[1, 4, 5] for other fuels; they are excellent in figure 4.8, while the predicted slope is a little higher than the average experimental data in figure 4.9. The experiments in this last figure were performed over a range of pressures, with values of the pressure not specified for each specific data point, and for each point it is possible to select a value of the pressure within the range that produces agreement between the prediction and the measurement. It is unclear whether the noticeably greater theoretical slope, which agrees with the slope of Li [26], should be attributable to erroneous values of rate parameters or to systematic experimental error, which becomes more difficult to avoid at these low pressures in shock tubes of the dimensions employed.

It was found that although the step 24, $CO+O_2 \rightarrow CO_2+O$, has no measurable influences on burning velocities and had not been retained previously as part of the mechanism, it does have a noticeable influence on these ignition times at low hydrogen content, contributing to initiation. This step therefore is now added to the mechanism, with rate parameters giving half the rate recommended by Tsang and Hampson [45]. This selection improves agreements somewhat in figure 4.8 and lies in the range of other values in the literature, even lower rates having been reported [46].

There are recent studies on ignition delay times from shock tubes [47] and laminar burning velocities [48] at higher pressures. The proposed mechanism underpredicts the autoignition delay time under these conditions. Further studies is required in accessing the rate parameters of elementary steps such as $CO+HO_2 \rightarrow CO_2+OH$ and $CO+O+M \rightarrow CO_2+M$, observed to have insignificant effect in the conditions studied here, are expected to play an important role at higher pressures.

4.6 CONCLUSIONS

The testing for hydrogen and carbon monoxide led to a few revisions of rate parameters for elementary steps in the mechanism for hydrogen and to deletion of a hydrogen initiation step and addition of an initiation step for carbon monoxide. Small increases in three-body recombination rates for certain steps and some changes in chaperon efficiencies were identified. With these alterations, reasonable agreement is obtained with available measured burning velocities, diffusion-flame extinction conditions and autoignition times. There is, however, need for further studies in assessing the validity of the mechanism for burning velocities and ignition delay times at intermediate and higher pressures for carbon monoxide hydrogen mixtures.

ACKNOWLEDGEMENT

This chapter, in part, is a reprint of the material as it appears in the article: P. Saxena and F.A. Williams, “Testing a small detailed chemical-kinetic mechanism for the combustion of hydrogen and carbon monoxide”, *Combustion and Flame*, 145, 2006, pp. 316-323. The dissertation author was the primary researcher in that publication.

Table 4.1 Chemical-Kinetic Mechanism for Hydrogen and Carbon Monoxide

Reaction		A[a]	n[a]	E[a]	Reference
		Hydrogen-Oxygen Chain			
1. $H + O_2 \rightarrow OH + O$		3.52×10^{16}	-0.7	71.4	[12]
2. $H_2 + O \rightarrow OH + H$		5.06×10^{4}	2.7	26.3	[13]
3. $H_2 + OH \rightarrow H_2O + H$		1.17×10^{9}	1.3	15.2	[14]
4. $H_2O + O \rightarrow OH + OH$		7.60×10^{0}	3.8	53.4	[13]
		Direct Recombination			
5[b]. $H + H + M \rightarrow H_2 + M$		1.30×10^{18}	-1.0	0.0	See text
6[c]. $H + OH + M \rightarrow H_2O + M$		4.00×10^{22}	-2.0	0.0	See text
7[d]. $O + O + M \rightarrow O_2 + M$		6.17×10^{15}	-0.5	0.0	See text
8[e]. $H + O + M \rightarrow OH + M$		4.71×10^{18}	-1.0	0.0	See text
9[e]. $O + OH + M \rightarrow HO_2 + M$		8.00×10^{15}	0.0	0.0	See text
		Hydroperoxyl Reactions			
10[f]. $H + O_2 + M \rightarrow HO_2 + M$	k_0	5.75×10^{19}	-1.4	0.0	See text
	k_∞	4.65×10^{12}	0.4	0.0	
11. $HO_2 + H \rightarrow OH + OH$		7.08×10^{13}	0.0	1.2	[15]
12. $HO_2 + H \rightarrow H_2 + O_2$		1.66×10^{13}	0.0	3.4	[15]
13. $HO_2 + H \rightarrow H_2O + O$		3.10×10^{13}	0.0	7.2	[16]
14. $HO_2 + O \rightarrow OH + O_2$		2.00×10^{13}	0.0	0.0	[17]
15. $HO_2 + OH \rightarrow H_2O + O_2$		2.89×10^{13}	0.0	-2.1	[16]
		Hydrogen Peroxide Reactions			
16[g]. $OH + OH + M \rightarrow H_2O_2 + M$	k_0	2.30×10^{18}	-0.9	-7.1	See text
	k_∞	7.40×10^{13}	-0.4	0.0	
17. $HO_2 + HO_2 \rightarrow H_2O_2 + O_2$		3.02×10^{12}	0.0	5.8	[13]
18. $H_2O_2 + H \rightarrow HO_2 + H_2$		4.79×10^{13}	0.0	33.3	[13]
19. $H_2O_2 + H \rightarrow H_2O + OH$		1.00×10^{13}	0.0	15.0	[13]
20. $H_2O_2 + OH \rightarrow H_2O + HO_2$		7.08×10^{12}	0.0	6.0	[13]
21. $H_2O_2 + O \rightarrow HO_2 + OH$		9.63×10^{6}	2.0	16.7	[13]
		Conversion of CO to CO_2			
22. $CO + OH \rightarrow CO_2 + H$		4.40×10^{6}	1.5	-3.1	[10]
23. $CO + HO_2 \rightarrow CO_2 + OH$		6.00×10^{13}	0.0	96.0	[10]
24. $CO + O_2 \rightarrow CO_2 + O$		1.00×10^{12}	0.0	199.4	See text
		Formyl Reactions			
25[h]. $HCO + M \rightarrow CO + H + M$		1.86×10^{17}	-1.0	71.1	[18]
26. $HCO + H \rightarrow CO + H_2$		1.00×10^{14}	0.0	0.0	[10]
27. $HCO + O \rightarrow CO + OH$		3.00×10^{13}	0.0	0.0	[10]
28. $HCO + O \rightarrow CO_2 + H$		3.00×10^{13}	0.0	0.0	[10]
29. $HCO + OH \rightarrow CO + H_2O$		5.02×10^{13}	0.0	0.0	[10]
30. $HCO + O_2 \rightarrow CO + HO_2$		3.00×10^{12}	0.0	0.0	[10]

[a]Specific reaction-rate constant $k = AT^n e^{-E/R^o T}$; units mol/cm^3, s^{-1}, K, kJ/mol.

[b]Chaperon efficiencies are 2.5 for H_2, 12.0 for H_2O, 1.9 for CO, 3.8 for CO_2, 0.5 for Ar and He and 1.0 for all other species.
[c]Chaperon efficiencies are 2.5 for H_2, 12.0 for H_2O, 1.9 for CO, 3.8 for CO_2, 0.4 for Ar and He and 1.0 for all other species.
[d]Chaperon efficiencies are 2.5 for H_2, 12.0 for H_2O, 1.9 for CO, 3.8 for CO_2, 0.2 for Ar and He and 1.0 for all other species.
[e]Chaperon efficiencies are 2.5 for H_2, 12.0 for H_2O, 1.9 for CO, 3.8 for CO_2, 0.7 for Ar and He and 1.0 for all other species.
[f]Chaperon efficiencies are 2.5 for H_2, 16.0 for H_2O, 1.2 for CO, 2.4 for CO_2, 0.7 for Ar and He and 1.0 for all other species; Troe falloff with $F_c = 0.5$.
[g]Chaperon efficiencies are 2.0 for H_2, 6.0 for H_2O, 1.5 for CO, 2.0 for CO_2, 0.4 for Ar and He and 1.0 for all other species; Troe falloff with $F_c = 0.265 \exp(-T/94\text{ K}) + 0.735 \exp(-T/1756\text{ K}) + \exp(-5182\text{ K}/T)$.
[h]Chaperon efficiencies are 1.9 for H_2, 12.0 for H_2O, 2.5 for CO, 2.5 for CO_2 and 1.0 for all other species.

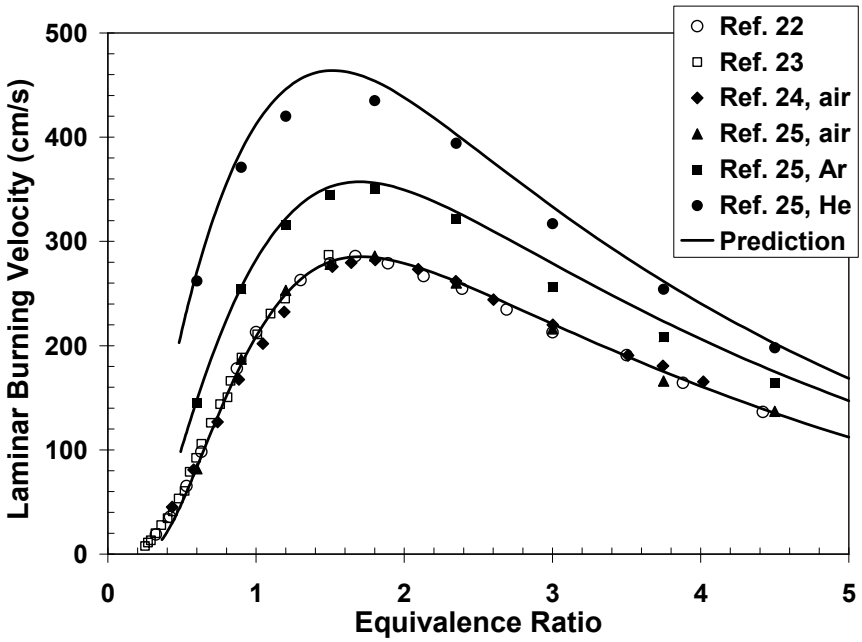

Figure 4.1: Measured and predicted laminar burning velocities of hydrogen-oxygen-inert flames at 1 atm and initially at 298 K with a dilution factor $f = 0.214$, for inerts nitrogen (air), argon and helium.

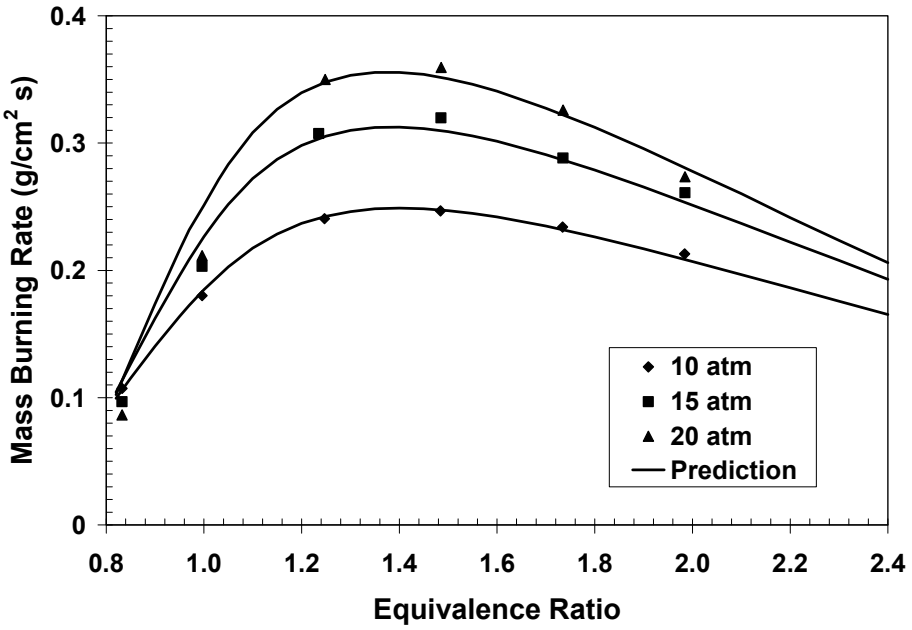

Figure 4.2: Measured [24] and predicted laminar mass burning rates of hydrogen-oxygen-helium mixtures with a dilution factor $f = 0.08$, initially at 298 K, for pressures from 10 atm to 20 atm.

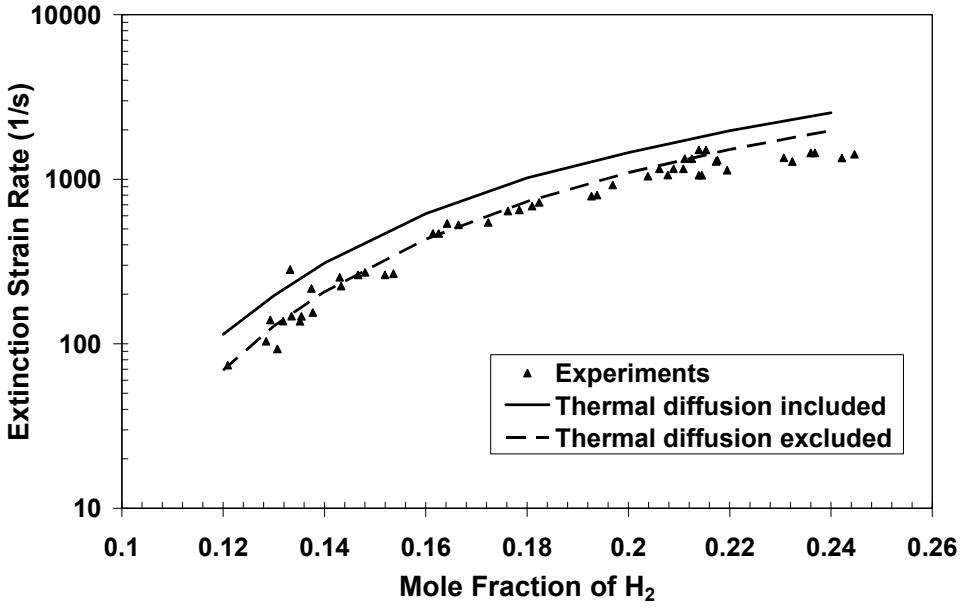

Figure 4.3: Measured [36] and predicted extinction strain rate as a function of the mole fraction of hydrogen in a hydrogen-nitrogen fuel mixture for a counterflow diffusion flame of the diluted fuel and air.

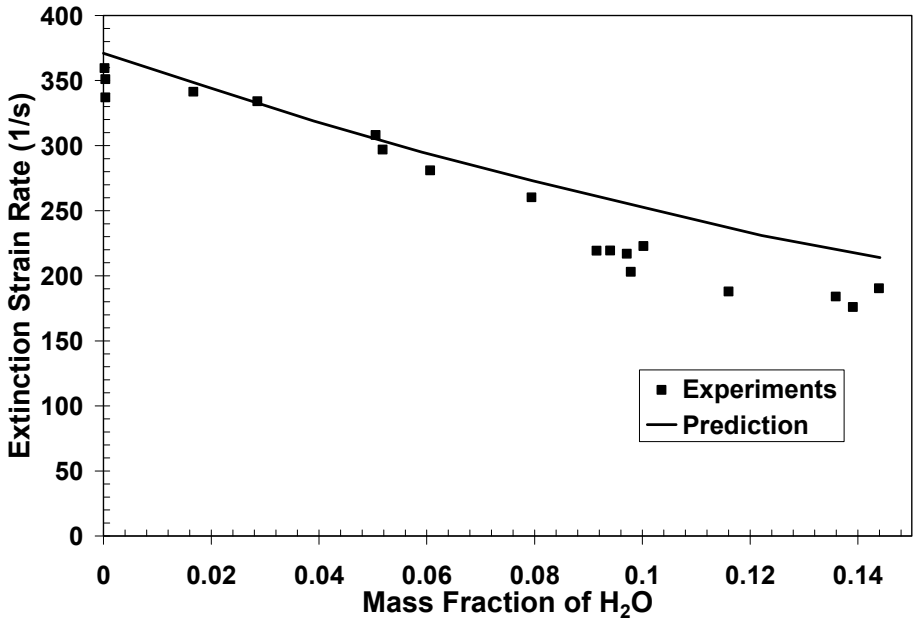

Figure 4.4: Measured [38] and predicted extinction strain rate as a function of the mass fractions of water in the oxidizer stream for a counterflow diffusion flame having a hydrogen-nitrogen mixture at room temperature as fuel (hydrogen mole fraction between 0.28 and 0.29) and an oxygen-nitrogen-water mixture at 383 K (dilution *f* approximately 0.1) as oxidizer.

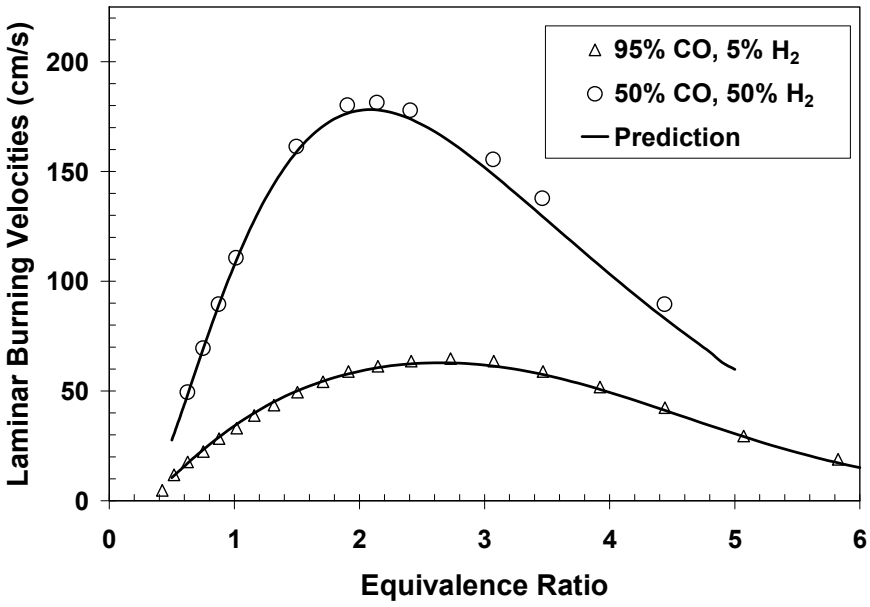

Figure 4.5: Measured [40] and predicted laminar burning velocities as functions of the equivalence ratio for two different mixtures of hydrogen and carbon monoxide in air at 1 atm and initially at 298 K.

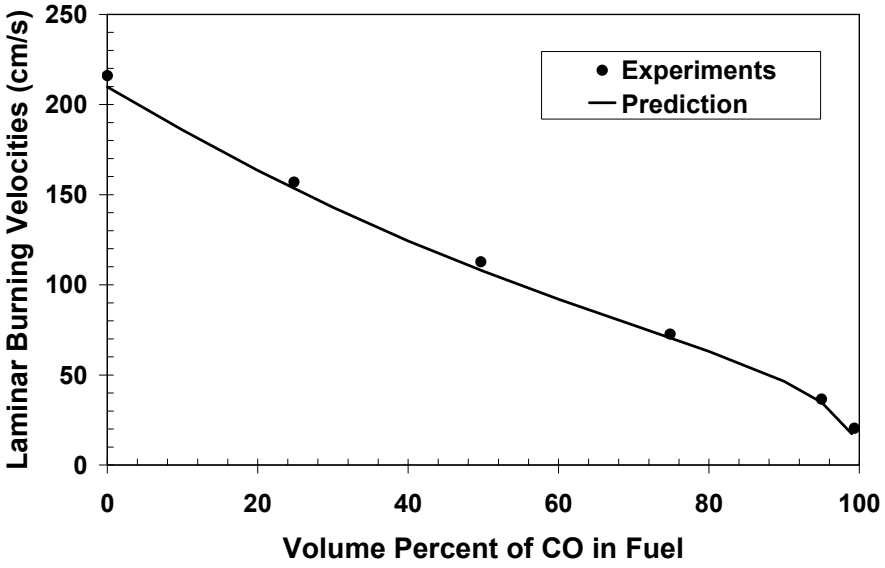

Figure 4.6: Measured [40] and predicted laminar burning velocities of stoichiometric fuel-air mixtures at 1 atm and initially at 298 K, as a function of the percentage of carbon monoxide in a fuel consisting of a mixture of hydrogen and carbon monoxide.

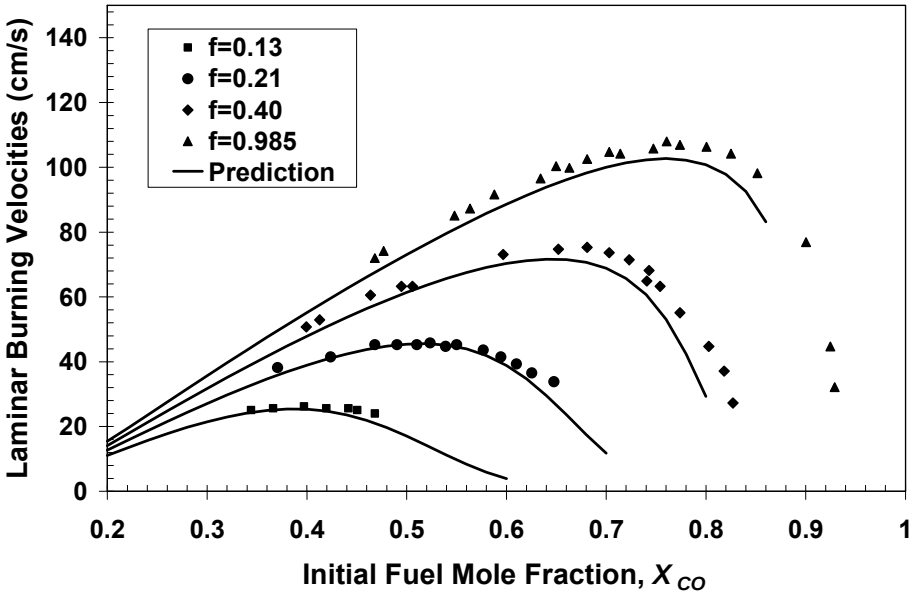

Figure 4.7: Measured [42] and predicted laminar burning velocities at 1 atm and initially at 298 K, as functions of the initial fuel mole fraction of carbon monoxide X_{CO} at various dilutions *f*, for flames of carbon monoxide with initial hydrogen mole fraction $X_{H_2} = 0.015(X_{CO} + X_{H_2} + X_{H_2O})$.

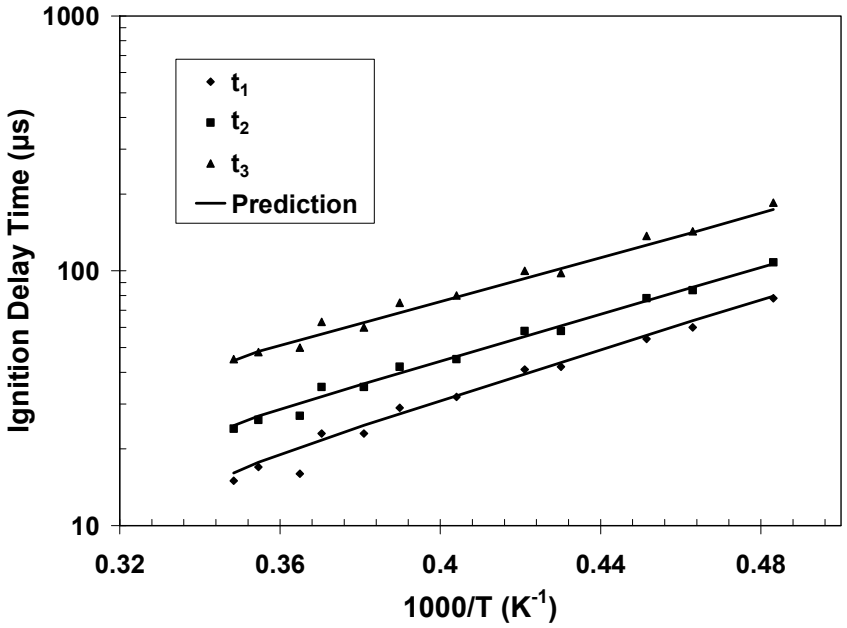

Figure 4.8: Measured [43] and predicted ignition times of a mixture of 12.15% CO, 0.05% H_2, 1.0% O_2 and 86.8% Ar by volume at pressures between 1.4 atm and 2.2 atm, according to three different definitions of the ignition times based on concentration-time profiles of carbon dioxide, namely, the time t_1 of the zero intercept of the maximum-slope straight line, the time t_2 at which the concentration is 10^{16} molecules/cm^3, and the time t_3 at which the concentration is $3x10^{16}$ molecules/cm^3.

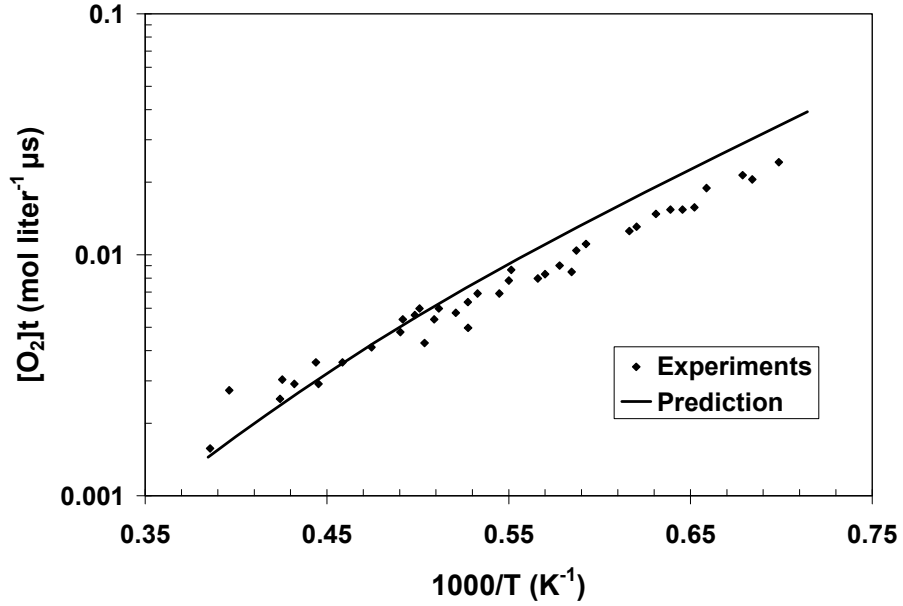

Figure 4.9: Measured [44] and predicted ignition times, defined as hydroxyl concentrations reaching $2.5x10^{-10}$ mol/cm^3, for a mixture of 3% CO, 1% H_2, 5% O_2 and 91% Ar by volume, at pressures between 0.15 and 0.30 atm.

4.7 REFERENCES

1. Petrova, M.V. and Williams, F.A., "A small detailed chemical-kinetic mechanism for hydrocarbon combustion", Combustion and Flame, 144, 2006, pp. 526-544.

2. Li, S.C. and Williams, F.A., "NO_x formation in two-stage methane-air flames", Combustion and Flame, 118, 1999, pp. 399-414.

3. Waly, M.M.Y., Li, S.C. and Williams, F.A., "Experimental and numerical studies of two-stage ethane-air flames", Journal of Engineering for Gas Turbines and Power, 122, 2000, pp. 651-658.

4. Varatharajan, B. and Williams, F.A., "Ethylene ignition and detonation chemistry, Part 1: Detailed modeling and experimental comparison", Journal of Propulsion and Power, 18, 2002, pp. 344-351.

5. Waly, M.M., Li, S.C. and Williams, F.A., "Structures of non-sooting counterflow diluted acetylene-air flames", Proceedings of the Combustion Institute, 28, 2000, pp. 2005-2012.

6. Varatharajan, B. and Williams, F.A., "Chemical-kinetic descriptions of high-temperature ignition and detonation of acetylene-oxygen-diluent systems", Combustion and Flame, 124, 2001, pp. 624-645.

7. Li, S.C. and Williams, F.A., "Experimental and numerical studies of two-stage methanol flames", Proceedings of the Combustion Institute, 26, 1996, pp. 1017-1024.

8. Li, S.C. and Williams, F.A., "Formation of NO_x, CH_4, and C_2 species in laminar methanol flames", Proceedings of the Combustion Institute, 27, 1998, pp. 485-493.

9. Del Alamo, G., Williams, F.A. and Sanchez A. L, "Hydrogen-oxygen induction times above crossover temperatures", Combustion Science and Technology, 176, 2004, 1599-1626.

10. Rightley, M.L. and Williams, F.A., "Structures of CO diffusion flames near extinction", Combustion Science and Technology, 125, 1997, pp. 181-200.

11. Rightley, M.L. and Williams, F.A., "Analytical approximation for structures of wet CO flames with one-step reduced chemistry", Combustion and Flame, 101, 1995, pp. 287-301.

12. Masten, D.A., Hanson, R.K. and Bowman, C.T., "Shock tube study of the reaction $H+O_2 \rightarrow OH+O$ using OH laser absorption", Journal of Physical Chemistry, 94, 1990, pp. 7119-7128.

13. Yetter, R.A., Dryer, F.L. and Rabitz, H., "A comprehensive reaction mechanism for carbon monoxide/hydrogen/oxygen kinetics", Combustion Science and Technology, 79, 1991, pp. 97-128.

14. Smooke, M.D., "Solution of burner-stabilized premixed laminar flames by boundary value methods", Journal of Computational Physics, 48, 1982, pp. 72-105.

15. Mueller, M.A., Kim, T.J., Yetter, R.A. and Dryer, F.L., "Flow reactor studies and kinetic modeling of the H_2/O_2 Reaction", International Journal of Chemical Kinetics, 31, 1999, pp. 113-125.

16. Baulch, D.L., Cobos, C.J., Cox, R.A., Esser, C., Frank, P., Just, Th., Kerr, J.A., Pilling, M.J., Troe, J., Walker, R.W. and Warnatz, J., "Evaluated kinetic data for combustion modeling", Journal of Physical and Chemical Reference Data, 21, 1992, pp. 411-734.

17. Warnatz, J., "Rate coefficients in the C/H/O system". In W.C. Gardiner (ed.), Combustion Chemistry, Springer-Verlag, Berlin, pp. 197-360, 1984.

18. Lindstedt, R.P. and Skevis, G., "Chemistry of acetylene flames", Combustion Science and Technology, 125, 1997, pp. 73-137.

19. Kee, R.J., Rupley, F.M., Miller, J.A., Coltrin M.E., Grcar, J.F., Meeks, E., Moffat, H.K., Lutz, A.E., Dixon-Lewis, G., Smooke, M.D., Warnatz, J., Evans, G.H., Larson, R.S., Mitchell, R.E., Petzold, L.R., Reynolds, W.C., Caracotsios, M., Stewart, W.E., Glarborg, P., Wang, C., Adigun, O., Houf, W.G., Chou, C.P. and Miller, S.F., Chemkin Collection, Release 3.7.1, Reaction Design Inc., San Diego, CA, 2003.

20. Pitsch, H., "Entwicklung eines Programmpakets zur Berechnung eindimensionaler Flammen am Beispiel einer Gegenstromdiffusionflamme", M.S. Thesis, RWTH Aachen, Germany, 1993.

21. Balakrishnan, G. and Williams, F.A., "Turbulent combustion regimes for hypersonic propulsion employing hydrogen-air diffusion flames", Journal of Propulsion and Power, 10, 1995, pp. 434-437.

22. Dowdy, D.R., Smith, D.B., Taylor, S.C. and Williams, A., "The use of expanding spherical flames to determine burning velocities and stretch effects in hydrogen/air mixtures", Proceedings of the Combustion Institute, 23, 1990, pp. 325-332.

23. Egolfopoulos, F.N. and Law, C.K., "An experimental and computational study of the burning rates of ultra-lean to moderately-rich $H_2/O_2/N_2$ laminar flames with pressure variations", Proceedings of the Combustion Institute, 23, 1990, pp. 333-340.

24. Tse, S.D., Zhu, D.L. and Law, C.K., "Morphology and burning rates of expanding spherical flames in H_2/O_2/Inert mixtures up to 60 atmospheres", Proceedings of the Combustion Institute, 28, 2000, pp. 1793-1800.

25. Kwon, O.C. and Faeth, G.M., "Flame/Stretch interactions of premixed hydrogen-fueled flames: Measurements and predictions", Combustion and Flame, 124, 2001, pp. 590-610.

26. Li, J., "Experimental and numerical studies of ethanol chemical kinetics", PhD Thesis, Princeton University, 2004.

27. Michael, J.V., Sutherland, J.W., Harding, L.B. and Wagner, A.F., "Initiation in H_2/O_2: Rate constants for $H_2+O_2 \rightarrow H+HO_2$ at high temperature", Proceedings of the Combustion Institute, 28, 2000, pp. 1471-1478.

28. Li, J., Zhao, Z., Kazakov, A. and Dryer, F.L., "An updates comprehensive kinetic model of hydrogen combustion", International Journal of Chemical Kinetics, 36, 2004, pp. 566-575.

29. O Conaire, M., Curran H.J., Simmie, J.M., Pitz, W. J. and Westbrook, C.K., "A comprehensive modeling study of hydrogen oxidation", International Journal of Chemical Kinetics, 36, 2004, pp. 603-622.

30. Davis, S.G., Joshi, A.V., Wang. H. and Egolfopoulos, F., "An optimized kinetic model of H_2/CO combustion", Proceedings of the Combustion Institute, 30, 2005, pp. 1283-1292.

31. Hippler, H., Troe, J. and Willner, J., "Shock wave study of the reaction H_2/O_2: Rate constants for $H_2+O_2 \rightarrow H+HO_2$ Confirmation of a rate constant minimum near 700 K", Journal of Chemistry and Physics, 93, 1990, pp. 1755-1760.

32. Baldwin, R.R., Fuller, M.E., Hillman, J.S., Jackson, D., Walker, R.W., "Second limit of Hydrogen+Oxygen mixtures: the reaction $H+HO_2$", Transactions of the Faraday Society, 70, 1974, pp. 635-641.

33. Gutheil, E., Balakrishnan, G. and Williams, F. A., "Structure and extinction of hydrogen-air diffusion flames". In Peters, N. and Rogg, Bernd, "Reduced kinetic mechanisms for applications in combustion systems", Springer-Velag, 1993, Chapter 11.

34. Troe, J., "Detailed modeling of the temperature and pressure dependence of the reaction $H+O_2(+M) \rightarrow HO_2(+M)$", Proceedings of the Combustion Institute, 28, 2000, pp. 1463-1469.

35. Baulch, D.L., Cobos, C.J., Cox, R.A., Frank, P., Hayman, G., Just, Th., Kerr, J.A., Murrells, T., Pilling, M.J., Troe, J., Walker, R.W. and Warnatz, J., "Evaluated kinetic data for combustion modeling. Supplement I", Journal of Physical and Chemical Reference Data, 23, 1994, pp. 847-1033.

36. Balakrishnan, G., Trees, D. and Williams, F.A., "An experimental investigation of strain-induced extinction of diluted hydrogen-air counterflow diffusion flames", Combustion and Flame, 98, 1994, pp. 123-126.

37. Paul, P. and Warnatz, J., "A re-evaluation of the means used to calculate transport properties of reacting flows", Proceedings of the Combustion Institute, 27, 1998, pp. 495-504.

38. Seiser, R. and Seshadri, K., "The influence of water on extinction and ignition of hydrogen and methane flames", Proceedings of the Combustion Institute, 30, 2005, pp. 407-414.

39. Bates, R.W., Golden, D.M., Hanson, R.K. and Bowman, C.T., "Experimental study and modeling of the reaction $H+O_2+M \rightarrow HO_2+M$ (M=Ar, N_2, H_2O) at elevated pressures and temperatures between 1050 and 1250 K", Physical Chemistry Chemical Physics, 3, 2001, pp. 2337-2342.

40. McLean, I.C., Smith, D.B. and Taylor, S.C., "The use of carbon monoxide/hydrogen burning velocities to examine the rate of the CO + OH reaction", Proceedings of the Combustion Institute, 25, 1994, pp. 749-757.

41. Mueller, M.A., Yetter, R.A. and Dryer, F.L., "Flow reactor studies and kinetic modeling of the $H_2/O_2/NO_x$ and $CO/H_2O/O_2/NO_x$ reactions", International Journal of Chemical Kinetics, 31, 1999, pp. 705-724.

42. Lewis, B. and von Elbe, G., Combustion, Flames, and Explosions of Gases, 3rd ed., Academic, New York, 1987, p. 398.

43. Dean, A.M., Steiner, D.C. and Wang, E.E., "A shock tube study of the $H_2/O_2/CO/Ar$ and $H_2/N_2O/CO/Ar$ systems: Measurement of the rate constant for $H+N_2O \rightarrow N_2+OH^*$", Combustion and Flame, 32, 1978, pp. 73-83.

44. Gardiner Jr., W.C., McFarland, M., Morinaga, K., Takeyama, T. and Walker, B.F., "Initiation rate for shock-heated hydrogen-oxygen-carbon monoxide-argon mixtures as determined by OH induction time measurement", The Journal of Physical Chemistry, 75, 1971, pp. 1504-1509.

45. Tsang, W. and Hampson, R.F., "Chemical kinetic database for combustion chemistry. 1. Methane and related compounds", Journal of Physical Chemistry Reference Data, 15, 1986, pp. 1087-1276.

46. Dean, A.M. and Kistiakowsky, G.B., "Oxidation of carbon monoxide/methane mixtures in shock waves", The Journal of Chemical Physics, 54, 1971, pp. 1718-1725.

47. Kalitan, D.M., Petersen, E.L., Mertens, J.D., and Crofton, M.W., "Ignition of lean CO/H_2/Air mixtures at elevated pressures", Proceedings of GT2006, ASME Turbo Expo 2006: Power for Land, Sea and Air, May 8-11, 2006, Barcelona, Spain, Paper #GT2006-90488.

48. Sun, H.Y., Yang, S.I., Jomaas, G., and Law, C.K., "High-pressure laminar flame speeds and kinetic modeling of carbon monoxide/hydrogen combustion", Proceedings of the Combustion Institute, 31, 2007, pp. 439-446.

CHAPTER 5

TESTING C_1 AND C_2 SUBMECHANISMS

5.1 OVERVIEW

The San Diego Mech grew out of rate-constant evaluations for hydrogen-air diffusion flames [1], augmented by carbon monoxide [2, 3], then methane [4], methanol [5, 6], ethane [7], ethylene [8], acetylene [9, 10], and further extended to propane, propene, propyne and allene [11].

The hydrogen and carbon monoxide submechanism of the San Diego Mech has been validated against various experimental data, and related modifications are reported in Chapter 4. The major path of oxidation for most of the hydrocarbon and alcohol fuels, including ethanol, is via $CH_2O \rightarrow CHO \rightarrow CO \rightarrow CO_2$. Hence, in addition to H_2/CO, the CH_2O submechanism also constitutes an important building block for a detailed reaction mechanism. A few of the important radical production and consumption steps related to the formyl radical could not be tested by testing a submechanism for carbon monoxide. But they play a key role in C_1 (formaldehyde, methane, methanol) submechanisms. In addition, testing of methane and methanol submechanisms provide confidence in reaction-rate constants for elementary reactions related to radicals such as CH_3, CH_2OH and CH_3O. The prediction of trace species, such as soot precursors, in ethanol flames depend on the accuracy of the C_2 submechanism. Hence, in this chapter submechanisms for C_1 (formaldehyde, methane, and methanol) and C_2 (ethane, ethylene, and acetylene) fuels are developed for high-temperature combustion by revising the mechanisms published in [1-11].

Acetaldehyde is an important intermediate in ethanol combustion. The steps related to acetaldehyde combustion are included from [12]. The preliminary tests for ignition delay times are completed here. Nevertheless, there is a need for a thorough study of the acetaldehyde submechanism by studying rate constants for a few key steps in the submechanism [12] and including experimental data on acetaldehyde concentrations in ethanol flames.

Going further with our practice in the development of the San Diego Mech in a hierarchical way, the next step is to test the mechanism for formaldehyde, methane, methanol, ethane, ethylene, and acetylene. The effect of the updates made to C_1 and C_2 chemistry on the propane mechanism are also tested. Finally, the additional steps related to acetaldehyde combustion are tested for autoignition of acetaldehyde. In the following sections, comparisons of the predictions of the San Diego Mech are made with the experimental data available in the literature for the conditions of interest. The experimental conditions and associated references are identified in the Tables 5.1-5.8, where φ denotes equivalence ratio, T temperature in K, and P pressure in atm. Table 5.9 lists all the elementary steps which are updated or added to the reaction mechanisms (published in [1-11]) as a result of these tests. The rate-parameter revisions are discussed in connection with the test for which they are most relevant.

In the following sections, older version of the San Diego mechanism (SD Old) for a particular fuel refers to the mechanisms from [1-11] modified by the submechanisms of the lower fuels which have already been updated during the study. The modifications to the submechanism for the fuel under consideration, based on the updates in reaction-rate constant for certain key steps and tests made against the experimental conditions (Table

5.1 to 5.8), result in a newer version of the San Diego mechanism which we refer here as the San Diego Mech.

In the process of the mechanism development in the following sections, the calculations were carried out using CHEMKIN [44] and FlameMaster [45] programs in accordance with the assumptions and procedures discussed in Chapter 2.

5.2 C_1 FORMALDEHYDE SUBMECHANISM

Both formaldehyde and formyl radical are the critical intermediates in the oxidation of hydrocarbon and alcohol fuels, such as methane, methanol, ethanol, leading to CO and then to CO_2. Previous studies [46, 47, 48, 13, 49] include pyrolysis and oxidation of formaldehyde, where shock-tube autoignition data as well as chemical-kinetic models for formaldehyde combustion were reported. The San Diego Mech was never developed for the formaldehyde combustion, and it has been tested here for the first time. Table 5.1 is a list of the experimental conditions in the shock-tube experiments for which the formaldehyde submechanism was tested in this study. When the SD Old, constituted by reactions related to formaldehyde [4] with the modified H_2/CO submechanism from chapter 4, was tested for the autoignition-delay data, it was found to overpredict the ignition delay times by 4 times at 1340 K and underpredict by 30% at 1700 K. This resulted in an incorrect slope. Since not all initiation steps were present previously, the initiation step $CH_2O+O_2 \rightarrow CHO+HO_2$ and propagation reaction $CH_2O+HO_2 \rightarrow HCO+H_2O_2$ are included. Addition of these reactions and updates in a few steps resulted in good agreement of predictions with the ignition delay times data.

5.2.1 Autoignition of Formaldehyde

Seven mixtures were studied behind reflected shock waves in [13]. They were: (1) Series A: 1.97% CH_2O-Ar; (2) Series B: 1.46% CH_2O-Ar; (3) Series C: 1.47% CH_2O-0.25% O_2-Ar; (4) Series D: 1.0% CH_2O-0.6% O_2-Ar; (5) Series E: 1.5% CH_2O-1.5% O_2-Ar; (6) Series F: 0.49% CH_2O-1.98% O_2-Ar; (7) Series G: 1.0% CH_2O-5.96% O_2-Ar. Mixture compositions covered a range from pure pyrolysis to oxidation of lean, rich, and stoichiometric mixtures. The study covered almost all the conditions found in other studies [46, 47, 48, 49]. The experimental conditions selected from [13], for which the formaldehyde submechanism was developed, are listed in Table 5.1. The first and the second entries correspond to conditions for Series E and F, respectively, in the notation in [13].

Figure 5.1 (a) and (b) shows the comparison of predictions with the experimental data for Series E where symbols represents experimental data, dashed line refers to predictions of the SD Old, and solid line to the predictions of the San Diego Mech. Reference [13] reports three ignition delay time criteria based on 25%, 50% and 75% of the maximum CO concentration emission. The ignition delay times plotted in Figs. 5.1 and 5.2 correspond to 75% of $[CO]_{max}$ which is closer to the widely used temperature inflection criteria, $(dT/dt)_{max}$.

It was observed that the predictions of the SD Old were found to agree well with the experimental data for pyrolysis cases (not shown here). For oxidation cases, the ignition delay times were overpredicted by 4 times at 1340 K while underpredicted by 30% at 1720 K. The recombination reaction $H+O_2+M \rightarrow HO_2+M$, which is temperature independent, competes with $H+O_2 \rightarrow OH+O$ at lower temperatures and results in an

increased concentration of HO_2 radicals. Hence, step 1 of Table 5.9, $CH_2O+HO_2 \rightarrow HCO+H_2O_2$, was added to the formaldehyde submechanism. This step consumes less reactive HO_2 radicals and produces relatively more reactive HCO radicals, thereby lowering the ignition delay times at lower temperatures. The rate-parameter values for step 1 were adopted from [13].

The step 2, $CH_2O+H \rightarrow HCO+H_2$, consumes more reactive H radicals and produces relatively less reactive HCO radicals. The rate-parameter values were updated using [35] which are about two times higher than previously used [37] values. A more recent study [49] of low-temperature autoignition in a shock tube shows similar values for rate constants of the step. This modification improved the comparison at higher temperature values.

There are two initiation steps in the formaldehyde combustion: $CH_2O+M \rightarrow HCO+H+M$ and $CH_2O+O_2 \rightarrow HCO+HO_2$. The reaction-rate parameters for step 3, $CH_2O+M \rightarrow HCO+H+M$, from GRI Mech 1.2 [36], which includes pressure fall-off, were preferred for the updates in the San Diego Mech. The reaction $CH_2O+O_2 \rightarrow HCO+HO_2$, step 4, was included to the formaldehyde submechanism. Since the San Diego Mech is intended for high temperature oxidation processes, this step may be important at all conditions of interest. The values for rate parameters were obtained from [37].

The rate constants for the step 5, $HCO+O_2 \rightarrow CO+HO_2$, from different sources are plotted in the compilation [37], and the recommended value was adopted in [4]. However, from the plots it seems that the recommendation from [38], which was based on the experimental studies, is a better choice. Although the values of [38] at high

temperatures of interest are only 30% greater than those in [37], this modification helps in correlating the numerical and experimental data for formaldehyde ignition delay and in lowering the laminar burning velocities on the lean side in methane and methanol premixed flames, discussed in later sections.

With these above modifications, new formaldehyde submechanism, developed along with updated H_2/CO submechanisms, forms an important and accurate building block for the mechanisms for larger fuels. The reasonably good comparisons of the predictions of the San Diego Mech and the experimental data give confidence in the updated elementary steps and their rate constants. However, there remains a need for the validation of this mechanism for high-pressure data for ignition.

5.2.2 Laminar Burning Velocities of Formaldehyde

Although it would be desirable to test the mechanism against laminar burning velocities of formaldehyde systems for freely propagating flame, no data on this were found in the literature. These comparisons would be helpful in enhancing the accuracy of the kinetic model.

5.3 C_1 METHANE AND METHANOL SUBMECHANISMS

The updates in the hydrogen, carbon monoxide and formaldehyde submechanisms of the San Diego Mech, newer rate-constant data for a few elementary steps, and the availability of newer experimental data motivate the evaluation of the San Diego Mech for C_1 fuels, mainly methane and methanol. The updates in methane and methanol submechanisms need to be done simultaneously because any change made for one affects

the other. The submechanisms for methane and methanol have been developed previously for autoignition delay times for methane [50], for laminar burning velocities for methane [4] and methanol [6], and for diffusion-flame structures for methane [4] and methanol [5, 6]. The methanol submechanism has been extended to autoignition for the first time here. Calculations have been made to ensure that the updates to the San Diego Mech do not deteriorate the agreements of the predictions with the experiments shown in previous studies with the published methane and methanol mechanisms. In addition, the new tests are made for the recently published diffusion-flame extinction data for methane [16] and methanol [26], and nonpremixed flame structures for methanol [27].

5.3.1 Autoignition of Methane

In an extensive study [50], a methane mechanism was developed for autoignition of methane in a shock-tube for temperatures between 1000 K and 2000 K, pressures between 1 bar and 260 bar, and equivalence ratio between 0.4 and 6.0. This mechanism contained elementary steps related to C_1 and C_2 species. Further improvements to this mechanism based on later studies [5-11] are summarized in [11]. The first entry in Table 5.2 corresponds to the first plot in Fig. 2 of article [50]. Figures 5.3 and 5.4 shows the comparison of the experimental data (symbols) listed in Table 5.2 with the predictions of the SD Old (dashed lines) and the San Diego Mech (solid line). The predictions of the SD Old, the mechanism assembled by including reactions from [4, 11] with the modified H_2/CO, CH_2O submechanisms, underpredict the ignition delay times by about 35% through out the temperature range. Similar underpredictions were observed in [50] as well. Hence, there was a need for revision of the steps involved in methane autoignition.

A sensitivity analysis was performed for this case at 1518 K and 1918 K to determine the key reactions with high sensitivity coefficients. The autoignition delay times were found to be very sensitive to the step 6 in Table 5.9, $CH_3+O_2 \rightarrow CH_3O+O$. The previous values for the rate constants were taken from [37], where reaction-rate constants from different sources are plotted together. The recommendation in [39], which was based on experimental values, is 0.2 times the recommendation in [37] was used here. In [4] reaction $CH_3+O_2 \rightarrow CH_2O+OH$ rate-constant values were taken from [39]. This modification in step 6, $CH_3+O_2 \rightarrow CH_3O+O$, also from [39], maintains the branching ratio for these two steps, as recommended in [39].

The solid line, Figs. 5.3 and 5.4, refers to the prediction of the San Diego Mech after implementing the change in step 6. The ignition criteria used in both the cases in experiments and the simulations was time when pressure inflection, $(dP/dt)_{max}$, occurs. The comparisons of the predictions of the San Diego Mech for the data from two experimental conditions in the shock-tube experiments listed in Table 5.2 look acceptable within the experimental uncertainties.

5.3.2 Diffusion-Flame Extinction of Methane

The methane submechanism was developed for diffusion-flame structures and laminar burning velocities [4], and was tested for autoignition [50], but it was never tested for extinction of diffusion flames. There is a newer experimental measurement of methane diffusion flame extinction strain rate [18] in a counterflow setup for the conditions shown in table 5.2. The fuel-stream consists of methane diluted in nitrogen at 298 K, and the oxidizer-stream consists of oxygen and nitrogen mixed with water vapor

at 352 K. The amount of fuel in the fuel stream and the oxygen in oxidizer stream was determined by keeping the adiabatic temperature and stoichiometric mixture fraction constant. The fuel mole fraction in nitrogen varied from 0.35 to 0.40. The distance between the two ducts was 10 mm. The symbols in Fig. 5.5 shows the extinction strain rate plotted against the increasing mass fraction of water vapor in the oxidizer stream. When the mechanism developed in section 5.3.1 was used to calculate the extinction strain rates, the predictions agree well with the data within the experimental uncertainty for zero or lower concentrations of water vapor in the oxidizer stream. For the cases with higher water vapor concentrations, such as Y_{H2O}=0.2, the predicted extinction strain rates were about two times those of the experimental values.

In methane flames, step 7 of Table 5.9 $CH_3+H+M\rightarrow CH_4+M$ is a major route for the termination of reactive radicals H and CH_3. The reaction-rate constant, along with the pressure fall-off for this step in [4], were adopted from [37] and the third-body efficiency for water in the termination step $CH_3+H+M\rightarrow CH_4+M$ was equal to that of the nitrogen. Generic third-body efficiencies [36] were introduced for this step. The efficiencies for different bath gases are 2.0 for H_2, 6.0 for H_2O, 1.5 for CO, 2.0 for CO_2, 2.0 for CH_4, and 0.7 for Ar with respect to N_2. The reaction-rate constant for step 7 [37] with the enhanced chaperon efficiency for H_2O resulted in rate-constant values too high for the H_2O bath gas. An extensive literature review for this step [37, 36, 51, 52, 53] indicates that the Baulch et al. [37] values in Ar bath gas are too high with an order of magnitude discrepancy observed in the rate-constant values in the latest study [53].

In the current study, the GRI Mech [36] values along with the chaperon-efficiency values recommendations were adopted in the C_1 submechanism. The comparisons shown

in Fig. 5.5 between the predictions (solid line) of the San Diego Mech and the experimental values (symbol) are reasonably good. The discrepancies in these values at higher water vapor concentrations are within the experimental uncertainties.

5.3.3 Laminar Burning Velocities of Methane

The predictions of the laminar burning velocities for experimental conditions in Table 5.2 with the mechanism [4] agreed well with earlier data [17]. Advancement in the methods [18] of the counter-flow twin flame techniques led to more accurate measurements of the laminar burning velocities. These values are found to be about 10 % lower than the measurements in [17] in the entire range of equivalence ratios.

The selection of [36] values for step 7 (in Table 5.9) was based on the nature of the slope of k v/s 1/T plot. In the flames this step competes with $CH_3+CH_3+M \rightarrow C_2H_6+M$, and plays a very significant role in C_1 and C_2 chemistry in predicting the laminar burning velocities, and the formation and consumption of CH_4 and C_2H_6 trace species in methane and methanol flames. This selection helped in increasing the near-stoichiometric mixture burning velocities while decreasing these predictions for the rich-side in freely-propagating methane flames.

A few other steps were modified within the uncertainties of their rate-constant values in the literature. Step 8, $HCO+H \rightarrow CO+H_2$, reaction-rate parameters in [4] were used from [2]. The newer values, which are one-half of the values in [2], were used. Values ($A=4.0\times10^{13}$, n=0.0, E=0.0) lower than the ones adopted here are also observed [54]. For the step $HCO+OH \rightarrow CO+H_2O$, step 9 in Table 5.9, previously used reaction-rate values [2] were decreased to Tsang and Hampson's recommendation [40]. Both these

modifications helped in increasing the near-stoichiometric burning velocities by 10%. In [4] for the reaction $CH_3+OH \rightarrow S\text{-}CH_2+H_2O$ (step 10 in Table 5.9), one-fourth of the reaction-rate values from Grotheer et al. [41] were used to fit the burning velocities data with a different H_2/CO submechanism. In the present study, with a better H_2/CO, CH_2O submechanisms, the original Grotheer et al. [41] recommendation for step 10 improves the agreement between predictions and data near the stoichiometric conditions.

The step 11, $CH_3+HCO \rightarrow CH_4+CO$, is added to the mechanism for the first time. It lowers the flamespeed in the rich side by consuming CH_3 radicals, which are relatively higher in concentration on the rich side in methane and methanol flames. Since the Tsang and Hampson [40] values for prefactor $A=1.0\times10^{14}$ seemed to be a too high, one-half of this value was used in the present study.

The comparisons of the predictions of laminar burning velocities with the experimental values selected in Table 5.2 are shown in Fig. 5.6. In reference [18] "Su, ex" denotes the burning velocities at zero strain rate determined by the linear-extrapolation method (old method), and "Su, tr" denotes the true value of the burning velocities at zero strain rate determined by a new method. The predictions with the current mechanism are in better agreement with the data in [18], confirming the choice of reaction-rate values for the key elementary reactions, since these are the most accurate experiments.

5.3.4 Diffusion-Flame Structure of Methane

The mechanism [4] was developed for methane flames and was validated against the data, listed in Table 5.2, for partially premixed flame in a counterflow setup. The fuel

stream consists of fuel-air mixture with equivalence ratios ranging between 1.5 and 3.0. The strain-rates value of 50 s^{-1} was reported in the article by assuming potential flow. The distance between the ducts was 18 mm.

The calculation for φ = 2.5 case is repeated with the San Diego Mech for the conditions in Table 5.2. Because of the lack of information about the input velocities of fuel and oxidizer streams, plug-flow conditions were assumed in the calculations. Corresponding to the input velocities used, the plug-flow strain rate on the oxidizer side was found to be 23 s^{-1}. Figure 5.7 (a) compares the predictions with the concentration profiles of CH_4, O_2, N_2, CO, CO_2, H_2, and Fig. 5.7 (b) reports temperature profiles, and the concentrations of the trace species (C_2H_2+C_2H_4, C_2H_6), and the NO production in the flame. The agreements are found to be similar for most of the data and in the case of C_2H_2+C_2H_4 and NO better than those in [4].

5.3.5 Autoignition of Methanol

Methanol is a basic alcohol fuel. The methanol mechanism was developed for partially premixed flame structures and burning velocities of freely-propagating flames [5, 6], but it was never developed for methanol autoignition. The mechanism has been augmented and tested for methanol autoignition for the first time in this study. The SD Old mechanism was assembled by mechanism from [11] and updated with the modified H_2/CO, CH_2O and CH_4 submechanisms of the present study. Figure 5.8 shows the comparison of experimental data (symbols) for the conditions of the first entry [19] of Table 5.3 with the predictions of the SD Old (dashed line) and from the San Diego Mech (solid line). The article [19] presented ignition delay times which were based on the onset

of CO_2 and OH. The experimental data plotted in Fig 5.8 is based on onset of CO_2. The numerical prediction is based on the inflection of $[CO_2]$, $(d[CO_2]/dt)_{max}$. This could be the reason for the slight overprediction of the data using the San Diego Mech. When the SD Old was used for the numerical prediction of autoignition delay times (dashed line in Fig. 5.8), the predictions were found to be two times larger than the experimental data. An addition of one important initiation step resulted in improving the agreement of prediction of the San Diego Mech with the experimental data.

There are three different routes for methanol initiation reaction [36], $CH_3OH+M \rightarrow CH_3+OH+M$, $CH_3OH+M \rightarrow CH_3O+H+M$, $CH_3OH+M \rightarrow CH_2OH+H+M$. Through sensitivity analysis and reaction flux analysis it was observed that the dependence of ignition delay times on the later two steps was insignificant. Hence only the first step, $CH_3OH+M \rightarrow CH_3+OH+M$, was included in the methanol submechanism. The reaction-rate parameters were adopted from Held and Dryer [42], which were based on the recommendation of [40]. In [42] the chaperon efficiencies for all the species were assumed to be 1.0. In the present study the generic chaperon efficiencies from GRI Mech [36] are included for this step. The reaction rate constant values are listed in Table 5.9 as step 12.

A wide range of mixtures were studied [20] out of which four conditions were selected to test the mechanism. The ignition delay times were defined as the time when the maximum of the product of the concentration of O and CO occurs. The experimental conditions are listed as entry 2 to 5 in Table 5.3. Figures 5.9 (a)-(d) show the comparison of ignition delay times data [20] with predictions of the San Diego Mech. The agreements show that the inclusion of a single initiation step with the selected rate parameters is

sufficient to enhance the San Diego Mech capabilities to methanol ignition, and at the same time keep the mechanism short.

5.3.6 Laminar Burning Velocities of Methanol

Li and Williams [6] tested the methanol mechanism for laminar burning velocities. The experimental data (symbols) is plotted in Fig. 5.10. The experimental conditions and methods of measurements are provided in the literature listed in Table 5.3. There is a lot of scatter in the data, especially near stoichiometric conditions. In [6], the predictions of the mechanism agreed well with the data from Gülder [23]. Gülder [23] data near stoichiometric conditions is 15% higher than those in [25]. The laminar burning velocities in [25], which were based on the counterflow twin-flame technique with stretch corrections applied, are expected to be more accurate, hence are chosen as the target values for the methanol mechanism development in the present study.

The SD Old mechanism was assembled with the mechanism published in [11] modified by the H_2/CO, CH_2O submechanisms from this study. When the predictions (dashed line) of this mechanism are plotted in Fig. 5.10 with the experimental data, 18% underprediction is observed. However, when the modified CH_4 submechanism from the current study was substituted in the SD Old mechanism, relatively better agreements were observed. However, the rich side burning velocities were overpredicted by about 10% compared to the data in [25]. This was observed mainly due to the lowering of the reaction-rate constant of step $CH_3+H+M \rightarrow CH_4+M$.

The burning velocities greatly depend on the branching ratios of radical attack on the fuel molecule, such as

$$CH_3OH+H \rightarrow CH_2OH+H_2, \quad \text{(R1)}$$

$$CH_3OH+H \rightarrow CH_3O+H_2, \quad \text{(R2)}$$

$$CH_3OH+OH \rightarrow CH_2OH+H_2O, \quad \text{(R3)}$$

$$CH_3OH+OH \rightarrow CH_3O+H_2O, \quad \text{(R4)}$$

where CH_2OH is more stable compared to CH_3O. A new theoretical study [43] based on RRKM calculations and comparison of the rate constants with the existing experimental values recommended the rate constant for the step $CH_3OH+H \rightarrow CH_2OH+H_2$ and $CH_3OH+H \rightarrow CH_3O+H_2$ where the branching ratio, R1/R2, is 32 at 1000 K and 9 at 2000 K. The previous reaction rate constants in [6] correspond to a branching ratio (R1/R2) of 0.8 at 1000 K and 0.6 at 2000 K. Rate parameter values for $CH_3OH+OH \rightarrow CH_3O+H_2O$ were obtained from GRI [36] in [6], where the branching ratio of the rate constant of step $CH_3OH+OH \rightarrow CH_2OH+H_2O$ to the rate constant of step $CH_3OH+OH \rightarrow CH_3O+H_2O$ was about 0.5. Bott and Cohen [55] suggested branching ratio for these steps to be 1.0. Hence, for reaction $CH_3OH+OH \rightarrow CH_3O+H_2O$, prefactor value was reduced by a factor of 0.7 to enhance the branching ratio (R3/R4) to 0.8. The current modifications caused the desired decrease in burning velocities on the rich side, as seen in Fig. 5.10.

The step 16, $CH_3O+M \rightarrow CH_2O+H+M$, from [41] was reduced by a factor of 5.5 in [6] to fit the burning velocities with the mechanism consisting of a different H_2/CO submechanism. In the methanol mechanism with the improved hydrogen, carbon monoxide, formaldehyde, and methane submechanisms, the original values were adopted from [41]. The rate constant in [41] was proposed from experiments in an argon gas bath. The generic chaperon efficiencies based on GRI [36] recommendations were added to this reaction as well. Since the third-body efficiencies for argon is 0.7 times that of the

value of nitrogen, and all the chaperon efficiencies values are with respect to $\eta_{N_2} = 1.0$, the prefactor of step 16 in Table 5.9 was divided by 0.7 resulting in prefactor value $A=7.8\times10^{13}$. This modification increased the burning velocities, especially near the stoichiometric conditions and improved the agreement with the experimental data [25].

The San Diego Mech, which includes the reaction mechanism from [11] modified by the H_2/CO, CH_2O, CH_4 and the modifications in the present section, was used in the calculations of the laminar burning velocities. Figure 5.10 shows the comparison of predictions and experimental data where the mechanism has targeted the experimental data in [25]. The agreements are reasonable in the rich and lean side, but at φ=1.1 values are underpredicted by 6% compared to what is believed to be the best experimental value. Figure 5.11 shows another set of experimental data from [25] for methanol-air mixtures at different initial temperatures. The agreements are reasonable within the experimental uncertainties.

5.3.7 Diffusion-Flame Structure of Methanol

The methanol mechanism was developed for the partially premixed flame structures in counterflow setup [5, 6]. The fuel stream consisted of fuel-air mixture with fuel-stream equivalence ratios of 2.0 and 2.3. The oxidizer stream was air. The strain-rates value of 50 s^{-1} was reported in the article by assuming a potential flow. The distance between the ducts was 18 mm.

The calculation for the φ = 2.0 case was repeated with the San Diego Mech for the conditions in Table 5.3. Because of the lack of information about the input velocities of fuel and oxidizer streams, the plug-flow conditions were assumed in the calculations.

Corresponding to the input velocities, the plug-flow strain rate on the oxidizer side was found to be 56 s^{-1}. Figure 5.12 (a) compares the predictions of the San Diego Mech with the concentration profiles of CH_3OH, O_2, N_2, CO, CO_2, H_2, and Fig. 5.12 (b) reports temperature profiles, and the concentrations of the trace species C_2H_2+C_2H_4+C_2H_6, and CH_4 production in the flame. The agreements of the predictions of the SD Old were found to be similar to those in [5] for most of the data, except that for CH_4, where the peak concentration was overpredicted by two times. These calculations are not shown in Figs. 5.12 (a) and 5.12 (b).

The methane formation in methanol flames occurs via $CH_2OH+H \rightarrow CH_3+OH$ and $CH_3+H+M \rightarrow CH_4+M$. A discussion on the reaction-rate constant for step $CH_2OH+H \rightarrow CH_3+OH$ was presented in [6]. In [6] the rate constant for this reaction was one-forth of the backward rate constant of Grotheer et al. [41]. When the backward rate constant was obtained with the newer thermodynamic data for CH_2OH, taking one-forth of their values resulted in reaction rate constant 30% lower than those used by [6]. The lowered rate constant of reaction $CH_2OH+H \rightarrow CH_3+OH$ helped in lowering the peak CH_4 concentration; predictions of the San Diego Mech are shown in Fig 5.12 (b). Though the peak CH_4 concentartion was still 15% higher it was well within the experimental error.

The San Diego Mech predictions were also compared with the newer data on nonpremixed flame structure in counterflow setup [26] in Fig 5.13 (a) and (b). The fuel stream consisted of 30% methanol in nitrogen. The oxidizer stream was air. These experiments were performed by carefully maintaining the plug-flow conditions at the duct exits. The plug-flow strain rate on the oxidizer side was 100 s^{-1}. The distance between the ducts was 10 mm. In the calculations, the exact conditions for velocity and

composition for fuel and oxidizer streams as in experiments were implemented. The predictions are compared for temperature and concentration profiles of CH_3OH, O_2, N_2, CO, CO_2, H_2O, H_2 in Fig. 5.13 (a) and CH_4, C_2H_2+C_2H_4, and C_2H_6 in Fig. 5.13 (b). The experiments and predictions agree well except for C_2H_2+C_2H_4, where the prediction of the peak concentration is lower by 20 %.

5.3.8 Diffusion-Flame Extinction of Methanol

The newer data on extinction strain rate for nonpremixed flame were reported recently [27]. The experimental conditions are listed in Table 5.3. Figure 5.14 shows the plot of extinction strain rates against increasing mass fraction of fuel in the fuel stream. The fuel stream consisted of methanol diluted in nitrogen flowing against the oxidizer stream, which was air. The distance between the ducts was 10 mm. The predictions using the San Diego Mech with two different transport models - multicomponent and mixture averaged values - are presented. Although the multicomponent diffusion model is considered better, the agreements of results using the mixture-averaged model are found to be better. At lower fuel mass fractions, the extinction strain rate values from the multicomponent and mixture averaged transport models are similar. At a fuel mass fraction of 0.3 the predicted values are lower by 10% for mixture averaged and by 20% for the multicomponent case compared to the experimental data. There is a need for more research in the kinetic model for this set of experiments. Relatively lower temperatures are encountered in flames at strain rates as high as these. Hence, there is a need to review the temperature dependence of the reaction rate for key reactions for these cases and of the transport properties.

5.4 C_2 SUBMECHANISM

Since C_2 chemistry plays an important role in determining the soot precursors (sum of C_2H_2, C_2H_4, and C_2H_6) in ethanol flames, it is very important to establish confidence in elementary steps related to ethane, ethylene and acetylene. It also establishes confidence in the rate constants used for steps $CH_3+H+M\rightarrow CH_4+M$ and $CH_3+CH_3+M\rightarrow C_2H_6+M$, and the extent of competition between these two steps for CH_3 radicals. The first step is one of the major sources of formation and consumption of CH_4, while the second step is for the formation of C_2H_6. Correct rate constants for these two steps facilitate the accurate prediction of the soot precursors in flames for practical fuels.

The mechanism for ethane was first developed by Waly et al. [7] for partially premixed flame structures. The mechanism for ethylene was developed by Bala and Williams [8] for ignition delay in shock tubes. The mechanism for acetylene was developed by Waly et al. [9] for laminar partially premixed flame structures. It was also tested for laminar burning velocities for ethane, ethylene, and acetylene in the same article. This mechanism was further enhanced for autoignition delay times for acetylene in [10]. In the following sections, a few of these calculations are repeated with the updated San Diego Mech to assess the effect of modifications in the hydrogen, carbon monoxide, and C_1 chemistry on the C_2 submechanism.

5.4.1 Laminar Burning Velocities of Ethane, Ethylene, and Acetylene

The C_2 submechanism was tested [9] for freely propagating flame burning velocity data for mixtures of ethane, ethylene, acetylene at an initial temperature and pressure of 298 K and 1 atm, respectively against the experimental conditions listed in

Tables 5.4, 5.5, and 5.6. As has been seen for methane in a previous section, recent burning velocity measurements for ethane in [18] were found to be lower than the previous data [17, 22, 29]. In the present study, modifications in the ethane submechanism were targeted to match data in [18] as it is expected to be more accurate because of the new methodology used for stretch-effect correction.

Figure 5.15 shows the comparison of experimental data (symbols) with the predictions of the SD Old mechanism (dashed line) and the San Diego Mech (solid lines). The SD Old mechanism was assembled from reactions in [11] and modified by the updated H_2/CO, CH_2O, and C_1 submechanisms. The predictions of this mechanism were found to be 10% higher than the experimental data in the near-stoichiometric and rich side. The sensitivity analysis was done for φ=1.0 and 1.6. The laminar burning velocities were found to be highly sensitive to the reaction 17, $C_2H_3+H \rightarrow C_2H_2+H_2$. This reaction terminates highly reactive H atoms to form stable products. The reaction-rate parameter values $A=4.0\times10^{13}$, n=0.0, E=0.0 are used, which results in reaction rate constant values 3.3 times the previous value [37]. The updated rate parameters lie within the uncertainty of the rate-constant values from the literature. The higher value of $A=9.6\times10^{13}$, n=0.0, E=0.0 were recommended in the compilation by Tsang and Hampson [40]. With just this one modification, the predictions of the San Diego Mech agreed well against [18] experimental data, Fig. 5.15. The agreements improved in the rich side and remain the same in the lean side.

The mechanism in Waly [9] was tested for ethylene and acetylene for the experimental conditions as listed in Tables 5.5 and 5.6. The initial mixtures were diluted in N_2 with a dilution factor f=0.1 and f=0.13 for ethylene and acetylene, respectively. The

dilution factor was defined as $f = [O_2]/([O_2]+[I])$, where I is the inert gas. The lower dilution factors were employed due to safety reasons associated with mixture pressure above 1.0 atm, especially for acetylene-air mixture.

The tests for ethylene-air and acetylene-air mixtures were repeated with the updated San Diego Mech. Figure 5.16 show the comparison of the experimental ethylene-air laminar burning velocities data with the numerical predictions of the San Diego Mech. Figure 5.17 shows the comparison of experimental acetylene-air laminar burning velocities data with numerical predictions of the San Diego Mech. The updated values for the rate constants for step $C_2H_3+H \rightarrow C_2H_2+H_2$ helped in lowering the burning velocities by 10% in the rich and near-stoichiometric conditions in ethylene and acetylene flames as well.

5.4.2 Autoignition of Ethane, Ethylene, and Acetylene

The C_2 mechanism in [7, 9, 11] was tested for autoignition of ethylene [8] and acetylene [10], but never tested for ignition of ethane. Table 5.4 lists the experimental condition for which the San Diego Mech, consisting of reactions from [11] modified by updates in the H_2/CO, CH_2O, C_1 and C_2 submechanisms of this study, was tested. Figure 5.18 shows the comparison of predictions (lines) with the experimental data (symbols). The ignition delay times were defined in the article based on the inflection of the concentrations of CO_2, OH and CH. The predictions of the San Diego Mech are plotted based on inflection of [CO_2] and [OH]. The agreements between the predictions and the experimental data are reasonable within the uncertainties in the experimental data. One elementary step $C_2H_6+HO_2 \rightarrow C_2H_5+H_2O_2$ has been added to the mechanism, with rate

constant values adopted from Baulch et al. [37] In sensitivity analyses, ignition delay time was found to be insensitive to this step. However, H abstraction by HO_2 radical attack on fuel plays a major role in the analytical formula for ignition delay time, motivating the inclusion of this step to the mechanism. This will be discussed further in Chapter 7.

The mechanisms were developed [8] for autoignition of ethylene/oxygen mixtures diluted in nitrogen or argon for φ=0.5-2.0 in the temperature and pressure ranges of 1000-2300 K and 0.4-6.7 bar, respectively. The experimental data with similar conditions were used in [10] for acetylene autoignition. The fuel/O_2 mixture in nitrogen or argon for φ=0.006-2.0 in the temperature and pressure ranges of 1000-2300 K and 0.7-9.4 bar, respectively were used for the tests. One of these conditions for ethylene and acetylene fuels was selected to test the San Diego Mech developed in this study. These experimental conditions are listed in Tables 5.5 and 5.6.

The comparison of experimental ignition delay times and their numerical predictions of the San Diego Mech are found to be same as those in previous studies or better, as seen in Figs. 5.19 and 5.20.

5.4.3 Partially Premixed Flame Structure of Ethane

The ethane mechanism was originally developed for partially premixed flame structures by Waly [7] in a counterflow setup. The strain-rate value of 90 s^{-1} was reported in the article. The distance between the ducts was 15 mm. The calculation for the φ = 2.2 case was repeated with the San Diego Mech for the conditions in Table 5.4. Because of the lack of information about the input velocities of fuel and oxidizer streams, the plug-

flow conditions were assumed in the calculations. Corresponding to the input velocities, the plug-flow strain rate on the oxidizer side was found to be 80 s^{-1}. The tests were repeated here with the San Diego Mech to assess its performance under these conditions. Figures 5.21 (a), (b), and (c) show the profiles for the temperature and concentration profiles of C_2H_6, CO, CO_2, C_2H_2, C_2H_4, and CH_4. The agreements of the predictions of the San Diego Mech with the experimental values are within the experimental error except in the case of methane where the peak CH_4 concentration is overpredicted by 50%.

5.5 GENERIC CHAPERON EFFICIENCIES

In addition to the modifications described in the sections above, the generic third-body efficiencies were included for following three-body reactions based on the GRI Mech [36] recommendations.

$$CH_3+CH_3+M\rightarrow C_2H_6+M$$

$$C_2H_6+M\rightarrow C_2H_5+H+M$$

$$C_2H_5+M\rightarrow C_2H_4+H+M$$

$$C_2H_4+M\rightarrow C_2H_3+H+M$$

$$C_2H_4+M\rightarrow C_2H_2+H_2+M$$

$$C_2H_3+M\rightarrow C_2H_2+H+M$$

It has been observed that many other mechanisms in the literature do not use the chaperon-efficiencies for all the three body reactions consistently. The chaperon efficiency for H_2O and CO_2, when used equal to that of N_2, can be critical in calculations of flame structures and burning velocities in the oxidation-zone where high

concentrations of water vapor, carbon monoxide and carbon dioxide are observed. However, more thorough evaluation of the effect of the inclusion of these third-body efficiencies is required. For this, experiments at high pressures with different bath gases are required.

5.6 PROPANE SUBMECHANISM

The submechanism for propane was developed by Petrova and Williams [11] in an extensive study for autoignition delay times and laminar burning velocities. A few of these tests are repeated here to assess the effect of the modifications in the San Diego Mech based on the present study. The experimental conditions are listed in table 5.7. Figure 5.22 presents a comparison of auotingition delay time predictions of the San Diego Mech with the experimental data. Figure 5.23 shows the comparison of the predictions of the San Diego Mech with laminar burning velocities data. In reference [18] "Su, ex" denotes the burning velocities at zero strain rate determined by the linear-extrapolation method (old method), and "Su, tr" denotes the true value of the burning velocities at zero strain rate determined by the new method. Both the predictions agree well with the experimental data. However, there is a need to identify the reason for the underprediction of about 5 % of the rich-side burning velocities. Also, the effect of the inclusion of generic chaperon-efficiencies to the three-body reactions needs to be evaluated.

5.7 ACETALDEHYDE SUBMECHANISM

Acetaldehyde is one of the major routes in the combustion of ethanol in counterflow diffusion flames studied in Chapter 6. The elementary reactions related to acetaldehyde that were taken from [12] are listed in Table 5.9 as steps 20-41. These 22 reactions involve acetaldehyde or one of the two isomers produced by abstraction of H from it, CH_2CHO and CH_3CO. The mechanism was tested for the experimental conditions listed in Table 5.8. The ignition time in experiments and numerical calculations was based on onset of rapid pressure rise. Figure 5.24 shows the comparison of the predictions of the San Diego Mech with the experimental data. There is an underprediction of ignition delay times for the φ=0.5 case by 20%. However, within the experimental uncertainties, these agreements are reasonable and give credence to the predictions of the concentration of acetaldehyde in ethanol flames that are presented in Chapter 6.

There is a need for the re-evaluation of the step 21, $CH_3CO+M \rightarrow CH_3+CO+M$. The rate constant for this step was based on the recommendation of Warnatz [56]. Further refinement of acetaldehyde submechanism is needed.

5.8 CONCLUSIONS

A thorough testing of the submechanisms of formaldehyde, methane, methanol, ethane, ethylene, and acetylene fuels in the San Diego Mech has been conducted. Tests were also made for propane and acetaldehyde fuels with the updated San Diego Mech. The updates in the rate constant of a few key reactions, and the newly included reactions are reported along with the significance for these changes. The mechanism is developed for the autoigntion of formaldehyde, methanol, and ethane for the first time. Various tests

have been repeated for the abovementioned fuels for selected experimental conditions, as mentioned in the articles where the mechanism for the particular fuel was first developed. The comparisons of predictions with the experimental data are found to be as good as those in the original publications or even better in some cases. The San Diego Mech developed in this chapter is ready to be used for fuels such as formaldehyde, methane, methanol, ethane, ethylene, acetylene, acetaldehyde, and propane. It also forms a robust building block for the ethanol mechanism developed in the next chapter. However, the need remains for further research in assessing the performance of the mechanism for various components at high pressure experimental conditions.

Table 5.1 Formaldehyde Experiments

Experiment	Mixture	φ	T (K)	P (atm)	Ref.
Shock-tube	1.5%CH_2O/1.5%O_2 /97.0%Ar	1.0	1338-1941	0.77-2.23	[13]
	0.49%CH_2O/1.98%O_2/97.5%Ar	0.25	1421-1658	0.84-2.10	[13]

Table 5.2 Methane Experiments

Experiment	Mixture	φ	T (K)	P (atm)	Ref.
Shock-tube	3.5%CH_4/7.0%O_2/89.5%Ar	1.0	1516-1918	5.8-8.0	[14]
	9.5%CH_4/19%O_2 /71.5%Ar	1.0	1407-1604	2.3-2.6	[15]
Diffusion flame extinction	$CH_4/O_2/N_2$		298	1.0	[16]
Laminar burning velocities	$CH_4/O_2/N_2$	0.5-2.0	298	1.0	[17], [18]
Diffusion flame structure	$CH_4/O_2/N_2$	2.5	298	1.0	[4]

Table 5.3 Methanol Experiments

Experiment	Mixture	φ	T (K)	P (atm)	Ref.
Shock-tube	2.0%CH_3OH/3.0%O_2 /95.0%Ar	1.0	1573-1860	0.33	[19]
	2.0%CH_3OH/4.0%O_2/94.0%Ar	0.75	1570-1925	1.2-1.74	[20]
	1.0%CH_3OH/1.0%O_2 /98.0%Ar	1.5	1575-2090	2.85-3.25	[20]
	1.0%CH_3OH/4.0%O_2 /95.0%Ar	0.375	1555-2030	2.9-3.2	[20]
	2.0%CH_3OH/1.0%O_2 /97.0%Ar	3.0	1555-1975	2.8-3.2	[20]
Laminar burning velocities	$CH_3OH/O_2/N_2$	0.5-2.0	298	1.0	[21]-[25]
	$CH_3OH/O_2/N_2$	0.5-2.0	318-368	1.0	[25]
Partially premixed flame structure	$CH_3OH/O_2/N_2$	2.0	F: 310 Ox:298	1.0	[5]
Nonpremixed flame structure	$CH_3OH/O_2/N_2$		F: 323 Ox:298	1.0	[26]
Diffusion flame extinction	$CH_3OH/O_2/N_2$		F: 323 Ox; 298	1.0	[27]

Table 5.4 Ethane Experiments

Experiment	Mixture	φ	T (K)	P (atm)	Ref.
Shock-tube	1.11%C_2H_6/3.89%O_2 /95.0%Ar	1.0	1503-1773	0.335	[28]
Laminar burning velocities	$C_2H_6/O_2/N_2$	0.5-1.7	298	1.0	[17], [18], [22], [29]
Diffusion flame structure	$C_2H_6/O_2/N_2$	2.2	298	1.0	[7]

Table 5.5 Ethylene Experiments

Experiment	Mixture	φ	T (K)	P (atm)	Ref.
Shock-tube	1.0%C_2H_4/3.0%O_2/96.0%Ar	1.0	1438-1745	1.0	[30]
Laminar burning velocities	$C_2H_4/O_2/N_2$	0.5-2.0	298	1.0	[17], [22], [29]

Table 5.6 Acetylene Experiments

Experiment	Mixture	φ	T (K)	P (atm)	Ref.
Shock-tube	1.4%C_2H_2/3.6%O_2/95.0%Ar	1.0	1142-1448	1.0-2.6	[31]
Laminar burning velocities	$C_2H_2/O_2/N_2$	0.5-2.0	298	1.0	[17], [22], [32]

Table 5.7 Propane Experiments

Experiment	Mixture	φ	T (K)	P (atm)	Ref.
Shock-tube	0.2%C_3H_8/1.0%O_2/98.8%Ar	1.0	1431-1680	1.5	[33]
Laminar burning velocities	$C_3H_8/O_2/N_2$	0.5-2.0	298	1.0	[18]

Table 5.8 Acetaldehyde Experiments

Experiment	Mixture	φ	T (K)	P (atm)	Ref.
Shock-tube	1.0%CH_3CHO/5.0%O_2/94.0%Ar	0.5	1277-1411	5.0	[34]
	1.0%CH_3CHO/2.5%O_2/96.5%Ar	1.0	1255-1478	5.0	[34]

Table 5.9 Updates to the elementary steps in C_1 and C_2 submechanisms

Reaction		A[a]	n[a]	E[a]	Reference
Based on formaldehyde ignition					
1. $CH_2O + HO_2 \rightarrow HCO + H_2O_2$		4.11×10^{04}	2.50	42.7	[13]
2. $CH_2O + H \rightarrow HCO + H_2$		5.74×10^{07}	1.90	11.5	[35]
3[b]. $H + HCO + M \rightarrow CH_2O + M$	k_0	1.35×10^{24}	-2.60	1.8	[36]
	k_∞	1.09×10^{12}	0.48	-1.1	
4. $CH_2O + O_2 \rightarrow HCO + HO_2$		6.00×10^{13}	0.00	170.2	[37]
5. $HCO + O_2 \rightarrow CO + HO_2$		7.58×10^{12}	0.00	1.7	[38]
Based on methane ignition					
6. $CH_3 + O_2 \rightarrow CH_3O + O$		1.10×10^{13}	0.00	116.4	[39]
Based on methane flame extinction and burning velocities					
7[c]. $CH_3 + H + M \rightarrow CH_4 + M$	k_0	2.47×10^{33}	-4.76	10.2	[36]
	k_∞	1.27×10^{16}	-0.63	1.6	
8. $HCO + H \rightarrow CO + H_2$		5.00×10^{13}	0.00	0.0	See text
9. $HCO + OH \rightarrow CO + H_2O$		3.00×10^{13}	0.00	0.0	[40]
10. $CH_3 + OH \rightarrow S\text{-}CH_2 + H_2O$		4.00×10^{13}	0.00	10.5	[41]
11. $HCO + CH_3 \rightarrow CH_4 + CO$		5.00×10^{13}	-0.00	0.0	See text
Based on methanol ignition					
12[c]. $CH_3OH + M \rightarrow CH_3 + OH + M$	k_0	2.95×10^{44}	-7.35	399.4	[42, 36]
	k_∞	1.90×10^{16}	0.00	383.8	
Based on methanol burning velocities					
13. $CH_3OH + H \rightarrow CH_2OH + H_2$		1.35×10^{03}	3.20	14.6	[43]
14. $CH_3OH + H \rightarrow CH_3O + H_2$		6.83×10^{01}	3.40	30.3	[43]
15. $CH_3OH + OH \rightarrow CH_2OH + H_2$		4.40×10^{06}	2.00	6.3	See text
16[d]. $CH_3O + M \rightarrow CH_2O + H + M$		7.78×10^{13}	0.00	56.5	See text
Based on methanol flame structure					
17. $CH_2OH + H \rightarrow CH_3 + OH$		2.50×10^{17}	-0.93	21.5	See text
Based on C_2 species burning velocities					
18. $C_2H_3 + H \rightarrow C_2H_2 + H_2$		4.00×10^{13}	0.00	0.0	See text
Based on ethane ignition					
19. $C_2H_6 + HO_2 \rightarrow C_2H_5 + H_2O_2$		1.32×10^{13}	0.00	85.6	[37]
Based on acetaldehyde ignition					
20. $CH_3CHO \rightarrow CH_3 + HCO$		7.00×10^{15}	0.00	341.8	[12]
21[e]. $CH_3CO + M \rightarrow CH3 + CO + M$	k_0	1.20×10^{15}	0.00	52.3	[12]

Table 5.9 Continued

Reaction	A[a]	n[a]	E[a]	Reference
k_∞	3.00×10^{12}	0.00	69.9	
22. $CH_3CHO + OH \rightarrow CH_3CO + H_2O$	3.37×10^{12}	0.00	-2.6	[12]
23. $CH_3CHO + OH \rightarrow CH_2CHO + H_2O$	3.37×10^{11}	0.00	-2.6	[12]
24. $CH_3CHO + O \rightarrow CH_3CO + OH$	1.77×10^{18}	-1.90	12.5	[12]
25. $CH_3CHO + O \rightarrow CH_2CHO + OH$	3.72×10^{13}	-0.20	14.9	[12]
26. $CH_3CHO + H \rightarrow CH_3CO + H_2$	4.66×10^{13}	-0.30	12.5	[12]
27. $CH_3CHO + H \rightarrow CH_2CHO + H_2$	1.85×10^{12}	0.40	22.4	[12]
28. $CH_3CHO + CH_3 \rightarrow CH_3CO + CH_4$	3.90×10^{-7}	5.80	9.2	[12]
29. $CH_3CHO + CH_3 \rightarrow CH_2CHO + CH_4$	2.45×10^{01}	3.10	24.0	[12]
30. $CH_3CHO + HO_2 \rightarrow CH_3CO + H_2O_2$	3.60×10^{19}	-2.20	58.6	[12]
31. $CH_3CHO + HO_2 \rightarrow CH_2CHO + H_2O_2$	2.32×10^{11}	0.40	62.3	[12]
32. $CH_3CHO + O_2 \rightarrow CH_3CO + HO_2$	1.00×10^{14}	0.00	176.6	[12]
33. $CH_2CHO + H \rightarrow CH_3 + HCO$	5.00×10^{13}	0.00	0.0	[12]
34. $CH_2CHO + H \rightarrow CH_2CO + H_2$	2.00×10^{13}	0.00	0.0	[12]
35. $CH_2CHO + O \rightarrow CH_2O + HCO$	1.00×10^{14}	0.00	0.0	[12]
36. $CH_2CHO + OH \rightarrow CH_2CO + H_2O$	3.00×10^{13}	0.00	0.0	[12]
37. $CH_2CHO + O_2 \rightarrow CH_2O + CO + OH$	3.00×10^{10}	0.00	0.0	[12]
38. $CH_2CHO + CH_3 \rightarrow C_2H_5 + CO + H$	4.90×10^{14}	-0.50	0.0	[12]
39. $CH_2CHO + HO_2 \rightarrow CH_2O + HCO + OH$	7.00×10^{12}	0.00	0.0	[12]
40. $CH_2CHO + HO_2 \rightarrow CH_3CHO + O_2$	3.00×10^{12}	0.00	0.0	[12]
41. $CH_2CHO \rightarrow CH_3 + CO$	1.17×10^{43}	-9.80	183.3	[12]

[a]Specific reaction-rate constant $k = AT^n e^{-E/R^o T}$; units mol/cm^3, s^{-1}, K, kJ/mol.
[b]Chaperon efficiencies are 2.0 for H_2, 6.0 for H_2O, 1.5 for CO, 2.0 for CO_2, 3.0 for CH_4, 3.0 for C_2H_6, 0.7 for Ar and 1.0 for all other species; Troe falloff with F_c = 0.2176 exp (-T/271.0 K) + 0.7824 exp (-T/2755.0 K) + exp (-6570.0 K/T).
[c]Chaperon efficiencies are 2.0 for H_2, 6.0 for H_2O, 1.5 for CO, 2.0 for CO_2, 2.0 for CH_4, 0.7 for Ar and 1.0 for all other species; Troe falloff with F_c = 0.217 exp (-T/74.0 K) + 0.783 exp (-T/2941.0 K) + exp (-6964.0 K/T).
[c]Chaperon efficiencies are 2.0 for H_2, 6.0 for H_2O, 1.5 for CO, 2.0 for CO_2, 2.0 for CH_4, 0.7 for Ar and 1.0 for all other species; Troe falloff with F_c = 0.586 exp (-T/279.0 K) + 0.414 exp (-T/5459.0 K).
[d]Chaperon efficiencies are 2.0 for H_2, 6.0 for H_2O, 1.5 for CO, 2.0 for CO_2, 2.0 for CH_4, 0.7 for Ar and 1.0 for all other species.
[e]Chaperon efficiencies are 2.0 for H_2, 6.0 for H_2O, 1.5 for CO, 2.0 for CO_2, 2.0 for CH_4, 0.7 for Ar and 1.0 for all other species; Troe falloff with F_c = 1.0.

(a)

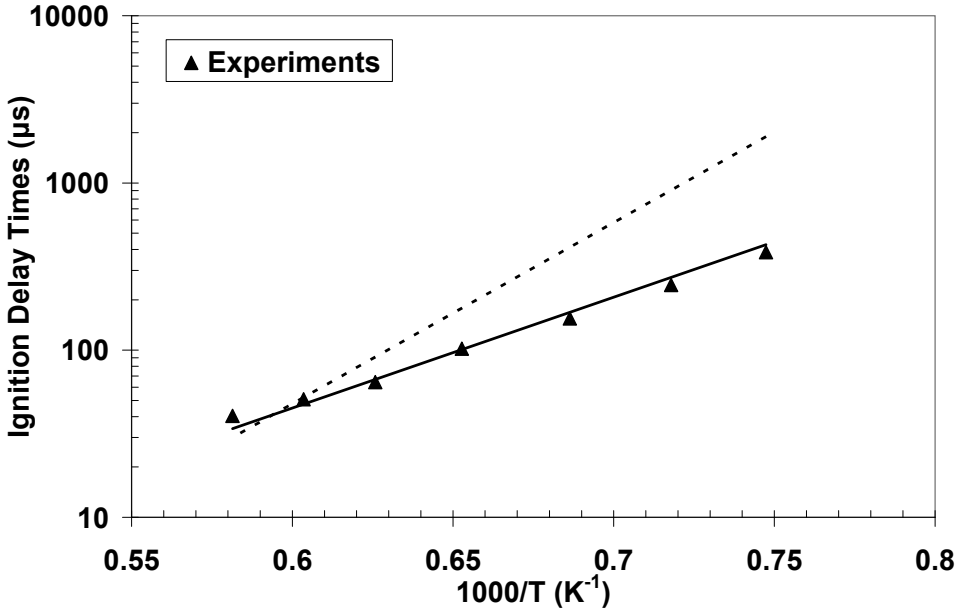

Figure 5.1 (a) Measured [13] and predicted autoignition delay times for Series E mixture φ=1.0 (1.5% CH_2O, 1.5% O_2, and 97.0% Ar by volume) at pressures between 1.2 and 1.5 atm; solid line represents the prediction of the San Diego Mech; dashed line represents the prediction of the SD Old.

(b)

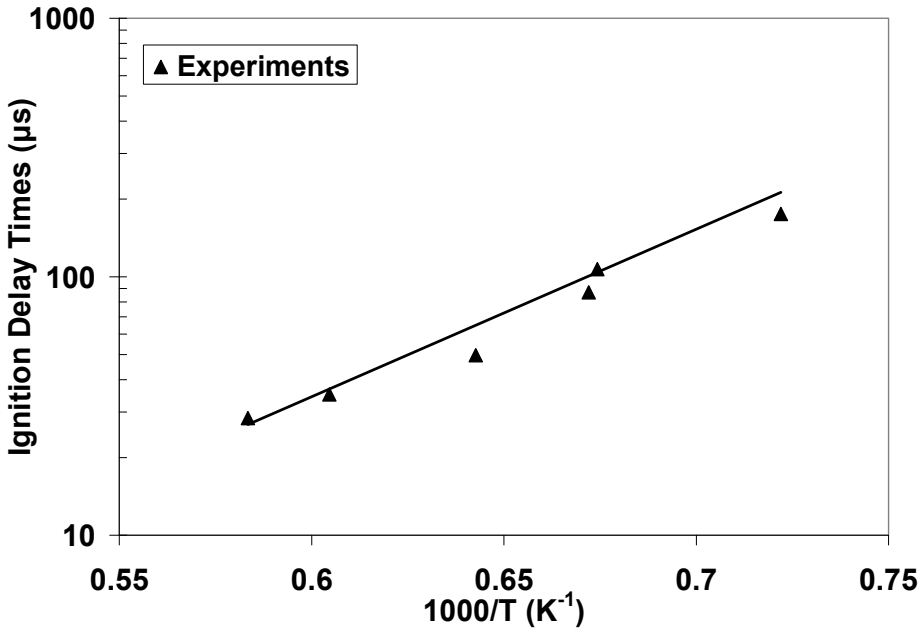

Figure 5.1 (b) Measured [13] and predicted autoignition delay times for Series E mixture φ=1.0 (1.5% CH_2O, 1.5% O_2, and 97.0% Ar by volume) at pressures between 1.8 and 2.2 atm; solid line represents prediction of the San Diego Mech.

(a)

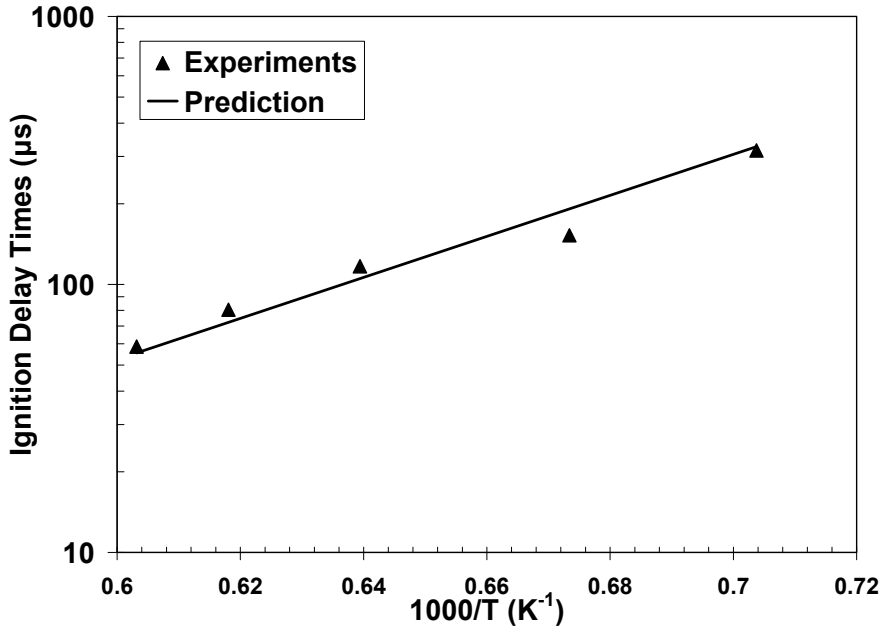

Figure 5.2 (a) Measured [13] and predicted autoignition delay times for Series F mixture φ=0.25 (0.49% CH_2O, 1.98% O_2, and 97.5% Ar by volume) at pressures between 1.25 and 1.43 atm; solid line represents prediction of the San Diego Mech.

(b)

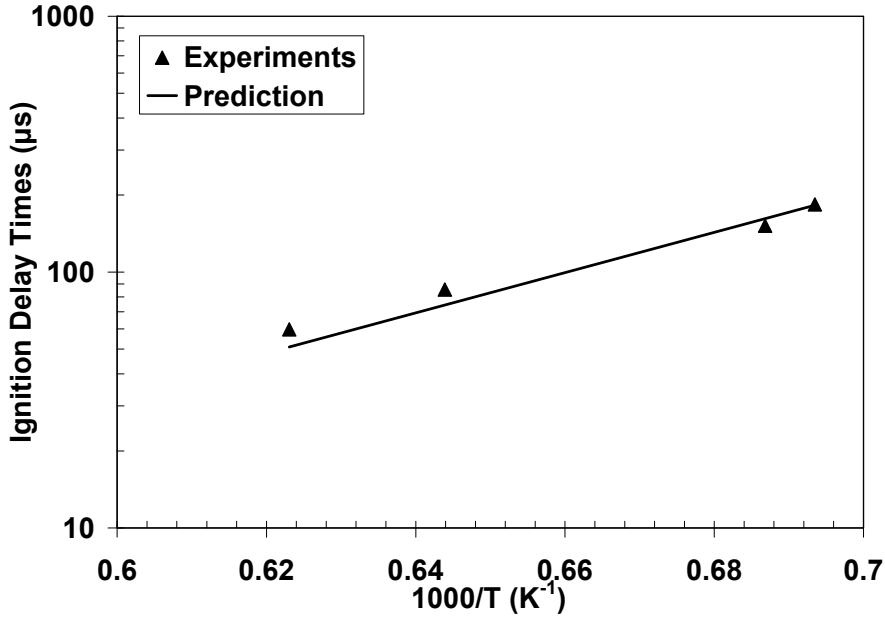

Figure 5.2 (b) Measured [13] and predicted autoignition delay times for Series F mixture φ=0.25 (0.49% CH_2O, 1.98% O_2, and 97.5% Ar by volume) at pressures between 1.89 and 2.0 atm; solid line represents prediction of the San Diego Mech.

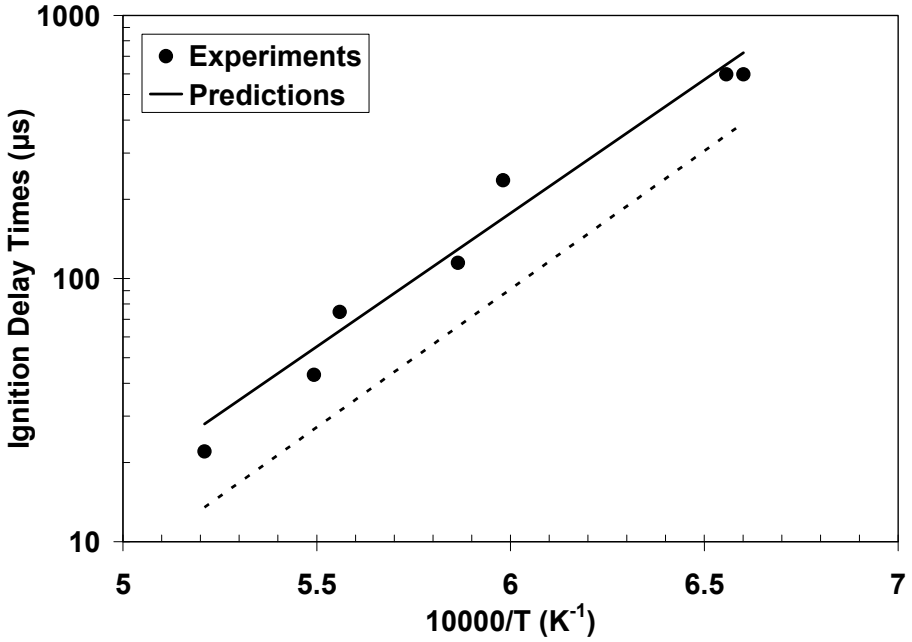

Figure 5.3 Measured [14] and predicted autoignition delay times for methane-oxygen-argon mixture φ=1.0 (3.5% CH_4, 7.0% O_2, and 89.5% Ar by volume) at pressures between 5.8 and 8.0 atm; solid line represents prediction of the San Diego Mech; dashed line represents prediction of the SD Old.

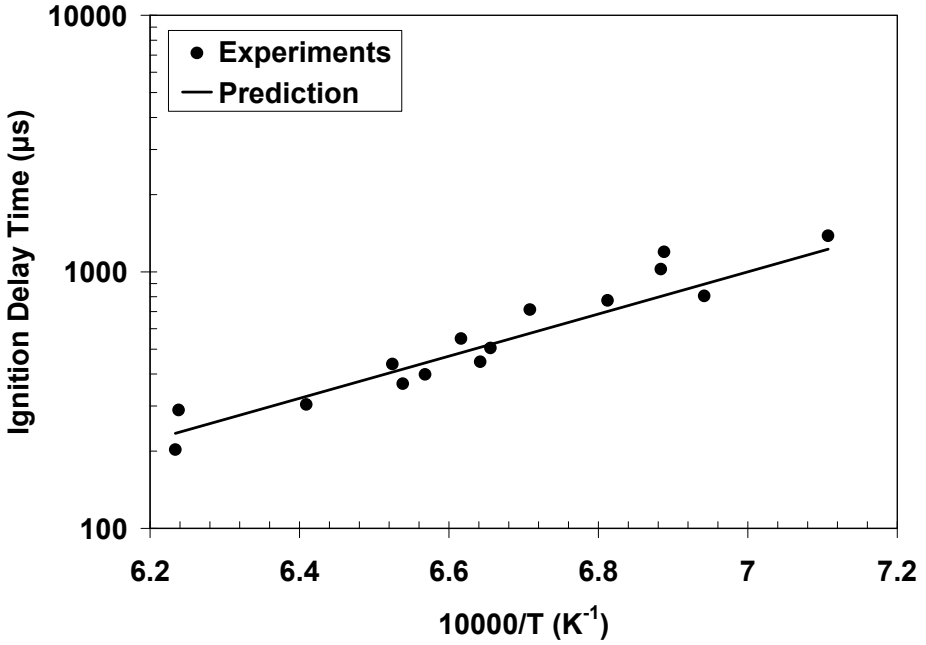

Figure 5.4 Measured [15] and predicted autoignition delay times for methane-oxygen-argon mixture φ=1.0 (9.5% CH_4, 19.0% O_2, and 71.5% Ar by volume) at pressures between 2.3 and 2.6 atm; solid line represents prediction of the San Diego Mech.

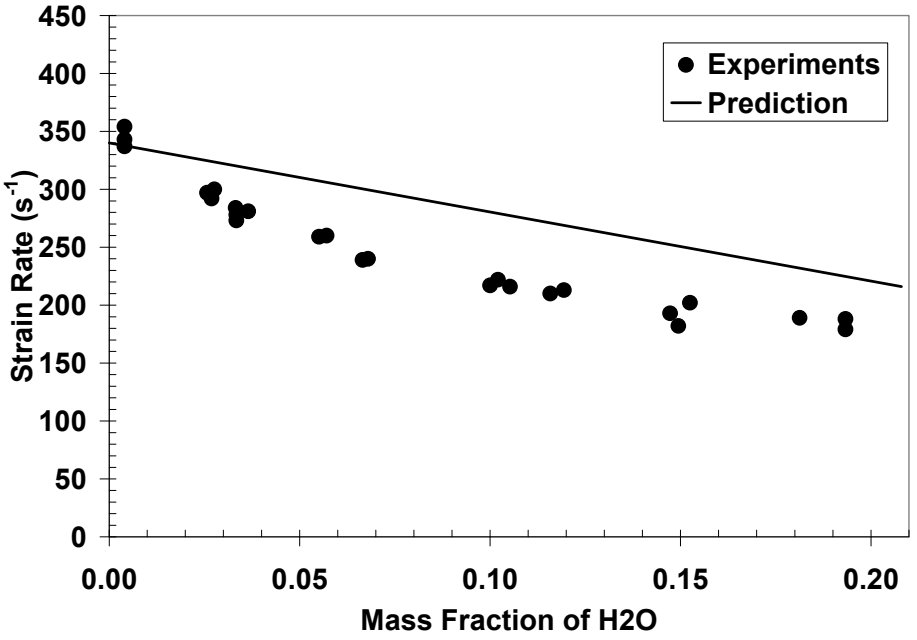

Figure 5.5 Measured [16] and predicted extinction strain rate for a counterflow diffusion flame at P=1 atm as a function of the mass fraction of water in the oxidizer stream having a methane-nitrogen mixture at room temperature as fuel and an oxygen-nitrogen-water mixture at 352 K as oxidizer; solid line represents prediction of the San Diego Mech.

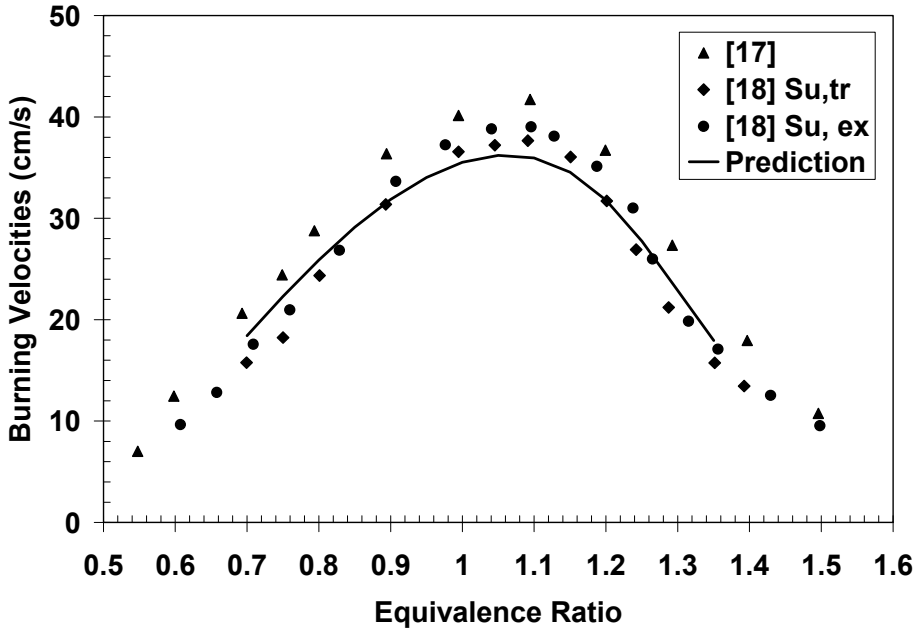

Figure 5.6 Measured [17, 18] and predicted laminar burning velocities for methane-air mixtures at initial temperature of 298 K at P = 1 atm; solid line represents prediction of the San Diego Mech.

(a)

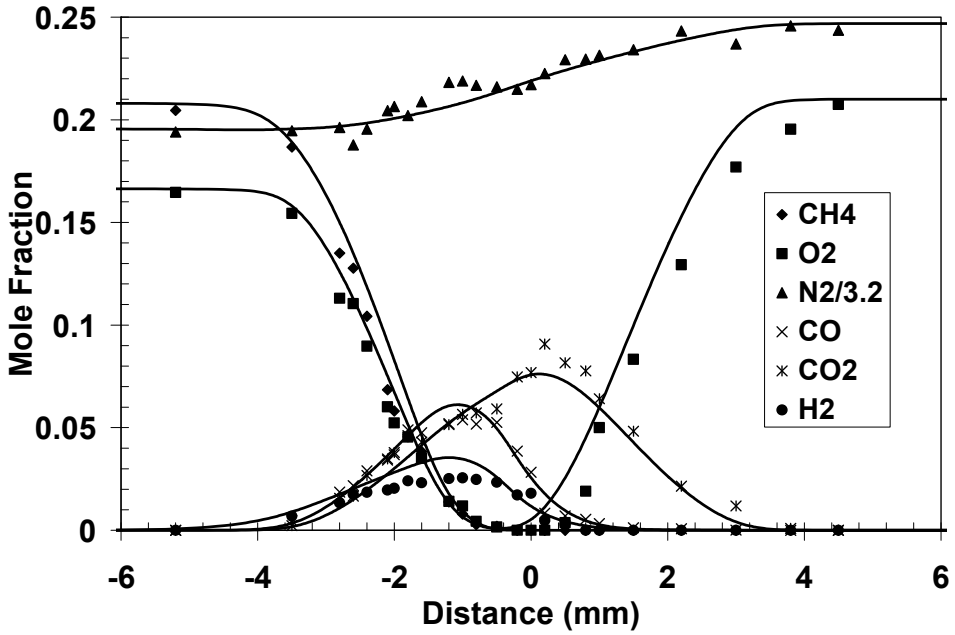

(b)

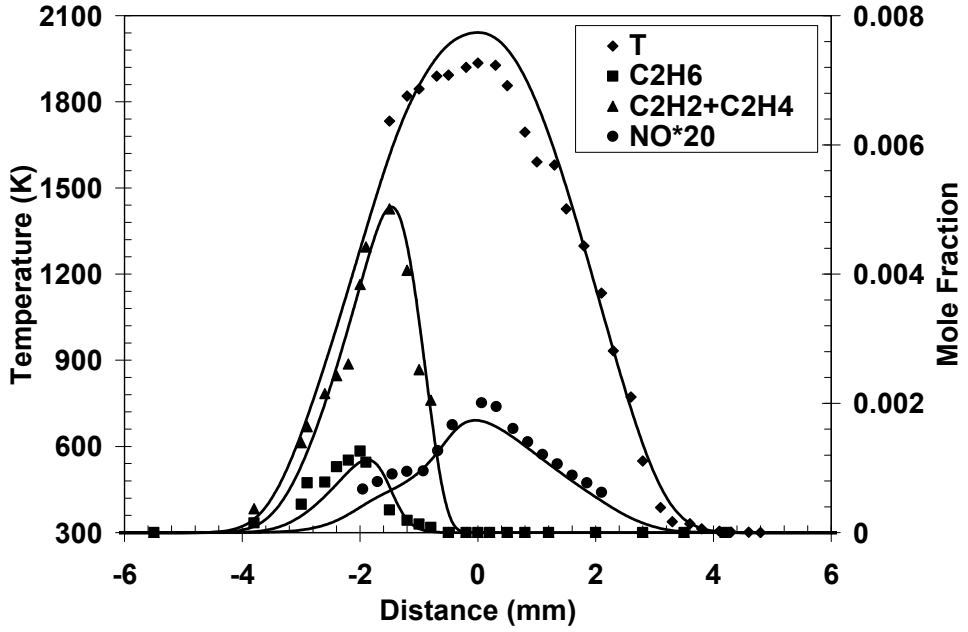

Figure 5.7 Measured [4] and predicted methane-air partially premixed flame structure: (a) Concentration profiles for CH_4, O_2, N_2, CO, CO_2, and H_2, (b) Temperature profile and concentration profiles for C_2H_6, C_2H_2+C_2H_4, and NO; solid line represents prediction of the San Diego Mech.

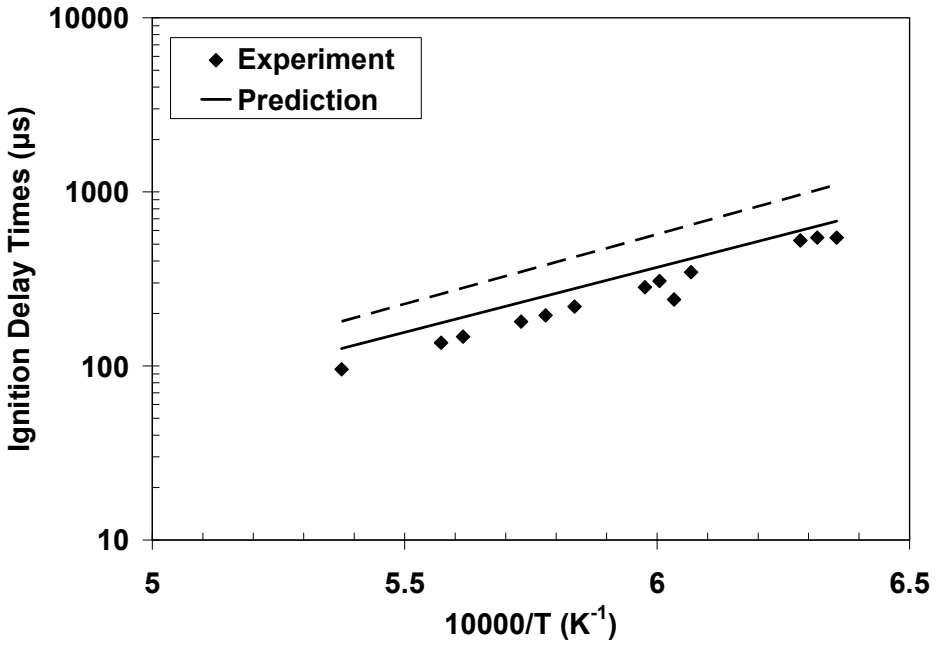

Figure 5.8 Measured [19] and predicted autoignition delay times for methanol-oxygen-argon mixture φ=1.0 (2.0% CH_3OH, 3.0% O_2, and 95.0% Ar by volume) at pressure 0.33 atm; solid line represents prediction of the San Diego Mech; dashed line represents prediction of the SD Old.

(a)

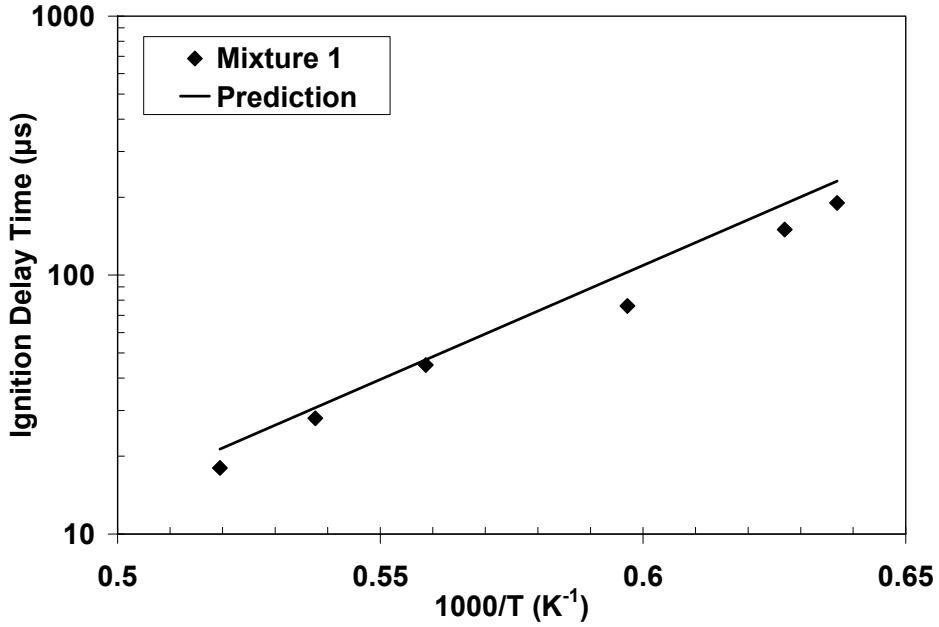

Figure 5.9 (a) Measured [20] and predicted autoignition delay times for methanol-oxygen-argon mixture φ=0.75 (2.0% CH_3OH, 4.0% O_2, and 94.0% Ar by volume) at pressures between 1.2 and 1.74 atm; solid line represents prediction of the San Diego Mech.

(b)

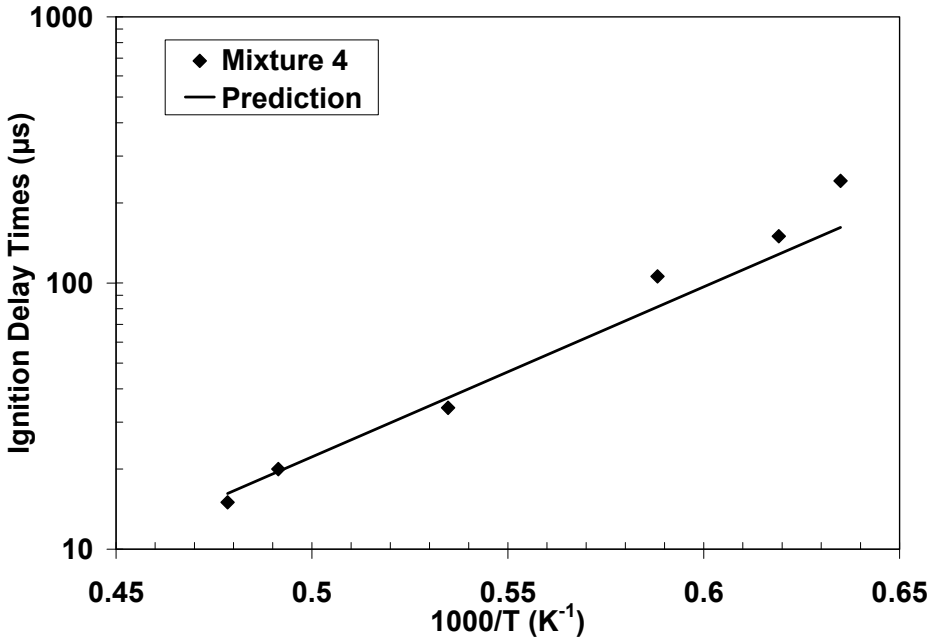

Figure 5.9 (b) Measured [20] and predicted autoignition delay times for methanol-oxygen-argon mixture φ=1.5 (1.0% CH_3OH, 1.0% O_2, and 98.0% Ar by volume) at pressures between 2.85 and 3.25 atm; solid line represents prediction of the San Diego Mech.

(c)

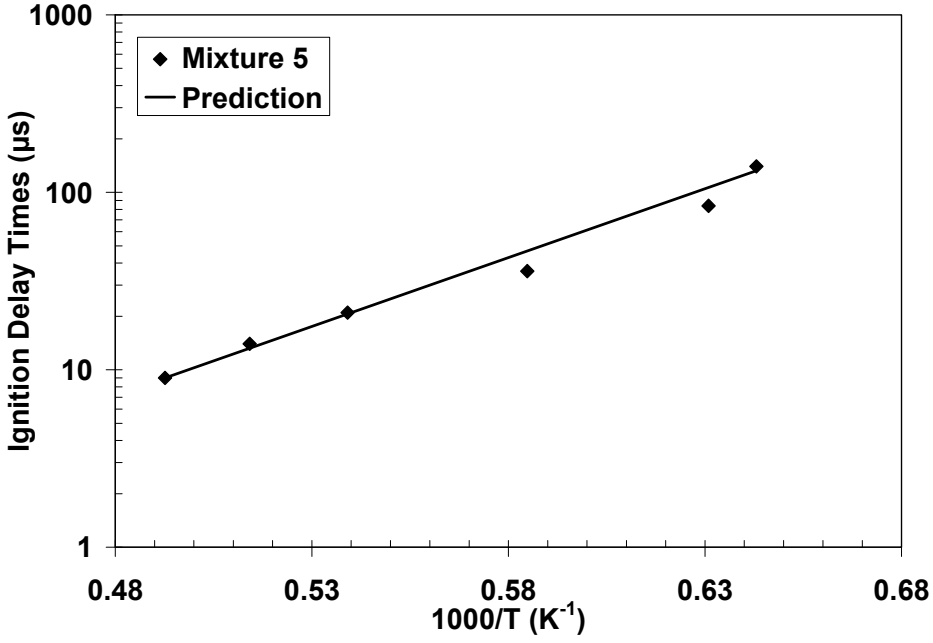

Figure 5.9 (c) Measured [20] and predicted autoignition delay times for methanol-oxygen-argon mixture φ=0.375 (1.0% CH_3OH, 4.0% O_2, and 95.0% Ar by volume) at pressures between 2.9 and 3.2 atm; solid line represents prediction of the San Diego Mech.

(d)

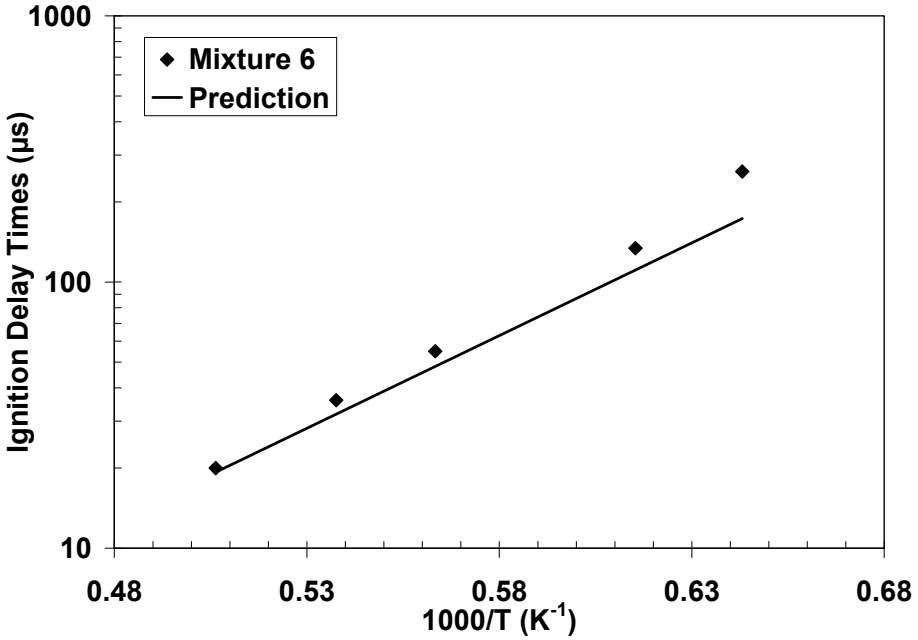

Figure 5.9 (d) Measured [20] and predicted autoignition delay times for methanol-oxygen-argon mixture φ=3.0 (2.0% CH_3OH, 1.0% O_2, and 97.0% Ar by volume) at pressures between 2.8 and 3.2 atm; solid line represents prediction of the San Diego Mech.

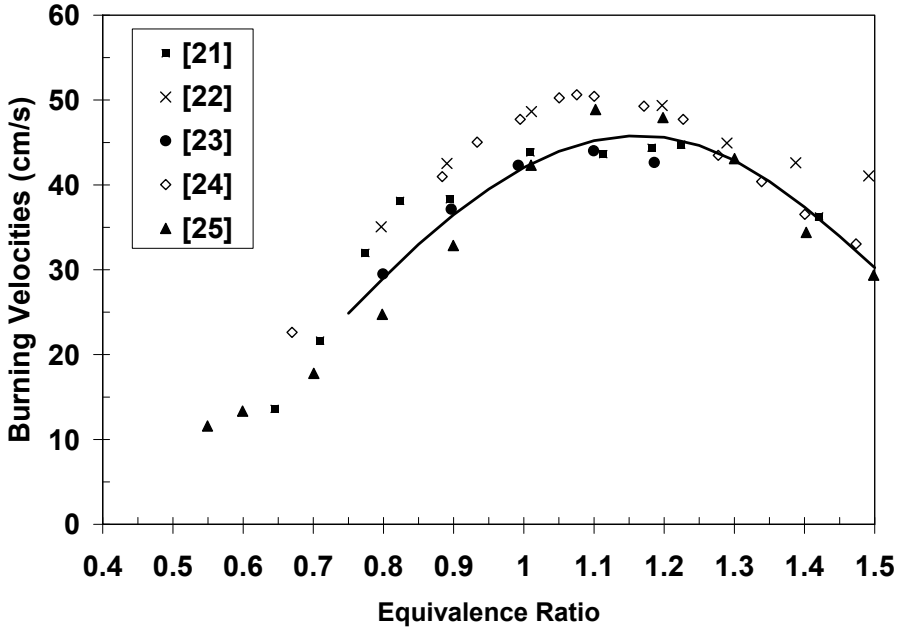

Figure 5.10 Measured [21-25] and predicted laminar burning velocities for methanol-air mixtures at initial temperature of 298 K at P = 1 atm; solid line represents prediction of the San Diego Mech; dashed line represents prediction of the SD Old.

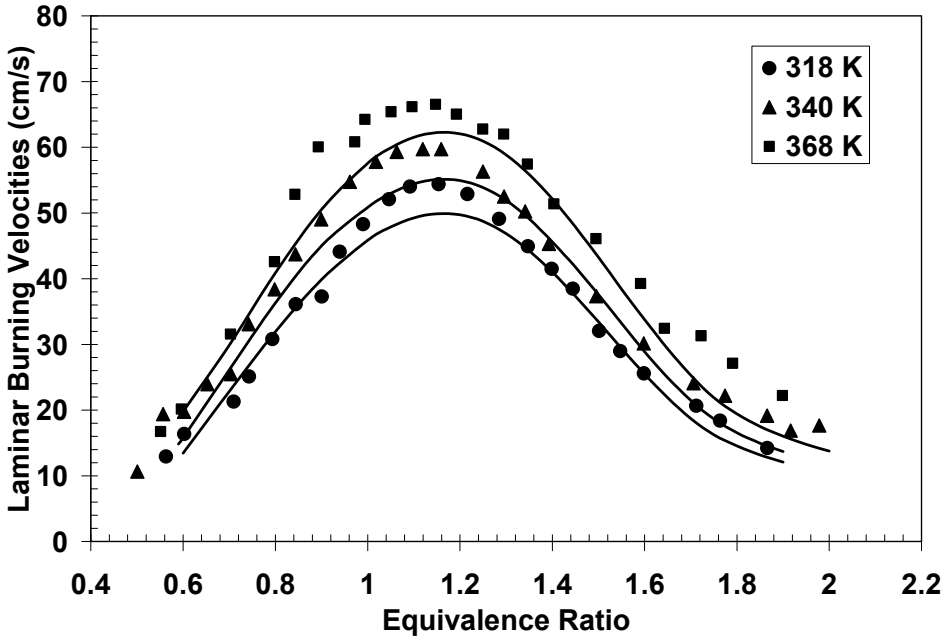

Figure 5.11 Measured [22] and predicted laminar burning velocities for methanol-air mixtures at initial temperatures of 318 K, 340 K, and 368 K at P=1atm; solid lines represent prediction of the San Diego Mech.

(a)

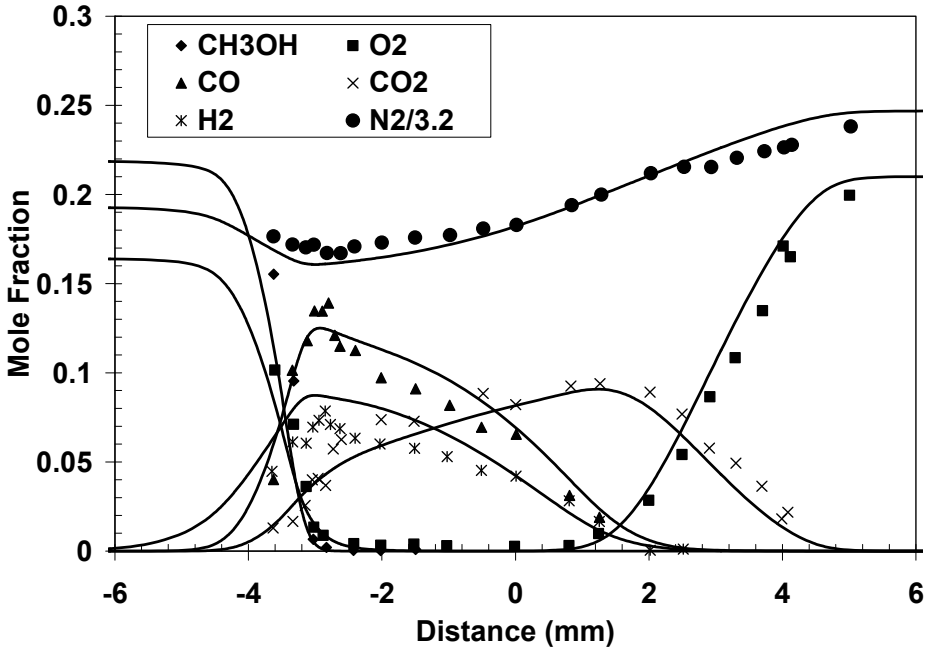

(b)

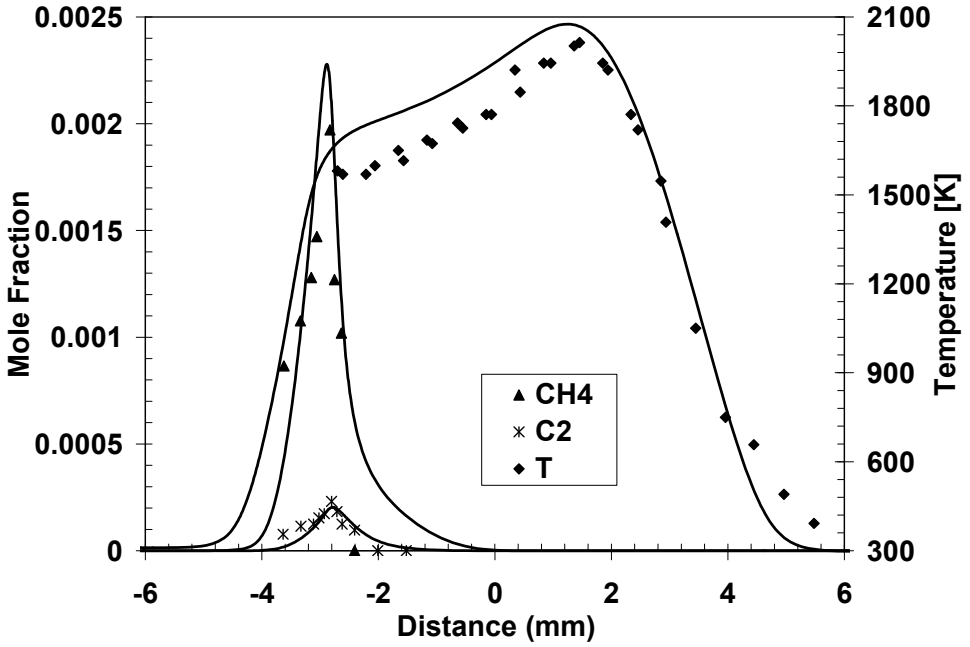

Figure 5.12 Measured [5] and predicted methanol-air partially premixed flame structure: (a) Concentration profiles for CH_3OH, O_2, CO, CO_2, and H_2, (b) Temperature profile and concentration profiles for CH_4, and C_2 (C_2H_6+C_2H_2+C_2H_4); solid line represents prediction of the San Diego Mech.

(a)

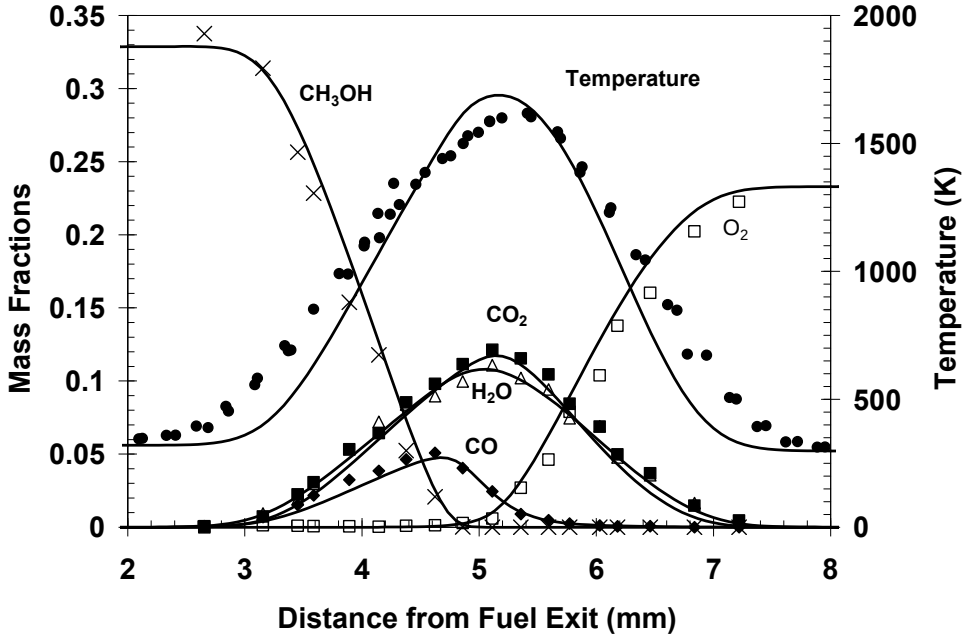

(b)

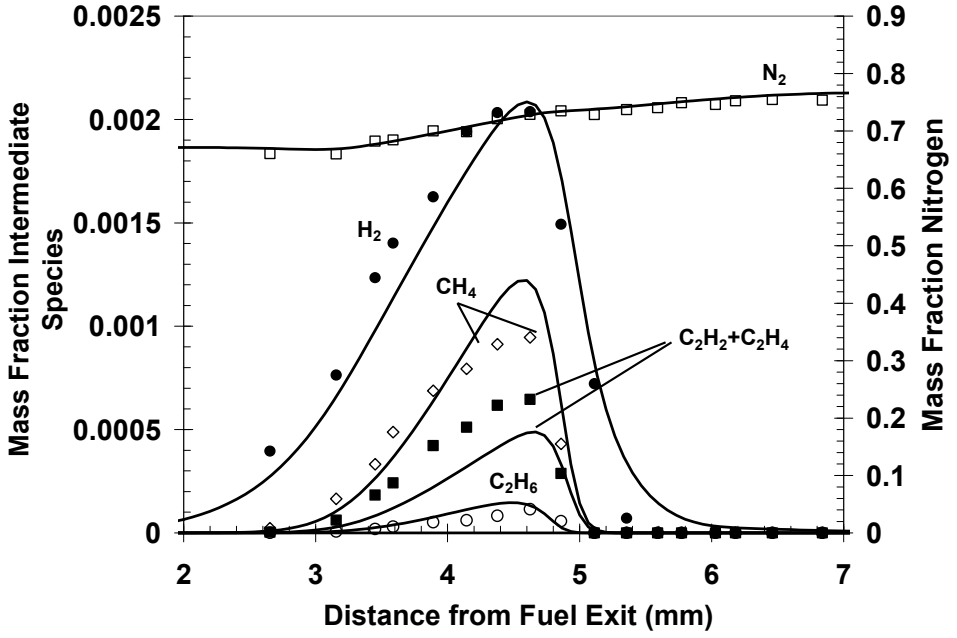

Figure 5.13 Measured [26] and predicted methanol-air nonpremixed flame structure: (a) Temperature and concentration profiles for CH_3OH, O_2, CO, CO_2, and H_2O, (b) Concentration profiles for CH_4, C_2H_6, C_2H_2+C_2H_4, N_2, and H_2; solid line represents prediction of the San Diego Mech.

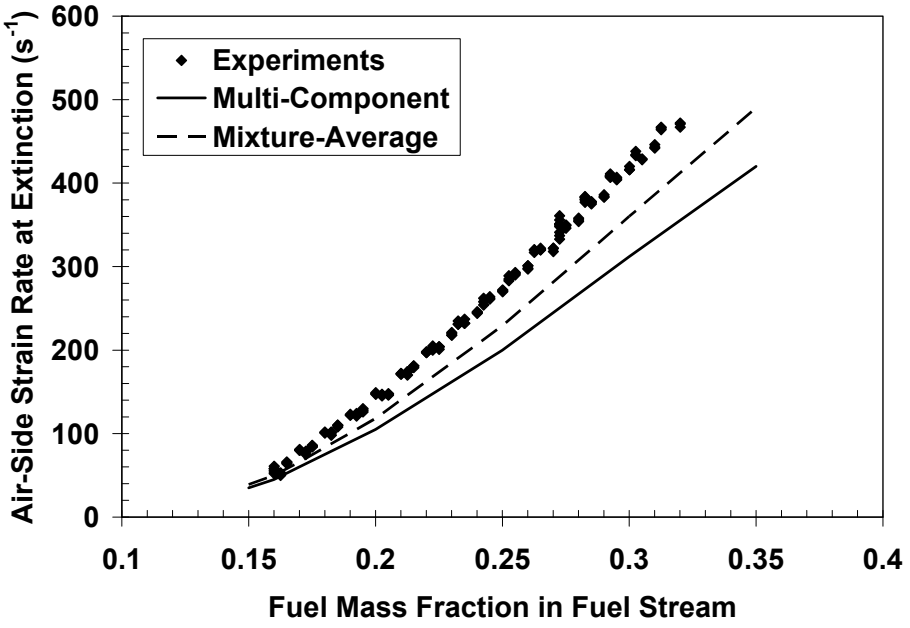

Figure 5.14 Measured [27] and predicted nonpremixed flame extinction strain rates at P=1 atm for fuel-stream temperature T_F=323 ± 10 K and air temperature T_{Ox}=298 K; lines represent the predictions of the San Diego Mech.

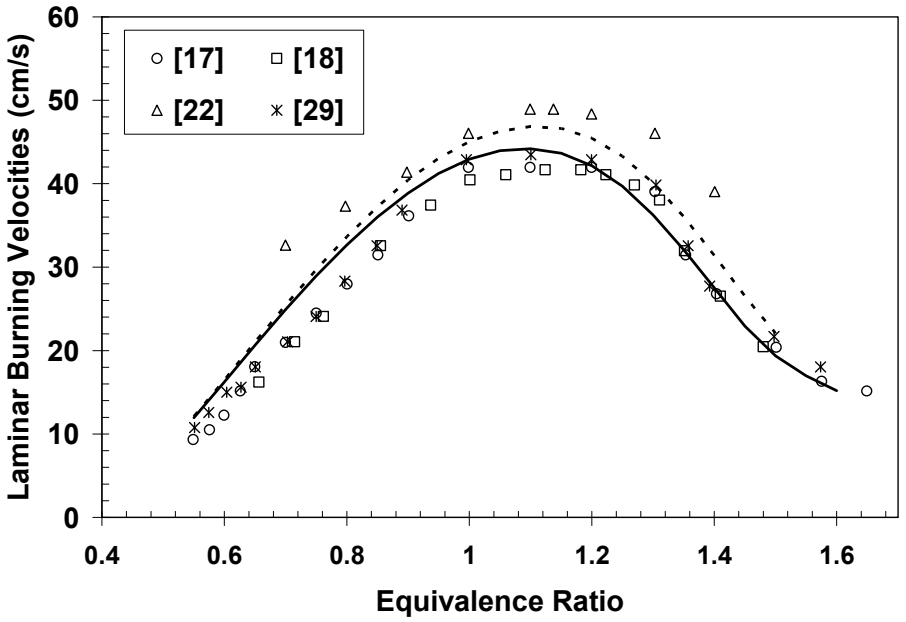

Figure 5.15 Measured [17, 18, 22, 29] and predicted laminar burning velocities for ethane-air mixtures at initial temperature of 298 K at P = 1 atm; solid line represents prediction of the San Diego Mech; dashed line represents prediction of the SD Old.

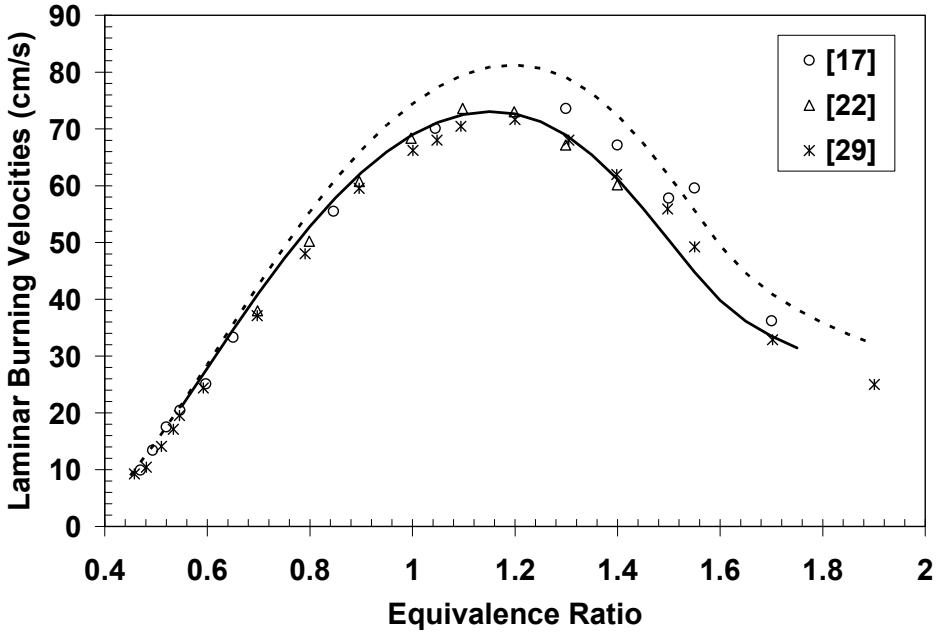

Figure 5.16 Measured [17, 22, 29] and predicted laminar burning velocities for ethylene-air mixtures at initial temperature of 298 K at P = 1 atm; solid line represents prediction of the San Diego Mech; dashed line represents prediction of the SD Old.

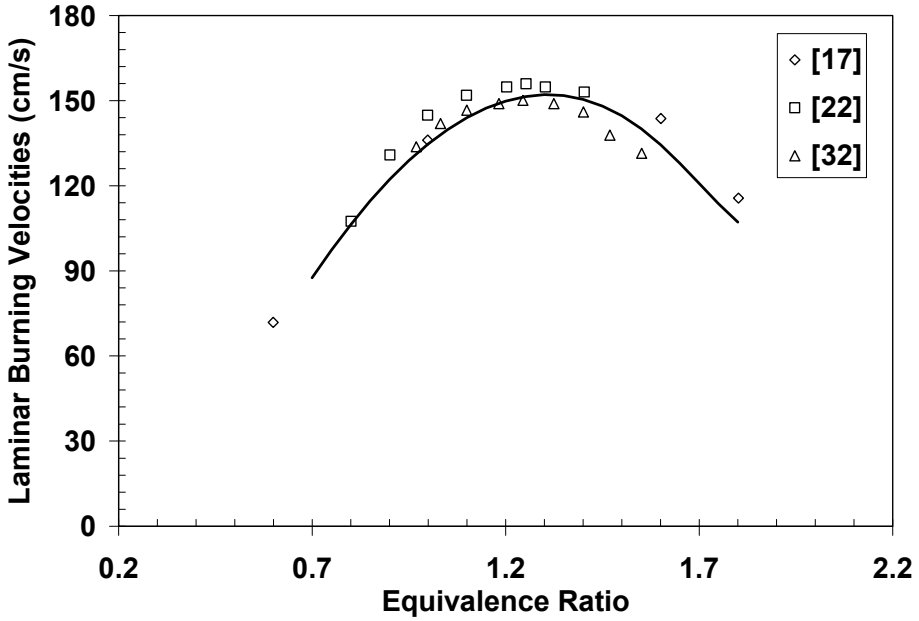

Figure 5.17 Measured [17, 22, 32] and predicted laminar burning velocities for acetylene-air mixtures at initial temperature of 298 K at P = 1 atm; solid line represents prediction of the San Diego Mech.

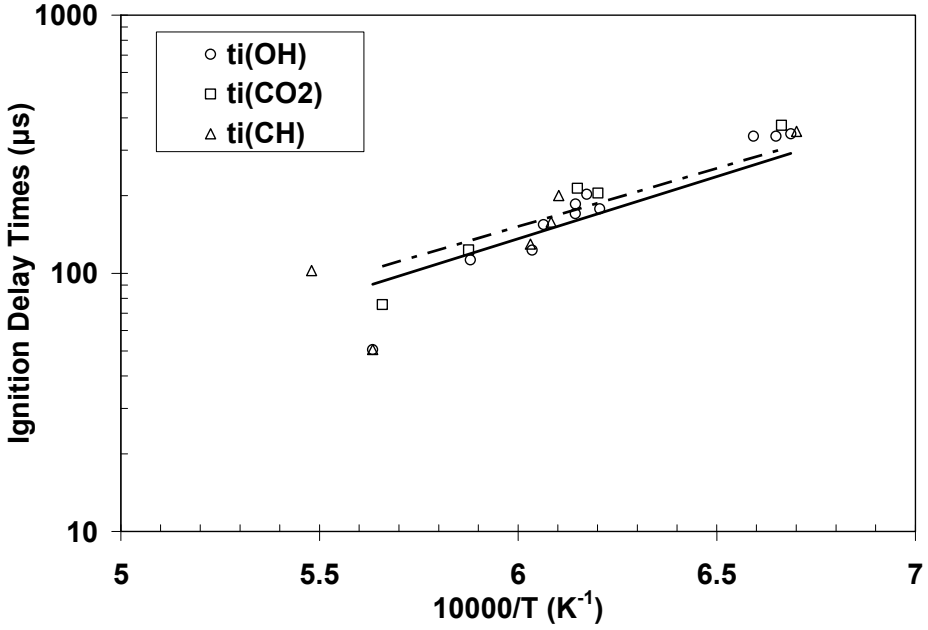

Figure 5.18 Measured [28] and predicted autoignition delay times for ethane-oxygen-argon mixture φ=1.0 (1.11% C_2H_6, 3.89% O_2, and 95.0% Ar by volume) at pressure 0.335 atm; lines represent prediction of the San Diego Mech; dot-dashed line represents prediction based on [CO_2] inflection criterion; solid line represents prediction based on [OH] inflection criterion.

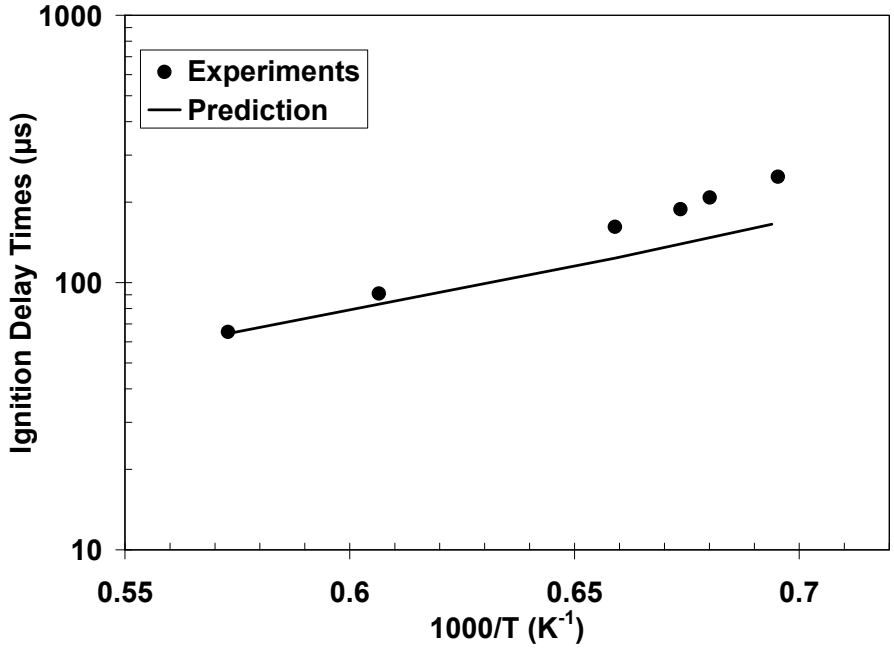

Figure 5.19 Measured [30] and predicted autoignition delay times for ethylene-oxygen-argon mixture φ=1.0 (1.0% C_2H_4, 3.0% O_2, and 96.0% Ar by volume) at pressure 1.0 atm; solid line represents prediction of the San Diego Mech.

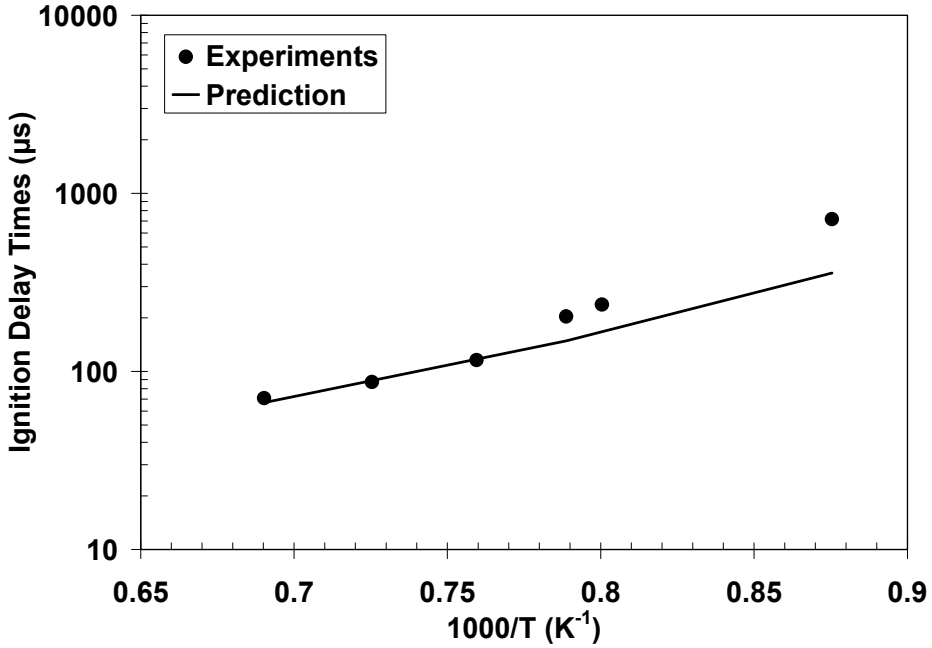

Figure 5.20 Measured [31] and predicted autoignition delay times for acetylene-oxygen-argon mixture φ=1.0 (1.4% C_2H_2, 3.6% O_2, and 95.0% Ar by volume) at pressures between 1.0 and 2.6 atm; solid line represents prediction of the San Diego Mech.

(a)

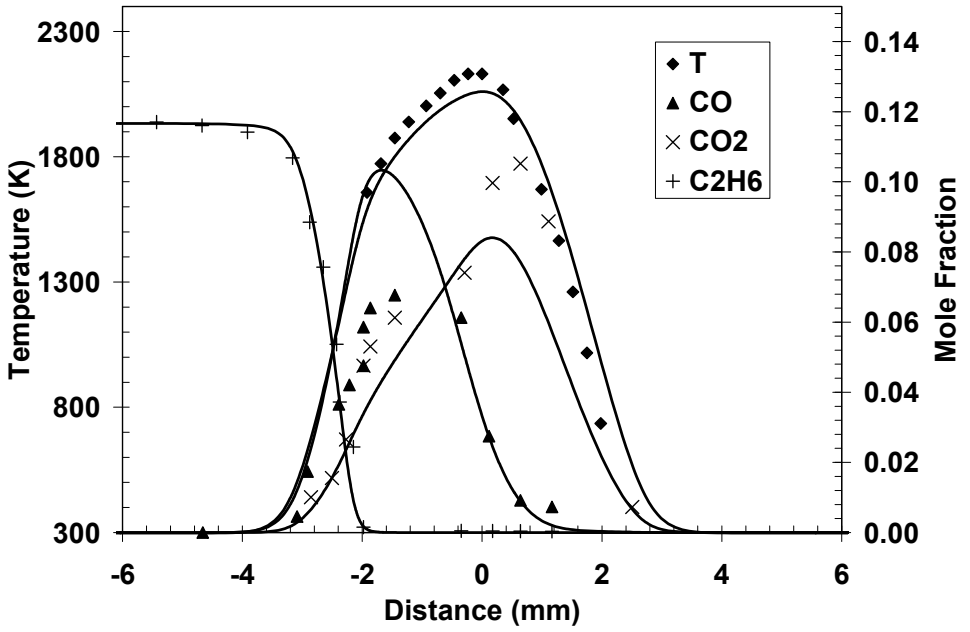

(b)

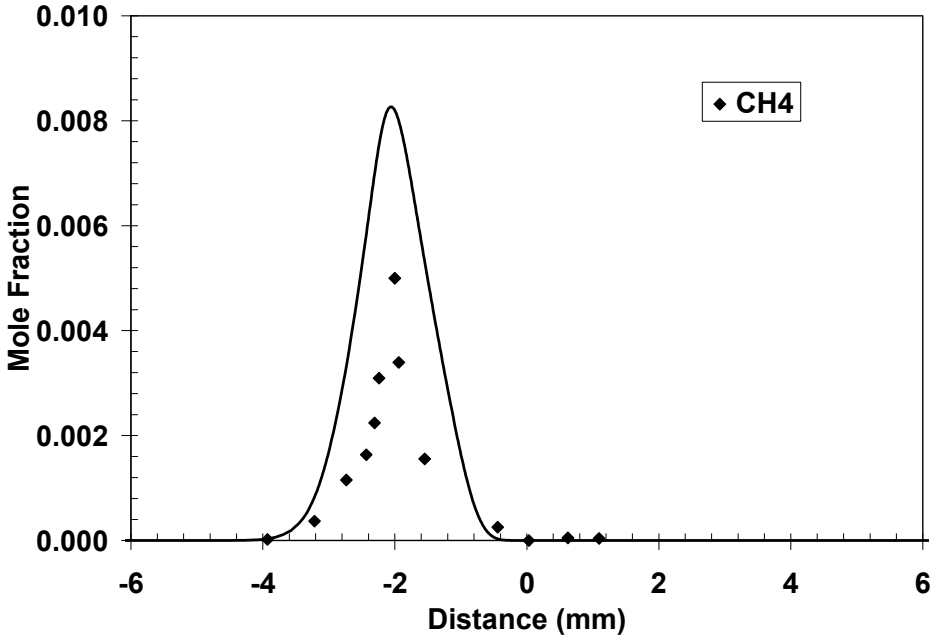

Figure 5.21 Measured [7] and predicted ethane-air partially premixed flame structure: (a) Temperature and concentration profiles for C_2H_6, O_2, CO, and CO_2; (b) Concentration profile for CH_4; solid line represents prediction of the San Diego Mech.

(c)

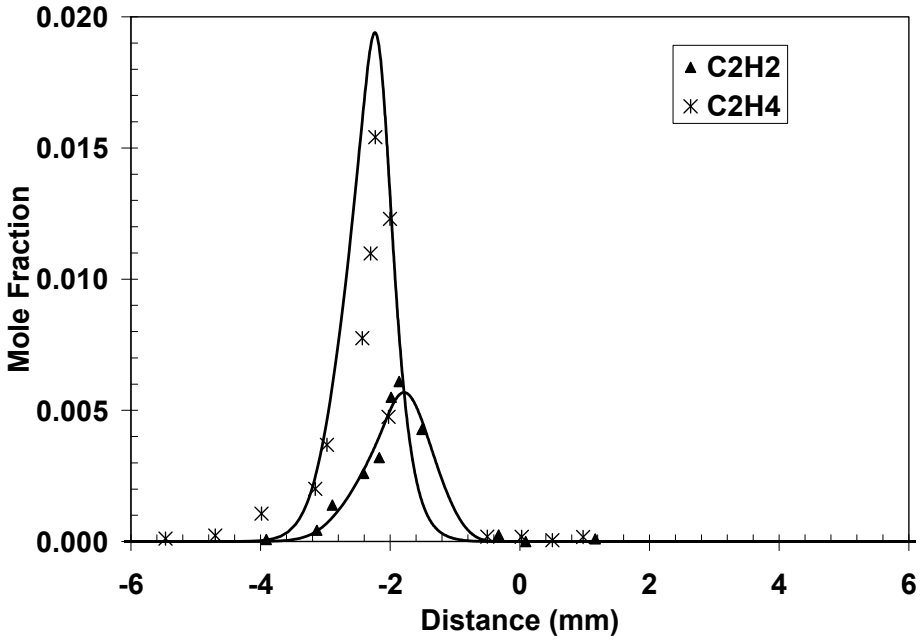

Figure 5.21 (c) Measured [7] and predicted ethane-air partially premixed flame structure: Concentration profiles for C_2H_2, and C_2H_4; solid line represents prediction of the San Diego Mech.

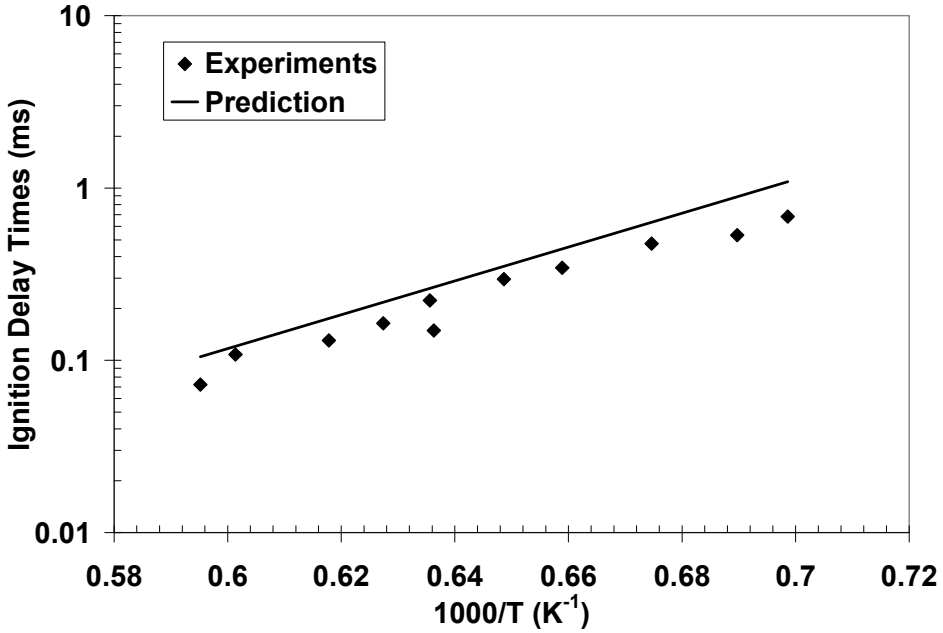

Figure 5.22 Measured [33] and predicted autoignition delay times for propane-oxygen-argon mixture φ=1.0 (0.2% C_2H_4, 1.0% O_2, and 98.8% Ar by volume) at pressure 1.5 atm; solid line represents prediction of the San Diego Mech.

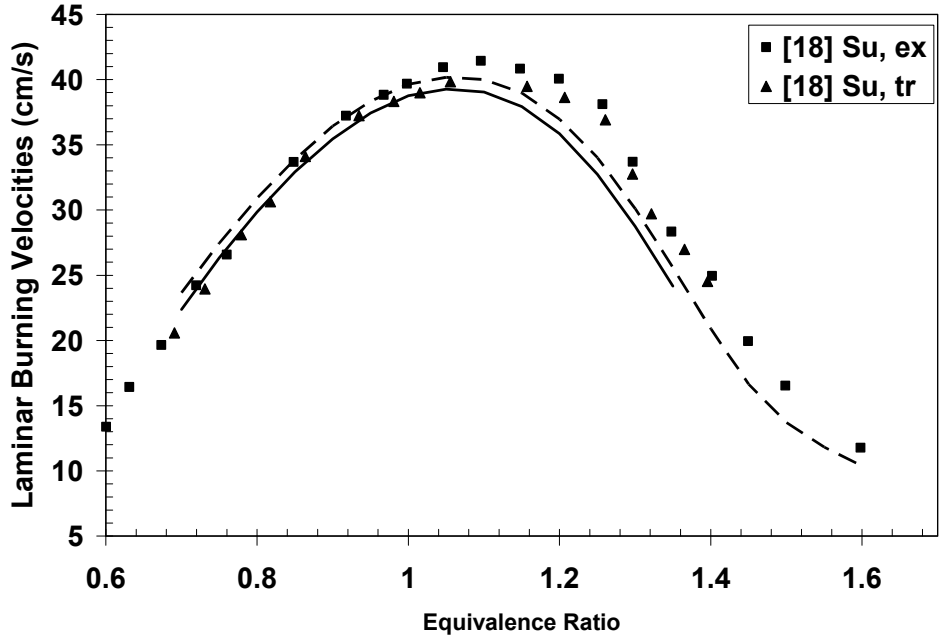

Figure 5.23 Measured [18] and predicted laminar burning velocities for propane-air mixtures at initial temperature of 298 K at P = 1 atm; solid line represents prediction of the San Diego Mech.

(a)

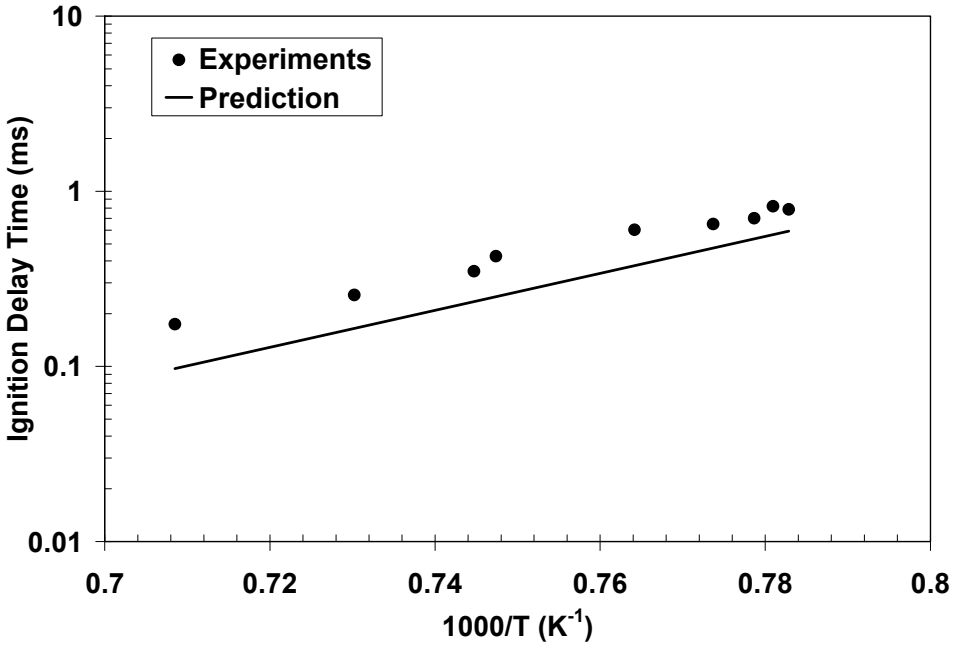

Figure 5.24 (a) Measured [34] and predicted autoignition delay times for acetaldehyde-oxygen-argon mixture φ=0.5 (1.0% CH_3CHO, 5.0% O_2, and 94.0% Ar by volume) at pressure 5.0 atm; solid line represents prediction of the San Diego Mech.

(b)

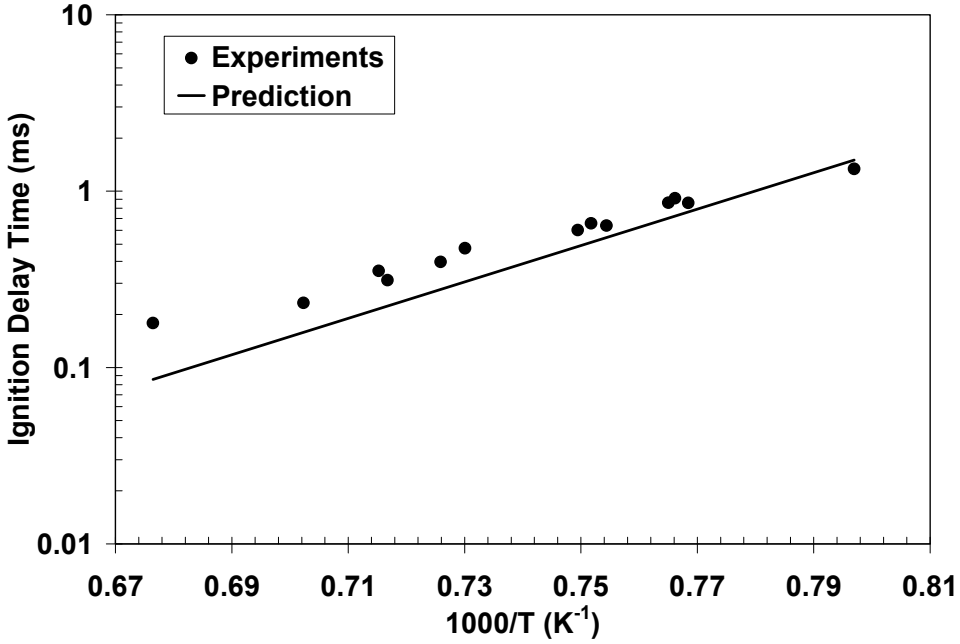

Figure 5.24 (b) Measured [34] and predicted autoignition delay times for acetaldehyde-oxygen-argon mixture φ=1.0 (1.0% CH_3CHO, 2.5% O_2, and 96.5% Ar by volume) at pressure 5.0 atm; solid line represents prediction of the San Diego Mech.

5.9 REFERENCES

1. Balakrishnan, G. and Williams, F.A., "Turbulent combustion regimes for hypersonic propulsion employing hydrogen-air diffusion flames", Journal of Propulsion and Power, 10, 1995, pp. 434-437.

2. Rightley, M.L. and Williams, F.A., "Structures of CO diffusion flames near extinction", Combustion Science and Technology, 125, 1997, pp. 181-200.

3. Rightley, M.L. and Williams, F.A., "Analytical approximation for structures of wet CO flames with one-step reduced chemistry", Combustion and Flame, 101, 1995, pp. 287-301.

4. Li, S.C. and Williams, F.A., "NO_x formation in two-stage methane-air flames", Combustion and Flame, 118, 1999, pp. 399-414.

5. Li, S.C. and Williams, F.A., "Experimental and numerical studies of two-stage methanol flames", Proceedings of the Combustion Institute, 26, 1996, pp. 1017-1024.

6. Li, S.C. and Williams, F.A., "Formation of NO_x, CH_4, and C_2 species in laminar methanol flames", Proceedings of the Combustion Institute, 27, 1998, pp. 485-493.

7. Waly, M.M.Y., Li, S.C. and Williams, F.A., "Experimental and numerical studies of two-stage ethane-air flames", Journal of Engineering for Gas Turbines and Power, 122, 2000, pp. 651-658.

8. Varatharajan, B. and Williams, F.A., "Ethylene ignition and detonation chemistry, Part 1: Detailed modeling and experimental comparison", Journal of Propulsion and Power, 18, 2002, pp. 344-351.

9. Waly, M.M., Li, S.C. and Williams, F.A., "Structures of non-sooting counterflow diluted acetylene-air flames", Proceedings of the Combustion Institute, 28, 2000, pp. 2005-2012.

10. Varatharajan, B. and Williams, F.A., "Chemical-kinetic descriptions of high-temperature ignition and detonation of acetylene-oxygen-diluent systems", Combustion and Flame, 125, 2001, pp. 624-645.

11. Petrova, M.V. and Williams, F.A., "A small detailed chemical-kinetic mechanism for hydrocarbon combustion", Combustion and Flame, 144, 2006, pp. 526-544.

12. Li, J., "Experimental and numerical studies of ethanol chemical kinetics," PhD Thesis, Princeton University, 2004.

13. Eiteneer, B., Yu, C.L., Goldenberg, M. and Frenklach, M., "Determination of rate coefficients for reactions of formaldehyde pyrolysis and oxidation in the gas phase", Journal of Physical Chemistry A., 102, 1998, pp. 5196-5205.

14. Spadiccini, L.J., and Colket. III, M.B., "Ignition delay characteristics of methane fuels", Progress in Energy and Combustion Science, 20, 1994, pp. 431-460.

15. Frenklach, M. and Bornside, D.E., "Shock-initiated ignition in methane-propane mixtures", Combustion and Flame, 56, 1984, pp. 1-27.

16. Seiser, R. and Seshadri, K., "The influence of water on extinction and ignition of hydrogen and methane flames", Proceedings of the Combustion Institute, 30, 2005, pp. 407-414.

17. Law, C.K., "Compilation of experimental data on laminar burning velocities", in Reduced Kinetic Mechanisms for Applications in Combustion Systems (N. Peters and B. Rogg, Eds.), Springer-Verlag, Berlin, 1993, p. 15-26.

18. Vagelopoulos, C.M. and Egolfopoulos, F.N., "Direct experimental determination of laminar flame speeds", Proceedings of the Combustion Institute, 27, 1998, pp. 513-519.

19. Cooke, D.F., Dodson, M.G., and Williams, A., "A shock-tube study of the ignition of methanol and ethanol with oxygen", Combustion and Flame, 16, 1971, pp. 233-236.

20. Bowman, C.T., "A shock-tube investigation of the high-temperature oxidation of methanol", Combustion and Flame, 25, 1975, pp. 343-354.

21. Wiser, W.H. and Hill, G.R., "A kinetic comparison of the combustion of methyl alcohol and methane", Proceedings of the Combustion Institute, 5, 1955, pp. 553-558.

22. Gibbs, C.J. and Calcote, H.F., "Effect of molecular structure on burning velocity", Journal of Chemical and Engineering Data, 4, 1959, pp. 226-237.

23. Gülder, O.L., "Laminar burning velocities of methanol, ethanol and isooctane-air mixtures", Proceedings of the Combustion Institute, 9, 1982, pp. 275-281.

24. Metghalchi, M. and Keck, J.C., "Burning velocities of mixtures of air with methanol, isooctane, and indolene at high pressure and temperature", Combustion and Flame, 48, 1982, pp. 191-210.

25. Egolfopoulos, F.N., Du, D.X. and Law, C.K., "A comprehensive study of methanol kinetics in freely-propagating and burner-stabilized flames, flow and

static reactors, and shock tubes", Combustion Science and Technology, 83, 1992, pp. 33-75.

26. Seiser, R., Humer, S., Seshadri, K., and Pucher, E., "Experimental investigation of methanol and ethanol flames in nonuniform flows", Proceedings of the Combustion Institute, 31, 2007, pp. 1173-1180.

27. Seiser, R. and Seshadri, K., "Counterflow extinction of premixed and nonpremixed methanol and ethanol flames", Western States Section, The Combustion Institute, 2002 Spring Meeting, University of California at San Diego, La Jolla, CA 92093-0411, March 25-26, 2002, Paper # 02S-27.

28. Cooke, D.F. and Williams, A., "Shock tube studies of methane and ethane oxidation", Combustion and Flame, 24, 1975, pp. 245-256.

29. Egolfopoulos, F.N., Zhu, D.L., and Law, C.K., "Experimental and numerical determination of laminar flame speeds: Mixtures of C_2-Hydrocarbons with oxygen and nitrogen", Proceedings of the Combustion Symposium, 23, 1990, pp. 471-478.

30. Horning, D.C., "A study of the high-temperature autoignition thermal decomposition of hydrocarbons", Ph.D. Dissertation, Department of Mechanical Engineering, Stanford University, Stanford, CA, June 2001.

31. Hidaka, Y., Hattori, K., Okuno, T., Inami, K., Abe, T., and Koike, T., "Shock-tube and modeling study of acetylene pyrolysis and oxidation", Combustion and Flame, 107, 1996, pp. 401-417.

32. Scholte, T.G. and Vaags, P.B., "The burning velocity of hydrogen-air mixtures and mixtures of some hydrocarbons with air", Combustion and Flame, 3, 1959, pp. 495-501.

33. Gray, J.A. and Westbrook, C.K., "High-temperature ignition of propane with MTBE as an additive: Shock tube experiments and modeling", International Journal of Chemical Kinetics, 26, 1994, pp. 757-770.

34. Dagaut, P., Reuillon, M., Voisin, D., Cathonet, M., McGuinness, M. and Simmie, J.M., "Acetaldehyde oxidation in a JSR and ignition in shock waves: Experimental and comprehensive kinetic modeling", Combustion Science and Technology, 107, 1995, pp. 301-316.

35. Irdham, E.A. and Kiefer, J.H., "The formaldehyde decomposition chain mechanism", International Journal of Chemical Kinetics, 25, 1993, pp. 285-303.

36. GRI Mech 1.2: http://www.me.berkeley.edu/gri-mech/

37. Baulch, D.L., Cobos, C.J., Cox, R.A., Frank, P., Just, Th., Kerr, J.A., Pilling, M.J., Troe, J., Walker, R.W. and Warnatz, J., "Evaluated kinetic data for combustion modeling", Journal of Physical and Chemical Reference Data, 21, 1992, pp. 411-734.

38. Timonen, R.S., Ratajczak, E. and Gutman, D., "Kinetics of the reactions of the formyl radical with oxygen, nitrogen dioxide, chlorine and bromine", Journal of Physical Chemistry, 92, 1988, pp. 651-655.

39. Zellner, R. and Ewig, F., "Computational study of the CH_3+O_2 chain branching reaction", Journal of Physical Chemistry, 92, 1988, pp. 2971-2974.

40. Tsang, W. and Hampson, R.F., "Chemical kinetic database for combustion chemistry. 1. Methane and related compounds", Journal of Physical Chemistry Reference Data, 15, 1986, pp. 1087-1276.

41. Grotheer, H.H., Kelm, S., Driver, H.S.T., Hutcheon, R.J., Lockett, R.D. and Robertson, G.N., "Elementary reactions in the methanol oxidation system. Part I. Establishment of the mechanism and modeling of laminar burning velocities", Ber. Bunsenges. Phys. Chem., 96, 1992, pp. 1376-1387.

42. Held, T.J. and Dryer, F.L., "A comprehensive mechanism for methanol oxidation", International Journal of Chemical Kinetics, 30, 1998, pp. 805-830.

43. Jodkowski, J.T., Rayez, M.T., Rayez, J.C., Bréces, T. and Dóbé, S., "Theoretical study of the kinetics of the hydrogen abstraction from methanol. 3. Reaction of methanol with hydrogen atom, methyl and hydroxyl radicals", Journal of Physical Chemistry A, 103, 1999, pp. 3750-3765.

44. Kee, R.J., Rupley, F.M., Miller, J.A., Coltrin M.E., Grcar, J.F., Meeks, E., Moffat, H.K., Lutz, A.E., Dixon-Lewis, G., Smooke, M.D., Warnatz, J., Evans, G.H., Larson, R.S., Mitchell, R.E., Petzold, L.R., Reynolds, W.C., Caracotsios, M., Stewart, W.E., Glarborg, P., Wang, C., Adigun, O., Houf, W.G., Chou, C.P. and Miller, S.F., Chemkin Collection, Release 3.7.1, Reaction Design Inc., San Diego, CA, 2003.

45. Pitsch, H., "Entwicklung eines Programmpakets zur Berechnung eindimensionaler Flammen am Beispiel einer Gegenstromdiffusionflamme", M.S. Thesis, RWTH Aachen, Germany, 1993.

46. Dean, A.M., Craig, B.L., Johnson, L., Schultz, M.C. and Wang, E.E., "Shock tube studies of formaldehyde pyrolysis", Proceedings of Combustion Institute, 7, 1979, pp. 577-586.

47. Dean, A.M., Johnson, R.L. and Steiner, D.C., "Shock-tube studies of formaldehyde oxidation", Combustion and Flame, 37, 1980, pp. 41-62.

48. Hidaka, Y., Taniguchi, T., Tanaka, H., Kamesawa, T., Inami, K. and Kawano, H., "Shock-tube study of CH_2O pyrolysis and oxidation", Combustion and Flame, 92, 1993, pp. 365-376.

49. Friedrichs, G., Davidson, D.F. and Hanson, R.K., "Validation of a thermal decomposition mechanism of formaldehyde by detection of CH_2O and HCO behind shock waves," International Journal of Chemical Kinetics, 36, 2004, pp. 157-169.

50. Li, S.C. and Williams, F.A., "Reaction mechanisms for methane ignition", Journal of Engineering for Gas Turbines and Power, 124, 2000, pp. 471-480.

51. Klemm, R.B., Sutherland, J.W., Rabinowitz, M.J., Patterson, P.M., Quaertemont, J.M. and Tao, W., "Shock tube kinetic study of methane dissociation: 1726 K $\leq$ T $\leq$ 2134 K", Journal of Physical Chemistry, 96, 1992, pp. 1786-1793.

52. Marinov, N.M., "A detailed chemical kinetic model for high temperature ethanol oxidation", International Journal Chemical Kinetics, 31, 1999, pp. 183-220.

53. Sutherland, J.W., Su, M.-C., and Michael, J.V., "Rate constants for $H+CH_4$, CH_3+H_2, and CH_4 dissociation at high temperature", International Journal of Chemical Kinetics, 33, 2001, pp. 669-684.

54. Cherian, M.A, Rhodes, P., Simpson, R.S., and Dixon-Lewis, G., "Kinetic modeling of the oxidation of carbon monoxide in flames", Proceedings of the Combustion Institute, 18, 1981, pp. 385-396.

55. Bott, J.F. and Cohen, N., "A shock-tube study of the reactions of the hydroxyl radical with several combustion species", International Journal of Chemical Kinetics, 23, 1991, pp. 1075-1094.

56. Warnatz, J., "Rate coefficients in the C/H/O system". In W.C. Gardiner (ed.), Combustion Chemistry, Springer-Verlag, Berlin, pp. 197-360, 1984.

CHAPTER 6

DETAILED MECHANISM FOR THE COMBUSTION OF ETHANOL

6.1 OVERVIEW

Although ethanol is attractive for use as a possible low-pollution source of renewable energy, significant uncertainties remain in its combustion chemistry. Despite the availability of a number of detailed chemical-kinetic mechanisms for ethanol combustion [1-6], there are differences in predictions of these mechanisms, and most of them have not been tested entirely thoroughly against experimental combustion data. A need therefore exists to investigate possibilities of improving the mechanisms and to attempt to validate them against measurements made in flames. The present study addresses this need by suggesting a different detailed mechanism and by comparing predictions with new measurements of structures of partially premixed and diffusion flames in a counterflow geometry. It also investigates computationally profiles of concentrations of pollutants in these and related flames.

6.2 THE REACTION MECHANISM

The chemical-kinetic mechanism is an augmentation of a mechanism developed for the combustion of hydrogen [7], carbon monoxide [7], methane [8, 9], ethane [10], ethylene [11], acetylene [12, 13], propane [14], propene [14], propyne [14], allene [14] and methanol [15, 16]. The recent tests of these submechanisms are presented in Chapters 4 and 5. The mechanism is relatively short for a detailed mechanism, simplifications

having been achieved by restricting attention to temperatures above about 1000 K, pressure below about 100 bar, equivalence ratios less than about 3 in premixed systems and potential-flow strain rates greater than about 50 s^{-1} in nonpremixed or partially premixed systems. These restrictions preclude addressing soot formation and cool flames, for example. The mechanism is extended here to ethanol by adding many of the steps and rate parameters of Li [6].

Specifically, 33 reactions are added that involve C_2H_5OH or one of the three isomers produced by abstraction of an H atom from it, CH_3CHOH, CH_2CH_2OH and CH_3CH_2O, and 22 reactions are added that involve acetaldehyde or one of the two isomers produced by abstraction of H from it, CH_2CHO and CH_3CO. Thus, in total, 55 new reactions and 6 new species are added. Consistent with our earlier practice and high-temperature objective, the peroxide $HOC_2H_4O_2$ and reactions related to it, which are included by Li [6], are not part of the present mechanism. All rate parameters for the newly added reactions are those of Li [6], except for the two initiation steps for which Li gives values only at particular pressures and for which, seeking simplicity within bounds of present uncertainty, we constructed a Troe-type falloff fit with F_c=0.5 and with zero temperature exponents at both low and high pressures, resulting in low-pressure and high-pressure specific reaction-rate constants given in Table 6.1. Because of falloff complexities, the low-pressure rate parameters may not apply below about 10^{-2} bar, and rates calculated at the highest temperatures likely are too high in Table 6.1. The resulting mechanism, available on the web [17], incorporates revisions of rates discussed in previous chapters and involves 288 elementary steps among 57 chemical species where the 53 steps among 14 species needed to address NO_x formation and the 43 steps among

7 species needed to address formation of compounds involving three carbon atoms are appended. All revisions other than those indicated above have been discussed in chapter 4 and 5.

Figure 6.1 shows a representative reaction-path diagram for this mechanism. The conditions selected for construction of this figure correspond to the partially premixed case of Table 6.2, and the figure tracks the carbon history, the arrows that show the main pathways being labeled with the agents and the percentage of their contributions. These percentages are obtained by integrating consumption rates over the entire field. Indications of the fates of some of the minor species, such as C_2H, C_3H_4, C_3H_6 and C_3H_8, are omitted for clarity because they are present in very small quantities and do not affect the rest of the chemistry significantly.

Direct fuel decomposition by the second step listed in Table 6.1 seems to be more important for these ethanol flames than is direct decomposition in corresponding flames of many other fuels; this path contributes more than 20% of the fuel removal in Fig. 6.1 and nearly 50% in the corresponding diffusion flame for the conditions of Table 6.2. Ethylene concentrations will be high in these flames because it is produced not only by this direct decomposition but also by decomposition of one of the hydroxy ethyl radicals formed by H abstraction, seen at the upper left of Fig. 6.1; (it will be even higher in the diffusion flame than in the partially premixed flame since about 70% of the fuel is calculated to go to C_2H_4 in the diffusion flame). The other hydroxy ethyl radical, as well as the ethoxy radical, at the upper right of Fig. 6.1, are seen to lead instead to acetaldehyde, the peak concentrations of which will be quite appreciable, computationally about twice that of formaldehyde (which arises from oxygen attack on

vinyl and hydroxyl attack on ketene in these particular flames, in addition to the familiar oxygen attack on methyl). The acetaldehyde concentration nevertheless is still less than half that of ethylene. Acetaldehyde is seen in Fig. 6.1 to play a major role in the formation of CH_3 radicals, directly by $CH_3CHO+M \rightarrow CH_3+HCO+M$, or indirectly, either through the set of reactions $CH_3CHO+H \rightarrow CH_2CHO+H_2$, $CH_2CHO \rightarrow CH_2CO+H$ and $CH_2CO+H \rightarrow CH_3+CO$ or by radical attack forming CH_3CO, which in turn decomposes to CH_3 and CO. Ethoxy also appreciably contributes to formation of CH_3 directly (the path at the far right), since nearly 40% of it decomposes by $CH_3CH_2O+M \rightarrow CH_3+CH_2O+M$, the other 60% of passing through acetaldehyde. Ketene is produced from acetaldehyde via CH_2CHO and also from the ethylene path at the left, through vinyl and acetylene, which thereby provides an additional, relatively smaller contribution to methyl. In this mechanism, both methane and ethane come only from CH_3, at the bottom of the figure. For simplicity, the fate of HCCO, namely forming CO and CO_2, is not shown in the figure.

The paths shown in Fig. 6.1 are not quantitatively representative of other conditions or other combustion processes. For example, although the first entry in Table 6.1 plays no significant role here, it is important in autoignition. The general ideas, however, such as the observation that ethylene and acetaldehyde are very important stable intermediates in ethanol combustion, extend to all processes considered here.

6.3 AUTOIGNITION, LAMINAR BURNING VELOCITIES AND DIFFUSION-FLAME EXTINCTION

It is of interest to test predictions of the mechanism against experimental data on combustion processes that are available in the literature. The computer program CHEMKIN 3.7 [18] mainly was employed for this purpose, although the FlameMaster [19] program also was often used to make sure that the predictions of the two different programs were the same. The autoignition computations were performed for homogeneous, adiabatic, isochoric conditions, with the maximum rate of increase of temperature employed as the criterion to define the ignition time. For the cases computed this was found to correspond closely to the maximum rate of increase of pressure and is a very good approximation to the shock-tube conditions to which the calculations are applied; in these cases the dependence of the ignition time on the ignition criterion is weak, and the results would be not too different if isobaric rather than isochoric conditions had been selected for the computation. The burning-velocity computations included multicomponent transport, the Soret effect and radiant energy loss from CO_2 and H_2O bands, while the diffusion-flame computations included these as well as an alternative mixture-averaged transport approximation.

There are various sources of shock-tube ignition-delay data [20, 21, 22], and Figs. 6.2 and 6.3 show representative comparisons. The agreements in Fig. 6.2, where the experiments were performed in 90% Ar at different equivalence ratios φ and pressures P, are quite good. It is seen that, under these conditions, there is practically no dependence of the ignition delay on φ, and there is a small decrease in delay with increasing P, both experimentally and computationally. For the leaner conditions at higher pressures shown in Fig. 6.3, where the dilution was 92% Ar [21], the experimental pressure dependence of the ignition time is slightly greater than predicted, and the experimental slopes of the

curves are somewhat less than predicted. These differences, which are exhibited to an even greater extent by other mechanisms, also extend to other data in this pressure range at richer conditions [21, 22] and may reflect a combination of inadequacies in the mechanisms and experimental difficulties at the lower temperatures. For purposes of comparison, the prediction of the mechanism of Li [6] at 2 bar is shown as light dashed curves in Figs. 6.2 and 6.3; other mechanisms are in poorer agreement.

Figure 6.4 compares predictions of the present mechanism with measurements of laminar burning velocities at various initial temperatures [23]. Agreements are seen to be good, except between equivalence ratios of 0.7 and 0.9, where burning velocities are overpredicted by up to 20%. The predictions in Fig. 6.4 agree with those of Li [6] and are in better agreement with the data than are the predictions of a mechanism of Marinov [5].

Measurements have been made of counterflow diffusion-flame extinction at normal atmospheric pressure for fuel streams of prevaporized ethanol with mass fraction in nitrogen varying between 0.18 and 0.39, flowing against air at room temperature [24]. Figure 6.5 compares this data with predictions of the present mechanism based on two different transport-property descriptions, multicomponent and mixture-averaged formulations as implemented in CHEMKIN 3.7. There are known deficiencies of transport-model implementation in CHEMKIN 3.7 [26, 27], and it is unclear which of the two is better. It is seen from Fig. 6.5 that, although the mixture-averaged computation produces excellent agreement with experiment, the multicomponent description, which might be thought to be better, exhibits noticeable differences. At present it is uncertain whether the differences between computation and experiment reflect transport uncertainties, experimental departures from plug-flow boundary conditions or

deficiencies in the mechanism. In any event, the same types of differences are shared by the other mechanisms in the literature.

6.4 COUNTERFLOW FLAME STRUCTURES

Experiments on flame structures were performed using a counterflow burner described previously [28]. The details of the experimental setup are given in Chapter 3. In this burner, fine wire meshes at the duct exits promote plug-flow boundary conditions there. The opposing ducts, 23.1 mm in inner diameter with shielding annular nitrogen curtains, were separated by 12 mm in these experiments. Air flows through the top duct and fuel through the bottom duct at flow rates adjusted according to a momentum balance to maintain the stagnation plane halfway between the duct exits. An insulated vaporizer, temperature-controlled to provide the desired ethanol mole fraction in nitrogen, generates the fuel vapor which flows through a heated line to the lower duct, first having been mixed with oxygen to reconstitute air for the partially premixed experiments. Computer-controlled flowmeters adjust the flow rates, which in these experiments provided an air-side strain rate of 100 s^{-1} according to the plug-flow formula [25].

Temperature profiles were measured by an uncoated Pt-Pt13%Rh (Type R) thermocouple, except in the high-temperature region of the partially premixed flame. The maximum temperature experienced in the partially premixed flame was much higher than that in the diffusion flame and surpassed the melting point of Pt, necessitating use of an uncoated Pt-6%Rh vs. Pt-30%Rh (Type B) thermocouple for near-flame-temperature measurements in the partially premixed flame. Standard radiation corrections were made [29], but catalytic effects were neglected, leading to temperatures estimated to be about

120 K too high at the highest temperatures, based on experimental observations and the ideas in the literature [29].

Following best established practice [28] gas samples were collected 5 mm off axis by a quartz microprobe, tip 88 μm inner diameter and 168 μm outer diameter, contoured for rapid cooling to quench reactions and inserted radially to minimize flow disturbances. The location of the sampling probe and the thermocouple in the flow field was determined using a digital camera with a pixel size corresponding to a distance in the flow field of approximately 17 μm. The samples from the quartz probe flowed steadily, through lines heated to prevent condensation, to a SRI 8610C gas chromatograph, equipped with a 4.5 ft mole-sieve (80/100 mesh) for separating H_2, O_2 plus Ar, N_2, CH_4, and CO and a 12 ft Porapaq Q column for separating CO_2, C_2H_6, C_2H_2+C_2H_4, and C_2H_5OH. Temperature programming and valve switching were employed to optimize the separation performance of both columns. The species eluting from the column were sensed by a thermal-conductivity detector (TCD) and a flame-ionization detector (FID). The chromatograms were analyzed by in-house software, absolute mole fractions being determined by comparing with runs of known samples. Since ethylene and acetylene appear as a single peak, their sum was reported using the calibration for ethylene as in earlier work [30]. Since argon eluted together with oxygen from the columns, a correction was made for this [31]. Recently developed methods [31] were employed to overcome difficulties in measuring water concentrations. The expected accuracy for the maximum concentrations is better than ± 10% for species that can be clearly identified on either the FID or TCD. Hydrogen gives a very small signal on the TCD, so its

concentration is estimated to be accurate to within $\pm 25\%$, while the expected accuracy for water is estimated to be $\pm 20\%$.

Figures 6.6 and 6.7 show the results of these flame-structure measurements. In these figures, the experimental results are compared with predictions of the chemical-kinetic mechanism, which are shown by the solid curves. These computations included multicomponent diffusion, the Soret effect and radiative heat loss from carbon dioxide and water bands, with buoyancy neglected and plug-flow boundary conditions. Figures 6.6 (a) and 6.7 (a) give the concentrations of the major species in the partially premixed flame and in the diffusion flame, respectively. The excellent agreements between the experimental and computational results in these figures are mutually supportive and help to verify the ability to measure H_2O with good accuracy. The minimum of the N_2 mole fraction somewhat on the air side of stoichiometry has also been seen for other fuels and is associated with differential diffusion effects and changes in the numbers of moles, since N_2 is not consumed chemically. The disappearance of the reactants at the premixed-flame and diffusion-flame sheets is evident in these figures, and the H_2, CO, H_2O and CO_2 profiles also are all just as would be expected for these conditions. The computational results in these figures are indistinguishable from those obtained when the mechanism of Li [6] is employed, but some of the earlier mechanisms exhibit different results and poorer agreement with experiment.

Figures 6.6 (b) and 6.7 (b) show the profiles of temperature and of mole fractions of measured stable intermediates. The measured temperature profiles agree with computations within experimental error. The catalytic effect of the high-temperature thermocouple, not accounted for in data reduction, is seen between the premixed flame

and the diffusion flame in Fig. 6.6 (b) where the measured values are too high by roughly 100 K; the displacement of the temperature profile on the air side in Fig. 6.7 (b) is within experimental positioning uncertainty. Because of the more stringent spatial resolution requirements in the diffusion flame, observed differences in profile shapes in Fig. 6.7 cannot definitively be attributed to deficiencies in the computational results.

The agreements of the profiles of methane and of ethylene plus acetylene (computationally about 80% ethylene) are good in both of these figures, thereby lending experimental support to the present mechanism. In contrast, the mechanism of Li [6] produces poorer agreement, giving slightly high predictions of C_2H_2+C_2H_4 peaks and underpredicting the height of the CH_4 peaks by nearly a factor of two, the latter illustrated by the light dashed curve in Fig. 6.6 (b). It may be noted that in the diffusion flame the peak CH_4 concentration is only about 60% that in the partially premixed flame, while the peak C_2H_4 concentration is 25% greater, illustrating the proportionally larger contributions of the paths on the left-hand side of Fig. 6.1 for the diffusion flame. The mechanism underpredicts ethane concentrations somewhat, by about 30% for the partially premixed flame and nearly 50% for the diffusion flame; the underpredictions by other mechanisms [5, 6] are comparable to this. This difference can be removed for the present mechanism by decreasing the rate of the step $C_2H_6+H \rightarrow C_2H_5+H_2$ by a factor of two (within uncertainties) or by adding a step $C_2H_5OH+H \rightarrow C_2H_6+OH$ at a rate somewhat less than that of other H attacks on the fuel; the latter of these has not been considered in studies [32] of this system and may not be likely.

6.5 CONCENTRATION PROFILES RELATED TO POLLUTANTS

Figures 6.6 (b) and 6.7 (b) also show computed NO_x profiles in these flames. Here NO_x is defined as the sum of NO and NO_2, but in all cases NO dominates in the flames. Based on methanol-flame studies, general belief was that in contrast to hydrocarbon flames, the thermal mechanism is much more important than the prompt mechanism for alcohol flames in these counterflow, atmospheric-pressure experiments because the CH concentrations are smaller. They are entirely negligible in methanol flames and, for these ethanol flames, less than half the values calculated for hydrocarbon flames. However, the reaction-pathways analysis of these flames show that in these ethanol flames the prompt mechanism is more important than the thermal mechanism; almost all NO was from the prompt route in the nonpremixed flame, and about 70% of NO produced in the partially premixed flame was from the prompt route. In Fig. 6.6 (b) the peak NO_x concentration, about 40 ppm, is nearly twice that in Fig. 6.7 (b), mainly because the peak flame temperature of the partially premixed flame is higher in these two experiments. In general, peak NO concentrations in ethanol flames were calculated to be comparable with those in methanol flames and about half those in hydrocarbon flames. Although NO profiles were not measured in these experiments, they have been measured earlier in our laboratory by T. Hiraiwa under quite similar conditions and are shown in Fig. 6.8 along with a curve giving computed results for those conditions. The close agreement in Fig. 6.8 lends credence to the computational NO_x results.

For these types of counterflow flames, extending to partial-premixing equivalence ratios of 1.5, peak methane concentrations in ethanol flames are calculated to be about twice those in methanol or hydrocarbon flames, while peak total concentrations of C_2 species (sum of C_2H_2, C_2H_4 and C_2H_6) in ethanol flames are calculated to be comparable

with those of most hydrocarbon flames, more than twice those in methane flames and nearly one hundred times those in methanol flames. This last result may help to account for the relatively high sooting tendency of ethanol (and higher alcohols); ethylene has been seen to be a very significant decomposition product of ethanol in these flames. Alcohol diffusion and partially premixed flames also exhibit higher maximum CO concentrations than hydrocarbon flames. These observations, along with the previously noted high acetaldehyde and formaldehyde concentrations in the ethanol flames studied here, suggest that pollutant-emission concerns will be different for ethanol than they are for methanol or for hydrocarbons.

6.6 CONCLUSIONS

Although the ethanol studies show that agreements between experiments and predictions for near-atmospheric pressures are reasonably good, more work should be done in the chemical-kinetic model in evaluating the performance of the mechanism. This would necessitate additional experimental, chemical-kinetic and computational work. It would be of interest to measure additional species in these flames at normal atmospheric pressure and also to perform experiments and make comparisons at higher pressures, since many of the applications of interest are at elevated pressures. The current study is a step forward in the effort to minimize the uncertainties in the predictions of ethanol combustion and to identify the associated chemical-kinetic channels. Similar to methanol, ethanol is expected to reduce NO_x emissions, but it may not be comparably effective in soot reduction and may exacerbate concerns about aldehydes. This study may contribute

towards enhancement of understanding of ethanol combustion and assessment of its utility as a fuel.

Comment

Eva Gutheil, Heidelberg, Germany: As you go from the nonpremixed flame to the partially premixed flame, a second green premixed flame zone appears at a certain degree of premixedness. How does this flame affect the NO profile?

Reply

As the degree of partial premixing increases at a constant strain rate, the NO profile broadens, but the peak remains at the diffusion flame, where the temperature is highest. The variation of the peak NO concentration with the degree of partial premixing depends, however, on the degree of dilution of the fuel stream, as a consequence of the competition between the prompt and thermal pathways. Of our two experiments, the diffusion-flame experiment involved nitrogen-diluted fuel against air and had a lower flame temperature, resulting in a calculated peak NO concentration of 25 ppm, almost all from the prompt mechanism. The partially premixed flame, on the other hand, involved a fuel-air mixture against air, resulting in a higher flame temperature and a peak NO concentration of 40 ppm, about 30% of which was attributable to the thermal mechanism. For the latter case, computations indicated very slight increases in peak NO concentrations with increasing premixing until a fuel-side equivalence ratio of about 10 was reached, beyond which, at lower equivalence ratios, there was a sharp drop in the peak NO concentrations with increasing premixing through reduction in the prompt

pathways. If oxygen were added to the fuel stream in our diffusion-flame experiment, on the other hand, computations predict significantly increased peak NO concentrations, partially through onset of the thermal mechanism (which occurs at about an equivalence ratio of 5) as a consequence of the increased flame temperature, followed again by a sharp decrease at high premixing through suppression of the prompt mechanism.

ACKNOWLEDGEMENT

This chapter, in full, is a reprint of the material as it appears in the article: P. Saxena and F.A. Williams, "Numerical and Experimental Studies of Ethanol Flames", *Proceedings of the Combustion Institute*, 31, 2007, pp.1149-1156. The dissertation author was the primary researcher in that publication.

Table 6.1 New ethanol rate parameters

Step	
$C_2H_5OH + M^a \rightarrow CH_3 + CH_2OH + M$	$k_0 = 3.0\times10^{16}\, e^{(-242.4/RT)}$ cm^3/mol s $k_\infty = 5.0\times10^{15}\, e^{(-342.8/RT)}$ s^{-1}
$C_2H_5OH + M^a \rightarrow C_2H_4 + H_2O + M$	$k_0 = 1.0\times10^{17}\, e^{(-225.7/RT)}$ cm^3/mol s $k_\infty = 8.0\times10^{13}\, e^{(-271.7/RT)}$ s^{-1}

[a]Chaperon efficiencies are 2.0 for H_2, 6.0 for H_2O, 1.5 for CO, 2.0 for CO_2, 2.0 for CH_4, 0.7 for Ar and He and 1.0 for all other species; Troe falloff with F_c = 0.5; units of activation energies are kJ/mol.

Table 6.2 Experimental conditions and boundary conditions used in the numerical calculations (symbols: X = mole fraction, V = duct exit velocity, T = temperature; subscripts: F = fuel stream, Ox = oxidizer stream, ad = adiabatic flame)

FUEL STREAM	NON PREMIXED	PARTIALLY PREMIXED
$X_{C_2H_5OH}$	0.3	0.1385
X_{N_2}	0.7	0.6803
X_{O_2}	0	0.1812
V_F	29.8 cm/s	30.22 cm/s
T_F	340 K	327 K
OXIDIZER STREAM		
X_{N_2}	0.79	0.79
X_{O_2}	0.21	0.21
V_{Ox}	30 cm/s	30 cm/s
T_{Ox}	298 K	298 K
T_{ad}	2070 K	2240 K

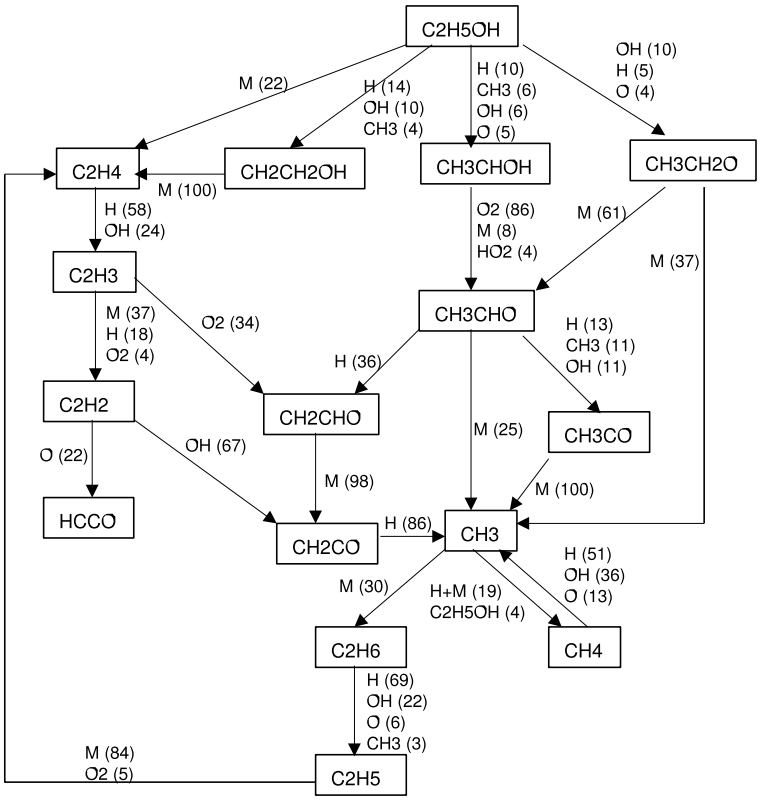

Figure 6.1 Reaction-path diagram of the ethanol partially premixed flame listed in Table 2.

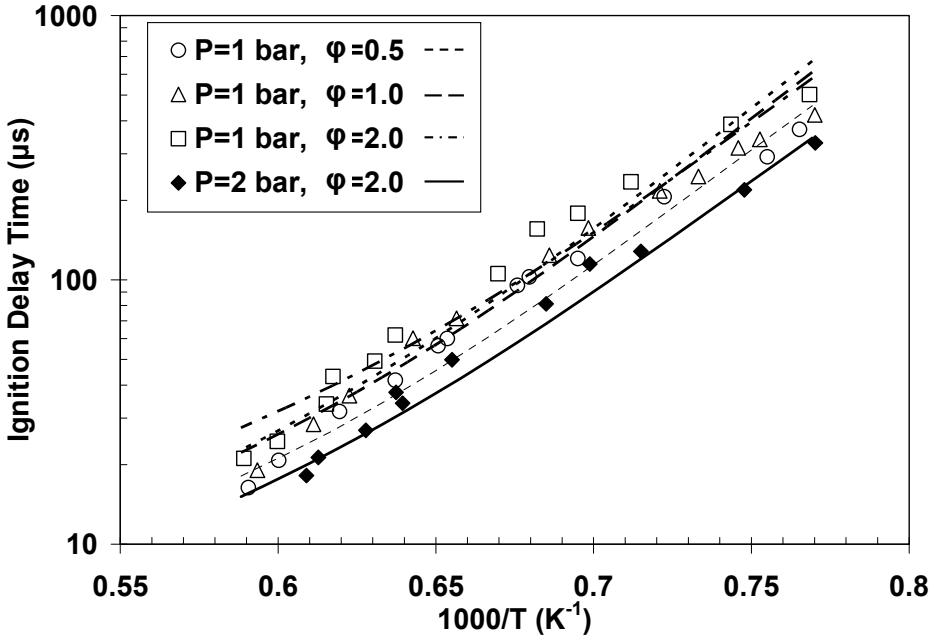

Figure 6.2 Comparisons of measured [20] and calculated autognition delay times for φ=0.5, 1.0 and 2.0 at P=1 bar and for φ=2.0 at P=2 bar, with 90% Ar dilution; the experimental ignition criterion was first visible light emission.

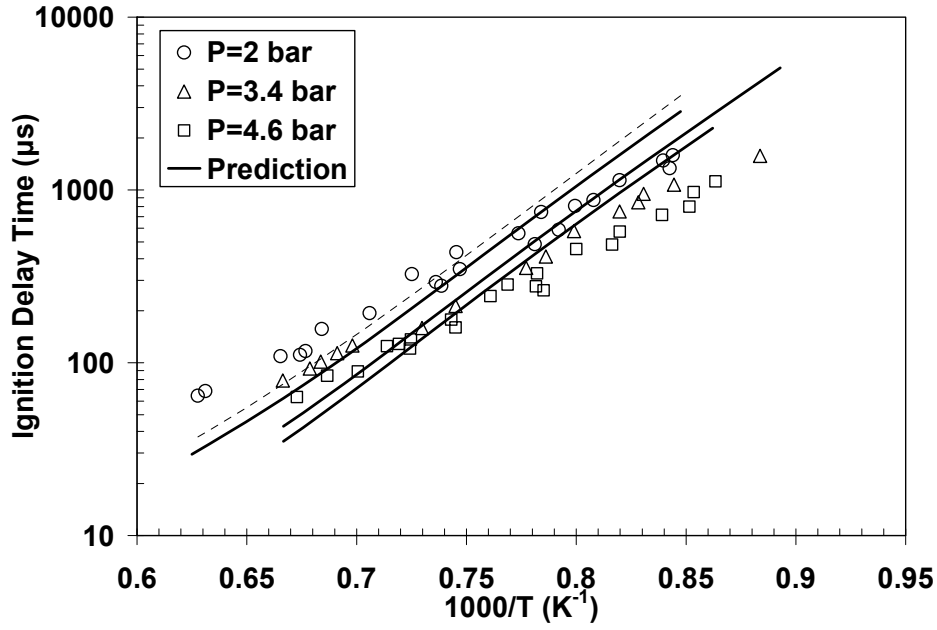

Figure 6.3 Comparisons of measured [21] and calculated autognition delay times for autognition delay times for φ=0.25 at P=2 bar, P=3.5 bar and P=4.6 bar, with 92% Ar dilution; the experimental ignition criteria were pressure rise, OH emission and the chemiluminesent reaction between CO and O.

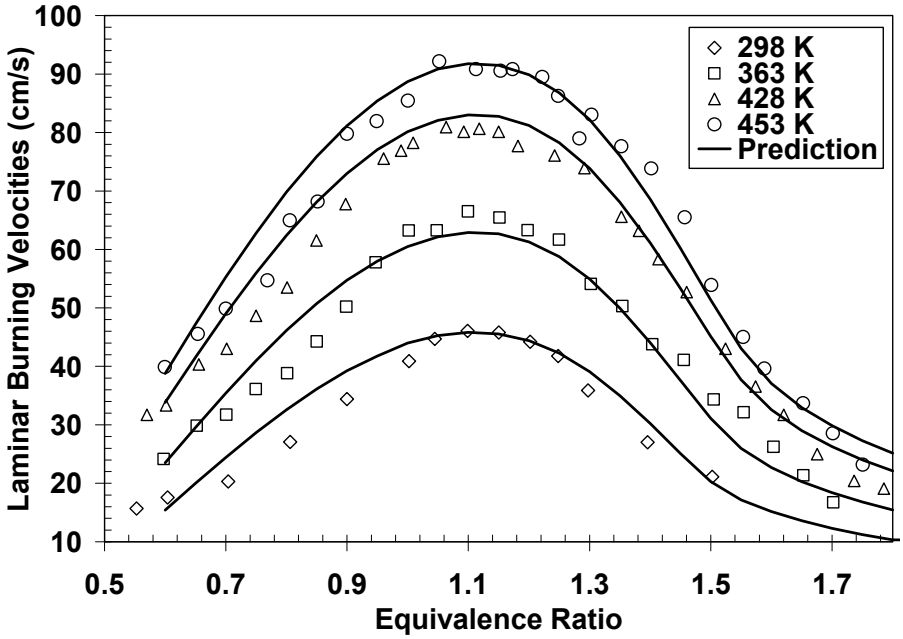

Figure 6.4 Comparison of measured [23] and calculated laminar burning velocities for ethanol-air mixtures at initial temperatures of 298 K, 363 K, 428 K, 453 K at P=1atm.

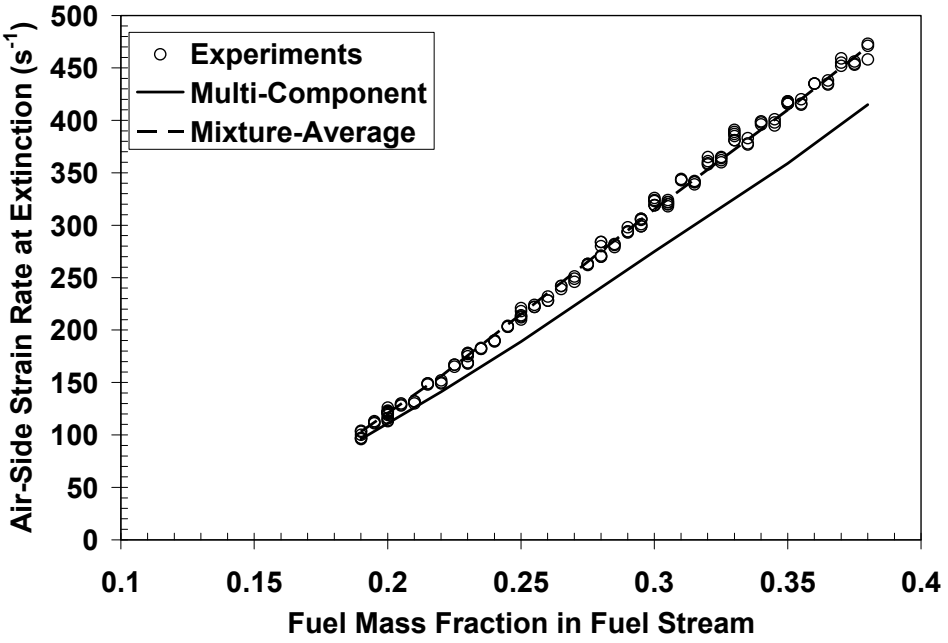

Figure 6.5 Comparison of measured [24] and calculated diffusion-flame extinction strain rates at P=1 atm for fuel-stream temperature T_F=323 ± 10 K and air temperature T_{Ox}=298 K; distance between the exit ducts was 10 mm, and the strain rate was calculated from measured flow rates using a plug-flow formula [25].

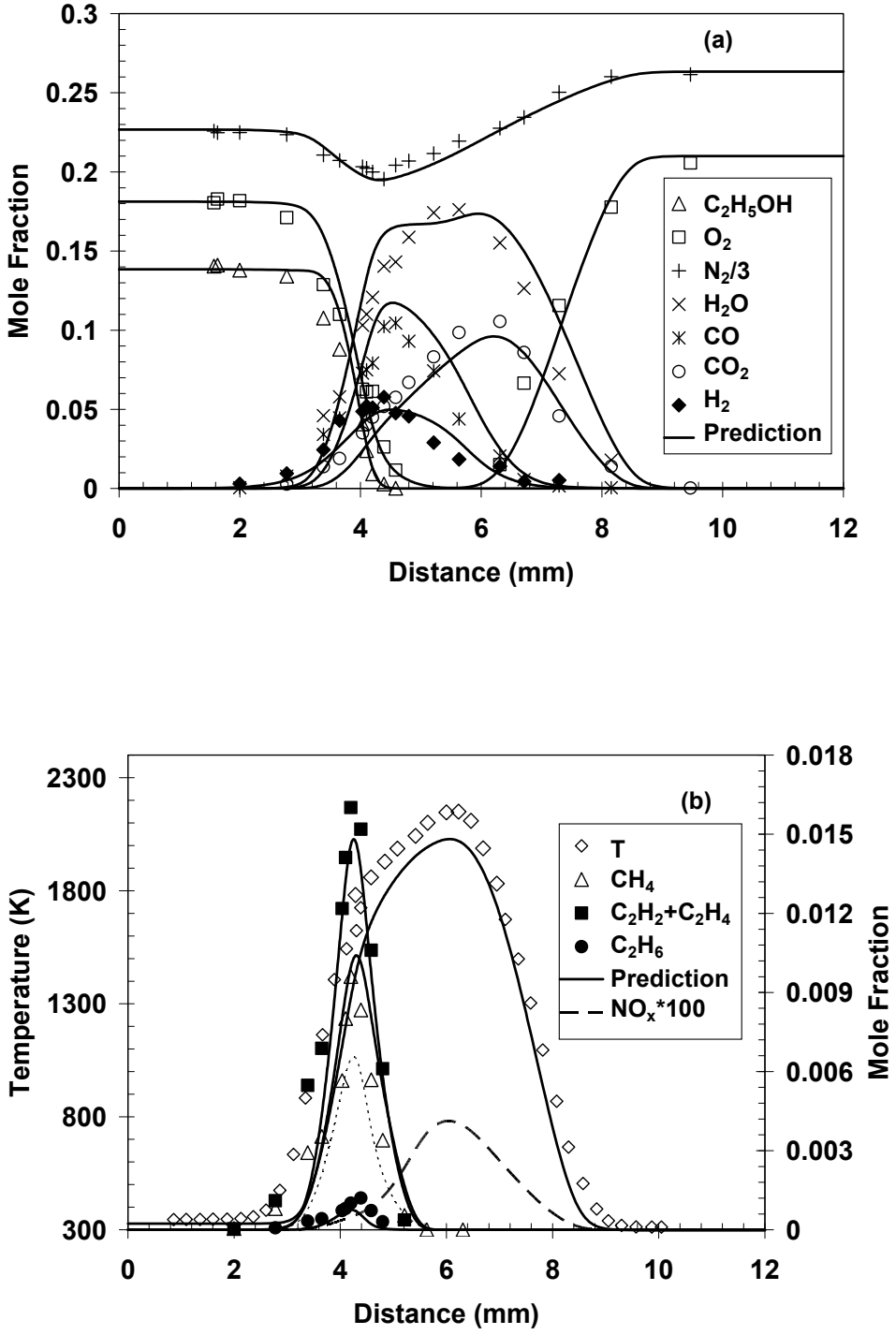

Figure 6.6 Ethanol partially premixed flame structures: (a) Concentration profiles for C_2H_5OH, N_2, O_2, H_2O, CO, CO_2 and H_2, (b) Temperature profile and concentration profiles for CH_4, C_2H_2+C_2H_4, C_2H_6 and NO_x.

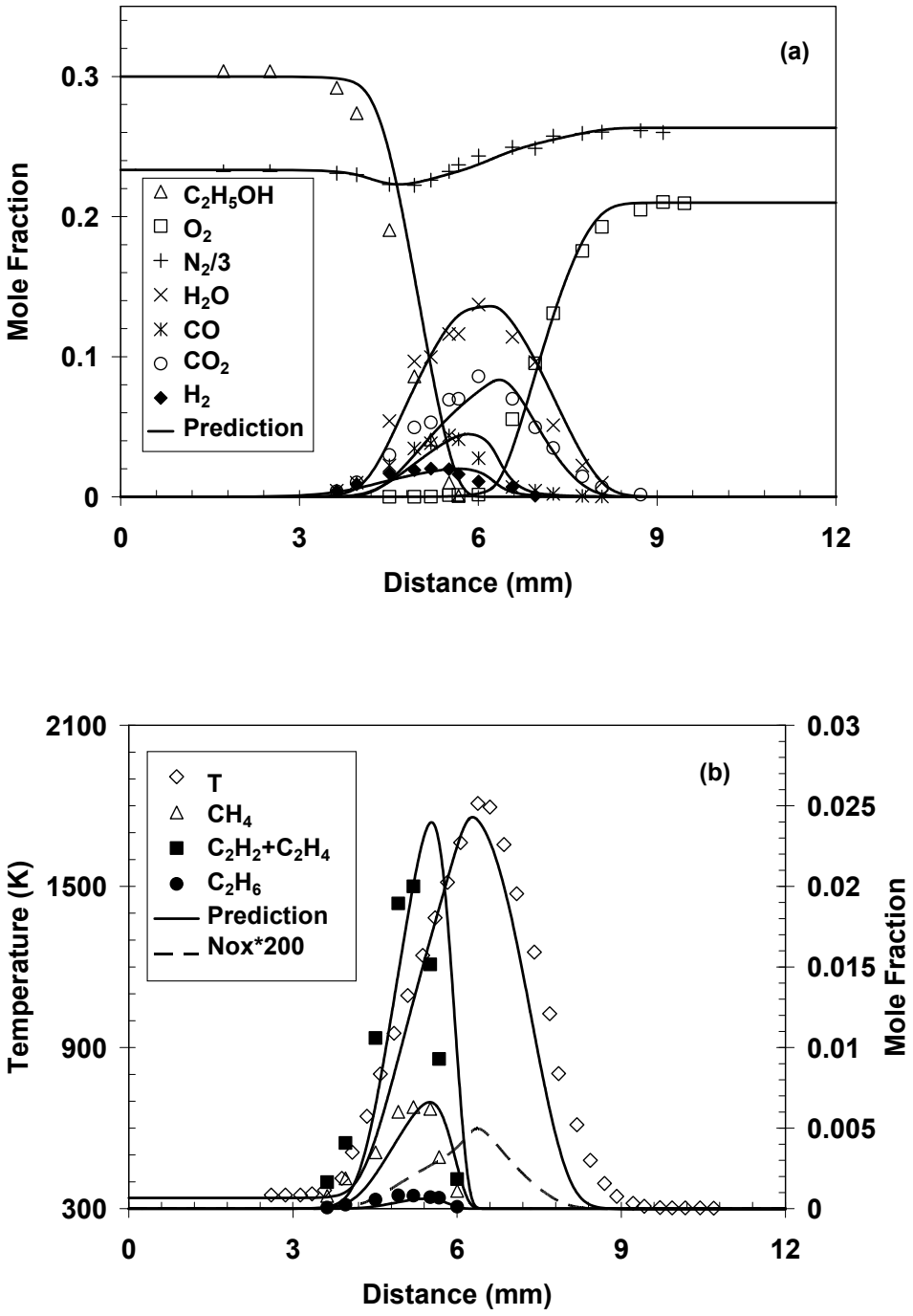

Figure 6.7 Ethanol nonpremixed flame structures: (a) Concentration profiles for C_2H_5OH, N_2, O_2, H_2O, CO, CO_2 and H_2, (b) Temperature profile and concentration profiles for CH_4, C_2H_2+C_2H_4, C_2H_6 and NO_x.

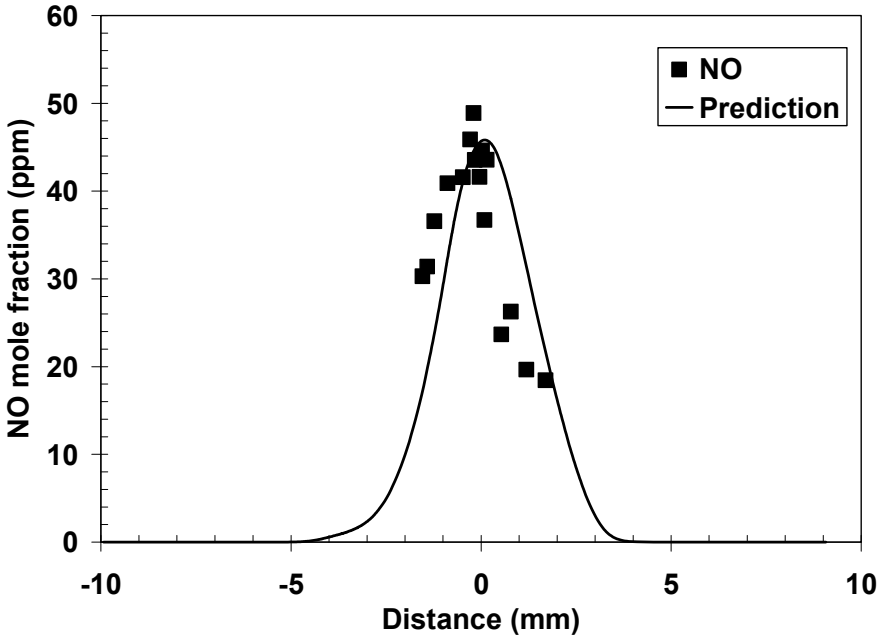

Figure 6.8 Comparison of measured and calculated NO concentration profiles for a partially premixed ethanol-air flame with fuel-side equivalence ratio φ = 2.3, and plug-flow strain rate 53 s^{-1}.

6.7 REFERENCES

1. Dunphy, M.P., Patterson, P.M. and Simmie, J.M., "High-temperature oxidation of ethanol. Part II – Kinetic modeling", Journal of the Chemical Society, Faraday Transactions, 87, 1991, pp. 2549-2559.

2. Borisov, A.A., Zamanskii, V.M., Konnov, A.A., Lisyanskii, V.V., Rusakov, S.A. and Skachkov, G.I., "A mechanism of high-temperature ethanol ignition", Soviet Journal of Chemistry and Physics, 9, 1992, pp. 2527-2537.

3. Dagaut, P., Boettner, J.C. and Cathonnet, M., "Kinetic modeling of ethanol pyrolysis and combustion", Journal de Chimie Physique, 89, 1992, pp. 867-884.

4. Norton, T.S. and Dryer, F.L., "An experimental and modeling study of ethanol oxidation kinetics in an atmospheric pressure flow reactor", International Journal of Chemical Kinetics, 24, 1992, pp. 319-344.

5. Marinov, N.M., "A detailed chemical kinetic model for high temperature ethanol oxidation", International Journal Chemical Kinetics, 31, 1999, pp. 183-220.

6. Li, J., "Experimental and numerical studies of ethanol chemical kinetics," PhD Thesis, Princeton University, 2004.

7. Saxena, P., and Williams, F. A., "Testing a small detailed chemical-kinetic mechanism for the combustion of hydrogen and carbon monoxide", Combustion and Flame, 145, 2006, pp. 316-323**.**

8. Li, S.C. and Williams, F.A., "NO_x formation in two-stage methane-air flames", Combustion and Flame, 118, 1999, pp. 399-414.

9. Shimizu, T., Williams, F.A. and Frassoldati, A., "Concentrations of nitric oxide in laminar counterflow methane/air diffusion flames", Journal of Propulsion and Power, 21, 2005, pp. 1019-1028.

10. Waly, M.M.Y., Li, S.C. and Williams, F.A., "Experimental and numerical studies of two-stage ethane-air flames", Journal of Engineering for Gas Turbines and Power, 122, 2000, pp. 651-658.

11. Varatharajan, B. and Williams, F.A., "Ethylene ignition and detonation chemistry, Part 1: Detailed modeling and experimental comparison", Journal of Propulsion and Power, 18, 2002, pp. 344-351.

12. Waly, M.M., Li, S.C. and Williams, F.A., "Structures of non-sooting counterflow diluted acetylene-air flames", Proceedings of the Combustion Institute, 28, 2000, pp. 2005-2012.

13. Varatharajan, B. and Williams, F.A., "Chemical-kinetic descriptions of high-temperature ignition and detonation of acetylene-oxygen-diluent systems", Combustion and Flame, 124, 2001, pp. 624-645.

14. Petrova, M.V. and Williams, F.A., "A small detailed chemical-kinetic mechanism for hydrocarbon combustion", Combustion and Flame, 144, 2006, pp. 526-544.

15. Li, S.C. and Williams, F.A., "Experimental and numerical studies of two-stage methanol flames", Proceedings of the Combustion Institute, 26, 1996, pp. 1017-1024.

16. Li, S.C. and Williams, F.A., "Formation of NO_x, CH_4, and C_2 species in laminar methanol flames", Proceedings of the Combustion Institute, 27, 1998, pp. 485-493.

17. Available at: http://maemail.ucsd.edu/combustion/cermech/

18. Kee, R.J., Rupley, F.M., Miller, J.A., Coltrin M.E., Grcar, J.F., Meeks, E., Moffat, H.K., Lutz, A.E., Dixon-Lewis, G., Smooke, M.D., Warnatz, J., Evans, G.H.,

Larson, R.S., Mitchell, R.E., Petzold, L.R., Reynolds, W.C., Caracotsios, M., Stewart, W.E., Glarborg, P., Wang, C., Adigun, O., Houf, W.G., Chou, C.P. and Miller, S.F., Chemkin Collection, Release 3.7.1, Reaction Design Inc., San Diego, CA, 2003.

19. Pitsch, H., "Entwicklung eines Program-pakets zur Berechnung eindimensionaler Flammen am Beispiel einer Gegenstvomdiffusionflamme", M.S. Thesis, RWTH Aachen, Germany, 1993.

20. Natarajan, K. and Bhaskaran, K.A., "An experimental and analytical investigation of high temperature ignition of ethanol", Thirteenth International Symposium on Shock Waves, 1982, pp. 834-842.

21. Dunphy, M.P. and Simmie, J.M., "High-temperature oxidation of ethanol", Journal of Chemical Society Faraday Transaction, 87, 1991, pp. 1691-1696.

22. Curran, H.J., Dunphy, M.P., Simmie, J.M., Westbrook, C.K. and Pitz, W.J., "Shock tube ignition of ethanol, isobutene and MTBE: Experiments and modeling", Proceedings of the Combustion Institute, 24, 1992, pp. 769-776.

23. Egolfopoulos, F.N., Du, D.X. and Law, C.K., "A study on ethanol oxidation kinetics in laminar premixed flames, flow reactors, and shock tubes", Proceedings of the Combustion Institute, 24, 1992, pp. 833-841.

24. Seiser, R. and Seshadri, K., "Counterflow extinction of premixed and nonpremixed methanol and ethanol flames", Western States Section, The Combustion Institute, 2002 Spring Meeting, University of California at San Diego, La Jolla, CA 92093-0411, March 25-26, 2002, Paper # 02S-27.

25. Seshadri, K. and Williams, F.A., "Laminar flow between parallel plates with injection of a reactant at high Reynolds number", International Journal of Heat and Mass Transfer, 21, 1978, pp. 251-253.

26. Paul, P. and Warnatz, J., "A re-evaluation of the means used to calculate transport properties of reacting flows", Proceedings of the Combustion Institute, 27, 1998, pp. 495-504.

27. Dong, Y., Holley, A.T., Andac, M.G., Egolfopoulos, F.N., Davis, S.G., Middha, P. and Wang, H., "Premixed extinction of H_2/air flames: Chemical Kinetics and Diffusion Effects", WSS/CI 2004 Spring Meeting, Paper 04S-19.

28. Seiser, R., "Nonpremixed combustion of liquid hydrocarbon fuels", Ph.D. thesis, Technical University of Graz, 2000.

29. Shaddix C.R., “Practical aspects of correcting thermocouple measurements for radiation loss”, Western State Section/The Combustion Institute, University of Washington, Seattle WA, Oct. 26-27, 1998, WSS/CI 98F-24.

30. Seiser, R., Truett, L., Trees, D. and Seshadri, K., “Structure and extinction of non-premixed n-heptane flames”, Proceedings of the Combustion Institute, 27, 1998, pp. 649-657.

31. Tanoue, K., Seiser, R., and Seshadri, K., “The structure of nonpremixed n-decane flames”, Proceedings of the Third Joint Meeting of the U.S. sections of The Combustion Institute, The University of Illinois at Chicago, Chicago, March 16-19, 2003, Paper A31.

32. Park, J., Xu, Z.F. and Lin, M.C., “Thermal decomposition of ethanol. II. A computational study of the kinetics and mechanism for the $H+C_2H_5OH$ reaction”, Journal of Chemical Physics, 118, 2003, pp. 9990-9996.

CHAPTER 7

AUTOIGNITION THEORY FOR HIGHER ALKANES

7.1 OVERVIEW

In both propulsion and explosion-safety applications, as well as in fundamental investigations such as computational approaches to descriptions of combustion processes, there is a need for simple analytical expressions for autoignition induction times. Expressions of that type can be obtained empirically from experiment, as they often have been [1-5], but this requires experiments to be performed for each fuel over the full range of conditions of interest. At the opposite extreme, programs are now readily available [6, 7] that enable autoignition times in homogeneous, adiabatic systems to be computed readily with full detailed chemical-kinetic mechanisms, and empirical fits to the computational results can be made. This, however, does not aid in understanding or in extension to conditions that have not been computed.

Autoignition times of most fuels, especially higher hydrocarbons, seem to be remarkably similar in both value and temperature dependence in the temperature range between about 1000 K and 2500 K. This suggests that the length of the induction period may be controlled by chemistry that the fuels have in common, not strongly dependent on the specific fuel and not reliant on the full complex details of the true chemical mechanism. A simple set of key elements of that common chemistry, however, has not yet been identified. Once that set is determined, if it is simple enough then it can readily be used to derive a general analytical autoignition-time formula from basic first

principles. Simplifying the chemistry and deriving such a formula is the objective of the present study.

7.2 BASIS OF THE APPROACH

It has been observed from computational ignition studies that, in high-temperature autoignition of propane and higher alkanes, during the induction stage that follows the very short initiation stage, the parent fuel molecule is a major sink for radicals [8-11]. The extent to which this statement is true varies somewhat, of course, with the fuel and the conditions. It is of interest to present here a representative demonstration. For that purpose, consider a homogeneous, isochoric, adiabatic, stoichiometric propane-air mixture at 1 atm and initially at 1500 K. Results of computations employing the detailed San Diego reaction mechanism [12], obtained by using the FlameMaster program [7], are shown in Fig. 7.1, where, following a brief initiation period, lasting perhaps 1 μs and seen most clearly in the profiles of the H and O mole fractions, there is a long induction period, lasting on the order of 100μs, during which the fuel concentration gradually decreases, prior to an abrupt, sharp temperature increase, at what usually is termed an induction time or an autoignition time. From the temperature profile shown in Fig. 7.1 it may be inferred that the time at which the inflection point occurs in the temperature profile is one convenient precise definition of an autoignition time. Assessment of the extent to which the fuel is the main radical sink therefore may be made by focusing attention on the history up until this inflection point.

For the conditions of Fig. 7.1, Fig. 7.2 shows the calculated fraction of the radical-depletion steps attributable directly to interactions with the parent fuel molecule,

for the most reactive radicals, H, O and OH. This fraction, defined as the ratio of the forward rate of the reaction with fuel to the total rate of consumption (excluding all generation steps for the radical in question), was calculated as a function of time by post-processing FlameMaster output. It is evident from Fig. 7.2 that, for the first 70% of the induction period, most of the sink of the key H radical is attributable to the parent fuel. Figure 7.2 shows that the fuel is also the major contributor to O-atom removal but that this is not the case for OH, and it is even less true for HO_2, for which fuel interactions constitute only a minor component of its consumption. The radical OH, however, cycles through H and O, for example in the hydrogen-oxygen shuffle reactions, notably $OH+H_2 \rightarrow H_2O+H$, and therefore the H and O sinks indirectly generate an OH sink as well. Although the parent fuel contribution to the H and O removal, of course, decreases sharply towards the end of induction, as its concentration decreases and the concentrations of secondary fuel species and radicals increase, during much of the induction period, 60% or more of the consumption of what is usually the most important radical, the H atom, is through its collision with the original fuel molecules. This, moreover, is a lower limit in the sense that computations for higher hydrocarbons than propane have shown even greater percentage contributions from fuel. The statement of effective domination of chain-branching radical removal by the parent fuel therefore is reasonably accurate.

Given this fact, it may be concluded that the rapid radical buildup and associated heat release cannot occur until after the fuel concentration has decayed to a level comparable with that of the H and O radical concentrations. This is evident in Fig. 7.1. In a qualitative sense, it may thus be stated that autoignition cannot occur until after the fuel

is gone. There are three reasons for this. One is that, while H, O and OH interactions with oxygen have a net branching effect, their interactions with fuel species have a net termination effect. A second is that the elementary rates of H and O reactions with the parent fuel are comparable with or larger than the rates of reactions with most secondary fuel species. The third is that, during most of the induction period, the concentration of the parent fuel is the largest fuel-species concentration. There is a lot of it around, and it has a voracious appetite for gobbling up the highest-quality radicals. In view of these characteristics, a useful criterion for defining the autoignition time is the time required for fuel depletion to occur. What is needed, then, is a simple enough description of the chemistry of fuel depletion to produce a formula for the time that it takes the fuel to disappear. That chemistry is presented in the following section, after which methods are discussed and the ignition-time formula is derived. The formula is tested against experimental results for various fuels in subsequent sections.

7.3 HIGH-TEMPERATURE REDUCED CHEMISTRY OF FUEL DEPLETION

In an earlier paper, Peters et al. [8] addressed n-heptane autoignition, identifying chemistry operative in low-temperature, intermediate-temperature and high-temperature ranges, including the negative temperature coefficient in the intermediate-temperature range. The present work restricts attention to the high-temperature range and generalizes their n-heptane results for that range to other fuels. Chain initiation by fuel decomposition or by reactive fuel-oxidizer molecular collisions is slow and dominant only briefly at the beginning of induction. Subsequently during induction, fuel is consumed mainly through attacks by radicals such as H, O, OH and HO_2, producing from C_mH_n the radical C_mH_{n-1},

which is very reactive and decompose often unimolecularly. Here C_mH_{n-1} stands for all of the isomers, and therefore the rate of fuel consumption is the sum of the rates of production of isomers, which for HO_2 attack, for example, involves one to five elementary steps in the mechanisms for different fuels for which calculations will be made.

Table 7.1 presents a formal derivation of the reduced chemistry. It seems appropriate to give a descriptive derivation here. Although the O atom contributes to fuel consumption, its effect generally is small compared with the effects of H and OH, and therefore it is not taken into account here, excluding extremely fuel-lean conditions. Over a wide range of stoichiometry, then, the remaining dominant radicals that consume the fuel are H, OH and HO_2. The first two of these obey excellent steady-state approximations during nearly all of the induction period, and a steady-state approximation for HO_2 also seems reasonable. This is illustrated in Fig. 7.3 for the fuel and conditions of Fig. 7.1. This figure shows the calculated ratio of the magnitude of the difference between the production and consumption rates, to the production rate, as functions of time for H, O, OH and HO_2. It is seen from this figure that, during most of the induction period, the error in the steady-state approximation is much less than 10% for the main radicals and on the order of 10%, even for HO_2. There is a period of net consumption of OH, at the beginning and end of which the OH curves go to zero, and the HO_2 curve also goes to zero shortly before autoignition, when it begins to be consumed (see Fig. 7.1). Since computations for higher hydrocarbons than propane have shown even better satisfaction of steady states for these radicals, these approximations are quite

reasonable in seeking autoignition times with accuracies such that errors are on the order of 10%.

As indicated above, the computations also have shown that the main sink of H is its fuel-consumption step, $H+C_mH_n \rightarrow C_mH_{n-1}+H_2$, while its main source can be taken to be $OH+H_2 \rightarrow H_2O+H$, so that the rates of these two elementary steps are equated. Similarly, the main sink of OH is its fuel-consumption step, $OH + C_mH_n \rightarrow C_mH_{n-1} + H_2O$, and especially at high temperatures it is produced mainly by the decomposition of hydrogen peroxide, step 6 of Table 7.1, $H_2O_2+(M) \rightarrow 2OH+(M)$, for which falloff needs to be included, as is done throughout the present study. The OH steady state then requires that the rate of step 6 is half the sum of the rates of the steps $OH+C_mH_n \rightarrow C_mH_{n-1}+H_2O$ and $OH+H_2 \rightarrow H_2O+H$, steps 2 and 5 of Table 7.1, which, from the H steady state, is half the sum of the rates of H and OH attack on the fuel, steps 1 and 2 of Table 7.1. The total rate of fuel consumption thus is twice the rate of step 6 plus the rate of $C_mH_n+HO_2 \rightarrow C_mH_{n-1}+H_2O_2$, step 3 of Table 7.1.

To calculate this total rate, it is evident that the concentrations of H_2O_2 and of HO_2 must be determined in the analysis. An expression for the HO_2 concentration may be obtained from its steady state by observing that, as each fuel radical C_mH_{n-1} goes through its series of rapid decompositions, at one step along the way it produces a radical that attacks oxygen to form HO_2. A major assumption underlying the analysis is then that the resulting effective decomposition step for C_mH_{n-1} is $C_mH_{n-1}+O_2 \rightarrow HO_2+$smaller, more stable products, step 4 of Table 7.1, which is the only overall (non-elementary) step in the mechanism. An example of this is provided by the dominant chemistry for n-heptane [8]

for which C_2H_5 and C_3H_7 are the intermediate fuel radicals that attack oxygen to form HO_2.

The principle radicals produced by H abstraction from C_7H_{16} are 1-C_7H_{15} and 2-C_7H_{15}, the 3-C_7H_{15} and 4-C_7H_{15} radicals being of lesser importance and not addressed in the chemistry [8]. The first of these radicals, 1-C_7H_{15}, decomposes to $C_5H_{11}+C_2H_4$, and the second, 2-C_7H_{15}, decomposes to $C_4H_9+C_3H_6$. The C_5H_{11}, in turn, decomposes to $C_2H_4+C_3H_7$, while C_4H_9 decomposes to $C_2H_4+C_2H_5$, the C_5H_{11} and C_4H_9 radicals both being relatively unstable above 1000 K, like C_7H_{15}. The steps $C_3H_7+O_2\rightarrow C_3H_6+HO_2$ and $C_2H_5+O_2\rightarrow C_2H_4+HO_2$ are the dominant elementary steps by which another O_2 is consumed and HO_2 is produced under the conditions addressed in the paper [8]. Since propene and ethylene are more stable than the propyl and ethyl radicals, but, unlike C_5H_{11} and C_4H_9 the latter two are stable enough to primarily react with O_2 before decomposing, the hydroperoxyl radical is produced from these two lower alkyl radicals without appreciable influence of the alkenes. Sequences such as this, resulting in step 4, will be different for different fuels and for different conditions.

If the assumption in step 4 is accepted, then the steady-state approximation for C_mH_{n-1}, which is an excellent approximation during induction, implies that the total rate of production of C_mH_{n-1} minus the rate of step 3 equals the net positive rate of production of HO_2 in the fuel-consumption chemistry. Besides being produced in this way, HO_2 is consumed by the important elementary step $2HO_2\rightarrow H_2O_2+O_2$, step 7 of Table 7.1, so that the steady-state approximation for HO_2 implies that the rate of step 7 is half the difference between the total rate of production of C_mH_{n-1} and the rate of step 3. Since the total rate of production of C_mH_{n-1} equals the total rate of consumption of fuel, this

observation results in the rate of step 7 being equal to the rate of step 6, so that the concentration of the hydroperoxyl radical is given by

$$[\mathrm{HO_2}] = \sqrt{\left(\frac{k_6}{k_7}\right)[M][\mathrm{H_2O_2}]}, \tag{1}$$

where k_i denotes the specific reaction-rate constant for step i of Table 7.1. The formal derivation of these results is given in Table 7.1.

It is straightforward to write these results in terms of a two-step overall reduced chemistry. Adding steps 3 and 4 to eliminate the steady-state species HO_2 shows that the overall step

$$\mathrm{C_mH_n + O_2 \rightarrow H_2O_2 + P} \tag{2}$$

occurs at the rate ω_3 of step 3 which, in view of Eq. 1, is

$$\omega_3 = k_3\sqrt{\left(\frac{k_6}{k_7}\right)[M]\,[\mathrm{H_2O_2}]\,[\mathrm{C_mH_n}]}\ . \tag{3}$$

This formula demonstrates the general autocatalytic character of the overall step in Eq. (2), which results in the fuel actually disappearing completely at a finite time under the current set of approximations. Considering steps 2, 4, 6 and 7 to eliminate the steady-state species OH and HO_2 produces the overall step

$$2C_mH_n + O_2 \rightarrow 2H_2O + 2P, \qquad (4)$$

which then occurs at the rate ω_6, the only other finite rate that affects the species evolution under these steady states.

7.4 SENSITIVITY AND REACTION-PATH ANALYSES

The present analysis is based on the observation that, through the systematic reduction described above, the chemistry can be expressed by the seven steps in Table 7.1, with steady states leading to the conclusion that only the rate parameters of steps 3, 6 and 7 affect the fuel-depletion history and hence, by implication, the autoignition time. Although the reasoning has not made use of any formal routines for sensitivity analysis or for reaction-path diagrams, it is of interest to examine these methods within the context of the reduction that has been obtained. By way of illustration, therefore, for propane-air mixtures under the conditions of Fig. 7.1, a sensitivity analysis of the temperature-inflection autoignition time was run using the San Diego mechanism in the FlameMaster code. With forward and backward steps counted separately, there are 358 steps in this detailed mechanism, the sensitivities to the rate constants for all of which are given by the code. Under these conditions, the step with the highest sensitivity coefficient was the initiation step, $C_3H_8+M\rightarrow CH_3+C_2H_5+M$. The second highest sensitivity was for the branching step $H+O_2\rightarrow OH+O$, which exhibits high sensitivity under all conditions. The step with rate constant k_6, $H_2O_2+(M)\rightarrow 2OH+(M)$, was sixteenth on the list of sensitivity, the highest of the two steps $C_3H_8+HO_2\rightarrow C_3H_7+H_2O_2$, namely that for 1-$C_3H_7$ in the rate

constant k_3, was 54th (the other 65th), and the step with rate constant k_7, $2HO_2 \rightarrow H_2O_2+O_2$, was 157th. Yet the ignition-time formula agrees with the ignition time predicted by the detailed mechanism within 10%, as will be seen later.

It certainly is counterintuitive that such excellent agreement can be obtained by using only rate constants of steps that are 16, 54, 65 and 157 in the list of 358. This emphasizes the many adjustments that must occur in the steady-state balances during autoignition. There are many cancellations of large terms that finally leave small terms in control. Sensitivities to many of the steps vary strongly with conditions, indicating that the cancellations correspondingly vary. This observation emphasizes that sensitivity analysis is seldom a very useful tool in identifying reduced chemistry that will work well over a wide range of conditions when multiple steady-state approximations are involved in the reduction. This conclusion applies for two reasons; first, the radical pools are so tightly bound together by the chain reactions that rates of steps with low sensitivities finally control overall rates, and second, relative sensitivities of most steps vary so strongly with conditions that specific reduced chemistries derived from sensitivities generally apply only over limited ranges of conditions, much narrower than the range of the present study.

Within the context of the present mechanism, it is relevant to ask how the autoignition time can be so sensitive to the rate parameters of steps such as $H+O_2 \rightarrow OH+O$, while yet the chemistry summarized in Table 7.1 does not involve these rate parameters. The answer must lie in step 4 of Table 7.1, the ultimate one-to-one production of hydroperoxyl from the H-abstracted fuel radical. The effective stoichiometry of this step must depend on those rate parameters, leading to greater or

lesser amounts of ultimate HO_2 production when the values of the parameters are changed. From this viewpoint, it can be considered to be a remarkable coincidence that the true rate parameters happen to conspire to make step 4 be such an excellent approximation over so wide a range of conditions. Where the analysis does become inaccurate, as will be seen to occur under high-dilution conditions, the failure can be viewed as a consequence of inaccuracy of step 4.

It is common to believe that, if sensitivity analysis alone cannot identify a suitable reduced mechanism, then sensitivity analysis in conjunction with reaction-path analysis surely can. Just as there are a variety of different versions of sensitivity analyses, so there also are many different types of reaction-path (or reaction-flux) analyses that have been constructed for different purposes [13]. They have in common, however, the objective of identifying the major pathways of the chemistry and the elementary steps having the greatest contributions to these pathways. For the autoigntion processes addressed here, irrespective of what type of path analysis is selected, it is found that the major contributions to fuel consumption occur through steps 1 and 2 of Table 7.1, and the flux through step 3 is secondary to these. Yet the rate parameters for steps 1 and 2 do not appear in the reduced chemistry; the only relevant fuel-consumption rate parameter is that of step 3. This again emphasizes the complex adjustments that occur through the steady states. There is no combination of existing automated sensitivity and reaction-flux analyses that can produce the preceding overall reduced chemistry. Although the problem is one that could well be addressed by computational singular perturbations [14], to give approximately the same results that have been obtained here, we find the insights provided by the analytical presentation given here to be more revealing.

7.5 DERIVATION OF THE IGNITION-TIME FORMULA

When Eq. 1 is used in the expression for the total rate of consumption of fuel, it is found that, in a homogeneous system,

$$\frac{d[\mathrm{C_mH_n}]}{dt} = -k_3[\mathrm{C_mH_n}]\sqrt{\left(\frac{k_6}{k_7}\right)[M][\mathrm{H_2O_2}]} - 2k_6[M][\mathrm{H_2O_2}] \,. \tag{5}$$

Since the rate of step 6 equals the rate of step 7, the corresponding expression for the evolution of the concentration of hydrogen peroxide is simply

$$\frac{d[\mathrm{H_2O_2}]}{dt} = k_3[\mathrm{C_mH_n}]\sqrt{\left(\frac{k_6}{k_7}\right)[M][\mathrm{H_2O_2}]} \,, \tag{6}$$

as implied by Eq. 2. Under isothermal, isobaric conditions with [*M*] approximated as constant, a nondimensional time can be defined as

$$\tau = t\left\{\frac{2k_6^2k_3^2}{k_7}[M]^2\,[\mathrm{C_mH_n}]_o\right\}^{1/3} , \tag{7}$$

where the subscript *o* identifies the concentration at time t=0. With the further definitions

$$x = \frac{[\mathrm{C_mH_n}]}{[\mathrm{C_mH_n}]_o} \,, y = \frac{[\mathrm{H_2O_2}]}{[\mathrm{C_mH_n}]_o}\left\{\frac{4k_6k_7[M]}{k_3^2[\mathrm{C_mH_n}]_o}\right\}^{1/3} , \tag{8}$$

Eqs. 5 and 6 become

$$\frac{dx}{d\tau} = -y - ax\sqrt{y}, \quad \frac{dy}{d\tau} = x\sqrt{y}\,, \tag{9}$$

where

$$a = \left\{ \frac{\left(k_3^2 \left[\mathrm{C_m H_n} \right]_o \right)}{\left(4k_6 k_7 \left[M \right] \right)} \right\}^{1/3}. \tag{10}$$

The pair of first-order ordinary differential equations given in Eq. 9 is to be solved subject to the initial conditions that x=1 and y=0 at τ=0.

It is convenient to introduce the variable $z = \sqrt{y}$, so that Eq. 9 becomes

$$\frac{dx}{d\tau} = -z^2 - axz, \quad \frac{dz}{d\tau} = \frac{x}{2}, \tag{11}$$

giving the second-order, nonlinear problem

$$\frac{d^2 z}{d\tau^2} + az\frac{dz}{d\tau} + \frac{z^2}{2} = 0; \quad z = 0, \frac{dz}{d\tau} = \frac{1}{2} \text{ at } \tau=0. \tag{12}$$

The parameter a generally is small, and to leading order in an expansion for small a, with $u = \frac{dz}{d\tau}$, Eq. 12 then becomes

$$\frac{d\left(u^2\right)}{dz} = -z^2; \;\; u = \frac{1}{2} \text{ at } z=0 \quad , \tag{13}$$

the solution to which is

$$u = \sqrt{\frac{1}{4} - \frac{z^3}{3}} \quad . \tag{14}$$

Since the induction period ends when the fuel has been consumed completely, that is, when x=0, which corresponds to u=0, the nondimensional induction time is found to be

$$\tau_i = \int_0^{(3/4)^{1/3}} u^{-1} dz = 6^{1/3} \int_0^1 \left(1 - v^3\right)^{-1/2} dv = 2.548 \, , \tag{15}$$

in which the substitution $v = z/(3/4)^{1/3}$ has been employed, and the definite integral has been evaluated by numerical integration. In view of this result, Eq. 7 provides, for the dimensional induction time, the expression

$$t_i = \left\{ 8.27 \frac{k_7}{k_6^2 k_3^2 \left[M\right]^2 \left[\mathrm{C_m H_n}\right]_o} \right\}^{1/3} \quad . \tag{16}$$

7.6 TESTS OF IGNITION-TIME PREDICTIONS

The ignition-time predictions for the various fuels employ the reaction-rate parameters listed in Table 7.2, which are obtained from the San Diego mechanism [12], supplemented as described below separately for each fuel. Figure 7.4 compares the prediction of Eq. 16 with experimental ignition-delay results for five normal alkanes. The experimental conditions and associated references are identified in the figure captions, where φ denotes equivalence ratio and P pressure. Since rate parameters for the HO_2 attack on the fuel were available [12] only for propane, values of the parameters for n-butane were obtained from Marinov et al. [15], for n-pentane from Curran et al. [16], for n-heptane from Held et al. [17] and for n-decane from Zhao et al. [18]. Agreements are well within experimental uncertainty for all fuels. The agreements are especially good for the higher alkanes, and even for propane, the predictions are as good as those obtained with a full detailed mechanism [11]. Very extensive data are available for propane over wide ranges of conditions [11], and the agreement shown in Fig. 7.4 is representative of that found under other conditions (above 1000 K) as well.

Argon is the diluent in the experiments shown in Fig. 7.4. There also are experimental results for propane, heptane and decane with nitrogen as the diluent. These experimental results are compared with the predictions of the formula in Fig. 7.5. Again the agreements are seen to be very good, except at the lower temperatures, approaching 1000 K, as the chemistry for the intermediate-temperature range, not included in the present mechanism, begins to become important and decreases the ignition time.

Since the fuel-specific aspects of the chemistry are H abstraction from the fuel by H, OH and HO_2 and the subsequent production of HO_2 in the course of decay of the

radical formed by the abstraction, the theory may be expected to work for all fuels for which these abstractions are the main source of fuel consumption and lead to this HO_2 production. Fuels with three or more carbon atoms that have C-C single bonds are all good candidates for having these properties. With this in mind, tests were made for various fuels other than normal alkanes. Figure 7.6 shows comparisons for iso-octane, for which the rate parameters for HO_2 attack on fuel were obtained from Curran et al. [19], and for JP-10, a pure hydrocarbon, $C_{10}H_{16}$, of three intertwined rings, all with single C-C bonds. The agreements are seen to be quite good in Fig. 7.6, although for iso-octane the data are seen to depart from the prediction at lower temperatures, likely because of the system beginning to enter the intermediate-temperature regime, as in Fig. 7.5.

To investigate further the range of applicability of the theory, calculations were made for other aliphatics. Figure 7.7 shows comparisons for propene and ethylene. The agreement for propene is good, as might be expected from the fact that, in addition to the double bond, it has a single C-C bond, but the agreement for ethylene, which only has the double bond, is poor, exhibiting differences in excess of an order of magnitude. Tests also were made for some aromatics, and while the disagreement for benzene is comparable with (and in the same direction as) that for ethylene, the agreement for toluene is better, suggesting that, for aromatics with enough aliphatic components having a sufficient number of C-C single bonds, Eq. (16) no longer will overpredict ignition times. Just for curiosity comparisons also were made for methane, ethane, methanol, ethanol, formaldehyde and acetaldehyde. Even though the chemistry does not apply to these fuels, the slopes were found to be in reasonable agreement with experiment, and even the values fortuitously agreed for methanol and formaldehyde. These last

observations emphasize that autoignition-time agreements do not necessarily imply that the chemistry is correct.

A restriction imposed in deriving Eq. 16 was that the parameter *a* of Eq. 10 must be small. This was checked for the fuels and conditions of Fig. 7.4-7.7, and it was found that typically the values of *a* were of the order of 10^{-4}, never reaching 10^{-3} and therefore always entirely negligible. The value is especially small for the low-pressure, high-dilution conditions typical of shock-tube experiments, where *a* is less than 10^{-4}, but even at high pressure with no dilution, corrections would be small, as implied by Fig. 7.8, which indicates that the largest *a* may ever become (for example at 100 bar with no dilution at an equivalence ratio of 2) is still less than 0.1. Since these evaluations indicate that the largest ignition-time corrections associated with $a \neq 0$ will always be expected to be less than 1%, there is no motivation for carrying the analysis to higher order. The smallness of *a* is associated with the rate of fuel consumption by HO_2 being slow compared with that by H and OH.

7.7 RANGE OF VALIDITY OF THE THEORY

It should be clear intuitively that, even above 1000 K, the quantitative conversion described by step 4 of Table 7.1 cannot be accurate over the complete ranges of pressure, dilution and equivalence ratio for any given fuel. It therefore is worthwhile to investigate the range of validity of the theory by comparing its predictions with other available information. Since experiments necessarily cover only a restricted range of conditions, most of these comparisons must be with results of computations that employ detailed chemical mechanisms.

One question concerns the pressure dependence of the ignition time. The lower curves in Fig. 7.9 contrast the predicted pressure dependence of the ignition time for stoichiometric propane-air mixtures at 1500 K with results derived from a recent detailed mechanism [11, 12], employing temperature inflection under adiabatic, isochoric conditions as the ignition criterion. While the agreement is seen to be good everywhere, it is better at low pressure than at high pressure, but differences are always less than a factor of two. Similar good agreement has been shown earlier for heptane [8], where a 56-step mechanism was employed for the comparison. The upper curves in Fig. 7.9 explore the effect of dilution on agreements, again for stoichiometric systems with propane [11, 12] at 1500 K, now at 1 atm only. The trends again agree well, there being a tendency for the theory to underpredict ignition times at high dilution, but differences still remaining within a factor of two. At high dilution, the ignition time can become more sensitive to the ignition criterion, and the temperature-inflection criterion employed in the detailed-chemistry calculation gives ignition times that can differ from those based on other criteria by as much as a factor of two.

Finally, Fig. 7.10 contrasts dependences of ignition times on equivalence ratio for heptane. Results are shown for the present theory (the solid curves), for two sets of detailed-chemistry data (the 56-step mechanism [8] and the San Diego mechanism [12]) and for two different sets of experimental measurements. The experimental data points shown involve very small interpolations (for the top curves) or extrapolations (for the bottom curves) of reported results [5, 25] to the temperature selected for the figure (1100 K for the top curves and 1500 K for the bottom curves). For the top curves in the figure the equivalence ratio was varied by varying the fuel-air ratio in purely fuel-air systems,

which corresponds mainly to varying the fuel concentration, since the oxygen mole fraction is practically constant, always between 20% and 21%. For the bottom curves, on the other hand, the equivalence ratio was varied mainly by varying the oxygen concentration, the fuel concentrations being held fixed; in the highly diluted system of the bottom curves, which have argon as the diluent, the diluent mole fraction varies from about 90% to more than 97% as the oxygen concentration is decreased.

For the top curves in Fig. 7.10, which correspond to moderate-pressure, low-dilution conditions with nearly constant oxygen concentrations, the agreements between theory, experiment and computation are seen to be excellent, but for the bottom curves, which correspond to low-pressure, high-dilution conditions with varying oxygen concentrations, the detailed chemistry and experiment both exhibit an increase in ignition time with increasing equivalence ratio, while the theory predicts no change in ignition time. Although the experimental ignition criterion in this last set of data was the maximum CH emission [5], this maximum, which typically occurs somewhat later than the temperature inflection employed in the detailed-chemistry calculations, computationally exhibits approximately the same oxygen-concentration dependence as the temperature inflection. There thus clearly exists a qualitative influence of the oxygen concentration which the theory fails to capture.

From these comparisons it appears that the theory is most accurate for low dilution, moderate pressure and near stoichiometry, conditions that typically are of greatest practical interest. The theory tends to underpredict ignition times at high-pressure, high-dilution and fuel-rich conditions and to overpredict ignition times at fuel-lean conditions. The last tendency was observed in calculations performed under other

conditions as well, notably with propane as the fuel, and the discrepancies were observed in that case to be negligible at 1000 K but to increase with temperature. Although predictions could be improved in these respects by allowing some variability of the stoichiometry of step 4 in Table 7.1 with experimental conditions, the simplicity of the theory in its present form, along with its acceptable predictions in most cases of practical interest, argues against this extension.

7.8 CONCLUSIONS

For hydrocarbon fuels that contain at least three carbon atoms and at least one carbon-carbon single bond, the high affinity of the fuel for active radicals enables fuel depletion to be employed as a criterion for defining the delay time in autoignition. The simple analytical expression for the autoignition time, derived here from this criterion by introducing steady-state approximation for H, OH, HO_2 and the alkyl or alkyl-like radical, correctly predicts high-temperature ignition times for these fuels at conditions of practical interest, namely moderate pressures, near stoichiometry and without excessive dilution. The predictions seldom differ from experimental results or from results of computations with detailed chemistry by as much as a factor of two. These agreements point to the importance of H_2O_2 in the autoignition chemistry and emphasize the role of the steady-state balances in removing branching reaction rates of the most active radicals from the ignition-time formula. The results provide a new perspective on high-temperature autoignition chemistry and a general means of easily estimating ignition times of the large number of fuels addressed.

ACKNOWLEDGEMENT

This chapter, in full, is a reprint of the material as it appears in the article: P. Saxena, N. Peters, and F.A. Williams, "An Analytical Approximation for High-Temperature Autoignition Times of Higher Alkanes", *Combustion and Flame*, to appear, 2007. The dissertation author was the primary researcher in that publication.

Table 7.1 Formal Derivation of Reduced Chemistry

Elementary steps (except #4)

1. $C_mH_n+H\rightarrow C_mH_{n-1}+H_2$
2. $C_mH_n+OH\rightarrow C_mH_{n-1}+H_2O$
3. $C_mH_n+HO_2\rightarrow C_mH_{n-1}+H_2O_2$
4. $C_mH_{n-1}+O_2\rightarrow HO_2 + P$
5. $OH+H_2\rightarrow H_2O+H$
6. $H_2O_2+(M)\rightarrow OH+OH+(M)$
7. $HO_2+HO_2\rightarrow H_2O_2+O_2$

Introduce H, OH, HO_2 and C_mH_{n-1} steady states.
With ω_i denoting the rate of step i, moles
per unit volume per unit time,
$\omega_1 = \omega_5, \omega_2 + \omega_5 = 2\omega_6, \omega_3 + 2\omega_7 = \omega_4,$
$\omega_1 + \omega_2 + \omega_3 = \omega_4$. Therefore,
$\omega_1 + \omega_2 = 2\omega_6, \omega_7 = \omega_6,$

$$k_7[HO_2]^2 = k_6[M][H_2O_2].$$

Fuel consumption rate:

$$\omega_{C_mH_n} = -\omega_1 - \omega_2 - \omega_3 = -2\omega_6 - \omega_3$$

Rate of production of H_2O_2:

$$\omega_{H_2O_2} = \omega_3 + \omega_7 - \omega_6 = \omega_3$$

Table 7.2 Reaction-Rate Parameters Employed

Reaction			A[a]	n[a]	E[a]	Ref.
$HO_2 + HO_2 \rightarrow H_2O_2 + O_2$	(k_7)		3.02×10^{12}	0.0	5.8	[12]
[b]$H_2O_2 + (M) \rightarrow OH + OH + (M)$	(k_6)	k_0	8.15×10^{23}	-1.92	207.6	[12]
		k_∞	2.60×10^{19}	-1.4	214.7	
$C_3H_8 + HO_2 \rightarrow 1\text{-}C_3H_7 + H_2O_2$			9.64×10^{3}	2.6	58.2	[12]
$C_3H_8 + HO_2 \rightarrow 2\text{-}C_3H_7 + H_2O_2$			4.76×10^{4}	2.55	69.0	[12]
$C_4H_{10} + HO_2 \rightarrow 1\text{-}C_4H_9 + H_2O_2$			1.70×10^{13}	0.0	85.5	[15]
$C_4H_{10} + HO_2 \rightarrow 2\text{-}C_4H_9 + H_2O_2$			1.12×10^{13}	0.0	74.0	[15]
$C_5H_{12} + HO_2 \rightarrow 1\text{-}C_5H_{11} + H_2O_2$			1.68×10^{13}	0.0	85.4	[16]
$C_5H_{12} + HO_2 \rightarrow 2\text{-}C_5H_{11} + H_2O_2$			1.12×10^{13}	0.0	73.9	[16]
$C_5H_{12} + HO_2 \rightarrow 3\text{-}C_5H_{11} + H_2O_2$			5.60×10^{12}	0.0	73.9	[16]
$C_7H_{16} + HO_2 \rightarrow 1\text{-}C_7H_{15} + H_2O_2$			4.76×10^{4}	2.55	68.9	[17][c]
$C_7H_{16} + HO_2 \rightarrow 2\text{-}C_7H_{15} + H_2O_2$			1.93×10^{4}	2.6	58.1	[17]
$C_7H_{16} + HO_2 \rightarrow 3\text{-}C_7H_{15} + H_2O_2$			2.00×10^{4}	2.6	58.1	[17]
$C_7H_{16} + HO_2 \rightarrow 4\text{-}C_7H_{15} + H_2O_2$			9.64×10^{3}	2.6	58.1	[17]
$C_{10}H_{22} + HO_2 \rightarrow 1\text{-}C_{10}H_{21} + H_2O_2$			4.76×10^{4}	2.55	69.0	[18]
$C_{10}H_{22} + HO_2 \rightarrow 2\text{-}C_{10}H_{21} + H_2O_2$			1.93×10^{4}	2.6	58.1	[18]
$C_{10}H_{22} + HO_2 \rightarrow 3\text{-}C_{10}H_{21} + H_2O_2$			1.93×10^{4}	2.6	58.1	[18]
$C_{10}H_{22} + HO_2 \rightarrow 4\text{-}C_{10}H_{21} + H_2O_2$			1.93×10^{4}	2.6	58.1	[18]
$C_{10}H_{22} + HO_2 \rightarrow 5\text{-}C_{10}H_{21} + H_2O_2$			1.93×10^{4}	2.6	58.1	[18]
$C_{10}H_{16} + HO_2 \rightarrow C_3H_5 + C_2H_2 + C_5H_8 + H_2O_2$			1.93×10^{4}	2.6	58.1	[12][c]
$C_{10}H_{16} + HO_2 \rightarrow C_3H_3 + C_2H_4 + C_5H_8 + H_2O_2$			4.76×10^{4}	2.55	69.0	[12]
$C_8H_{18} + HO_2 \rightarrow 1\text{-}C_8H_{17} + H_2O_2$			2.52×10^{13}	0.0	85.4	[19]
$C_8H_{18} + HO_2 \rightarrow 2\text{-}C_8H_{17} + H_2O_2$			5.60×10^{12}	0.0	73.9	[19]
$C_8H_{18} + HO_2 \rightarrow 3\text{-}C_8H_{17} + H_2O_2$			2.80×10^{12}	0.0	66.9	[19]
$C_8H_{18} + HO_2 \rightarrow 4\text{-}C_8H_{17} + H_2O_2$			1.68×10^{13}	0.0	85.4	[19]
$C_3H_6 + HO_2 \rightarrow C_3H_5 + H_2O_2$			9.60×10^{3}	2.6	58.1	[20]
$C_2H_4 + HO_2 \rightarrow C_2H_3 + H_2O_2$			1.13×10^{13}	0.0	127.0	[12]

[a]Specific reaction-rate constant $k = AT^n e^{-E/R^o T}$; units mol/cm^3, s^{-1}, K, kJ/mol.
[b]Chaperon efficiencies are 2.0 for H_2, 6.0 for H_2O, 1.5 for CO, 2.0 for CO_2, 0.4 for Ar and He and 1.0 for all other species; Troe falloff with F_c = 0.265 exp (-T/94 K) + 0.735 exp (-T/1756 K) + exp (-5182 K/T).

[c]The steps shown include the lumping employed in the reference, but the rate is that of the hydrogen abstraction.

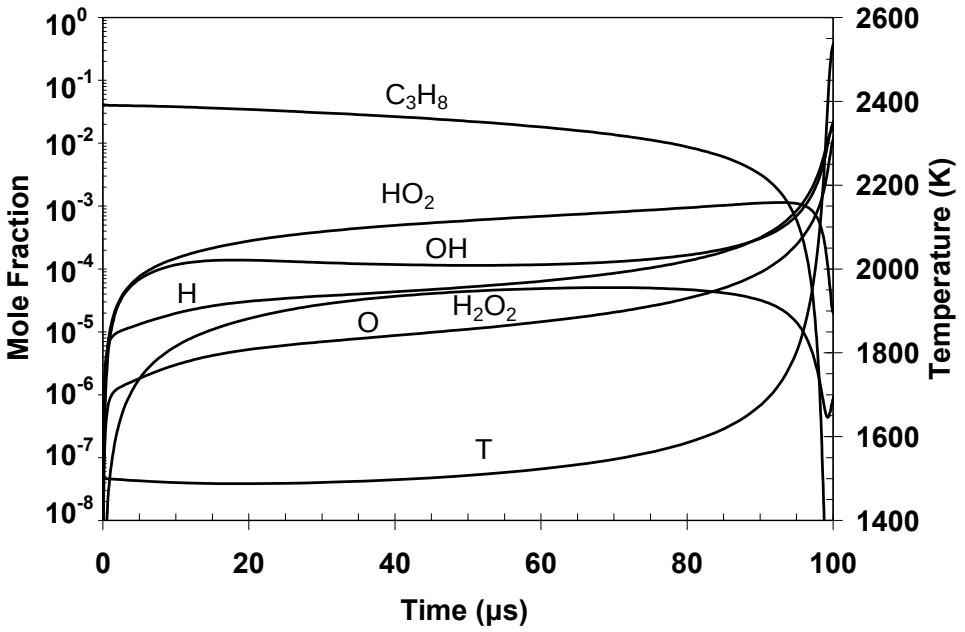

Figure 7.1 Computed histories of temperature and mole fractions for isochoric, adiabatic, stoichiometric propane-air mixtures at 1 atm and initially at 1500 K.

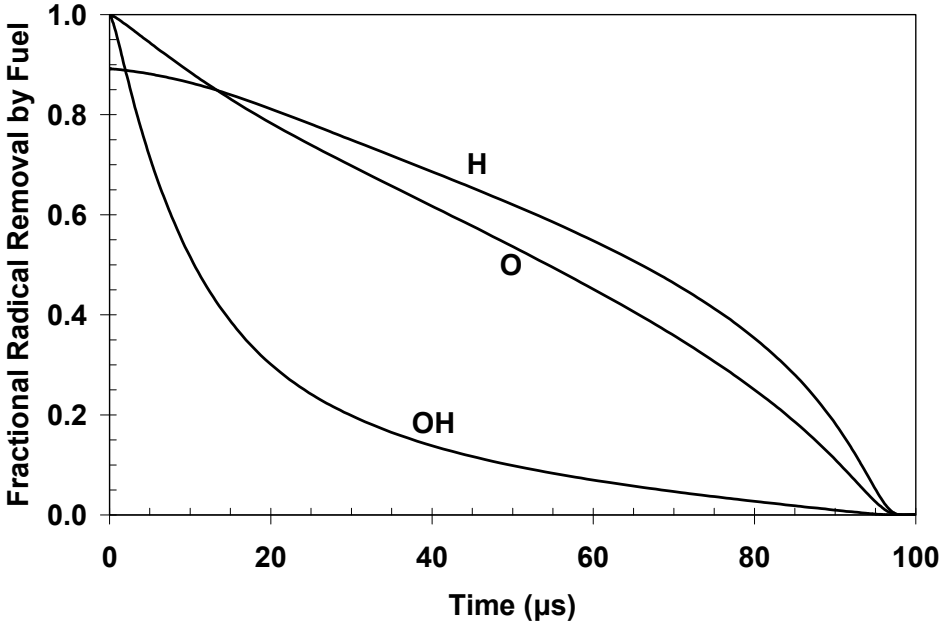

Figure 7.2 Computed ratio of the rate of reaction of the radical with the parent fuel to the total rate of consumption of the radical, for H, O and OH, as functions of time, for the fuel and conditions of Fig. 1.

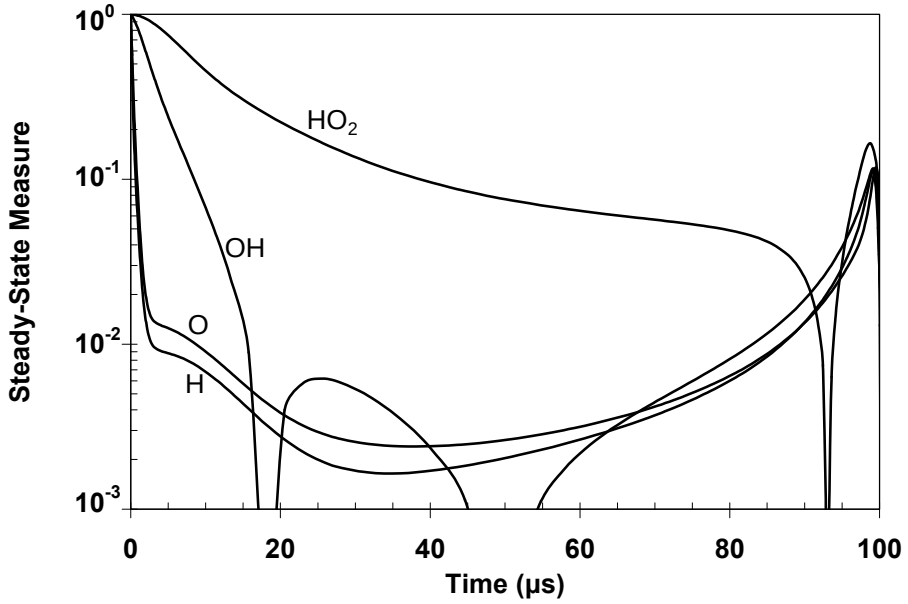

Figure 7.3 Computed magnitude of the difference between the production rate and the consumption rate, divided by the production rate, for four radicals, as functions of time, for the fuel and conditions of Fig. 1.

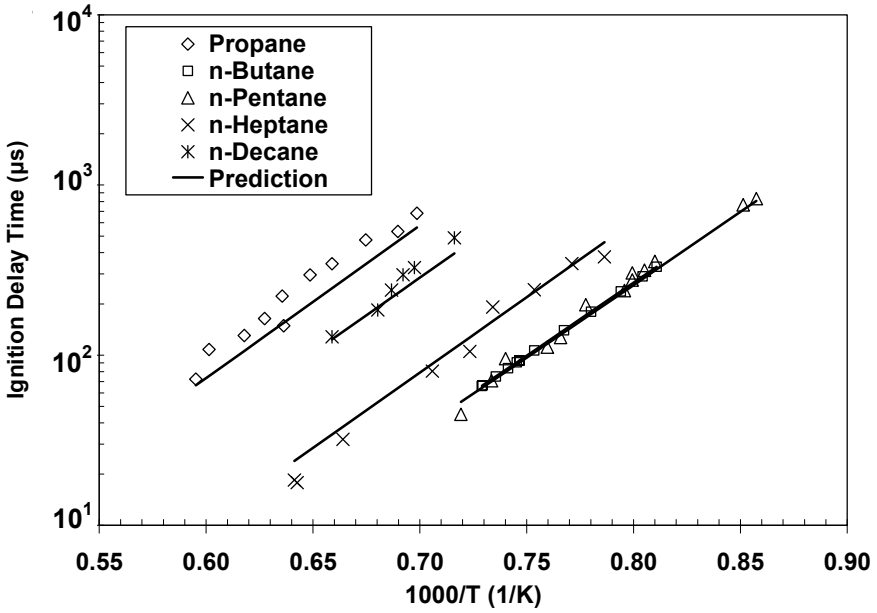

Figure 7.4 Comparison of theoretical and experimental ignition times for normal alkanes with argon as the inert (a) propane [21], φ=1.0; 0.2% C_3H_8, 1% O_2, 98.8% Ar; P=1.5 atm; T=1431-1680 K; (b) n-butane [22], φ=1.0; 2.5% C_4H_{10}, 16.25% O_2, 81.25% Ar; P=9.19-10.58 atm; T=1233-1372 K; (c) n-pentane [22], φ=1.0; 2.04% C_5H_{12}, 16.32% O_2, 81.64% Ar; P=8.27-9.46 atm; T=1166-1390 K; (d) n-heptane [23], φ=1.0; 2.5% C_7H_{16}, 27.5% O_2, 70% Ar; P=1-4 atm; T=1272-1559 K; (e) n-decane [5], φ=1.0; 0.2% $C_{10}H_{22}$, 3.1% O2, 96.78% Ar; P=1.2 atm; T=1396-1518 K.

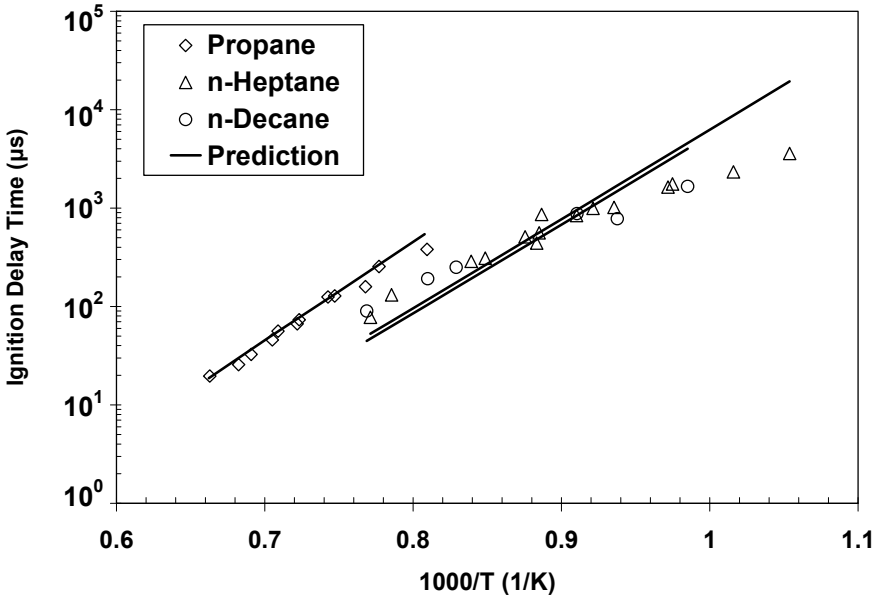

Figure 7.5 Comparison of theoretical and experimental ignition times for normal alkanes with nitrogen as the inert (a) propane [24], φ=1.0; 4.17% C_3H_8, 20.83% O_2, 75.0% N_2; P=3.4-5.0 atm; T=1238-1510 K; (b) n-heptane [25], φ=1.0; 1.87% C_7H_{16}, 20.61% O_2, 77.51% N_2; P=13.3 atm; T=949-1297 K; (c) n-decane [26], φ=1.0; 1.34% $C_{10}H_{22}$, 20.73% O_2, 77.94% N_2; P=12.83 atm; T=1015-1300 K.

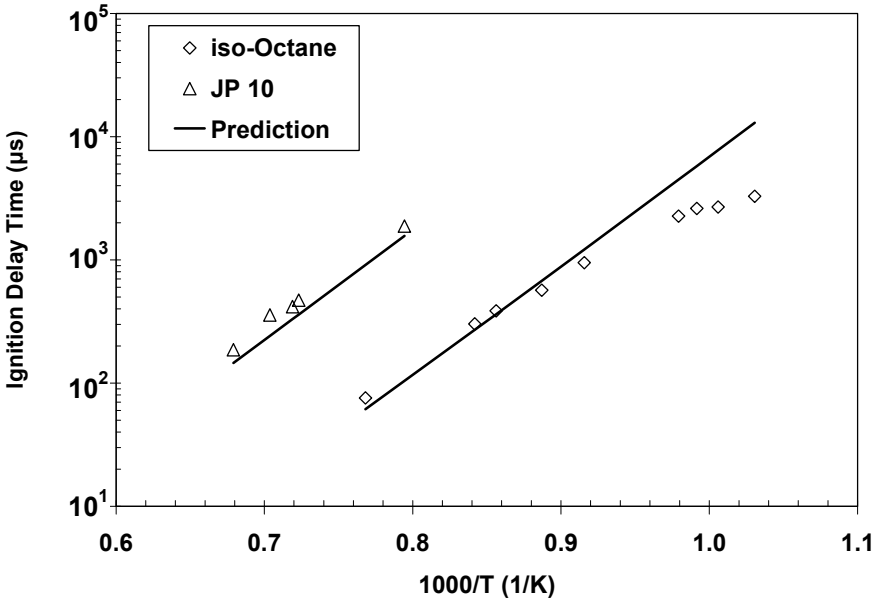

Figure 7.6 Comparison of theoretical and experimental ignition times for (a) iso-octane [27], φ=1.0; 1.65% iC_8H_{18}, 20.7% O_2, 77.7% N_2; P=13.3 atm; T=970-1301 K; (b) JP 10 [28], φ=1.0; 0.4% $C_{10}H_{16}$, 5.6% O_2, 94% Ar; P=2.5 atm; T=1259-1472 K.

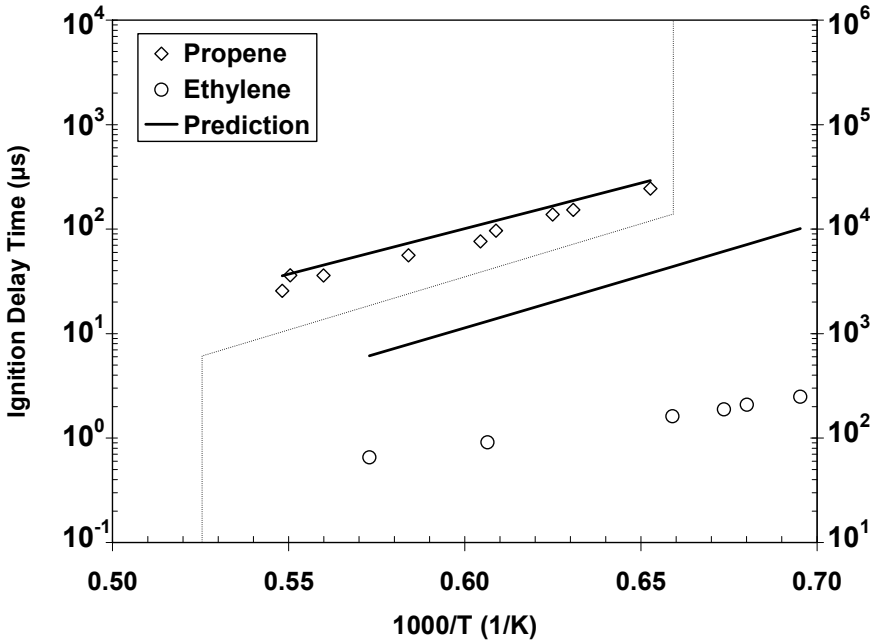

Figure 7.7 Comparison of theoretical and experimental ignition times for (a) propene [29], φ=1.0; 1.6% C_3H_6, 7.2% O_2, 91.2% Ar; P=1 atm; T=1532-1824 K; (b) ethylene [30], φ=1.0; 1% C_2H_4, 3% O_2, 96% Ar; P=1 bar; T=1440-1745 K.

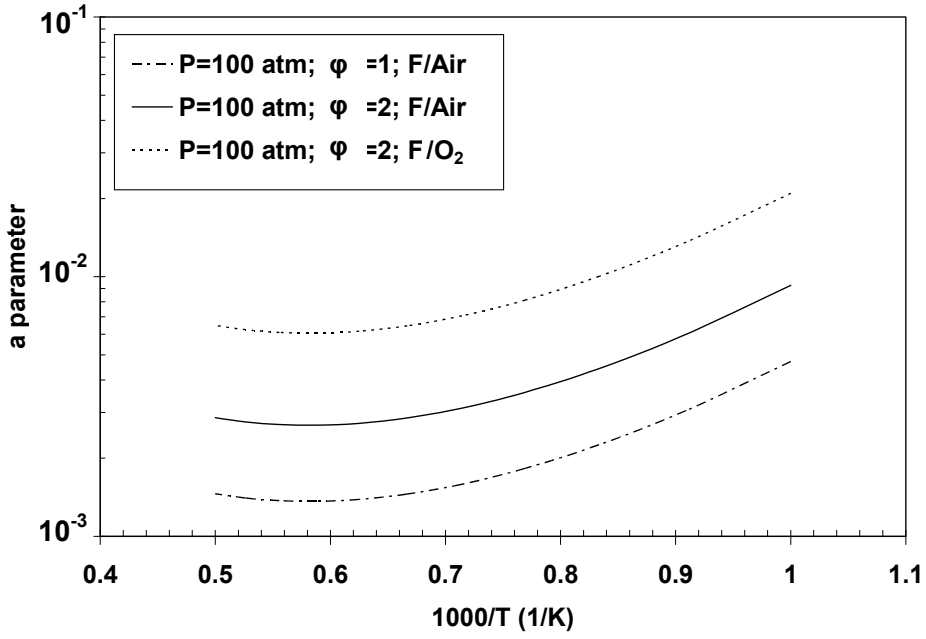

Figure 7.8 Variation of the parameter *a* with temperature for n-heptane at 100 atm and different dilutions and equivalence ratios.

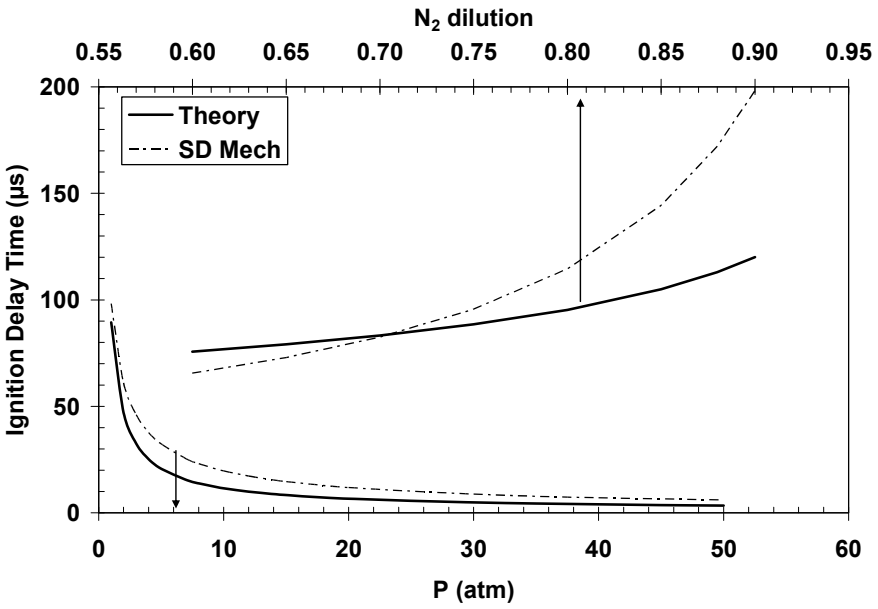

Figure 7.9 Comparison of theoretical and numerical predictions of (a) the effect of pressure on ignition delay time for stoichiometric propane-air mixtures at 1500 K (lower curves) and of (b) the effect of nitrogen dilution on ignition delay time for stoichiometric propane-air mixtures at 1 atm and 1500 K (upper curves).

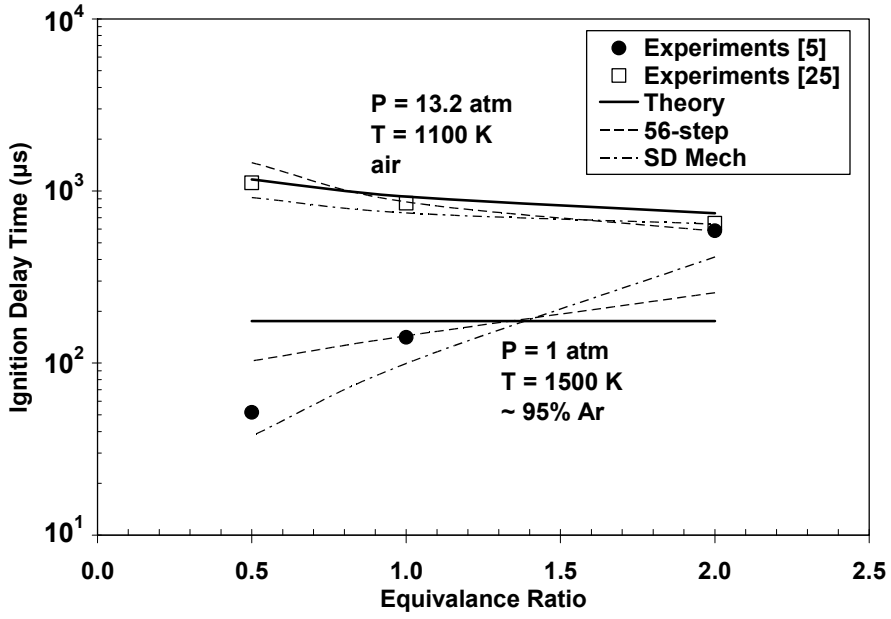

Figure 7.10 Comparison of experimental, theoretical and numerical predictions of the effect of equivalence ratio on ignition delay time for n-heptane, with fuel mole fraction fixed at 0.4%, at 1 atm and 1500 K in oxygen-argon mixtures (lower curves) and for fuel-air mixtures at 13.2 atm and 1100 K (upper curves).

7.9 REFERENCES

1. Cooke, D.F. and Williams, A., "Shock tube studies of methane and ethane oxidation", Combustion and Flame, 24, 1975, pp. 245-256.

2. Spadaccini and Colket III, M.B., "Ignition delay characteristics of methane fuels", Progress in Energy and Combustion Science, 20, 1994, pp. 431-460.

3. Petersen, E.L., Davidson, D.F. and Hanson, R.K., "Kinetic modeling of shock-induced ignition in low-dilution CH_4/O_2 mixtures at high pressures and intermediate temperatures", Combustion and Flame, 117, 1999, pp. 272-290.

4. Colket III, M.B. and Spadaccini, L.J., "Scramjet fuels autoignition study", Journal of Propulsion and Power, 17, 2001, pp. 315-323.

5. Horning, D.C., Davidson, D.F. and Hanson, R.K., "Study of the high-temperature autoignition of n-Alkane/O2/Ar mixtures", Journal of Propulsion and Power, 18, 2002, pp. 363-371.

6. Kee, R.J., Rupley, F.M., Miller, J.A., Coltrin M.E., Grcar, J.F., Meeks, E., Moffat, H.K., Lutz, A.E., Dixon-Lewis, G., Smooke, M.D., Warnatz, J., Evans, G.H., Larson, R.S., Mitchell, R.E., Petzold, L.R., Reynolds, W.C., Caracotsios, M., Stewart, W.E., Glarborg, P., Wang, C., Adigun, O., Houf, W.G., Chou, C.P. and Miller, S.F., Chemkin Collection, Release 3.7.1, Reaction Design Inc., San Diego, CA, 2003.

7. Pitsch, H., "Entwicklung eines Programmpakets zur Berechnung eindimensionaler Flammen am Beispiel einer Gegenstromdiffusionflamme", M.S. Thesis, RWTH Aachen, Germany, 1993.

8. Peters, N., Paczko, G., Seiser, R. and Seshadri, K., "Temperature cross-over and non-thermal runaway at two-stage ignition of n-heptane", Combustion and Flame, 128, 2002, pp. 38-59.

9. Varatharajan, B., Petrova, M., Williams, F.A., and Tangirala, "Two-step chemical-kinetic descriptions for hydrocarbon-oxygen-diluent ignition and detonation applications", Proceedings of Combustion Institute, 30, 2004, pp. 1869-1877.

10. Petrova, M.V. and Williams, F.A., "A phenomenological model for hydrocarbon high-temperature autoignition", Combustion Theory and Modeling, 10, 2006, pp. 344-360.

11. Petrova, M.V. and Williams, F.A., "A small detailed chemical-kinetic mechanism for hydrocarbon combustion", Combustion and Flame, 144, 2006, pp. 526-544.

12. Available at: http://maemail.ucsd.edu/combustion/cermech.

13. Grcar, J.F., Day, M.S., and Bell, J.B., “A taxonomy of integral reaction path analysis”, Combustion Theory and Modeling, 10, 2006, pp. 559-579.

14. Lam, S.H., “Using CSP to understand complex chemical kinetics”, Combustion Science and Technology, 89, 1993, pp. 375-404.

15. Marinov, N. M., Pitz, W. J., Westbrook, C. K., Vincitore, A. M., Castaldi, M. J., and Senkan, S. M, "Aromatic and polycyclic aromatic hydrocarbon formation in a laminar premixed n-butane flame", Combustion and Flame, 114, 1998, pp. 192-213.

16. Curran, H. J., Gaffuri, P., Pitz, W. J., and Westbrook, C. K. "A comprehensive modeling study of n-heptane oxidation", Combustion and Flame 114, 1998, pp. 149-177; available at: http://www-cms.llnl.gov/combustion/nc7_2b_mech.txt

17. Held, T.J., Marchese, A.J., and Dryer, F.L., “A semi-empirical reaction mechanism for n-heptane oxidation and pyrolysis”, Combustion Science and Technology, 123, 1997, pp. 107-146.

18. Zhao, Z., Li, J., Kazakov, A., and Dryer, F.L., “Burning velocities and a high temperature skeletal kinetic model for n-decane”, Combustion Science and Technology, 177, 2005, pp. 89-106; available at: http://www.princeton.edu/~combust/database.

19. Curran, H. J., Gaffuri, P., Pitz, W. J., and Westbrook, C. K. "A comprehensive modeling study of iso-octane oxidation" Combustion and Flame, 129, 2002, pp. 253-280.

20. Tsang, W., “Chemical kinetic data base for combustion chemistry. Part V. Propene”, Journal of Physical and Chemical Reference Data, 20, 1991, pp. 221-273.

21. Gray, J.A. and Westbrook, C.K., “High-temperature ignition of propane with MTBE as an additive: Shock tube experiments and modeling”, International Journal of Chemical Kinetics, 26, 1994, pp. 757-770.

22. Burcat, A., Scheller, K., and Lifshitz, A., “Shock-tube inverstigation of comparative ignition delay times for C_1-C_5 alkanes”, Combustion and Flame, 16, 1971, pp. 29-33.

23. Vermeer, D.J., Meyer, J.W., and Oppenheim, A.K., “Auto-ignition of hydrocarbon behind reflected shock waves”, Combustion and Flame, 18, 1972, pp. 327-336.

24. Brown, C.J. and Thomas, G.O., "Experimental studies of shock-induced ignition and transition to detonation in ethylene and propane mixtures", Combustion and Flame, 117, 1999, pp. 861-870.

25. Ciezki, H.K. and Adomeit, G., "Shock-tube investigation of self-ignition of n-heptane-air mixtures under engine relevant conditions", Combustion and Flame, 93, 1993, pp. 421-433.

26. Pfahl, U., Fieweger, K. and Adomeit, G., "Self-ignition of diesel relevant hydrocarbon-air mixtures under engine conditions", Proceedings of the Combustion Institute, 26, 1996, pp. 781-789.

27. Fieweger, K., Blumenthal, R., and Adomeit, G., "Self-ignition of s.i. engine model fuels: A shock tube investigation at high pressure", Combustion and Flame, 109, 1997, pp. 599-619.

28. Davidson, D.F., Horning, D.C., Herbon, J.T., and Hanson, R.K., "Shock-tube measurements of JP-10 ignition", Proceedings of the Combustion Institute, 28, 2001, pp. 1687-1692.

29. Quin, Z., Yang, H. and Gardiner, Jr., W.C., "Measurement and modeling of shock-tube ignition delay for propene", Combustion and Flame, 124, 2001, pp. 246-254.

30. Horning, D.C., "A study of the high-temperature autoignition thermal decomposition of hydrocarbons", Ph.D. Dissertation, Department of Mechanical Engineering, Stanford University, Stanford, CA, June 2001.

CHAPTER 8

SUMMARY AND FUTURE WORK

In the following sections, the major conclusions from this research are summarized and the possibilities of future research as an extension to this work are highlighted. The discussion is presented separately for ethanol-flame studies and autoignition theory for higher alkane fuels.

8.1 ETHANOL-FLAME STUDIES

The extent to which the possible benefits of ethanol as an alternative fuel are realizable can only be assessed by understanding its combustion at a fundamental level. The first part of the thesis attempts to elucidate ethanol combustion at a fundamental level and reduce existing uncertainties in ethanol combustion chemistry. It has both numerical and experimental components. In the numerical studies, a small detailed chemical-kinetic mechanism, the San Diego Mech, for ethanol combustion is developed in a hierarchical way. During the mechanism development for ethanol, the sub-mechanisms for the simpler fuels were developed and thoroughly tested against as many relevant experimental data as possible.

The testing of the San Diego Mech for hydrogen and carbon monoxide led to a few revisions of rate parameters for elementary steps in the mechanism for hydrogen and to deletion of a hydrogen initiation step and addition of an initiation step for carbon monoxide. Small increases in three-body recombination rates for certain steps and some changes in chaperon efficiencies were identified. With these alterations, reasonable agreement is obtained with available measured burning velocities, diffusion-flame

extinction conditions and autoignition times. There is, however, need for further studies in assessing the validity of the mechanism for burning velocities and ignition delay times at intermediate and higher pressures for carbon monoxide hydrogen mixtures. There is a need to review the effect of reactions $CO+HO_2 \rightarrow CO_2+OH$ and $CO+O+M \rightarrow CO_2+M$, which do not play any role at low-pressure conditions, but are expected to play a significant role at intermediate and high-pressure conditions. There is a lack of information available in the literature concerning the pressure falloff for the step $CO+O+M \rightarrow CO_2+M$. Hence more studies are required for this step in determining the behavior of the rate constant at higher pressures and also the chaperon efficiencies for different species.

The hydrogen and carbon monoxide submechanism, thus developed, provided a building block upon which the C_1 and C_2 submechanisms for the San Diego mechanism were developed. A thorough testing of the submechanisms of formaldehyde, methane, methanol, ethane, ethylene, and acetylene fuels in the San Diego Mech has been conducted. The mechanism was tested for autoignition, premixed-flame burning velocities, and structures and extinction of nonpremixed flames and of partially premixed flames of many of these fuels. Tests were also made for propane and acetaldehyde fuels with the updated San Diego Mech. The updates in the rate constant of a few key reactions, and the newly included reactions are reported along with the significance for these changes. The mechanism is developed for the autoigntion of formaldehyde, methanol, and ethane for the first time in this study. Various tests have been repeated for the abovementioned fuels for selected experimental conditions, as mentioned in the articles where the mechanism for a particular fuel was first developed. The comparisons

of predictions with the experimental data are found to be as good as those in the original publications or even better in some cases. Hence, the San Diego Mech is considered ready to be used for fuels such as formaldehyde, methane, methanol, ethane, ethylene, acetylene, acetaldehyde, and propane.

Although reactions related with formyl radical consumptions play a key role in the combustion of alkane and alcohol fuels, it was observed during the studies that more research is needed in reducing the uncertainies in these reactions, especially, H, OH, O, and O_2 attack on HCO. Large uncertainties were observed in the pressure dependence of rate constants of recombination steps $HCO+H+M \rightarrow CH_2O+M$ and $CH_3+H+M \rightarrow CH_4+M$. The first of which, in backward direction, is a significant route that leads a fuel to HCO and then to CO and CO_2. The second step is a crucial one in determining the formation of methane and soot precursors in a reaction mechanism. Hence, both theoretical and experimental studies are needed for these two steps to reduce the uncertainties in their rates and pressure fall offs. During the study, generic third-body efficiencies with respect to nitrogen are assigned for all the pressure-dependent reactions. Yet, validation of these generic efficiencies, included in pressure-dependent elementary steps, would reduce the uncertainties in their rate implementation. Also, the need remains for the inclusion of pressure falloff for some of the key steps such as $CH_3O+M \rightarrow CH_2O+H+M$ and others.

The reaction mechanism for C_1 and C_2 fuels, thus developed, consists of 137 reactions among 30 species, and provided a robust building block upon which the ethanol mechanism was developed. The San Diego Mech is extended for ethanol combustion by adding 55 new reactions and 6 new species based on the extensive literature survey. Specifically, 33 reactions are added that involve C_2H_5OH or one of the three isomers

produced by abstraction of an H atom from it, CH_3CHOH, CH_2CH_2OH and CH_3CH_2O, and 22 reactions are added that involve acetaldehyde or one of the two isomers produced by abstraction of H from it, CH_2CHO and CH_3CO.

Ethanol combustion was investigated on the basis of a new reaction mechanism, thus developed, consisting of 192 elementary steps among 36 species, augmented by 53 additional steps and 14 additional species to address the formation of oxides of nitrogen and 43 steps and 7 species to address formation of compounds involving three carbon atoms. The mechanism was tested against shock-tube autoignition-delay data, laminar burning velocities, counterflow diffusion-flame extinction, and measurements of structures of counterflow partially premixed and nonpremixed flames. Going along with our approach, these experiments were selected because they address all the features of high-temperature combustion in practical engines. The flame structures of ethanol in practically relevant partially premixed and nonpremixed systems are measured in counterflow setup for the first time in this study.

The ethanol-air flames were measured in a counterflow setup at a strain rate of 100 s^{-1}, employing prevaporized ethanol with a mole fraction of 0.3 in a nitrogen carrier stream, for the pure diffusion flame and for a partially premixed flame with a fuel-side equivalence ratio of 2.3. The temperatures were measured using the appropriate thermocouples, and the concentration profiles of C_2H_5OH, CO, CO_2, H_2, H_2O, O_2, N_2, CH_4, C_2H_6 and C_2H_2+C_2H_4 were determined by gas chromatographic analysis of samples withdrawn through fine quartz probes. The best practices developed in our laboratory in such measurements were followed to prevent the condensation of vapors of fuel and water.

There are serious concerns over the aldehydes and ketene emission in the use of ethanol as a fuel. During the study, species such as formaldehyde, acetaldehyde, and ketene could not be measured because of the difficulties associated with probe measurement of these species at such low concentrations. However, future experiments are required to quantitatively determine the concentrations of aldehydes and ketene in order to achieve better understanding of their production and consumption, providing a more stringent test to the ethanol mechanism, and hence controlling emissions of these harmful species. In the current study, the production of oxides of nitrogen was studied at atmospheric pressures. The next step would be to extend the NO_x mechanism for high-pressure description by including pressure falloff especially to the reactions related with N_2O chemistry. It would be of interest to perform additional experiments and make comparisons at higher pressures, since many of the applications of interest are at elevated pressures.

The comparison of the predictions of the ethanol mechanism with a wide range of experimental conditions provides confidence in the elementary steps and their reaction rate constants used in the mechanism. The agreements seen in predictions and data for soot precursors indicate that the reduction in the uncertainties in the description of the C_2 chemistry related with ethanol has been achieved. In general, the computational results with the present mechanism are in reasonable agreement with experiments and perform as well as or better than predictions of other, generally much larger, mechanisms available in the literature. Further research is, however, warranted for providing additional and more stringent tests of the mechanism and its predictions, especially for condition at higher pressures. The current study is a step forward in the effort to minimize

the uncertainties in the predictions of ethanol combustion and to identify the associated chemical-kinetic channels. Similar to methanol, ethanol is expected to reduce NO_x emissions, but it may not be comparably effective in soot reduction and may exacerbate concerns about aldehydes. These observations suggest that pollutant-emission concerns will be different for ethanol than they are for methanol or for hydrocarbons. This study may contribute towards enhancement of understanding of ethanol combustion and assessment of its utility as a fuel.

While detailed chemistry can be employed to describe combustion in homogeneous time-dependent and steady-flow one-dimensional systems, for practical applications, such as turbulent combustion in engines, computer limitations require simpler chemistry. In a further extension to this work, systematically reduced mechanisms for combustion predictions for ethanol can be developed. Through proper use of steady-state and partial-equilibrium approximations, the ethanol detailed reaction mechanism can be reduced to systems having much smaller numbers of overall steps. The reduced mechanisms are much more useful than the detailed mechanisms for computations of combustion processes because very often the detailed mechanisms are so large that they cannot be used computationally. This reduced chemistry for ethanol can also be used in theoretical studies such as rate-ratio asymptotics to obtain expressions for autoignition times, burning velocities, diffusion-flame structures and extinction conditions. Similar studies have been carried out for methane and methanol in the past. These studies provide analytical expressions for a particular combustion process that it is derived for, and can be used in complex engine analysis.

8.2 AUTOIGNITION THEORY FOR HIGHER ALKANES

Autoignition delay times of hydrocarbon fuels play a major role in the performance characteristics of new engine concepts such as HCCI (Homogeneous Charged Compression Ignition). There is a need for reduced-chemistry models and simple formula for the autoignition of practical hydrocarbon fuels for flex-fuel complex engine analysis, which are computationally less expensive compared to detailed chemical mechanisms. The second part of the thesis consists of analytical study of autoignition of higher alkane fuels. It has been observed that autoignition times of most fuels, especially higher hydrocarbons, seem to be remarkably similar in both value and temperature dependence in the temperature range between about 1000 K and 2500 K. A simplified chemistry, common to fuels such as propane and higher hydrocarbons, which controls the induction period, is identified by systematic reduction. Computationally, for propane and higher hydrocarbons, temperature runaway in autoignition occurs only after fuel is depleted to concentration levels compared with those of radicals. Based on this observation fuel depletion was employed as an ignition-time criterion in the development of a formula for autoignition delay times. As a result of this study, it is found that above about 1000 K, ignition delay times for propane and all higher alkanes, as well as for a number of other fuels, can be calculated well by employing rate parameters of only three types of elementary steps, namely $C_mH_n+HO_2 \rightarrow C_mH_{n-1}+H_2O_2$, $H_2O_2+M \rightarrow 2OH+M$ and $2HO_2 \rightarrow H_2O_2+O_2$, only the first of which is fuel-specific, the other two clearly being common to all fuels. The prediction of this remarkably simple result relies on a steady-state approximation for HO_2, as well as steady states for more active radicals (H, OH, and the alkyl or alkyl-like radicals) during induction. The resulting approximation to the

chemistry exhibits a slow, finite-rate buildup of H_2O_2 and removal of fuel during the induction period.

The numerical predictions from this formula are tested against the experimental data for higher alkane fuels such as propane, butane, pentane, heptane, decane, and isooctane. The formula is also shown to accurately predict the autoignition delay times for propene, JP-10, and toluene. The last three agreements indicate that this description of autoignition is valid for the fuels which contain at least three carbon atoms and one carbon-carbon single bond. One of the major assumptions that went into the development of the theory is one-to-one net production of HO_2 in fuel-radical decomposition-chemistry process. The predictions from the theory tend to deviate from the experimental data when this assumption breaks down in the conditions such as high dilution. Also, the formula does not predict the correct oxygen dependence of the ignition time. However, it is found to work best in the conditions of practical interests such as moderate pressures, near stoichiometry and without excessive dilution. The analytical approximation thus produces reasonable results for a wide range of fuels. These results provide a new perspective on high-temperature autoignition chemistry and a general means of easily estimating ignition times of the large number of fuels of practical importance.

As a further extension to this work, a similar reduced-chemistry determination for ethanol autoignition can be investigated. In order to obtain the correct oxygen dependence of ignition times, the assumption of one-to-one net production of HO_2 in fuel-radical decomposition-chemistry process has to be relaxed. However, this will lead to a formula not as simple as the one obtained in this study.

APPENDIX 1

THE SAN DIEGO MECH

All the elementary reactions in the San Diego Mech that were used in calculations for ethanol combustion are reported in the Table A1.1 along with their reaction-rate parameters. The references for the reaction-rate constants are provided. The modifications made to the reaction mechanism based on this study are marked as [TS]. Further extensions to the San Diego Mech are reported for propane [11], propene [11], propyne [11], and allene [11], n-heptane [13], JP-10 [14], and NO_x [15, 16]. In the calculations the reactions related with fuels with three carbon atoms were taken from [11] and the reactions related with nitrogen chemistry were taken from [15, 16].

Table A1.1 Chemical-Kinetic Mechanism for Ethanol

Reaction		A[a]	n[a]	E[a]	Reference
Hydrogen-Oxygen Chain					
1. $H + O_2 \rightarrow OH + O$		3.52×10^{16}	-0.70	71.4	[1]
2. $H_2 + O \rightarrow OH + H$		5.06×10^{04}	2.70	26.3	[2]
3. $H_2 + OH \rightarrow H_2O + H$		1.17×10^{09}	1.30	15.2	[3]
4. $H_2O + O \rightarrow OH + OH$		7.60×10^{00}	3.80	53.4	[2]
Direct Recombination					
5[c]. $H + H + M \rightarrow H_2 + M$		1.30×10^{18}	-1.00	0.0	[TS][b]
6[d]. $H + OH + M \rightarrow H_2O + M$		4.00×10^{22}	-2.00	0.0	[TS]
7[e]. $O + O + M \rightarrow O_2 + M$		6.17×10^{15}	-0.50	0.0	[TS]
8[f]. $H + O + M \rightarrow OH + M$		4.71×10^{18}	-1.00	0.0	[TS]
9[f]. $O + OH + M \rightarrow HO_2 + M$		8.00×10^{15}	0.00	0.0	[TS]
Hydroperoxyl Reactions					
10[g]. $H + O_2 + M \rightarrow HO_2 + M$	k_0	5.75×10^{19}	-1.40	0.0	[TS]
	k_∞	4.65×10^{12}	0.40	0.0	
11. $HO_2 + H \rightarrow OH + OH$		7.08×10^{13}	0.00	1.2	[4]
12. $HO_2 + H \rightarrow H_2 + O_2$		1.66×10^{13}	0.00	3.4	[4]
13. $HO_2 + H \rightarrow H_2O + O$		3.10×10^{13}	0.00	7.2	[5]
14. $HO_2 + O \rightarrow OH + O_2$		2.00×10^{13}	0.00	0.0	[6]
15. $HO_2 + OH \rightarrow H_2O + O_2$		2.89×10^{13}	0.00	-2.1	[5]

Table A1.1 Continued

Reaction	A[a]	n[a]	E[a]		Reference
Hydrogen Peroxide Reactions					
16[h]. $OH + OH + M \rightarrow H_2O_2 + M$	k_0	2.30×10^{18}	-0.90	-7.1	[TS]
	k_∞	7.40×10^{13}	-0.40	0.0	
17. $HO_2 + HO_2 \rightarrow H_2O_2 + O_2$		3.02×10^{12}	0.00	5.8	[2]
18. $H_2O_2 + H \rightarrow HO_2 + H_2$		4.79×10^{13}	0.00	33.3	[2]
19. $H_2O_2 + H \rightarrow H_2O + OH$		1.00×10^{13}	0.00	15.0	[2]
20. $H_2O_2 + OH \rightarrow H_2O + HO_2$		7.08×10^{12}	0.00	6.0	[2]
21. $H_2O_2 + O \rightarrow HO_2 + OH$		9.63×10^{6}	2.00	16.7	[2]
Conversion of CO to CO_2					
22. $CO + OH \rightarrow CO_2 + H$		4.40×10^{6}	1.50	-3.1	[7]
23. $CO + HO_2 \rightarrow CO_2 + OH$		6.00×10^{13}	0.00	96.0	[7]
24. $CO + O_2 \rightarrow CO_2 + O$		1.00×10^{12}	0.00	199.4	[TS]
Formyl (HCO) Reactions					
25[i]. $HCO + M \rightarrow CO + H + M$		1.86×10^{17}	-1.00	71.1	[8]
26. $HCO + H \rightarrow CO + H_2$		5.00×10^{13}	0.00	0.0	[TS]
27. $HCO + O \rightarrow CO + OH$		3.00×10^{13}	0.00	0.0	[7]
28. $HCO + O \rightarrow CO_2 + H$		3.00×10^{13}	0.00	0.0	[7]
29. $HCO + OH \rightarrow CO + H_2O$		3.00×10^{13}	0.00	0.0	[9]
30. $HCO + O_2 \rightarrow CO + HO_2$		7.58×10^{12}	0.00	1.7	[10]
31. $HCO + CH_3 \rightarrow CO + CH_4$		5.00×10^{13}	0.00	0.0	[TS]
Formaldehyde (CH_2O) Reactions					
32[j]. $H + HCO + M \rightarrow CH_2O + M$	k_0	1.35×10^{24}	-2.60	1.8	[TS]
	k_∞	1.09×10^{12}	0.48	-1.1	
33. $CH_2O + H \rightarrow HCO + H_2$		5.74×10^{07}	1.90	11.5	[TS]
34. $CH_2O + O \rightarrow HCO + OH$		3.50×10^{13}	0.00	14.7	[7]
35. $CH_2O + OH \rightarrow HCO + H_2O$		3.90×10^{10}	0.89	1.7	[7]
36. $CH_2O + O_2 \rightarrow HCO + HO_2$		6.00×10^{13}	0.00	170.2	[TS]
37. $CH_2O + HO_2 \rightarrow HCO + H_2O_2$		4.11×10^{04}	2.50	42.7	[TS]
Methane (CH_4) Consumption					
38. $CH_4 + H \rightarrow H_2 + CH_3$		1.30×10^{04}	3.00	33.6	[11]
39. $CH_4 + OH \rightarrow H_2O + CH_3$		1.60×10^{07}	1.83	11.6	[11]
40. $CH_4 + O \rightarrow OH + CH_3$		1.90×10^{09}	1.44	36.3	[11]
41. $CH_4 + O_2 \rightarrow HO_2 + CH_3$		3.98×10^{13}	1.44	238.0	[11]
42. $CH_4 + O_2 \rightarrow H_2O_2 + CH_3$		9.03×10^{12}	0.00	103.1	[11]
Methyl (CH_3) Reactions					
43. $CH_3 + H \rightarrow T\text{-}CH_2 + H_2$		1.80×10^{14}	0.00	63.2	[11]
44. $CH_3 + H \rightarrow S\text{-}CH_2 + H_2$		1.55×10^{14}	0.00	56.4	[11]
45. $CH_3 + OH \rightarrow S\text{-}CH_2 + H_2O$		4.00×10^{13}	0.00	10.5	[TS]
46. $CH_3 + O \rightarrow CH_2O + H$		8.43×10^{13}	0.00	0.0	[11]
47. $CH_3 + T\text{-}CH_2 \rightarrow C_2H_4 + H$		4.22×10^{13}	0.00	0.0	[11]
48. $CH_3 + HO_2 \rightarrow CH_3O + OH$		5.00×10^{12}	0.00	0.0	[11]

Table A1.1 Continued

Reaction	A[a]	n[a]	E[a]		Reference
49. $CH_3 + O_2 \rightarrow CH_2O + OH$		3.30×10^{11}	0.00	37.4	[11]
50. $CH_3 + O_2 \rightarrow CH_3O + O$		1.10×10^{11}	0.00	116.4	[TS]
51. $CH_3 + CH_3 \rightarrow C_2H_4 + H_2$		1.00×10^{14}	0.00	133.9	[11]
52. $CH_3 + CH_3 \rightarrow C_2H_6 + H$		3.16×10^{13}	0.00	61.5	[11]
53[k,l]. $H + CH_3 + M \rightarrow CH_4 + M$	k_0	2.47×10^{33}	-4.76	10.2	[TS]
	k_∞	1.27×10^{16}	-0.63	1.6	
54[m]. $CH_3 + CH_3 + M \rightarrow C_2H_6 + M$	k_0	1.27×10^{41}	-7.00	11.6	[11]
	k_∞	1.81×10^{13}	0.00	0.0	
Singlet Methylene (S-CH_2) Reactions					
55. $S\text{-}CH_2 + OH \rightarrow CH_2O + H$		3.00×10^{13}	0.00	0.0	[11]
56. $S\text{-}CH_2 + O_2 \rightarrow CO + OH + H$		3.13×10^{13}	0.00	0.0	[11]
57. $S\text{-}CH_2 + CO_2 \rightarrow CO + CH_2O$		3.00×10^{12}	0.00	0.0	[11]
58[k]. $S\text{-}CH_2 + M \rightarrow T\text{-}CH_2 + M$		6.00×10^{12}	0.00	0.0	[11]
Triplet Methylene (T-CH_2) Reactions					
59. $T\text{-}CH_2 + H \rightarrow CH + H_2$		6.02×10^{12}	0.00	-7.5	[11]
60. $T\text{-}CH_2 + OH \rightarrow CH_2O + H$		2.50×10^{13}	0.00	0.0	[11]
61. $T\text{-}CH_2 + OH \rightarrow CH + H_2O$		1.13×10^{07}	2.00	12.6	[11]
62. $T\text{-}CH_2 + O \rightarrow CO + H + H$		8.00×10^{13}	0.00	0.0	[11]
63. $T\text{-}CH_2 + O \rightarrow CO + H_2$		4.00×10^{13}	0.00	0.0	[11]
64. $T\text{-}CH_2 + O_2 \rightarrow CO_2 + H_2$		2.63×10^{12}	0.00	6.2	[11]
65. $T\text{-}CH_2 + O_2 \rightarrow CO + OH + H$		6.58×10^{12}	0.00	6.2	[11]
66. $T\text{-}CH_2 + T\text{-}CH_2 \rightarrow C_2H_2 + H + H$		1.00×10^{14}	0.00	0.0	[11]
Methyne (CH) Reactions					
67. $CH + O \rightarrow CO + H$		4.00×10^{13}	0.00	0.0	[11]
68. $CH + O_2 \rightarrow HCO + O$		1.77×10^{11}	0.76	-2.0	[11]
69. $CH + H_2O \rightarrow CH_2O + H$		1.17×10^{15}	-0.75	0.0	[11]
70. $CH + CO_2 \rightarrow HCO + CO$		4.80×10^{01}	3.22	-13.5	[11]
Methoxy (CH_3O) Reactions					
71. $CH_3O + H \rightarrow CH_2O + H_2$		2.00×10^{13}	0.00	0.0	[11]
72. $CH_3O + H \rightarrow S\text{-}CH_2 + H_2O$		1.60×10^{13}	0.00	0.0	[11]
73. $CH_3O + OH \rightarrow CH_2O + H_2O$		5.00×10^{12}	0.00	0.0	[11]
74. $CH_3O + O \rightarrow CH_2O + OH$		1.00×10^{13}	0.00	0.0	[11]
75. $CH_3O + O_2 \rightarrow CH_2O + HO_2$		4.28×10^{-13}	7.60	-14.8	[11]
76[k]. $CH_3O + M \rightarrow CH_2O + H + M$		7.78×10^{13}	0.00	56.5	[TS]
Ethane (C_2H_6) Reaction					
77. $C_2H_6 + H \rightarrow C_2H_5 + H_2$		5.40×10^{02}	3.50	21.8	[11]
78. $C_2H_6 + O \rightarrow C_2H_5 + OH$		1.40×10^{00}	4.30	11.6	[11]
79. $C_2H_6 + OH \rightarrow C_2H_5 + H_2O$		2.20×10^{07}	1.90	4.7	[11]
80. $C_2H_6 + CH_3 \rightarrow C_2H_5 + CH_4$		5.50×10^{-01}	4.00	34.7	[11]
81[n]. $C_2H_6 + M \rightarrow C_2H_5 + H + M$	k_0	4.90×10^{42}	-6.43	448.4	[11]

Table A1.1 Continued

Reaction	A^a	n^a	E^a		Reference
	k_∞	8.85×10^{20}	-1.23	427.7	
82. $C_2H_6 + HO_2 \rightarrow C_2H_5 + H_2O_2$		1.32×10^{13}	0.00	85.6	[TS]
Ethyl (C_2H_5) Reactions					
83. $C_2H_5 + H \rightarrow C_2H_4 + H_2$		3.00×10^{13}	0.00	0.0	[11]
84. $C_2H_5 + O \rightarrow C_2H_4 + OH$		3.06×10^{13}	0.00	0.0	[11]
85. $C_2H_5 + O \rightarrow CH_3 + CH_2O$		4.24×10^{13}	0.00	0.0	[11]
86. $C_2H_5 + O_2 \rightarrow C_2H_4 + H_2O$		2.00×10^{12}	0.00	20.9	[11]
87[o]. $C_2H_5 + M \rightarrow C_2H_4 + H + M$	k_0	3.99×10^{33}	-4.99	167.4	[11]
	k_∞	1.11×10^{10}	1.04	53.8	
Ethene (C_2H_4) Reactions					
88. $C_2H_4 + H \rightarrow C_2H_3 + H_2$		4.49×10^{07}	2.12	55.9	[11]
89. $C_2H_4 + OH \rightarrow C_2H_3 + H_2O$		5.53×10^{05}	2.31	12.4	[11]
90. $C_2H_4 + O \rightarrow CH_3 + HCO$		2.25×10^{06}	2.08	0.0	[11]
91. $C_2H_4 + O \rightarrow CH_2CHO + H$		1.21×10^{06}	2.08	0.0	[11]
92. $C_2H_4 + C_2H_4 \rightarrow C_2H_3 + C_2H_5$		5.01×10^{14}	0.00	270.7	[11]
93. $C_2H_4 + O_2 \rightarrow C_2H_3 + HO_2$		4.22×10^{13}	0.00	241.1	[11]
94. $C_2H_4 + HO_2 \rightarrow C_2H_4O + OH$		2.23×10^{12}	0.00	71.9	[11]
95. $C_2H_4O + HO_2 \rightarrow CH_3 + CO + H_2O_2$		4.00×10^{12}	0.00	71.2	[11]
96[k]. $C_2H_4 + M \rightarrow C_2H_3 + H + M$		2.60×10^{17}	0.00	404.0	[11]
97[k]. $C_2H_4 + M \rightarrow C_2H_2 + H_2 + M$		3.50×10^{16}	0.00	299.3	[11]
Vinyl (C_2H_3) Reactions					
98. $C_2H_3 + H \rightarrow C_2H_2 + H_2$		4.00×10^{13}	0.00	0.0	[TS]
99[p]. $C_2H_3 + M \rightarrow C_2H_2 + H + M$	k_0	1.51×10^{14}	0.10	136.7	[11]
	k_∞	6.38×10^{09}	1.00	157.4	[11]
100. $C_2H_3 + O_2 \rightarrow CH_2O + HCO$		1.70×10^{29}	-5.31	27.2	[11]
101. $C_2H_3 + O_2 \rightarrow CH_2CHO + O$		7.00×10^{14}	-0.61	22.0	[11]
102. $C_2H_3 + O_2 \rightarrow C_2H_2 + HO_2$		5.19×10^{15}	-1.26	13.9	[11]
Acetylene (C_2H_2) Reactions					
103. $C_2H_2 + O \rightarrow HCCO + H$		4.00×10^{14}	0.00	44.6	[11]
104. $C_2H_2 + O \rightarrow T\text{-}CH_2 + CO$		1.60×10^{14}	0.00	41.4	[11]
105. $C_2H_2 + O_2 \rightarrow CH_2O + CO$		4.60×10^{15}	-0.54	188.0	[11]
106. $C_2H_2 + OH \rightarrow CH_2CO + H$		1.90×10^{07}	1.70	4.2	[11]
107. $C_2H_2 + OH \rightarrow C_2H + H_2O$		3.37×10^{07}	2.00	58.6	[11]
CH_2CO Reactions					
108. $CH_2CO + H \rightarrow CH_3 + CO$		1.50×10^{09}	1.43	11.3	[11]
109. $CH_2CO + O \rightarrow T\text{-}CH_2 + CO_2$		2.00×10^{13}	0.00	9.6	[11]
110. $CH_2CO + O \rightarrow HCCO + OH$		1.00×10^{13}	0.00	8.4	[11]
111. $CH_2CO + CH_3 \rightarrow C_2H_5 + CO$		9.00×10^{10}	0.00	0.0	[11]
HCCO Reactions					

Table A1.1 Continued

Reaction	A^a	n^a	E^a		Reference
112. $HCCO + H \rightarrow S\text{-}CH_2 + CO$		1.50×10^{14}	0.00	0.0	[11]
113. $HCCO + OH \rightarrow HCO + CO + H$		2.00×10^{12}	0.00	0.0	[11]
114. $HCCO + O \rightarrow CO + CO + H$		9.64×10^{13}	0.00	0.0	[11]
115. $HCCO + O_2 \rightarrow CO + CO + OH$		2.88×10^{07}	1.70	4.2	[11]
116. $HCCO + O_2 \rightarrow CO_2 + CO + H$		1.40×10^{07}	1.70	4.2	[11]
C_2H Reactions					
117. $C_2H + OH \rightarrow HCCO + H$		2.00×10^{13}	0.00	0.0	[11]
118. $C_2H + O \rightarrow CO + CH$		1.02×10^{13}	0.00	0.0	[11]
119. $C_2H + O_2 \rightarrow HCCO + O$		6.02×10^{11}	0.00	0.0	[11]
120. $C_2H + O_2 \rightarrow CH + CO_2$		4.50×10^{15}	0.00	105.0	[11]
121. $C_2H + O_2 \rightarrow HCO + CO$		2.41×10^{12}	0.00	0.0	[11]
Hydroxymethyl (CH_2OH) Reactions					
122. $CH_2OH + H \rightarrow CH_2O + H_2$		3.00×10^{13}	0.00	0.0	[11]
123. $CH_2OH + H \rightarrow CH_3 + OH$		2.50×10^{17}	-0.93	21.5	[TS]
124. $CH_2OH + OH \rightarrow CH_2O + H_2O$		2.40×10^{13}	0.00	0.0	[11]
125. $CH_2OH + O_2 \rightarrow CH_2O + HO_2$		5.00×10^{12}	0.00	0.0	[11]
126[k]. $CH_2OH + M \rightarrow CH_2O + H + M$		5.00×10^{13}	0.00	105.1	[11]
127[k]. $CH_3O + M \rightarrow CH_2OH + M$		1.00×10^{14}	0.00	80.0	[11]
128. $CH_2CO + OH \rightarrow CH_2OH + CO$		1.02×10^{13}	0.00	0.0	[11]
Methanol (CH_3OH) Reactions					
129. $CH_3OH + OH \rightarrow CH_2OH + H_2O$		1.44×10^{06}	2.00	-3.5	[11]
130. $CH_3OH + OH \rightarrow CH_3O + H_2O$		4.40×10^{06}	2.00	6.3	[TS]
131. $CH_3OH + H \rightarrow CH_2OH + H_2$		1.35×10^{03}	3.20	14.6	[TS]
132. $CH_3OH + H \rightarrow CH_3O + H_2$		6.83×10^{01}	3.40	30.3	[TS]
133. $CH_3OH + O \rightarrow CH_2OH + OH$		1.00×10^{13}	0.00	19.6	[11]
134. $CH_3OH + HO_2 \rightarrow CH_2OH + H_2O_2$		6.20×10^{12}	0.00	81.1	[11]
135. $CH_3OH + O_2 \rightarrow CH_2OH + HO_2$		2.00×10^{13}	0.00	188.0	[11]
136[p]. $CH_3OH + M \rightarrow CH_3 + OH + M$	k_0	2.95×10^{44}	-7.35	399.4	[TS]
	k_∞	1.90×10^{16}	0.00	383.8	
CH_2CHO Reactions					
137. $CH_2CHO \rightarrow CH_2CO + H$		1.05×10^{37}	-7.19	185.5	[11]
138. $CH_2CHO + H \rightarrow CH_3 + HCO$		5.00×10^{13}	0.00	0.0	[12]
139. $CH_2CHO + H \rightarrow CH_2O + H_2$		2.00×10^{13}	0.00	0.0	[12]
140. $CH_2CHO + O \rightarrow CH_2O + HCO$		1.00×10^{14}	0.00	0.0	[12]
141. $CH_2CHO + OH \rightarrow CH_2CO + H_2O$		3.00×10^{13}	0.00	0.0	[12]
142. $CH_2CHO + O_2 \rightarrow CH_2O + CO + OH$		3.00×10^{10}	0.00	0.0	[12]
143. $CH_2CHO + CH_3 \rightarrow C_2H_5 + CO + H$		4.90×10^{14}	-0.50	0.0	[12]
144. $CH_2CHO + HO_2 \rightarrow CH_2O + HCO + OH$		7.00×10^{12}	0.00	0.0	[12]
145. $CH_2CHO + HO_2 \rightarrow CH_3CHO + O_2$		3.00×10^{12}	0.00	0.0	[12]
146. $CH_2CHO \rightarrow CH_3 + CO$		1.17×10^{43}	-9.80	183.3	[12]

Table A1.1 Continued

Reaction	A^a	n^a	E^a		Reference
Acetaldehyde (CH_3CHO) Reactions					
147. $CH_3CHO \rightarrow CH_3 + HCO$		7.00×10^{15}	0.00	341.8	[12]
148[q]. $CH_3CO + M \rightarrow CH_3 + CO + M$	k_0	1.20×10^{15}	0.00	52.3	[12]
	k_∞	3.00×10^{12}	0.00	69.9	
149. $CH_3CHO + OH \rightarrow CH_3CO + H_2O$		3.37×10^{12}	0.00	-2.6	[12]
150. $CH_3CHO + OH \rightarrow CH_2CHO + H_2O$		3.37×10^{11}	0.00	-2.6	[12]
151. $CH_3CHO + O \rightarrow CH_3CO + OH$		1.77×10^{18}	-1.90	12.5	[12]
152. $CH_3CHO + O \rightarrow CH_2CHO + OH$		3.72×10^{13}	-0.20	14.9	[12]
153. $CH_3CHO + H \rightarrow CH_3CO + H_2$		4.66×10^{13}	-0.30	12.5	[12]
154. $CH_3CHO + H \rightarrow CH_2CHO + H_2$		1.85×10^{12}	0.40	22.4	[12]
155. $CH_3CHO + CH_3 \rightarrow CH_3CO + CH_4$		3.90×10^{-7}	5.80	9.2	[12]
156. $CH_3CHO + CH_3 \rightarrow CH_2CHO + CH_4$		2.45×10^{01}	3.10	24.0	[12]
157. $CH_3CHO + HO_2 \rightarrow CH_3CO + H_2O_2$		3.60×10^{19}	-2.20	58.6	[12]
158. $CH_3CHO + HO_2 \rightarrow CH_2CHO + H_2O_2$		2.32×10^{11}	0.40	62.3	[12]
159. $CH_3CHO + O_2 \rightarrow CH_3CO + HO_2$		1.00×10^{14}	0.00	176.6	[12]
Ethanol (C_2H_5OH) Reactions					
160[r]. $C_2H_5OH + M \rightarrow CH_3 + CH_2OH + M$	k_0	3.0×10^{16}	0.00	242.4	[TS]
	k_∞	5.00×10^{15}	0.00	342.8	
161[r]. $C_2H_5OH + M \rightarrow C_2H_4 + H_2O + M$	k_0	1.0×10^{17}	0.00	225.7	[TS]
	k_∞	8.00×10^{13}	0.00	271.7	
162. $C_2H_5OH + OH \rightarrow CH_2CH_2OH + H_2O$		1.81×10^{11}	0.40	3.0	[12]
163. $C_2H_5OH + OH \rightarrow CH_3CHOH + H_2O$		3.09×10^{10}	0.50	-1.6	[12]
164. $C_2H_5OH + OH \rightarrow CH_3CH_2O + H_2O$		1.05×10^{10}	0.80	3.0	[12]
165. $C_2H_5OH + H \rightarrow CH_2CH_2OH + H_2$		1.90×10^{07}	1.80	21.3	[12]
166. $C_2H_5OH + H \rightarrow CH_3CHOH + H_2$		2.60×10^{07}	1.60	11.8	[12]
167. $C_2H_5OH + H \rightarrow CH_3CH_2O + H_2$		1.50×10^{07}	1.60	12.7	[12]
168. $C_2H_5OH + O \rightarrow CH_2CH_2OH + OH$		9.41×10^{07}	1.70	22.8	[12]
169. $C_2H_5OH + O \rightarrow CH_3CHOH + OH$		1.88×10^{07}	1.90	7.6	[12]
170. $C_2H_5OH + O \rightarrow CH_3CH_2O + OH$		1.58×10^{07}	2.00	18.6	[12]
171. $C_2H_5OH + CH_3 \rightarrow CH_2CH_2OH + CH_4$		2.19×10^{02}	3.20	40.3	[12]
172. $C_2H_5OH + CH_3 \rightarrow CH_3CHOH + CH_4$		7.28×10^{02}	3.00	33.3	[12]
173. $C_2H_5OH + CH_3 \rightarrow CH_3CH_2O + CH_4$		1.45×10^{02}	3.00	32.0	[12]
174. $C_2H_5OH + HO_2 \rightarrow CH_2CH_2OH + H_2O_2$		8.20×10^{03}	2.50	45.2	[12]
175. $C_2H_5OH + HO_2 \rightarrow CH_3CHOH + H_2O_2$		2.43×10^{04}	2.50	66.1	[12]
176. $C_2H_5OH + HO_2 \rightarrow CH_3CH_2O + H_2O_2$		3.80×10^{12}	0.00	100.4	[12]
C_2H_5O Reactions					
177. $C_2H_4 + OH \rightarrow CH_2CH_2OH$		2.41×10^{11}	0.00	-9.9	[12]
178. $C_2H_5 + HO_2 \rightarrow CH_3CH_2O + OH$		4.00×10^{13}	0.00	0.0	[12]
179[k]. $CH_3CH_2O + M \rightarrow CH_3CHO + H + M$		5.60×10^{34}	-5.90	105.9	[12]
180[k]. $CH_3CH_2O + M \rightarrow CH_3 + CH_2O + M$		5.35×10^{37}	-7.00	99.6	[12]
181. $CH_3CH_2O + O_2 \rightarrow CH_3CHO + HO_2$		4.00×10^{10}	0.00	4.6	[12]

Table A1.1 Continued

Reaction	A[a]	n[a]	E[a]		Reference
182. $CH_3CH_2O + CO \rightarrow C_2H_5 + CO_2$	4.68×10^{02}		3.20	22.5	[12]
183. $CH_3CH_2O + H \rightarrow CH_3 + CH_2OH$	3.00×10^{13}		0.00	0.0	[12]
184. $CH_3CH_2O + H \rightarrow C_2H_4 + H_2O$	3.00×10^{13}		0.00	0.0	[12]
185. $CH_3CH_2O + OH \rightarrow CH_3CHO + H_2O$	1.00×10^{13}		0.00	0.0	[12]
186. $CH_3CHOH + O_2 \rightarrow CH_3CHO + HO_2$	4.82×10^{13}		0.00	21.0	[12]
187. $CH_3CHOH + O \rightarrow CH_3CHO + OH$	1.00×10^{14}		0.00	0.0	[12]
188. $CH_3CHOH + H \rightarrow C_2H_4 + H_2O$	3.00×10^{13}		0.00	0.0	[12]
189. $CH_3CHOH + H \rightarrow CH_3 + CH_2OH$	3.00×10^{13}		0.00	0.0	[12]
190. $CH_3CHOH + HO_2 \rightarrow CH_3CHO + OH + OH$	4.00×10^{13}		0.00	0.0	[12]
191. $CH_3CHOH + OH \rightarrow CH_3CHO + H_2O$	5.00×10^{12}		0.00	0.0	[12]
192[k]. $CH_3CHOH + M \rightarrow CH_3CHO + H + M$	1.00×10^{14}		0.00	104.6	[12]

[a]Specific reaction-rate constant $k = AT^n e^{-E/R^o T}$; units mol/cm^3, s^{-1}, K, kJ/mol.
[b][TS] stands for This study
[c]Chaperon efficiencies are 2.5 for H_2, 12.0 for H_2O, 1.9 for CO, 3.8 for CO_2, 0.5 for Ar and He and 1.0 for all other species.
[d]Chaperon efficiencies are 2.5 for H_2, 12.0 for H_2O, 1.9 for CO, 3.8 for CO_2, 0.4 for Ar and He and 1.0 for all other species.
[e]Chaperon efficiencies are 2.5 for H_2, 12.0 for H_2O, 1.9 for CO, 3.8 for CO_2, 0.2 for Ar and He and 1.0 for all other species.
[f]Chaperon efficiencies are 2.5 for H_2, 12.0 for H_2O, 1.9 for CO, 3.8 for CO_2, 0.7 for Ar and He and 1.0 for all other species.
[g]Chaperon efficiencies are 2.5 for H_2, 16.0 for H_2O, 1.2 for CO, 2.4 for CO_2, 0.7 for Ar and He and 1.0 for all other species; Troe falloff with $F_c = 0.5$.
[h]Chaperon efficiencies are 2.0 for H_2, 6.0 for H_2O, 1.5 for CO, 2.0 for CO_2, 0.4 for Ar and He and 1.0 for all other species; Troe falloff with $F_c = 0.265 \exp(-T/94\text{ K}) + 0.735 \exp(-T/1756\text{ K}) + \exp(-5182\text{ K}/T)$.
[i]Chaperon efficiencies are 1.9 for H_2, 12.0 for H_2O, 2.5 for CO, 2.5 for CO_2 and 1.0 for all other species.
[j]Chaperon efficiencies are 2.0 for H_2, 6.0 for H_2O, 1.5 for CO, 2.0 for CO_2, 3.0 for CH_4, 3.0 for C_2H_6, 0.7 for Ar and 1.0 for all other species; Troe falloff with $F_c = 0.2176 \exp(-T/271.0\text{ K}) + 0.7824 \exp(-T/2755.0\text{ K}) + \exp(-6570.0\text{ K}/T)$.
[k]Chaperon efficiencies are 2.0 for H_2, 6.0 for H_2O, 1.5 for CO, 2.0 for CO_2, 2.0 for CH_4, 0.7 for Ar and 1.0 for all other species
[l]Troe falloff with $F_c = 0.217 \exp(-T/74.0\text{ K}) + 0.783 \exp(-T/2941.0\text{ K}) + \exp(-6964.0\text{ K}/T)$.
[m]Chaperon efficiencies are 2.0 for H_2, 6.0 for H_2O, 1.5 for CO, 2.0 for CO_2, 2.0 for CH_4, 3.0 C_2H_6, 0.7 for Ar and 1.0 for all other species; Troe falloff with $F_c = 0.38 \exp(-T/73.0\text{ K}) + 0.62 \exp(-T/1180.0\text{ K})$.
[n]Chaperon efficiencies are 2.0 for H_2, 6.0 for H_2O, 1.5 for CO, 2.0 for CO_2, 2.0 for CH_4, 3.0 C_2H_6, 0.7 for Ar and 1.0 for all other species; Troe falloff with $F_c = 0.16 \exp(-T/125.0\text{ K}) + 0.84 \exp(-T/2219.0\text{ K}) + \exp(-6882.0\text{ K}/T)$.

[o]Chaperon efficiencies are 2.0 for H_2, 6.0 for H_2O, 1.5 for CO, 2.0 for CO_2, 2.0 for CH_4, 0.7 for Ar and 1.0 for all other species; Troe falloff with F_c = 0.832 exp (-T/1203.0 K) + 0.168 exp (-T/0.0 K).
[p]Chaperon efficiencies are 2.0 for H_2, 6.0 for H_2O, 1.5 for CO, 2.0 for CO_2, 2.0 for CH_4, 0.7 for Ar and 1.0 for all other species; Troe falloff with F_c = 0.586 exp (-T/279.0 K) + 0.414 exp (-T/5459.0 K).
[q]Chaperon efficiencies are 2.0 for H_2, 6.0 for H_2O, 1.5 for CO, 2.0 for CO_2, 2.0 for CH_4, 0.7 for Ar and 1.0 for all other species; Troe falloff with F_c = 1.0.
[r]Chaperon efficiencies are 2.0 for H_2, 6.0 for H_2O, 1.5 for CO, 2.0 for CO_2, 2.0 for CH_4, 0.7 for Ar and 1.0 for all other species; Troe falloff with F_c = 0.5.

REFERENCES

1. Masten, D.A., Hanson, R.K. and Bowman, C.T., "Shock tube study of the reaction $H+O_2 \rightarrow OH+O$ using OH laser absorption", Journal of Physical Chemistry, 94, 1990, pp. 7119-7128.

2. Yetter, R.A., Dryer, F.L. and Rabitz, H., "A comprehensive reaction mechanism for carbon monoxide/hydrogen/oxygen kinetics", Combustion Science and Technology, 79, 1991, pp. 97-128.

3. Smooke, M.D., "Solution of burner-stabilized premixed laminar flames by boundary value methods", Journal of Computational Physics, 48, 1982, pp. 72-105.

4. Mueller, M.A., Kim, T.J., Yetter, R.A. and Dryer, F.L., "Flow reactor studies and kinetic modeling of the H_2/O_2 Reaction", International Journal of Chemical Kinetics, 31, 1999, pp. 113-125.

5. Baulch, D.L., Cobos, C.J., Cox, R.A., Esser, C., Frank, P., Just, Th., Kerr, J.A., Pilling, M.J., Troe, J., Walker, R.W. and Warnatz, J., "Evaluated kinetic data for combustion modeling", Journal of Physical and Chemical Reference Data, 21, 1992, pp. 411-734.

6. Warnatz, J., "Rate coefficients in the C/H/O system". In W.C. Gardiner (ed.), Combustion Chemistry, Springer-Verlag, Berlin, pp. 197-360, 1984.

7. Rightley, M.L. and Williams, F.A., "Structures of CO diffusion flames near extinction", Combustion Science and Technology, 125, 1997, pp. 181-200.

8. Lindstedt, R.P. and Skevis, G., "Chemistry of acetylene flames", Combustion Science and Technology, 125, 1997, pp. 73-137.

9. Tsang, W. and Hampson, R.F., "Chemical kinetic database for combustion chemistry. 1. Methane and related compounds", Journal of Physical Chemistry Reference Data, 15, 1986, pp. 1087-1276.

10. Timonen, R.S., Ratajczak, E. and Gutman, D., "Kinetics of the reactions of the formyl radical with oxygen, nitrogen dioxide, chlorine and bromine", Journal of Physical Chemistry, 92, 1988, pp. 651-655.

11. Petrova, M.V. and Williams, F.A., "A small detailed chemical-kinetic mechanism for hydrocarbon combustion", Combustion and Flame, 144, 2006, pp. 526-544.

12. Li, J., "Experimental and numerical studies of ethanol chemical kinetics," PhD Thesis, Princeton University, 2004.
13. Li, S.C. and Williams, F.A., "Counterflow heptane flame structure", Proceedings of the Combustion Institute, 28, 2000, pp. 1031-1038.

14. Li, S.C., Varatharajan, B. and Williams, F.A., "Chemistry of JP-10 ignition", AIAA Journal, 39, 2001, pp. 2351-2356.

15. Li, S.C. and Williams, F.A., "NO_x formation in two-stage methane-air flames", Combustion and Flame, 118, 1999, pp. 399-414.

16. Shimizu, T., Williams, F.A. and Frassoldati, A., "Concentrations of nitric oxide in laminar counterflow methane/air diffusion flames", Journal of Propulsion and Power, 21, 2005, pp. 1019-1028.

APPENDIX 2

VAPORIZER TEMPERATURE

During our experiments, a vaporizer was used to vaporize ethanol fuel. The vaporizer was elevated to a temperature based on the molefraction of the fuel required in the fuel stream. These temperatures can be obtained using Classius-Clapeyron equation or Antoine equation. These equations basically relate the partial pressure of the fuel in fuel-nitrogen mixture with the temperature.

A2.1 NONPREMIXED FLAME

In the nonpremixed case, the molefraction of ethanol in the fuel stream was equal to 0.3.

Classius Clapeyron equation

$$\ln\left(\frac{P_1}{P_2}\right) = \frac{h_{fg}}{R}\left(\frac{1}{T_1} - \frac{1}{T_2}\right) \qquad (1)$$

where, boiling point of ethanol at atmospheric pressure, T_1 = 78.3 °C = 351.3 K; latent heat of vaporization, h_{fg} = 840 kJ/kg; Gas constant, R = R°/MW = 0.181 kJ/kg K. The data was obtained from [1].

Since, in nonpremixed case, P_2/P_1 = 0.3, hence, vaporizer temperature, **T_2 = 322.0 K**

Antoine formula

$$\log_{10}(P_v) = A - \frac{B}{t + C} \qquad (2)$$

where, vapor pressure in mm of Hg, P_v = 0.3*760 = 228 mm; t is in degree celcius. Using constants, A = 8.04494, B = 1554.3, C=222.65, for ethanol from [2], vaporizer temperature, t = 50.7 °C = **323.9 K**

A2.2 PARTIALLY PREMIXED FLAME

In partially premixed case, fuel stream consists of $X_{C_2H_5OH}$ = 0.1385, X_{N_2} = 0.6803, X_{O_2} = 0.1812.

Classius Clapeyron equation

Since in the vaporizer, only nitrogen flow through the vaporizing fuel, P_2/P_1 = 0.1692; using equation 1, vaporizer temperature, T_2 = **309.7 K**

Antoine formula

The vapor pressure in mm of Hg in the vaporizer, P_v = 0.1692*760 = 128.6 mm. Using equation 2, vaporizer temperature, t = 39.2 °C = **312.3 K**.

For both the nonpremixed and partially premixed systems the values of the vaporizer temperature calculated with Antoine equation were used in the experiments.

REFRENCES

1. Cengel, Y.A. and Boles, M.A., Thermodynamics An Engineering Approach (3rd edition), McGraw-Hill, New York, 1998.

2. Dean, J.A., Lange's Handbook of Chemistry (13th edition). McGraw-Hill, New York, 1985.

APPENDIX 3

HYDROGEN AUTOIGNITION RESULTS

The hydrogen submechanism of the San Diego Mech was tested for autoignition delay times [1] against the selected experimental data under various conditions of pressure and composition. This mechanism has been tested for laminar burning velocities and diffusion-flame extinction in Chapter 4 of this study. The updates to this mechanism based on these tests are discussed. The autoignition calculations for the selected experiments in [1] are repeated here for isochoric, homogeneous, and adiabatic system with updated hydrogen mechanism. The ignition time in calculations is the time when maximum temperature inflection occurs. Figure A3.1 shows the comparison of experimental data (symbols) with the predictions (solid line) of the San Diego Mech. The agreements between predictions and the data are as good as those in [1]. The discrepancy in the data [2] and predicted values at high temperatures can be attributed to the different ignition criteria used in experiments and calculations. Experimental ignition delay time was based on the onset of light emission.

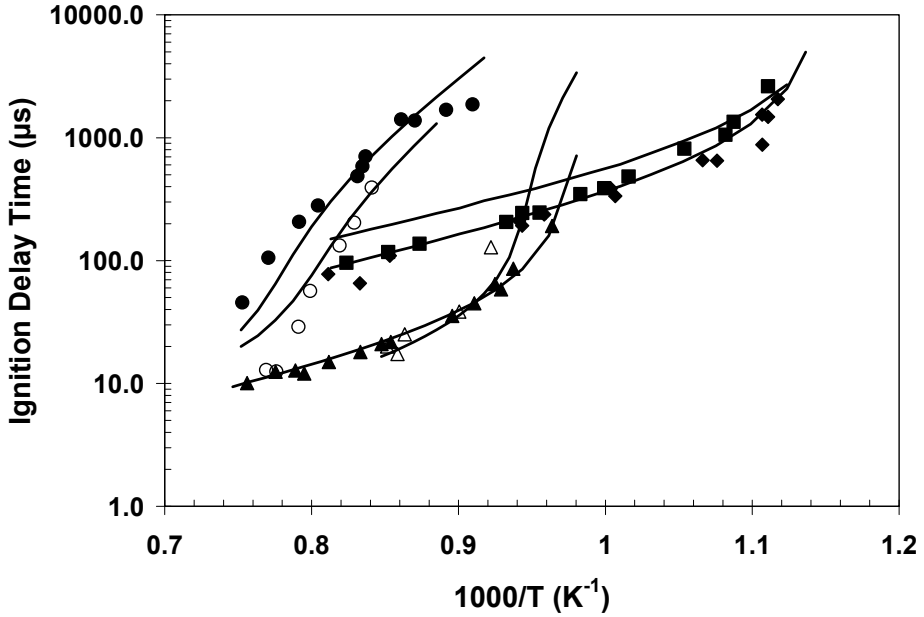

Figure A3.1 Measured and predicted autoignition delay times for hydrogen-oxygen-inert mixtures; solid diamonds [2] φ=1.0 (29.6% H_2, 14.8% O_2, and 55.6% N_2 by volume) at pressure 0.43 bar, solid squares [2] φ=0.1 (4.0% H_2, 20.2% O_2, and 75.8% N_2 by volume) at pressure 0.45 bar; solid triangles [3] φ=1.0 (29.6% H_2, 14.8% O_2, and 55.6% N_2 by volume) at pressure 2.5 bar; open circles [4] φ=1.0 (2.0% H_2, 1.0% O_2, and 97.0% Ar by volume) at pressure 33 bar; open triangles [5] φ=0.42 (15.0% H_2, 17.85% O_2, and 67.15% N_2 by volume) at pressure 4.0 bar; solid circle [5] φ=0.42 (9.0% H_2, 10.71% O_2, 40.0% H_2O, and 40.29.0% N_2 by volume) at pressure 4.5 bar; solid line represents prediction of the San Diego Mech.

REFERENCES

1. Del Alamo, G., Williams, F.A. and Sanchez A. L, "Hydrogen-oxygen induction times above crossover temperatures", Combustion Science and Technology, 176, 2004, 1599-1626.

2. Just, T. and Schmalz, F., "Measurements of ignition delays of hydrogen-air mixtures under sumulated conditions of supersonic combustion chambers", AGARD CP No. 34, Part2, 1968, Paper 19.

3. Bhaskaran, K.A., Gupta, M.C., and Just, T., "Shock-tube study of the effect of unsymmetric dimethyl hydrazine on the ignition characteristics of hydrogen-air mixtures", Combustion and Flame, 21, 1973, pp. 45-48.

4. Petersen, E.L., Davidson, D.F., Rohrig, M., and Hanson, R.K., "High-pressure shock-tube measurements of ignition times in stoichiometric H_2/O_2/Ar mixtures", Proceeding of the 20^{th} International Symposium on Shock Waves, World Scientific Publisher, River Edge, NJ, Vol. II, 1996, pp. 941-946.

5. Wang, B.L., Olivier, H., and Gronig, H., "Ignition of shock-heated H_2-air-steam mixtures", Combustion and Flame, 133, 2003, pp. 96-106.